SYNTHESES OF LIPOPHILIC WERNER COMPLEXES FOR APPLICATION AS CHIRAL HYDROGEN BOND DONORS IN ENANTIOSELECTIVE CATALYSIS AND INVESTIGATION OF THE EFFECT OF CHLORIDE ON FLUID CATALYTIC CRACKING CATALYSTS

A Dissertation

by

WILLIAM JOSEPH MAXIMUCK

Submitted to the Office of Graduate and Professional Studies of
Texas A&M University
in partial fulfillment of the requirements for the degree of

DOCTOR OF PHILOSOPHY

Chair of Committee,	John A. Gladysz
Committee Members,	François P. Gabbaï
	Daniel A. Singleton
	Patrick J. Shamberger
Head of Department,	Simon W. North

May 2021

Major Subject: Chemistry

ABSTRACT

Swiss chemist and 1913 Nobel laureate Alfred Werner is commonly referred to as the father of coordination chemistry. Werner synthesized a myriad of inorganic complexes and accurately predicted the bonding relationships between the metals, ligands, and anions. Werner was tremendously influential on the development of inorganic chemistry. In opposition to the theories of many of his contemporaries, Werner insisted chirality could exist at the metal center of certain coordination compounds. Demonstrating this point, Werner successfully resolved the enantiomers of $[Co(en)_3]^{3+}$ (en = 1,2-ethylenediamine) into their respective Λ and Δ forms via fractional crystallization from diastereomeric tartrate salts.

Analysis of crystal structures of tris(ethylenediamine) complexes reveals that the NH units of the ligands exhibit a propensity to function as exceptional hydrogen bond donors to counter anions. The century long dormancy of the use of these compounds in synthetic applications can be attributed to their meager organic solublity and low spin d^6 electron configuration, rendering these octahedral complexes kinetically substitution inert. Thankfully, anion methathesis with lipophilic counteranions unlocks substantial organic solubility, relieving competition between substrates and anions for NH active sites. The mechanism of hydrogen bond donating organocatalysts is not entirely understood. However, modifications to the ligands, anions, and metals has provided insight into catalytic enantioselectivity and kinetics.

In an unrelated project, nickel, a common contaminant in crude oil, deposits on Fluid catalytic cracking (FCC) catalysts and induces unwanted dehydrogenation reactions. These lead to an increase in hydrogen and coke, inhibiting the FCC unit from reaching its optimal operation. In this study, equilibrium catalyst samples obtained from industrial

FCC units are exposed to chloride ions, and changes in physicochemical characteristics, catalytic selectivity, and the reducibility of nickel are analyzed. Spectroscopic analyses show that the interaction with chloride ions alters the electronic environment of nickel and Advanced Cracking Evaluation studies show equilibrium catalysts that were exposed to chloride ions gave higher coke and H_2 yields. These results bridge the gap between existing literature and the FCC environment by demonstrating that chloride ions can interact and reactivate nickel contaminant on FCC catalysts.

DEDICATION

This dissertation is dedicated to my wife, Patricia Maximuck. She has persevered with me throughout this journey here in Texas. She has encouraged me to follow my dreams of attending Texas A&M University, temporarily sacrificing time away from family in the process. She has been there through the best and worst times. Her dedication means everything to me.

ACKNOWLEDGEMENTS

I am very grateful to my committee chair, Dr. John A. Gladysz. After my first interaction with him at the poster session during orientation, I appreciated how he was very straightforward with me and welcoming. When I joined the research group, he had thoughtfully planned projects for me, but also provided an abundance of independence and encouraged freedom to explore outside of these projects. He was patient with me during the research and writing processes, understanding when I made mistakes, but he also encouraged me when I needed it.

I am thankful for my committee members, Dr. François P. Gabbaï, Dr. Daniel A. Singleton, and Dr. Patrick J. Shamberger. Their thoughtful questions and offers of assistance during meetings, literature seminars, and preliminary exams has been much appreciated.

An unmeasurable amount of credit goes to my wife, Patricia Maximuck. I would not be here at Texas A&M University without her selflessness to allow us to move halfway across the country to pursue my dreams. All of this time, she has sacrificed valuable time with our families and I cannot thank her enough for that. She kept my head up during rough times, especially the coursework and cumulative exams during the first year of graduate studies. Together, we planned a wedding from halfway across the country and adopted a puppy during this time here and look forward to moving onto the next chapter of our lives.

My family has been very important to me and supportive to me throughout this journey. They have come to visit and have always inspired me to chase my dreams and they were there for the tougher times when I needed guidance.

I owe credit to the wonderful bunch of coworkers that I have had the pleasure to work with during these four past years. Some special credit goes to my Werner subgroup coworkers, Connor Kabes and Quang Luu. These two were always there for advice (in chemistry and in life) and provided me with ideas to move the projects that I was working on in the right direction.

CONTRIBUTORS AND FUNDING SOURCES

Contributors

This work was supervised by a dissertation committee consisting of Dr. John A. Gladysz, Dr. François P. Gabbaï, and Dr. Daniel A. Singleton of the Department of Chemistry and Dr. Patrick J. Shamberger of the Department of Materials Science and Engineering.

The work of section 2 of the dissertation was completed by the student, in collaboration with Dr. Carola Ganzmann of the Institut für Organische Chemie and Interdisciplinary Center for Molecular Materials, Friedrich-Alexander-Universität Erlangen-Nürnberg, Henkestraße 42, 91054 Erlangen (Germany), Ms. Scheherzad Alvi, and Mr. Karan R. Hooda of the Department of Chemistry.

The work of section 3 of the dissertation was completed by the student, in collaboration with Mr. Connor Q. Kabes, Dr. Subrata K. Ghosh, Dr. Anil Kumar, and Dr. Kyle G. Lewis of the Department of Chemistry.

The work of section 4 of the dissertation was completed by the student in collaboration with Mr. Karan R. Hooda of the Department of Chemistry.

The work of section 5 of the dissertation was completed by the student, in collaboration with Mr. Karan R. Hooda and Ms. Scheherzad Alvi of the Department of Chemistry.

The work of section 6 of the dissertation was completed by the student, in collaboration with Dr. Corbett Senter of BASF Refinery Catalysts, 11750 Katy Fwy. #120, Houston, TX 77079 USA, Dr. Melissa Clough Mastry of BASF Refinery Catalysts, Can Rabia 3-5, Barcelona 08017 Spain, Dr. Claire C. Zhang of BASF, Analytics & Materials

Characterization, 25 Middlesex-Essex Tpk., Iselin, NJ 08830 USA, and Dr. Bilge Yilmaz of BASF Refinery Catalysts, 25 Middlesex-Essex Tpk., Iselin, NJ 08830 USA.

All crystal structures were determined by crystallographers Dr. Kevin Gagnon of the Advanced Light Source, Lawrence Berkeley National Laboratory, 6 Cyclotron Road, Berkeley, CA 94720, and Dr. Nattamai Bhuvanesh and Dr. Joseph Reibenspies of the Department of Chemistry, although all crystallographic data were interpreted by the student.

All other work conducted for the dissertation was completed by the student independently.

Funding Sources

This work was made possible in part by Welch Foundation under Grant Number A-1656. Additionally, BASF provided funding for the research performed in section 6 of the dissertation.

NOMENCLATURE

δ	chemical shift
Δε	molar circular dichroism
ε	molar extinction coefficient
ν	stretching mode (IR)
$\{^1H\}$	proton decoupled
Å	Angstrom
ACE	advanced cracking evaluation
Anal.	analysis
Ar	aryl
aq	aqueous
br	broad
Bu	butyl
BINOLPA	1,1'-binaphthyl-2,2'-diyl hydrogenphosphate
Calcd.	Calculated
camphSO_3^-	3-bromocamphor-8-sulfonate
CD	circular dichroism
chxn	1,2-cyclohexanediamine
cm	centimeter
cm^{-1}	wavenumber
°C	degrees Celsius
d	doublet (NMR), days
dec	decomposition
DRIFTS	diffuse reflectance infrared Fourier transform spectroscopy
DMSO	dimethyl sulfoxide
dnen	1,2-dinaphthylethylenediamine
dpen	1,2-diphenylethylenediamine

DS^-	dodecyl sulfate
DSC	differential scanning calorimetry
Ecat	equilibrium catalyst
ee	enantiomeric excess
en	ethylenediamine
Et	ethyl
Et_3N	triethylamine
EtOAc	ethyl acetate
equiv	equivalent
FCC	fluid catalytic cracking
h	hour
HPLC	high pressure liquid chromatography
Hz	hertz
i	*ipso*
$^iJ_{jk}$	scalar coupling constant for coupling of nucleus j with nucleus k through i bonds
IR	infrared
L^n	$NH_2CH_2CH((CH_2)_nNMe_2)NH_2$ (n = 1-4)
lel	parallel to the C_3 axis
M	metal, mol/liter
m	multiplet (NMR), medium (IR)
m	*meta*
Me	methyl
MeOH	methanol
mg	milligram
min	minutes
mol	mole
mm^2	cubic millimeter
mmol	millimole

mp	melting point
MSA	matrix surface area
n	normal
nm	nanometer
NMM	N-methyl morpholine
NMR	nuclear magnetic resonance
o	*ortho*
OAc	acetate
ob	oblique to the C_3 axis
p	*para*
Ph	phenyl
pn	1,2-propylenediamine
ppm	parts per million
Pr	propyl
q	quartet
R	organic group
rac	racemic
REO	rare earth oxide
rt	room temperature
s	singlet (NMR), strong (IR)
sar	sarcophagine, 3,6,10,13,16,19-hexaazabicyclo[6.6.6]icosane
SDS	sodium dodecyl sulfate
SEM	scanning electron microscopy
sen	1,1,1-tris(2'-aminoethylaminomethyl)ethane
sep	sepulchrate, 1,3,6,8,10,13,16,19-octaazabicyclo[6.6.6]icosane
tart	tartrate
taetacn	1,4,7-tris(2-aminoethyl)-1,4,7-triazacyclononane
t	triplet
t	tertiary

T_c	extrapolated peak-offset temperature
T_e	extrapolated peak-onset temperature
temp	temperature
T_f	final peak temperature
TGA	thermogravimetric analysis
THF	tetrahydrofuran
T_i	initial peak temperature
T_p	maximum peak temperature
t_R	retention time
TSA	total surface area
UV	ultraviolet
VAPOLPA	2,2'-diphenyl-3,3'-biphenanthryl-4,4'-diyl hydrogenphosphate
v/v	volume/volume
vis	visible
vs	very strong
w	weak
W	watt
wt	weight
XRF	X-ray fluorescence
ZSA	zeolite surface area

TABLE OF CONTENTS

LIST OF FIGURES

LIST OF TABLES

1. INTRODUCTION

1.1 History of Alfred Werner

Alfred Werner was born in Mulhouse, Alsace, France in 1866. The territory that he grew up in was heavily disputed between France and Germany. Though he passed through the German education system, spoke the German language, was obligated to complete the compulsory German military service requirement, he aligned with the French ideals and politics.[1]

Werner's love of chemistry originated from conducting experiments in his parents' barn. When he was of age to attend university education, Werner left Alsace to further his scientific ambitions at the Swiss Federal Institute in Zürich, and later the University of Zürich as the former was not able to issue doctoral degrees at the time. Werner was an unsalaried lecturer at the Technical High School in Zürich when he wrote his most impactful publication, entitled "Beitrag zur Konstitution anorganischer Verbindungen" in 1893. Werner claimed that he was awaken one night by a classical "Eureka!" moment and scribed feverishly for an entire day about his theories on coordination chemistry.[1]

Werner proposed that coordination compounds existed as complex ions, where a transition metal was surrounded by neutral or anion ligands arranged in a tetrahedral, square planar, or octahedral geometry. Werner also suggested that counter anions were necessary to balance the charge of the complex.[2] In some instances, some species could exist as ligands or anions. Alfred Werner became an overnight success for his theories. On the other hand, that much attention was faced with fierce pushback for a multitude of reasons.[1] None of this work was empirically tested, given Werner's low standing in the hierarchy of chemistry, and publication in a lesser known journal.

In contrast to Werner's theories, well-respected Danish chemist Sophus Mads Jørgensen and Swedish chemist Christian Wilhelm Blomstrand had proposed a chain theory (Figure 1.1) to describe the structure of these complexes.[3] It was quite the controversial topic until Werner was able to experimentally prove his theories. In fact, Jørgensen was in line to be awarded the Nobel Prize in Chemistry until his theories were disproven by Werner.[1]

Another one of Werner's innovative ideas was that, in some cases, chirality could exist at the metal center depending upon the arrangement and character of the ligands. This idea was outlandish to many of Werner's contemporaries. The common thought among the scientific community was that chirality could only exist as stereocenters about carbon atoms. Werner realized that he would have to support his theories experimentally if they were to be widely accepted, especially due to their innovative nature to the community.[1]

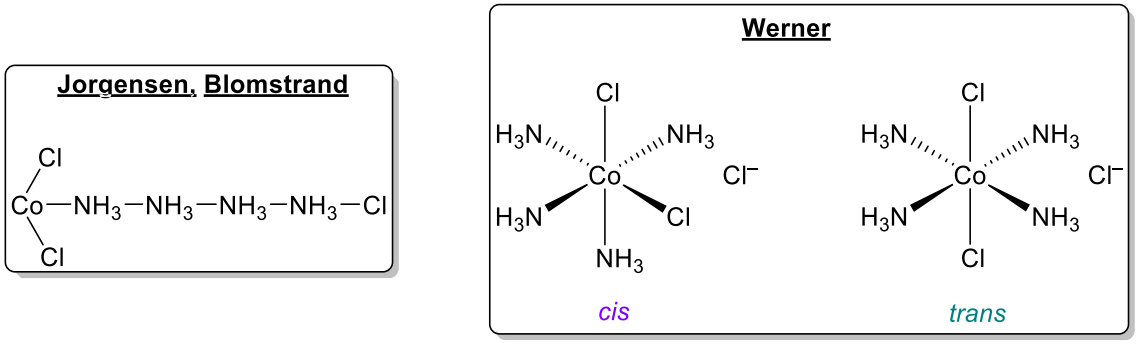

Figure 1.1. Jørgensen and Blomstrand's chain theory (left) and Werner's coordination theory (right) in description of the structure of $[Co(NH_3)_4(Cl)_2]^+ Cl^-$.

One of the most notable examples was $[Co(NH_3)_4(Cl)_2]^+ Cl^-$.[4] Werner noted that, based on his coordination theory, there would be two isomers for this complex. The one would have the two chloride ligands at a 90° angle relative to each other (*cis*) and the other

case, they would be 180° from each other (*trans*). The other factor was that the *cis* formed was violet in color, where the *trans* isomer was green.

The *cis* form is chiral when the NH_3 ligands are replaced by bidentate ethylenediamine ligands and Werner was able to resolve the $[Co(en)_2(Cl)_2]^+ Cl^-$ complex into its Λ and Δ forms by fractional crystallization of the diastereomeric bromocamphorsulfonate salts. Werner synthesized a myriad of complexes that possessed chirality at the metal center.[5] Still, not all of the community was convinced. They argued that the chirality originated from the carbon atoms in the molecule. In order to prove his point, Werner was able to resolve hexol, $([Co\{(OH)_2Co(NH_3)_4\}_3]^{6+}$ (Figure 1.2)). This marked the first synthetic chiral carbonless compound to be isolated.[6]

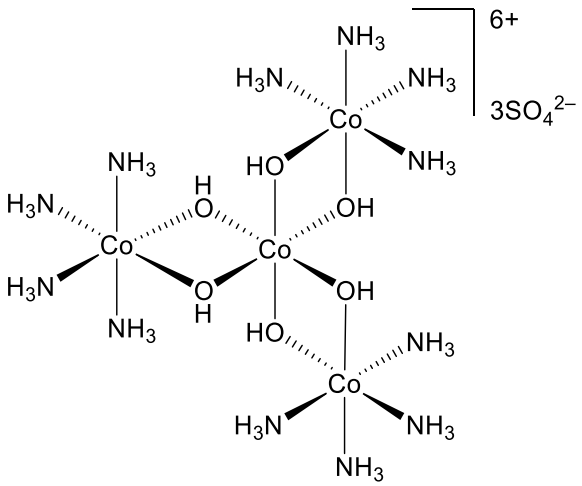

Figure 1.2. The structure of hexol, the first resolved synthetic chiral compound lacking carbon.

1.2 Bridging to organocatalysis

Much of the chemistry discussed to this point involves inorganic coordination chemistry that was developed between 100 and 150 years ago. Throughout the period that followed, these complexes were studied extensively. They had been derivatized, probed heavily through a variety of analytical methods, and introduced in countless undergraduate laboratories around the world.[7] Just as Alfred Werner bridged the gap between inorganic and organic chemistry, we must do the same.

The use of hydrogen bond donor organocatalysts was a foreign idea for some time. In the last few decades, the field has blossomed.[8a,b] Some of the earlier work was carried out by using thiourea-based catalysts.[8c] More recently, the catalysis has been shifted to include those containing metal ions (Figure 1.3). This is still considered organocatalysis by some definitions because the metal is not directly involved with the catalysis. Recent examples of other researchers that are utilizing these tactics include the Meggers group in Germany and Belokon group in Russia. Both groups feature nitrogen donor ligands bound to the chiral-at-metal center with NH units serving as hydrogen bond donors.[8d,e]

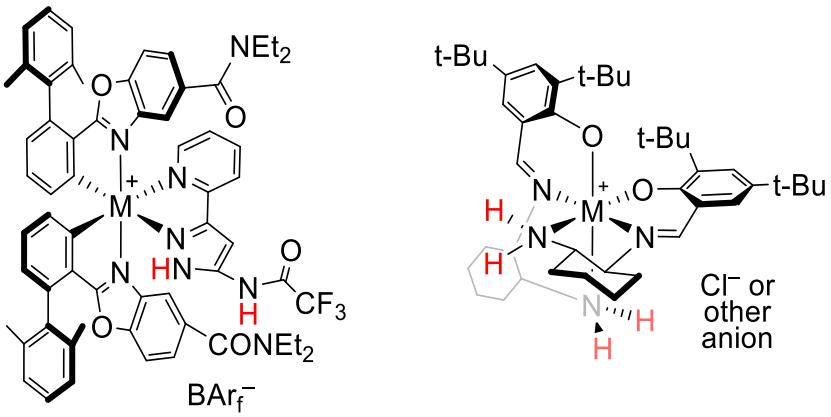

Figure 1.3. Other chiral, enantiopure metal and NH containing hydrogen bond donor catalysts.[8d,e]

It was during this time period, up to about ten years ago, that these inorganic coordination complexes had no applications in synthetic organic chemistry. This dormancy can be explained by the fact that most of inorganic catalysts feature the removal of a ligand from a coordination site or the redox potential of the metal. The low-spin cobalt(III) metal center is not conducive to this type of chemistry. Its d^6 electron configuration fully occupies the t_{2g} ground state energy level. The e_g energy level is elevated, thanks to the strong sigma-donor properties of the ligands, making it difficult to promote electrons to induce ligand substitution and, in turn, racemization.[9]

Thanks to the analysis of dozens of tris(ethylenediamine) complex crystal structures, the propensity for these complexes to form hydrogen bonds was realized.[10] These complexes could function as chiral hydrogen bond donors and were inexpensive, easy to synthesize and resolve. The major setback was that these complexes were exclusively soluble in water, making organocatalysis impossible. Not only would many organic substrates not be soluble in the reaction media, but the highly polar solvent and strong hydrogen bond accepting anions would undoubtedly outcompete Lewis basic substrates for NH active sites.

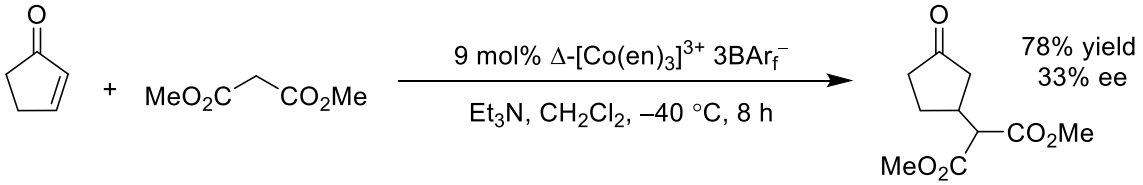

Figure 1.4. The enantioselective Michael addition of dimethyl malonate to 2-cyclopenten-1-one using Δ-$[Co(en)_3]^{3+}$ $3BAr_f^-$.[11a]

The cure to this shortcoming came in the form of anion metathesis with weakly coordinating lipophilic anions such as tetrakis(3,5-bis(trifluoromethyl)phenyl)borate (BAr_f^- or $B(3,5\text{-}C_6H_3(CF_3)_2)_4^-$). These catalysts were highly soluble in organic solvents

and produced modest enantioselectivities in the addition of dimethyl malonate to cyclopentenone (up to 33% ee, Figure 1.4).[11a] In later studies, enantioselectivity could be improved by sterically bulking up the ligands with the use of (*S*,*S*)- or (*R*,*R*)-1,2-diphenylethylenediamine (dpen = $H_2NCHPhCHPhNH_2$)[11b,d,e,j] or the addition of a pendant tertiary amine to the ligand to act as an internal base for the catalysis to occur.[11c]

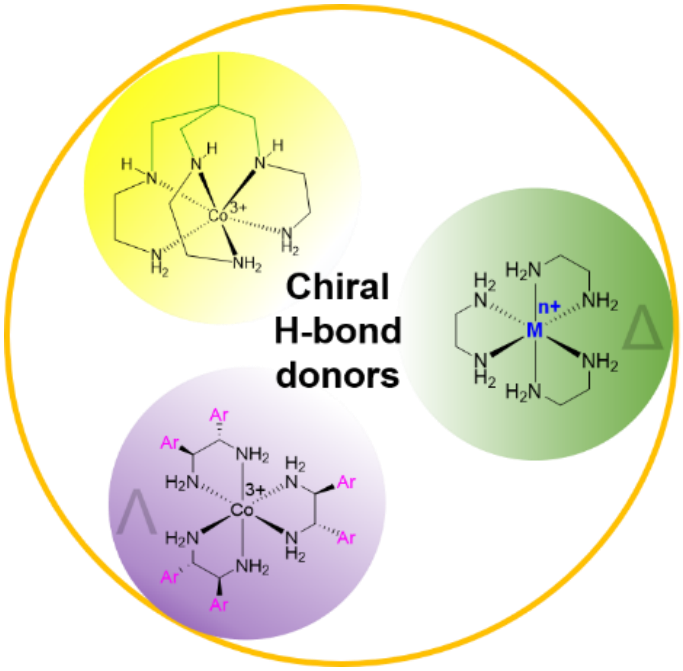

Figure 1.5. Representative image of the lipophilic Werner catalysts described in this dissertation.

This dissertation describes the effects that modifications to the metal, ligands, and anions of these lipophilic Werner catalysts have on their enantioselectivities (Figure 1.5, Table 1.1). The rationale for the development and results of these catalysts will be described herein.

Table 1.1. Published Gladysz group lipophilic Werner catalyst inventory.

#	Metal	Ligands[a]	Anions[a]	Config.	Coworker	Reference
1	Co	en	$3BAr_f^-$	Δ	Ganzmann	11a
2	Co	*rac*-chxn	$3BAr_f^-$	racemic	Ganzmann	11a
3	Co	(*R*,*R*)-chxn	$3BAr_f^-$	racemic	Ganzmann	11a
4	Co	(*S*,*S*)-dpen	$3BAr_f^-$	Λ	Ghosh/ Lewis	11b
5	Co	(*S*,*S*)-dpen	$2Cl^-BAr_f^-$	Λ	Ghosh/ Lewis	11b
6	Co	(*S*,*S*)-dpen	$2Cl^-BAr_f^-$	Δ	Ghosh/ Lewis	11b
7	Co	(*S*,*S*)-dpen	$3BAr_f^-$	Δ	Ghosh/ Lewis	11b
8	Co	(*S*,*S*)-dpen	$3BF_4^-$	Λ	Ghosh/ Lewis	11b
9	Co	(*S*,*S*)-dpen	$2BF_4^-BAr_f^-$	Λ	Ghosh/ Lewis	11b
10	Co	(*S*,*S*)-dpen	$2PF_6^-BAr_f^-$	Λ	Ghosh/ Lewis	11b
11	Co	(*S*,*S*)-dpen	$2Cl^-BAr_{f20}^-$	Λ	Ghosh/ Lewis	11d
12	Co	(*S*,*S*)-dpen	$2PhBF_3^-$ BAr_{f20}^-	Λ	Ghosh/ Lewis	11d
13	Co	(*S*,*S*)-dpen	$3BAr_{f20}^-$	Λ	Ghosh/ Lewis	11d
14	Co	(*S*,*S*)-dpen	$3PF_6^-$	Λ	Ghosh/ Lewis	11d
15	Co	(*S*,*S*)-dpen	$2Cl^-BAr_{f20}^-$	Δ	Ghosh/ Lewis	11d
16	Co	(*S*,*S*)-dpen	$2BF_4^-BAr_f^-$	Δ	Ghosh/ Lewis	11d
17	Co	(*S*,*S*)-dpen	$3PF_6^-$	Δ	Ghosh/ Lewis	11d
18	Co	(*S*,*S*)-dpen	$3BAr_f^-$	Δ	Ghosh/ Lewis	11d
19	Co	(*S*,*S*)-4-*n*-butyldpen	$2Cl^-BAr_f^-$	Λ	Ghosh	11d
20	Co	(*S*,*S*)-4-chlorodpen	$2Cl^-BAr_f^-$	Λ	Ghosh	11d

Table 1.1. Continued.

#	Metal	Ligands[a]	Anions[a]	Config.	Coworker	Reference
21	Co	(*S*,*S*)-4-chlorodpen	$2BF_4^-BAr_f^-$	Λ	Ghosh	11d
22	Co	(*S*,*S*)-4-(CF_3)dpen	$2Cl^-BAr_f^-$	Λ	Ghosh	11d
23	Co	(*S*,*S*)-4-(OMe)dpen	$2Cl^-BAr_f^-$	Λ	Lewis	11d
24	Co	(*S*,*S*)-4-(OMe)dpen	$2Cl^-BAr_f^-$	Δ	Lewis	11d
25	Co	(*S*,*S*)-αdnen	$2Cl^-BAr_f^-$	Λ	Lewis	11d
26	Co	(*S*,*S*)-αdnen	$2BF_4^-BAr_f^-$	Λ	Lewis	11d
27	Co	(*S*,*S*)-αdnen	$2Cl^-BAr_f^-$	Δ	Ghosh	11d
28	Co	(*S*,*S*)-βdnen	$2Cl^-BAr_f^-$	Λ	Ghosh	11d
29	Co	(*S*,*S*)-2-OBndpen	$2Cl^-BAr_f^-$	Λ	Ghosh	11d
30	Co	(*S*,*S*)-3,5-CF_3dpen	$Cl^-2BAr_f^-$	Λ	Ghosh	11d
31	Co	(*R*,*R*)-dpen	$2Cl^-BAr_f^-$	Λ	Lewis	12
32	Co	(*R*,*R*)-dpen	$2Cl^-BAr_f^-$	Δ	Lewis	12
33	Cr	en	$3BAr_f^-$	Δ	Maximuck	11i
34	Cr	en	$3BAr_f^-$	Λ	Maximuck	11i
35	Pt	en	$4BAr_f^-$	Δ	Alvi	11i
36	Pt	en	$4BAr_f^-$	Λ	Alvi	11i
37	Co	taetacn	$3BAr_f^-$	Λ	Maximuck	13
38	Co	sep	$3BAr_f^-$	Λ	Maximuck	11g
39	Co	sep	$3BAr_f^-$	Δ	Maximuck	11g
40	Co	sar	$3BAr_f^-$	Λ	Maximuck	11g
41	Co	sen	$3BAr_f^-$	Λ	Maximuck	11g
42	Co	$(NH_2)_2$sar	$3BAr_f^-$	Λ	Maximuck	11g
43	Co	(*S*,*S*)-furylen	$3BAr_f^-$	Λ	Maximuck	13
44	Co	(*S*,*S*)-furylen	$Cl^-2BAr_f^-$	Λ	Maximuck	13
45	Co	(*S*,*S*)-thiopen	$3BAr_f^-$	Λ	Maximuck	13
46	Co	(*S*,*S*)-thiopen	$3BF_4^-$	Λ	Maximuck	13

Table 1.1. Continued.

#	Metal	Ligands[a]	Anions[a]	Config.	Coworker	Reference
47	Co	(*S*,*S*)-thiopen	$3BAr_{f20}^-$	Λ	Maximuck	13
48	Co	(*S*,*S*)-dicyhexen	$3BAr_f^-$	Λ	Maximuck	13
49	Co	(*S*,*S*)-dicyhexen	$2Cl^-BAr_f^-$	Λ	Maximuck	13
50	Co	(*S*,*S*)-4-CNdpen	$2Cl^-BAr_f^-$	Δ	Maximuck/ Hooda	13
51	Co	(*S*,*S*)-dpen	(*R*,*R*)-$tart^{2-}$ BAr_f^-	Λ	Kabes/ Maximuck	11h
52	Co	(*S*,*S*)-dpen	(*S*,*S*)-$tart^{2-}$ BAr_f^-	Λ	Kabes/ Maximuck	11h
53	Co	(*S*,*S*)-dpen	Sb(*R*,*R*)-$tart^{2-}$ BAr_f^-	Λ	Kabes/ Maximuck	11h
54	Co	(*S*,*S*)-dpen	Sb(*S*,*S*)-$tart^{2-}$ BAr_f^-	Λ	Kabes/ Maximuck	11h
55	Co	(*S*,*S*)-dpen	2(*S*)-$(CF_3)_2$ BINOLPA$^-$ BAr_f^-	Λ	Kabes/ Maximuck	11h
56	Co	(*S*,*S*)-dpen	2(*S*)-$(i\text{Pr})_2$ BINOLPA$^-$ BAr_f^-	Λ	Kabes/ Maximuck	11h
57	Co	(*S*,*S*)-dpen	2(*S*)-$(SiPh_3)_2$ BINOLPA$^-$ BAr_f^-	Λ	Kabes/ Maximuck	11h
58	Co	(*S*,*S*)-dpen	2(*S*)-VAPOLPA$^-$ BAr_f^-	Λ	Kabes/ Maximuck	11h
59	Co	(*S*,*S*)-dpen	2(*R*)-VAPOLPA$^-$ BAr_f^-	Λ	Kabes/ Maximuck	11h
60	Co	(*S*,*S*)-dpen	2(*R*)-$(SiPh_3)_2$ BINOLPA$^-$ BAr_f^-	Λ	Kabes/ Maximuck	11h

Table 1.1. Continued.

#	Metal	Ligands[a]	Anions[a]	Config.	Coworker	Reference
61	Co	(*S*,*S*)-dpen	2(*R*)-$(CF_3)_2$ BINOLPA$^-$ BAr_f^-	Λ	Kabes/ Maximuck	11h
62	Co	(*S*,*S*)-dpen	2(*R*)-$(CF_3)_2$ BINOLPA$^-$ BAr_f^-	Λ	Kabes/ Maximuck	11h
63	Co	(*S*,*S*)-dpen	2(1*R*)-camphSO_3^- BAr_f^-	Λ	Lewis	11h
64	Co	(*S*,*S*)-dpen	2(1*S*)-camphSO_3^- BAr_f^-	Λ	Ghosh	11h
65	Co	(*S*,*S*)-dpen	2(1*R*)-camphSO_3^- BAr_f^-	Δ	Ghosh	11h
66	Co	(*S*,*S*)-dpen	2(1*S*)-camphSO_3^- BAr_f^-	Δ	Ghosh/ Kumar	11h
67	Co	(*S*,*S*)-dpen	2(*R*)-BINOLPA$^-$ BAr_f^-	Λ	Ghosh	11h
68	Co	(*S*,*S*)-dpen	2(*S*)-BINOLPA$^-$ BAr_f^-	Λ	Ghosh	11h
69	Co	(*S*,*S*)-dpen	3(*S*)-BINOLPA$^-$	Λ	Ghosh	11h
70	Co	(*S*,*S*)-dpen	3(*R*)-BINOLPA$^-$	Λ	Ghosh	11h
71	Co	(*S*,*S*)-dpen	2(*S*)-BINOLPA$^-$ BAr_f^-	Δ	Ghosh/ Kumar	11h
72	Co	(*S*,*S*)-dpen	3(1*R*)-camphSO_3^-	Λ	Kabes/ Maximuck	11h
73	Co	(*S*,*S*)-dpen	3(1*S*)-camphSO_3^-	Λ	Kabes/ Maximuck	11h
74	Co	(*S*,*S*)-dpen	$3I^-$	Λ	Luu	11f

Table 1.1. Continued.

#	Metal	Ligands[a]	Anions[a]	Config.	Coworker	Reference
75	Co	(*S*,*S*)-dpen	$2I^-BAr_f^-$	Λ	Luu	11f
76	Co	(*S*,*S*)-dpen	$2Br^-BAr_f^-$	Λ	Maximuck	11h
77	Co	$(en)_2(L^1)$	$3BAr_f^-$	Λ	Ghosh	11c
78	Co	$(en)_2(L^1)$	$3BAr_f^-$	Δ	Ghosh	11c
79	Co	$(en)_2(L^2)$	$3BAr_f^-$	Λ	Ghosh	11c
80	Co	$(en)_2(L^2)$	$3BAr_f^-$	Δ	Ghosh	11c
81	Co	$(en)_2(L^3)$	$3BAr_f^-$	Λ	Ghosh	11c
82	Co	$(en)_2(L^3)$	$3BAr_f^-$	Δ	Ghosh	11c
83	Co	$(en)_2(L^4)$	$3BAr_f^-$	Λ	Ghosh	11c
84	Co	$(en)_2(L^4)$	$3BAr_f^-$	Δ	Ghosh	11c
85	Co	(*S*,*S*)-dpen	$Cl^-BF_4^-BAr_f^-$	Λ	Maximuck	13
86	Co	(*S*,*S*)-dpen	$Cl^-PF_6^-BAr_f^-$	Λ	Maximuck	13
87	Co	(*S*,*S*)-dpen	$CO_2^{2-}BAr_f^-$	Λ	Maximuck	13
88	Rh	en	$3BAr_f^-$	Δ	Maximuck	11i
89	Rh	en	$3BAr_f^-$	Λ	Maximuck	11i
90	Ir	en	$3BAr_f^-$	Δ	Maximuck	11i
91	Ir	en	$3BAr_f^-$	Λ	Maximuck	11i
92	Co	(*S*,*S*)-dpen	$2DS^-BAr_f^-$	Λ	Maximuck/ Hooda	13
93	Co	(*S*,*S*)-dpen	$3DS^-$	Λ	Maximuck/ Hooda	13
94	Co	$(NMe_2)_2$sar	$3BAr_f^-$	Λ	Maximuck/ Hooda	11l
95	Co	(*S*,*S*)-dpen	$2PhCO_2^-BAr_f^-$	Λ	Maximuck/ Hooda	13
96	Co	(*S*,*S*)-dpen	$2CF_3CO_2^-$ BAr_f^-	Λ	Maximuck/ Hooda	13
97	Co	(*S*,*S*)-dpen	$SO_4^{2-}BAr_f^-$	Λ	Maximuck/ Hooda	13
98	Co	(*S*,*S*)-dpen	$3SbF_6^-$	Λ	Maximuck/ Hooda	13
99	Co	(*R*,*R*)-chxn	$3BAr_f^-$	Δ	Maximuck	13
100	Co	taetacn	$3BAr_f^-$	Δ	Maximuck	13

Table 1.1. Continued.

#	Metal	Ligands[a]	Anions[a]	Config.	Coworker	Reference
101	Co	CO_2Et-oxosen–H	$2BAr_f^-$	Λ	Maximuck	13
102	Co	en	$3BAr_f^-$	Λ	Ghosh	11c
103	Co	(*S*,*S*)-dpen	$2I^-BAr_{f20}^-$	Λ	Alimohammadi /Maximuck	11k
104	Co	(*S*,*S*)-dpen	$2OTf^-BAr_f^-$	Λ	Hasaninejad	11k

[a]See list of abbreviations.

1.3 Fluid catalytic cracking

Fluid catalytic cracking (FCC) is an important process along the way of the conversion of crude oil from inside the Earth into gasoline and diesel fuels. In fact, there are close to 430 FCC units worldwide today. They are utilized for the production of 31 million barrels of gasoline daily. The process is utilized to break down high molecular weight hydrocarbon chains into lighter hydrocarbons using high temperatures (525-575 °C) and a Ni/zeolite catalyst. The catalyst is primarily composed of zeolite, which has a high degree of surface area, but also features a matrix used for the cracking process (Figure 1.6). The binder acts similarly to glue to keep adhesion between the components, while the other parts of the system include fillers and additives, such as vanadium traps, ZSM-5, and CO promoters.[14]

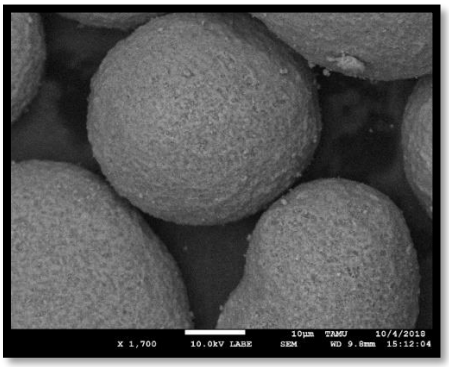

Figure 1.6. SEM image of FCC zeolite catalyst.

The FCC catalyst is used for cracking reactions and is relatively robust. However, the cracking process can lead to oxidation of contaminant nickel deposited on the catalyst from its Ni(0) state into nickel oxides. This chemical transformation immobilizes the nickel and minimizes the deleterious effects of dehydrogenation reactions that occur when Ni(0) is present. However, there have been earlier reports that the dehydrogenation activity may be able to be restored by forming nickel chloride species, which are mobile, allowing for better dispersion amongst the zeolite. Subsequent reduction using hydrogen gas essentially regenerates the harmful nickel species by reducing the Ni(II) to Ni(0), restoring activity to pre-oxidation levels.[15] Herein, we investigate the effect of gaseous HCl treatment on FCC catalysts and test the dispersion of nickel and catalytic efficiency via a variety of analytical methods.

1.4 References (All titles are given in the capitalization format of the original article)

(1) (a) Morral, F. R. Alfred Werner and Cobalt Complexes. In *Werner Centennial*; Kauffman, G. B., Ed.; American Chemical Society: Washington, D. C., 1967; Vol. 62; pp. 70-77. (b) Kauffman, G. B. Alfred Werner's Research on Optically Active Coordination Compounds. *Coord. Chem. Rev.* **1974**, *12*, 105-149.

(2) Werner, A. Beitrag zur Konstitution anorganischer Verbindungen. *Z. Anorg. Allg. Chem.* **1893**, *3*, 267-330.

(3) (a) Blomstrand, C. W. Ueber die Metallammoniake oder die Metallammine. *Ber. Dtsch. Chem. Ges.* **1871**, *4*, 40-52. (b) Jørgensen, S. M. Zur Konstitution der Kobalt-, Chrom- und Rhodiumbasen *Z. Anorg. Allg. Chem.* **1899**, *19*, 109-157.

(4) (a) Werner, A. Zur Kenntnis des asymmetrischen Kobaltatoms. I. *Ber. Dtsch. Chem. Ges.* **1911**, *44*, 1887-1898. King, V. L. is listed as an author for the experimental section. (b) Werner, A. Zur Kenntnis des asymmetrischen Kobaltatoms. II. *Ber. Dtsch. Chem. Ges.* **1911**, *44*, 2445-2455. (c) Werner, A. Zur Kenntnis des asymmetrischen Kobaltatoms. III. *Ber. Dtsch. Chem. Ges.* **1911**, *44*, 3272-3278. (d) Werner, A. Zur Kenntnis des asymmetrischen Kobaltatoms. IV. *Ber. Dtsch. Chem. Ges.* **1911**, *44*, 3279-3284. (e) Werner, A. Zur Kenntnis des asymmetrischen Kobaltatoms. V. *Ber. Dtsch. Chem. Ges.* **1912**, *45*, 121-130.

(5) (a) von Zelewsky, A. *Stereochemistry of Coordination Compounds*; John Wiley & Sons: Chichester, 1996. (b) *Chirality in Transition Metal Chemistry*; Amouri, H.; Gruselle, M.; John Wiley & Sons: Chichester, 2008. (c) Ehnbom, A.; Ghosh, S. K.; Lewis, K. G.; Gladysz, J. A. Octahedral Werner complexes with substituted ethylenediamine ligands: a stereochemical primer for a historic series of compounds now emerging as a modern family of catalysts. *Chem. Soc. Rev.* **2016**, *45*, 6799-6811.

(6) Werner, A; Kuh, H.; Wüst, P. Zur Kenntnis des asymmetrischen Kobaltatoms. X. *Ber. Dtsch. Chem. Ges.* **1914**, *47*, 1961-1979.

(7) Girolami, G. S.; Rauchfuss, T. B.; Angelici, R. J. *Synthesis and Technique in Inorganic Chemistry: A Laboratory Manual*, 3rd ed.; University Science Books: Sausalito, CA, 1999.

(8) (a) Taylor, M. S.; Jacobsen, E. N. Asymmetric Catalysis by Chiral Hydrogen-Bond Donors. *Angew. Chem., Int. Ed.* **2006***, 45,* 1520-1543; Asymmetrische Katalyse durch chirale Wasserstoffbrückendonoren. *Angew. Chem.* **2006**, *118*, 1550-1573. (b) Doyle, A. G.; Jacobsen, E. N. Small-Molecule H-Bond Donors in Asymmetric Catalysis. *Chem. Rev.* **2007**, *107*, 5713-5743. (c) Takemoto, Y. Recognition and activation by ureas and thioureas: stereoselective reactions using ureas and thioureas as hydrogen-bonding donors. *Org. Biomol. Chem.* **2005**, *3*, 4299-4306. (d) Xu, W.; Arieno, M.; Löw, H.; Huang, K.; Xie, X.; Cruchter, T.; Ma, Q.; Xi, J.; Huang, B.; Wiest, O.; Gong, L.; Meggers, E. Metal-Templated Design: Enantioselective Hydrogen-Bond-Driven Catalysis Requiring Only Parts-per-Million Catalyst Loading. *J. Am. Chem. Soc.* **2016,** *138*, 8774-8780. (e) Belokon, Y. N.; Maleev, V. I.; North, M.; Larionov, V. A.; Savel'yeva, T. F.; Nijland, A.; Nelyubina, Y. V. Chiral Octahedral Complexes of Co^{III} As a Family of Asymmetric Catalysts Operating under Phase Transfer Conditions. *ACS Catal.* **2013**, *3*, 1951-1955.

(9) (a) Taube, H. Rates and Mechanisms of Substitution in ang Complexes in Solution. *Chem. Rev*. 1952, 50, 69-126. (b) Data for $[Co(en)_3]^{3+}$: Friend, J. A.; Nunn, E. K. Substitution Reactions in the Trisethylenediaminecobalt(III) Ion. *J. Chem. Soc.* **1958**, 1567-1571. (c) For an entry level rationale, see *Selected Topics in Inorganic Chemistry*; Malik, W. U.; Tuli, G. D.; Madan, R. D.; S. Chand & Company: New Delhi, 2002. Chapter 14. (d) Sen, D.; Fernelius, W. C. Catalytic racemization of optically active complexes: Tris(ethylenediamine)cobalt(III), -platinum(IV), and -rhodium(III) halides. *J. Inorg. Nucl.*

Chem. **1959**, *10*, 269-274. (e) Douglas, B. D. Racemization of Tris-(ethylenediamine)-cobalt(III) Ion in the Presence of Decolorizing Carbon. *J. Am. Chem. Soc.* **1954**, *76*, 1020-1021. (f) Harnung, S. E.; Kallesøe, S.; Sargeson, A. M.; Schäffer, C. E. The Tris[(±)-1,2-propanediamine]cobalt(III) System. *Acta Chem. Scand.* **1974**, *A28*, 385-398; see especially the final paragraph of the experimental section.

(10) Ghosh, S. K.; Ehnbom, A.; Lewis, K. G.; Gladysz, J. A. Hydrogen bonding motifs in structurally characterized salts of the tris(ethylenediamine) cobalt trication, $[Co(en)_3]^{3+}$; An interpretive review, including implications for catalysis. *Coord. Chem. Rev.* **2017**, *350*, 30-48.

(11) (a) Ganzmann, C.; Gladysz, J. A. Phase Transfer of Enantiopure Werner Cations into Organic Solvents: An Overlooked Family of Chiral Hydrogen Bond Donors for Enantioselective Catalysis. *Chem. Eur. J.* **2008**, *14*, 5397-5400. (b) Lewis, K. G.; Ghosh, S., K.; Bhuvanesh, N.; Gladysz, J. A. Cobalt(III) Werner Complexes with 1,2-Diphenylethylenediamine Ligands: Readily Available, Inexpensive, and Modular Chiral Hydrogen Bond Donor Catalysts for Enantioselective Organic Synthesis. *ACS. Cent. Sci.* **2015**, *1*, 50-56. (c) Ghosh, S. K.; Ganzmann, C.; Bhuvanesh, N.; Gladysz, J. A. Werner Complexes with ω-Dimethylaminoalkyl Substituted Ethylenediamine Ligands: Bifunctional Hydrogen-Bond-Donor Catalysts for Highly Enantioselective Michael Additions. *Angew. Chem., Int. Ed.* **2016**, *55*, 4356-4360; Werner-Komplexe mit ω-Dimethylaminoalkyl-substitutierten Ethylendiaminliganden: bifunktionale H-Brückendonor-Katalysatoren für hoch enantioselektive Michael-Additionen. *Angew. Chem.* **2016**, *128*, 4429-4433. (d) Ghosh, S. K.; Lewis, K. G.; Kumar, A.; Gladysz, J. A. Syntheses of Families of Enantiopure and Diastereopure Cobalt Catalysts Derived from Trications of the Formula $[Co(NH_2CHArCHArNH_2)_3]^{3+}$. *Inorg. Chem.* **2017**, *56*, 2304-2320. (e) Joshi, H.; Ghosh, S. K.; Gladysz, J. A. Enantioselective Additions of Stabilized

Carbanions to Imines Generated from α-Amido Sulfones By Using Lipophilic Salts of Chiral Tris(1,2-diphenylethylenediamine) Cobalt(III) Trications as Hydrogen Bond Donor Catalysts. *Synthesis* **2017**, *49*, 3905-3915. (f) Luu, Q. H.; Lewis, K. G.; Banerjee, A.; Bhuvanesh, N.; Gladysz, J. A. The robust, readily available cobalt(III) trication $[Co(NH_2CHPhCHPhNH_2)_3]^{3+}$ is a progenitor of broadly applicable chirality and prochirality sensing agents. *Chem. Sci.* **2018**, *9*, 5087-5099. (g) Maximuck, W. J.; Gladysz, J. A. Lipophilic chiral cobalt(III) complexes of hexaamine ligands; Efficacies as enantioselective hydrogen bond donor catalysts. *Mol. Catal.* **2019**, *473*, 110360. (h) Kabes, C. Q.; Maximuck, W. J.; Ghosh, S. K.; Kumar, A.; Bhuvanesh, N.; Gladysz, J. A. Chiral Tricationic Tris(1,2-diphenylethylenediamine) Cobalt(III) Hydrogen Bond Donor Catalysts with Defined Carbon/Metal Configurations; Matched/Mismatched Effects upon Enantioselectivities with Enantiomeric Chiral Counter Anions. *ACS Catal.* **2020**, *10*, 3249-3263. (i) Maximuck, W. J.; Ganzmann, C.; Alvi, S.; Hooda, K. R.; Gladysz, J. A. Rendering classical hydrophilic enantiopure Werner salts $[M(en)_3]^{n+}$ nX^- lipophilic (M/*n* = Cr/3, Co/3, Rh/3, Ir/3, Pt/4); New chiral hydrogen bond donor catalysts and enantioselectivities as a function of metal and charge. *Dalton Trans.* **2020**, *49*, 3680-3691. (j) Luu, Q. H.; Gladysz, J. A. An Air- and Water- Stable Hydrogen-Bond-Donor Catalyst for the Enantioselective Generation of Quaternary Carbon Stereocenters by Additions of Substituted Cyanoacetate Esters to Acetylenic Esters. *Chem. Eur. J.* **2020**, *26*, 10230-10239. (k) Alimohammadi, M.; Hasaninejad, A.; Luu, Q. H.; Gladysz, J. A. Λ-$[Co((S,S)\text{-dpen})_3]^{3+}$ $2I^-B(C_6F_5)_4^-$: A Second Generation Air- and Water-Stable Chiral Solvating Agent for Chiral Sensing (dpen = $NH_2CHPhCHPhNH_2$). *J. Org. Chem.* **2020**, *85*, 11250-11257. (l) Wegener, A. R.; Kabes, C. Q.; Gladysz, J. A. Launching Werner Complexes into the Modern Era of Catalytic Enantioselective Organic Synthesis. *Acc. Chem. Res.* **2020**, *53*, 2299-2313.

(12) Lewis, K. G. The Development of Werner-Type Cobalt Complexes in Enantioselective Hydrogen Bond Mediated Catalysis, Texas A&M University, College Station, TX, USA, December 2013.

(13) Maximuck, W. J. Syntheses of Lipophilic Werner Complexes For Application as Chiral Hydrogen Bond Donors in Enantioselective Catalysis and Investigation of the Effect of Chloride on Fluid Catalytic Cracking Catalysts, Texas A&M University, College Station, TX, USA, May 2021.

(14) Vogt, E. T. C.; Weckhuysen, B. M. Fluid catalytic cracking: recent developments on the grand old lady of zeolite catalysts. *Chem. Soc. Rev.* **2015**, *44*, 7342-7370.

(15) (a) Chen, N. Y. Reactivation of deactivated zeolite catalysts. U.S. patent 3,684,738 (filed Mar. 16, 1970); *Chem. Abstr.* **1972**, *77*, 118822. (b) Ohtsuka, Y. Influence of hydrogen chloride treatment on the dispersion of nickel particles supported on carbon. *J. Mol. Catal.* **1989**, *54*, 225-235. (c) Foger, K.; Jaeger, H. Redispersion of Pt-Zeolite Catalysts with Chlorine. *Appl. Catal.* **1989**, *56*, 137-147.

2. RENDERING CLASSICAL HYDROPHILIC ENANTIOPURE WERNER SALTS $[M(en)_3]^{n+}$ nX^- LIPOPHILIC (M/*n* = Cr/3, Co/3, Rh/3, Ir/3, Pt/4); NEW CHIRAL HYDROGEN BOND DONOR CATALYSTS AND ENANTIOSELECTIVITIES AS A FUNCTION OF METAL AND CHARGE†

2.1 Introduction

The first chiral inorganic compounds to be synthesized in enantiopure form were reported by Alfred Werner in a series of five papers some 109 years ago.[1] These involved various adducts of cobalt(III) and at least two 1,2-ethylenediamine (en) ligands. For the trication $[Co(en)_3]^{3+}$, the diastereomeric tartrate salts were readily separable and easily metathesized to the enantiopure chloride salts $[Co(en)_3]^{3+}$ $3Cl^-$.[1e] This work has been extensively described in articles and textbooks dealing with the history of inorganic chemistry.[2] Somewhat less attention has been given to Werner's similar studies of enantiopure salts of the trications $[Cr(en)_3]^{3+}$,[3] $[Rh(en)_3]^{3+}$,[4] and $[Ir(en)_3]^{3+}$,[5] and tetracation $[Pt(en)_3]^{4+}$.[6] The metal configurations of such complexes are commonly denoted Λ and Δ, corresponding to left- and right-handed helices as represented in Figure 2.1 (top).[7]

†Reprinted with permission from "Rendering classical hydrophilic enantiopure Werner salts $[M(en)_3]^{n+}$ nX^- lipophilic (M/*n* = Cr/3, Co/3, Rh/3, Ir/3, Pt/4); new chiral hydrogen bond donor catalysts and enantioselectivities as a function of metal and charge" by Maximuck, W. J.; Ganzmann, C.; Alvi, S.; Hooda, K. R.; Gladysz, J. A., 2020. *Dalton Trans.*, 49, 3680-3691, Copyright 2020 by the Royal Society of Chemistry.

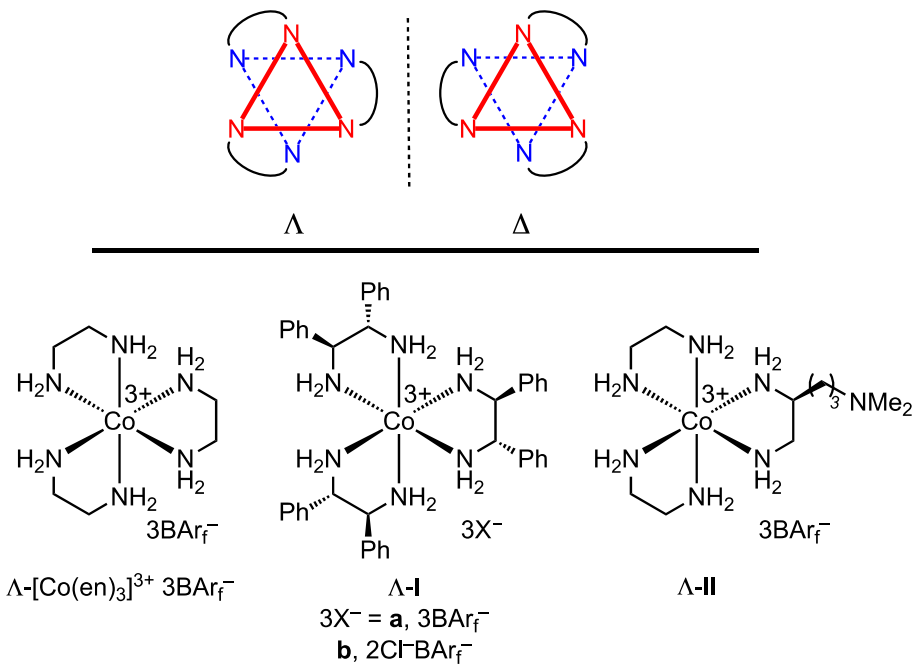

Figure 2.1. Configurations of the enantiomeric cations $[M(en)_3]^{n+}$ (top), and previously reported lipophilic enantiopure cobalt(III) tris(1,2-diamine) complexes (bottom).

Irrespective of the metal, for 100^+ years there has been a conspicuous absence of any applications of the preceding complexes in catalysis and in particular enantioselective catalysis. This is in large part due to the inertness of the cations towards substitution[8,9] – a consequence of the high field diamine ligands and the filled t_{2g} orbital sets associated with d^6 electronic configurations (Co(III), Rh(III), Ir(III), Pt(IV)) or the half-filled sets associated with d^3 electronic configurations (Cr(III)). Hence, conventional coordinative mechanisms for the activation of organic substrates by metal fragments are blocked. Also, none of these salts exhibit significant solubilities in organic solvents, which would normally necessitate heterogeneous reaction conditions.

In 2008, we communicated the synthesis of the enantiopure salt Δ-$[Co(en)_3]^{3+}$ $3BAr_f^-$ (Figure 2.1), which features three lipophilic "barf" counter anions ($B(3,5\text{-}C_6H_3(CF_3)_2)_4^-$).[10] Although this compound was soluble in numerous organic solvents, it also "carried" some water along, presumably via "second coordination sphere" NH/OH_2

hydrogen bonding, as often seen in the crystal structures of $[Co(en)_3]^{3+}$ salts.[11] In any case, Δ-$[Co(en)_3]^{3+}$ $3BAr_f^-$ was found to catalyze Michael additions of malonate esters to enones in organic solvents in the presence of Et_3N.[10] The mechanism was presumed to involve hydrogen bonding between the NH groups and organic substrates, an increasingly common mode of catalysis.[12] Turnover would be expected to be much slower in aqueous media due to the likelihood of water hydrogen bonding to the active site. Regardless, the product enantioselectivities never exceeded 33% ee.

In subsequent efforts, we developed second generation catalysts that gave highly enantioselective reactions.[13-16] These included the mixed salt Λ-$[Co((S,S)\text{-dpen})_3]^{3+}$ $2Cl^-$ BAr_f^- (Λ-**Ib**; Figure 2.1), in which dpen denotes 1,2-diphenyl-1,2-ethylenediamine,[13] and the bifunctional catalyst Λ-$[Co(en)_2(NH_2CH_2CH((CH_2)_3N(CH_3)_2)NH_2)]^{3+}$ $3BAr_f^-$ (Λ-**II**),[14] in which one of the ethylenediamine ligands carries a pendant tertiary amine. Although numerous structural variants in each series have been investigated, the possible influence of the metal has remained undefined.

One line of inquiry would involve a series of homologs of **I** or **II** with different metals, an undertaking that would require an extensive amount of synthesis and characterization. Another, simpler, approach would exploit the palette of enantiopure halide salts $[M(en)_3]^{n+}$ nX^- originally prepared by Werner. Given the moderate enantioselectivities obtained with the cobalt complex Δ-$[Co(en)_3]^{3+}$ $3BAr_f^-$, improvements would be conspicuous. In other words, the effect of the metal is easier to assay in series where the enantioselectivities are moderate as opposed to bunched in a narrow range of 90-95% ee.

Thus, as part of our ongoing efforts to optimize catalyst performance, define trends, and deepen mechanistic understanding, we synthesized the new lipophilic salts Λ- and Δ-$[M(en)_3]^{n+}$ $nBAr_f^-$ ($M^{n+} = Cr^{3+}$, Co^{3+}, Rh^{3+}, Ir^{3+}, Pt^{4+}) as described below. Their

efficacies as enantioselective catalysts for three types of addition reactions are then compared, together with those of $[Co(en)_3]^{3+}$ $3BAr_f^-$. Indeed, there can be a significant dependence upon the metal, and possible factors are analyzed. A portion of the data for $[Co(en)_3]^{3+}$ $3BAr_f^-$ was communicated earlier.[10] We note that several other research groups have also developed enantioselective catalysts that feature metal-containing NH hydrogen bond donors.[17-19] However, only in a few studies have catalysts with different metals been compared (always limited to two metals; *vide infra*).[17e,18a,b]

2.2 Results

2.2.1 Syntheses of catalysts

The enantiopure chloride or iodide salts Λ- and Δ-$[M(en)_3]^{n+}$ nX^- were prepared according to previously published procedures.[6,20-23] As shown in Figure 2.2, they were treated with an appropriate amount of Na^+ BAr_f^- under aqueous/organic biphase conditions. The CH_2Cl_2 layers were separated and the solvent allowed to evaporate. This gave the enantiopure "barf" salts Λ- and Δ-$[M(en)_3]^{n+}$ $nBAr_f^-\cdot zH_2O$ as canary yellow (Cr(III)), orange (Co(III)), ivory (Rh(III), Ir(III)), or pale yellow (Pt(IV)) hydrates in 87-97% yields as depicted in Figure 2.2. All were quite soluble in THF, CH_2Cl_2, acetone, CH_3CN, methanol, and ethanol.

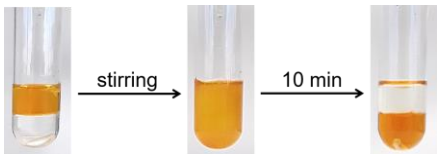

M^{n+}	*n*	*z*	yield (%)
Cr^{3+}	3	14	91
Co^{3+}	3	14	87
Rh^{3+}	3	11.5	97
Ir^{3+}	3	9	96-97
Pt^{4+}	4	17	95

Figure 2.2. Syntheses of the lipophilic tris(ethylenediamine) complexes Λ- and Δ-$[M(en)_3]^{n+}$ $nBAr_f^-$. The photograph in the left panel depicts the reactants for the Λ-$[Cr(en)_3]^{3+}$ $3BAr_f^-$ synthesis, that in the middle the stirred reaction, and that in the right the products.

The new complexes were characterized by microanalysis and IR and UV-visible spectroscopy. All except the paramagnetic adducts Λ- and Δ-$[Cr(en)_3]^{3+}$ $3BAr_f^-$ were further characterized by ^1H and $^{13}C\{^1H\}$ NMR. The water molecules were evidenced by broad OH ^1H NMR signals, and the stoichiometry suggested by integration was usually close to that calculated from the microanalytical data. When these differed, microanalytical values were given precedence since NMR integrations can be enhanced by protic impurities. The water molecules are included in all stoichiometry and yield calculations, as given in the experimental section, but for simplicity are often not represented in the graphics or main text. Attempts were made to dry CD_2Cl_2 or THF solutions of Λ- and Δ-$[Co(en)_3]^{3+}$ $3BAr_f^-$ with molecular sieves or P_2O_5, but this gave partial or complete decomposition, respectively, as independently verified on two continents.[24,25]

The ^1H NMR spectra showed separate signals for the diastereotopic N***HH'*** protons. These were further downfield for the tetracationic platinum complex (8.05, 8.48 ppm) than the tricationic cobalt (5.29, 5.69 ppm), rhodium (5.52, 6.00 ppm), and iridium (5.92, 6.42 ppm) complexes. The ***C***H_2NHH' ^{13}C NMR signal of the platinum complex (50.7 ppm) was also downfield of the others (cobalt (46.3 ppm), rhodium (47.0 ppm), iridium (48.5 ppm)).

2.2.2 Enantioselective catalysis

The enantiopure complexes $[M(en)_3]^{n+}$ $nBAr_f^-$ in Scheme 1 were screened as catalysts for the addition of dimethyl malonate to *trans*-β-nitrostyrene in the presence of *N*-methylmorpholine (NMM; 1.1:1.0:1.0 mol ratio). As summarized in Figure 2.3, all of the salts gave the addition product **1** in high yields (95-87%) and with appreciable albeit moderate enantioselectivities (23-39% ee; average 33%). The identity of the metal clearly affects the ee value. However, the enantioselectivities are much lower than those obtained

with appropriate salts of the tris(dpen) complex **I** or the bifunctional catalyst **II** (Figure 2.1; >90% ee).[13a,14]

The Cr(III) and Rh(III) complexes (entries 1-2, 5-6) boasted the highest enantioselectivities under the conditions investigated (37-39% ee). The Ir(III) complexes slightly outperformed the Co(III) complexes (entries 7-8 vs. 3-4; 34% vs. 31% ee). The Pt(IV) complexes furnished the lowest yields and enantioselectivities (entries 9-10; 23% ee). These trends are further analyzed in the discussion section.

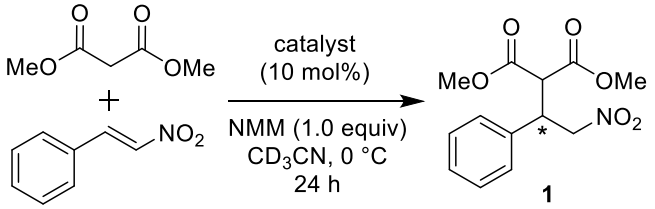

entry	catalyst	yield (%)[a]	ee (%) (config)
1	Λ-$[Cr(en)_3]^{3+}$ $3BAr_f^-$	95	37 (*R*)
2[b]	Δ-$[Cr(en)_3]^{3+}$ $3BAr_f^-$	95	37 (*S*)
3	Λ-$[Co(en)_3]^{3+}$ $3BAr_f^-$	95	31 (*R*)
4	Δ-$[Co(en)_3]^{3+}$ $3BAr_f^-$	95	31 (*S*)
5	Λ-$[Rh(en)_3]^{3+}$ $3BAr_f^-$	95	39 (*R*)
6	Δ-$[Rh(en)_3]^{3+}$ $3BAr_f^-$	95	39 (*S*)
7	Λ-$[Ir(en)_3]^{3+}$ $3BAr_f^-$	92	34 (*R*)
8	Δ-$[Ir(en)_3]^{3+}$ $3BAr_f^-$	92	34 (*S*)
9	Λ-$[Pt(en)_3]^{4+}$ $4BAr_f^-$	87	23 (*R*)
10	Δ-$[Pt(en)_3]^{4+}$ $4BAr_f^-$	87	23 (*S*)

[a]Yields were determined by ^{1}H NMR relative to the internal standard Ph_2SiMe_2 (experimental section). [b]Data under identical conditions in CD_2Cl_2 or acetone-d_6: yield, >99%, 96%; ee, 10%, 24%.

Figure 2.3. Additions of dimethyl malonate to *trans*-β-nitrostyrene catalyzed by lipophilic tris(ethylenediamine) complexes.

Various control experiments were conducted. First, when a reaction was carried out as in Figure 2.3 but using the hydrophilic iodide complex Λ-$[Co(en)_3]^{3+}$ $3I^-$ as the catalyst (a monohydrate), Et_3N as the base, and a biphasic water/CH_2Cl_2 mixture, the product **1** was obtained in only 19% yield and <1% ee. When a heterogeneous reaction

was carried out with the same catalyst in CD_3CN with NMM as the base, **1** was obtained in 20% yield and 6% ee (*R* dominant). Finally, the new Brønsted acidic salt $NMMH^+$ BAr_f^- was prepared from $NMMH^+$ Cl^- and Na^+ BAr_f^- as described in the experimental section. When this was used in place of the catalyst in Figure 2.3, no reaction occurred.

The same complexes were next screened as catalysts for the addition of the β-ketoester methyl 2-oxocyclopentanecarboxylate to di-*tert*-butylazodicarboxylate in the presence of NMM (1.0:1.0:1.0 mol ratio). As shown in Figure 2.4, the product (**2**) was again obtained in high yields (99-85%) and appreciable enantioselectivities (58-41% ee). The average ee value was higher than that in Figure 2.3 (52% vs. 33%), but lower than those found for appropriate tris(dpen) salts **I** (>90% ee).[15a]

The Cr(III) and Rh(III) complexes (entries 1-2, 5-6) again gave the highest enantioselectivities (58-57% ee), followed by the Ir(III) and Co(III) complexes (53-52% ee). In accord with Figure 2.3, the Pt(IV) complexes again furnished the lowest yields and enantioselectivities (entries 9-10; 41% ee).

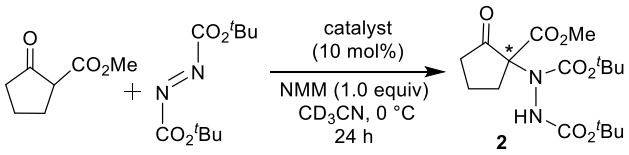

entry	catalyst	yield (%)[a]	ee (%) (config)
1	Λ-$[Cr(en)_3]^{3+}$ $3BAr_f^-$	99	58 (*S*)
2[b]	Δ-$[Cr(en)_3]^{3+}$ $3BAr_f^-$	99	58 (*R*)
3	Λ-$[Co(en)_3]^{3+}$ $3BAr_f^-$	94	52 (*S*)
4	Δ-$[Co(en)_3]^{3+}$ $3BAr_f^-$	94	52 (*R*)
5	Λ-$[Rh(en)_3]^{3+}$ $3BAr_f^-$	99	57 (*S*)
6	Δ-$[Rh(en)_3]^{3+}$ $3BAr_f^-$	99	57 (*R*)
7	Λ-$[Ir(en)_3]^{3+}$ $3BAr_f^-$	97	53 (*S*)
8	Δ-$[Ir(en)_3]^{3+}$ $3BAr_f^-$	97	53 (*R*)
9	Λ-$[Pt(en)_3]^{4+}$ $4BAr_f^-$	85	41 (*S*)
10	Δ-$[Pt(en)_3]^{4+}$ $4BAr_f^-$	85	41 (*R*)

[a]Yields were determined by ^1H NMR relative to the internal standard Ph_2SiMe_2 (experimental section). [b]Data under identical conditions in CD_2Cl_2 or acetone-d_6: yield, >99%, >99%; ee, 56%, 52%.

Figure 2.4. Additions of methyl 2-oxocyclopentanecarboxylate to di-*tert*-butylazodicarboxylate catalyzed by lipophilic tris(ethylenediamine) complexes.

Next, we returned to additions of malonate esters to cyclic enones, a reaction type briefly examined in our initial communication.[10] As shown in Figure 2.5, all of the complexes catalyzed the addition of diisopropyl malonate to 2-cyclopenten-1-one in the presence of Et_3N (1.0:1.0:1.0 mol ratio). However, the product (**3**) was obtained in much lower enantioselectivities than those in Figures 2.3 and 2.4, with an average ee value of 17% (range: 10-21%). In a second effort, the analogous reaction of dimethyl malonate was carefully optimized, using the cobalt catalyst Δ-$[Co(en)_3]^{3+}$ $3BAr_f^-$. As shown in entry 5, a somewhat higher ee value could be obtained (33%). The corresponding reaction of dimethyl malonate and 2-cyclohexen-1-one was briefly screened, but the yields and ee values of the addition product were lower.[24]

In any event, the Co(III) and Rh(III) catalysts give the highest enantioselectivities for the diisopropyl malonate additions in Figure 2.5 (21% ee) and the Pt(IV) catalyst the lowest (10% ee). It has not yet proved possible to effect such additions using salts of **I** or **II** with high enantioselectivities. A precipitate forms during all of the reactions in Figure 2.5. This is believed to be some less soluble salt of the catalyst, as with the reactions involving cobalt, treatment with Na^+ BAr_f^- regenerates $[Co(en)_3]^{3+}$ $3BAr_f^-$.[24] The reactions in Figures 2.3-2.5 were evaluated in other solvents, but the ee values were lower, per the data in the footnotes.

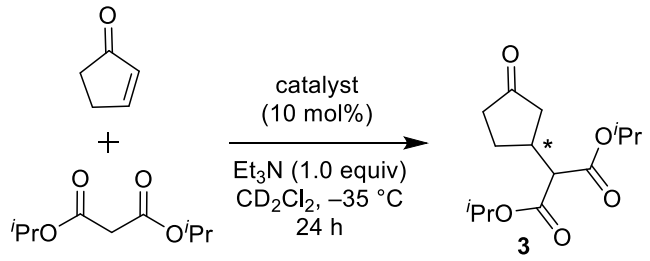

entry	catalyst	yield (%)[a]	ee (%) (config)
1	Λ-$[Cr(en)_3]^{3+}$ $3BAr_f^-$	98	16 (*S*)
2[b]	Δ-$[Cr(en)_3]^{3+}$ $3BAr_f^-$	98	16 (*R*)
3	Λ-$[Co(en)_3]^{3+}$ $3BAr_f^-$	99	21 (*S*)
4	Δ-$[Co(en)_3]^{3+}$ $3BAr_f^-$	99	21 (*R*)
5[c]	Δ-$[Co(en)_3]^{3+}$ $3BAr_f^-$	78[d]	33 (*R*)
6	Λ-$[Rh(en)_3]^{3+}$ $3BAr_f^-$	96	21 (*S*)
7	Δ-$[Rh(en)_3]^{3+}$ $3BAr_f^-$	96	21 (*R*)
8	Λ-$[Ir(en)_3]^{3+}$ $3BAr_f^-$	94	16 (*S*)
9	Δ-$[Ir(en)_3]^{3+}$ $3BAr_f^-$	94	16 (*R*)
10	Λ-$[Pt(en)_3]^{4+}$ $4BAr_f^-$	67	10 (*S*)
11	Δ-$[Pt(en)_3]^{4+}$ $4BAr_f^-$	67	10 (*R*)

[a]Yields were determined by ^{1}H NMR relative to the internal standard Ph_2SiMe_2 (experimental section). [b]Data under identical conditions in acetone-d_6 or CD_3CN: yield, 35%, 15%; ee, 15%, 14%. [c]Dimethyl malonate was used in place of the diisopropyl ester; –40 °C, 9 mol% catalyst, 8 h. [d]Isolated yield.

Figure 2.5. Additions of diisopropyl malonate to 2-cyclopenten-1-one catalyzed by lipophilic tris(ethylenediamine) complexes.

2.2.3 Stability data

During initial synthetic efforts, canary yellow CH_2Cl_2 solutions of the new salt $[Cr(en)_3]^{3+}$ $3BAr_f^-$ turned violet upon concentration. This could be avoided by allowing the CH_2Cl_2 to evaporate at 4 °C in the dark. Samples were subsequently stored at –35 °C in the dark. The decomposition could be followed visually or by UV-visible spectroscopy under homogeneous conditions in EtOH as shown in Figure 2.6. The initial spectrum of $[Cr(en)_3]^{3+}$ $3BAr_f^-$ consists of two peaks at 351 and 459 nm, which correspond to the $^4T_{1g} \leftarrow {}^4A_{2g}$ and $^4T_{2g} \leftarrow {}^4A_{2g}$ transitions respectively for the hydrophilic analog.[26] Aqueous solutions of racemic $[Cr(en)_3]^{3+}$ $3Cl^-$ have been reported to decompose to the violet bis(aquo) complex *cis*-$[Cr(en)_2(OH_2)_2]^{3+}$ $3Cl^-$ in the dark, and crystalline hydrates

behave analogously when exposed to sunlight.[26b] None of the other new salts in Figure 2.2 displayed the slightest lability at room temperature.

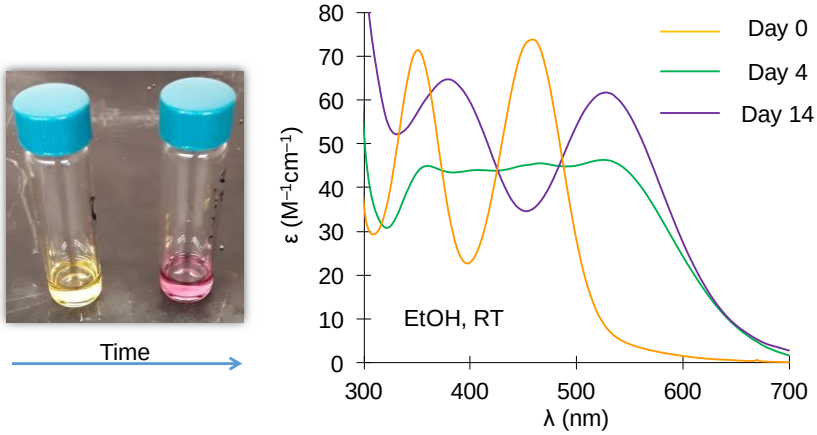

Figure 2.6. Decomposition of $[Cr(en)_3]^{3+}$ $3BAr_f^-$ in EtOH as assayed visually (left, RT) or by UV-visible spectroscopy (right, sample at RT but spectra at 12.0 °C).

The stabilities of the new lipophilic catalysts were also probed with respect to the degree of hydration (*z*, Figure 2.2), as this represents another factor that could influence rates and enantioselectivities. In addition, there are compounds that decompose when a certain threshold of accompanying water molecules are removed.[27] Furthermore, although the BAr_f^- anion is a feeble hydrogen bond acceptor,[16c] the lithium, sodium, and potassium salts are always isolated as hydrates (0.5 to 3.0 water molecules);[28] anhydrous alkali metal salts are conspicuously lacking. Thus, thermogravimetric analyses (TGA) were carried out for all of the new salts in Figure 2.2, and the results are summarized in Table 2.1. The traces are reproduced in the Appendix.

The onset of mass loss ranged from 71 °C for $[Pt(en)_3]^{4+}$ $4BAr_f^-\cdot 17H_2O$ to 151 °C for $[Rh(en)_3]^{3+}$ $3BAr_f^-\cdot 11.5H_2O$. Various mass loss regimes are noted in column 2 of Table 2.1. The temperature at which the mass loss is equal to the mass of all water molecules is given in column 3 (although the possibility of some mass loss originating from the en ligands is not excluded).

Next, open capillaries containing the lipophilic catalysts were heated. Column 4 of Table 2.1 shows that most of them decolorized before they liquefied at 118-190 °C. In a second set of experiments, the capillaries were heated to the temperature that the TGA data suggested should give complete dehydration. Only for Λ-$[Cr(en)_3]^{3+}$ $3BAr_f^-\cdot 14H_2O$ was this significantly above the decolorization temperature, and the violet sample was not further analyzed. The others were cooled and dissolved in acetone-d_6. The ^{1}H NMR spectra showed no significant decomposition of the cations, and the hydration levels were very close to those of the original samples. Thus, the dehydrated salts appear to be especially deliquescent.

Finally, the new complexes were similarly probed by differential scanning calorimetry (DSC). In all cases except for Λ-$[Ir(en)_3]^{3+}$ $3BAr_f^-\cdot 9H_2O$, there was at least one endotherm during the dehydration regime, as summarized in column 5 of Table 2.1. In all cases, there was an additional endotherm close to the liquefaction regime (somewhat separated for Λ-$[Pt(en)_3]^{4+}$ $4BAr_f^-\cdot 17H_2O$).

2.3 Discussion

The data in Figures 2.3-2.5 show that for three different types of addition reactions, the highest enantioselectivities are generally obtained with the Cr(III) and Rh(III) catalysts, and the lowest with Pt(IV). Both steric and electronic factors were considered in attempting to interpret these trends. For example, crystal structures of salts of each $[M(en)_3]^{n+}$ species have been determined, and these give average metal-nitrogen bond lengths ranging from 1.965 Å to 2.081 Å (Co, 1.965 Å;[29a] Cr, 2.076 Å;[29b] Rh, 2.071 Å;[29b] Ir, 2.080 Å;[30] Pt, 2.081 Å[31]). Alternatively, the ionic radii, which range from 0.545 Å to 0.680 Å, can be compared (Co(III), 0.545 Å; Cr(III), 0.615 Å; Rh(III), 0.665 Å; Ir(III), 0.680 Å; Pt(IV), 0.625 Å).[32] The most enantioselective catalysts (Cr(III), Rh(III)) seem to occupy a steric "middle ground".

Table 2.1. Thermal stability data (°C).

complex	TGA, T_i/T_f[a]	~temp., complete hydrate loss[b]	capillary thermolysis[c] (decolorization/ liquefaction)	DSC, $T_i/T_e/T_p/T_c/T_f$[a,d]
Λ-$[Cr(en)_3]^{3+}$ $3BAr_f^-$ $\cdot 14H_2O$	73.5/122.7[e] (7.7% or 13.1 H_2O) 122.7/220.9 (33.2% cumulative) 220.9/333.4 (83.5% cumulative) 333.4/494.3 (90.4% cumulative)	141.8 (8.2% or 14H_2O)	105[f]/118-121[g]	84.3/87.1/99.0/113.1/114.3 115.8/118.5/124.3/128.7/129.1
Λ-$[Co(en)_3]^{3+}$ $3BAr_f^-$ $\cdot 14H_2O$	124.8/128.1[e] (3.4% or 5.8 H_2O) 128.1/164.7 (17.7% cumulative) 164.7/211.3 (39.7% cumulative) 211.3/317.2 (86.9% cumulative) 317.2/494.8 (91.9% cumulative)	149.8 (8.2% or 14H_2O)	148[h]/157-159[g]	68.9/68.9/79.2/95.1/95.1 117.4/121.3/131.7/142.5/147.0 149.3/149.3/157.9/161.0/161.0
Λ-$[Rh(en)_3]^{3+}$ $3BAr_f^-$ $\cdot 11.5H_2O$	150.8/176.6[e] (6.7% or 11.5 H_2O) 176.6/207.3 (28.8% cumulative) 207.3/243.1 (59.2% cumulative) 243.1/276.5 (72.6% cumulative) 276.5/288.9 (79.7% cumulative) 288.9/494.9 (92.0% cumulative)	176.6 (6.7% or 11.5H_2O)	182[i]/184-186[g]	144.2/150.8/162.8/170.9/170.9 171.2/171.9/174.0/177.1/179.3
Λ-$[Ir(en)_3]^{3+}$ $3BAr_f^-$ $\cdot 9H_2O$	76.7/173.4[e] (5.7% cumulative) 173.4/495.0 (81.0% cumulative)	143.4 (5.2% or 9H_2O)	184[i]/188-190[g]	156.0/160.3/174.9/178.9/179.3 181.6/182.5/186.4/192.8/192.8
Λ-$[Pt(en)_3]^{4+}$ $4BAr_f^-$ $\cdot 17H_2O$	71.2/77.8[e] (4.7% or 10.8 H_2O) 77.8/120.4 (17.0% cumulative) 120.4/163.7 (22.7% cumulative) 163.7/261.8 (81.2% cumulative) 261.8/494.6 (88.8% cumulative)	90.4 (7.4% or 17H_2O)	92[i]/147-152[g]	67.1/76.0/92.0/108.5/115.2 130.8/133.1/137.8/140.7/141.5

[a]Data were treated as recommended by Cammenga, H. K.; Epple, M. *Angew. Chem., Int. Ed. Engl.* **1995**, *34*, 1171-1187; *Angew. Chem.* **1995**, *107*, 1284-1301. [b]Temperature at which the mass corresponding to the water molecules has been lost (this does not require that only water has been volatilized). In the case of Λ-$[Cr(en)_3]^{3+}$ $3BAr_f^-$, thermal decomposition occurs below this temperature. [c]Open capillary; conventional melting point apparatus. [d]All DSC features are endotherms. [e]This mass loss includes a small contribution from a featureless temperature regime starting at *ca.* 30°C. [f]Turns violet. [g]Liquefaction. [h]Darkens. [i]Turns yellow.

The idealized representations of the cations in Figure 2.1 (top) have D_3 symmetry, with a principal C_3 axis and three C_2 axes that lie in a perpendicular plane. This results in two "C_3 faces" and three "C_2 faces" as illustrated by the space filling depictions **III** and **IV** in Figure 2.7. These chiral binding sites feature three NH donor groups and two NH donor groups, respectively. Shorter metal-nitrogen distances or ionic radii lead to "tighter" chiral pockets, and longer distances or radii afford geometrically expanded or more diffuse chiral pockets. One interpretation is that a happy medium is required for optimum enantioselectivity. There is clearly the opportunity for additional insight via computational chemistry, but the large number of NH bonds and possible substrate binding modes renders this a complex and potentially long term undertaking.[16c] Another takeaway from this study is that the enantioselectivities between the catalysts are not drastically different for all of the reactions tested. This supports the hypothesis that the catalytic reactions are proceeding through a secondary coordination sphere mechanism and the metal is not directly involved, but can indirectly influence enantioselectivity.

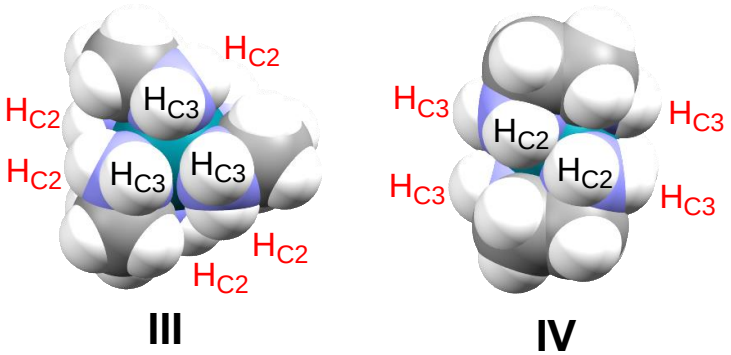

Figure 2.7. Space filling representations of the C_3 (**III**) and C_2 (**IV**) faces of Λ-$[M(en)_3]^{3+}$, as taken from the crystal structure of Λ-$[Rh(en)_3]^{3+}$ $3Cl^-\cdot 3.37H_2O$.[29b]

In the case of the Pt(IV) catalyst, the additional charge introduces the possibility of a significant electronic effect. Indeed, the NH bonds of $[Pt(en)_3]^{4+}$ $4Cl^-$ are much more acidic (pK_a^1/K_a^1 = 5.5/3.2 × 10^{-6})[33,34] than those of $[Co(en)_3]^{3+}$ $3Cl^-$ (pK_a^1/K_a^1 =

14.9/1.3 × 10^{-15}).[35] We initially considered this advantageous, as more acidic NH bonds are stronger hydrogen bond donors, which could potentially draw substrates or transition states deeper into the chiral C_3 and C_2 sites. However, the acidity of the $[Pt(en)_3]^{4+}$ tetracation is so great that it would be quantitatively deprotonated by NMM ($pK_a(BH^+)/K_a(BH^+)$ = 7.4/4.0 × 10^{-8})[36] or Et_3N ($pK_a(BH^+)/K_a(BH^+)$ = 10.7/2.0 × 10^{-11}).[36] The K_{eq} values in aqueous solution would be 80 and 1.6 × 10^5, respectively. This is likely the basis for the slower rates and reduced yields with the Pt(IV) catalyst.

The higher acidities associated with salts of $[Pt(en)_3]^{4+}$ may also factor into the greater degrees of hydration. Rates of hydrogen/deuterium exchange suggest that the thermodynamic acidities follow the order $[Pt(en)_3]^{4+}$ > $[Cr(en)_3]^{3+}$ > $[Co(en)_3]^{3+}$ > $[Rh(en)_3]^{3+}$ > $[Ir(en)_3]^{3+}$,[33] parallel to the hydration levels in Figure 2.2. Also, the lower thermal stability of $[Pt(en)_3]^{4+}$ $4BAr_f^-\cdot 17H_2O$ may reflect the abundance of water molecules, which may be difficult to optimally accommodate within a second (outer) coordination sphere. In this context, TGA data for the anhydrous chloride salt $[Pt(en)_3]^{4+}$ $4Cl^-$ shows a much higher onset of mass loss (220 °C vs. 71 °C).[37]

Interestingly, for the hydrophilic chloride and iodide salts of $[M(en)_3]^{n+}$, hydration levels are lower (4-0 molecules, as summarized in Table A-1), perhaps because the good hydrogen bond accepting halide ions[38] occupy some of the binding sites. Takamizawa has carried out in depth TGA and calorimetric studies of the chloride salts $[M(en)_3]^{3+}$ $3Cl^-\cdot zH_2O$ (M/z = Cr/3.72, Co/4.0, Rh/3.37).[29] He finds that single crystals readily dehydrate at 60 °C under vacuum with preservation of the crystal lattice (albeit with *ca.* 10% shrinkage of the dimensions). This stands in sharp contrast to the 71-151 °C temperatures required to initiate dehydration for the new complexes in Figure 2.2.

Meggers has synthesized the chiral, enantiopure rhodium(III) and iridium(III) containing NH hydrogen bond donor catalysts **Va** and **Vb** in Figure 2.8. These promote

highly enantioselective conjugate reductions of alkenes, but with essentially identical ee values.[17e] In these systems, the locus of reaction is likely more distant from the metal than in Figures 2.3-2.5, reducing the influence on the $\Delta\Delta G^{\ddagger}$ for the reaction coordinates leading to each enantiomer. Belokon has reported the use of the chromium(III) and cobalt(III) catalysts **VIa** and **VIb** (Figure 2.8) for enantioselective alkylations under phase transfer conditions.[18a,b] These feature metal bound NH donor groups like our lipophilic catalysts in Figure 2.2. Now the ee values show a greater dependence upon the metal (Cr/Co 70%/77% ee or 78/81% ee).

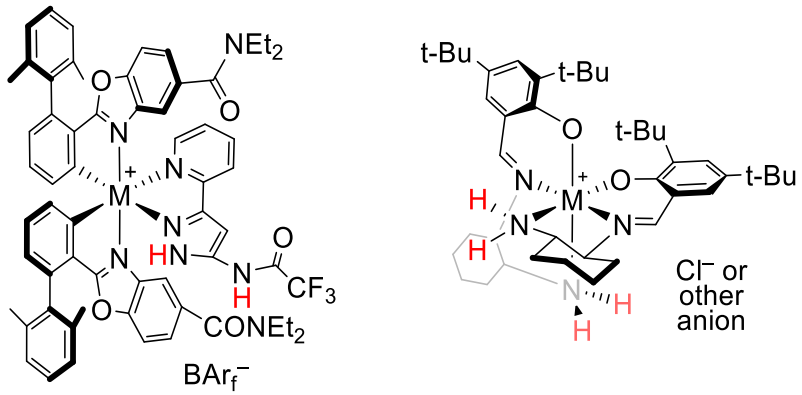

V
M = **a**, Rh
b, Ir

VI
M = **a**, Cr
b, Co

Figure 2.8. Other chiral, enantiopure metal and NH containing hydrogen bond donor catalysts where the metal has been varied.[17e,18a]

In summary, there are two principle conclusions from this study. The first is that of the new lipophilic enantiopure catalysts $[M(en)_3]^{n+}$ $n\mathrm{BAr_f^-}\cdot z\mathrm{H_2O}$ investigated, the chromium(III) and rhodium(III) complexes generally give the highest ee values, at least for the two reactions with higher enantioselectivities (Figures 2.3 and 2.4). In all cases, the platinum(IV) complex gives the lowest. The second is that the enantioselectivities remain considerably lower than those that can be realized with the second generation

catalysts **I** and **II** in Figure 2.1 (bottom), one of which is bifunctional, incorporating a tertiary amine base. This is unfortunate, given the "entry level" nature of the catalysts in Scheme 1, some of which can be prepared from scratch in enantiopure form in an afternoon, as described in undergraduate laboratory textbooks.[39] In this context, one productive strategy for future research may involve salts with chiral lipophilic anions,[15d] which are becoming increasingly available and are seeing broad application in enantioselective catalysis.[40]

2.4 Experimental section

General data. All reactions were conducted under aerobic conditions. Solvents and the educts and bases in Figures 2.3-2.5 were used as received from common commercial sources (generally given in previous reports).[10,13a,15a] The Na^+ BAr_f^- was purchased from Ark Pharm.[41]

NMR spectra were recorded on a Bruker 400 MHz spectrometer at ambient probe temperatures and referenced (δ/ppm) to solvent signals (^{1}H: residual $CHDCl_2$/5.32, acetone-d_5/2.05, or CHD_2CN/1.94; ^{13}C: acetone-d_6/29.8). IR spectra were recorded on a Shimadzu IRAffinity-1 spectrometer (Pike MIRacle ATR system, diamond/ZnSe crystal). UV-vis spectra were obtained with a Shimadzu UV-1800 spectrometer with a thermostat cell. HPLC analyses were carried out with a Shimadzu instrument package (pump/autosampler/detector LC-20AD/SIL-20A/SPD-M20A). Capillary thermolyses were monitored with an OptiMelt MPA100 instrument. TGA and DSC analyses were carried out on TA Instruments Q50 and TA Instruments Q20 systems, respectively, and data were treated according to literature conventions.[42] Microanalyses were conducted by Atlantic Microlab.

Λ-$[Cr(en)_3]^{3+}$ $3BAr_f^-$. A beaker was charged with Λ-$[Cr(en)_3]^{3+}$ $3Cl^-\cdot 1.6H_2O$ (0.0228 g, 0.0620 mmol),[20] H_2O (15 mL), CH_2Cl_2 (15 mL), and Na^+ BAr_f^- (0.1650 g,

0.1861 mmol; 3:1 mol ratio).[41] The biphasic mixture was vigorously stirred (10 min) and allowed to stand. The yellow lower phase was separated and allowed to slowly evaporate at 4 °C in the dark for several days. This gave Λ-$[Cr(en)_3]^{3+}$ $3BAr_f^-\cdot 14H_2O$ as a canary yellow solid (0.1734 g, 0.05642 mmol, 91%), which was stored at –35 °C in the dark to slow decomposition. Anal. Calcd. for $C_{102}H_{60}B_3CrF_{72}N_6\cdot 14H_2O$ (3074.17): C 39.85, H 2.89, N 2.73; found C 40.03, H 2.88, N 2.71. Capillary thermolysis, TGA, and DSC data: Table 2.1.

IR (powder film, cm^{-1}): 3254 (m, NH_2), 1611 (m, NH_2), 1356 (s, CF-aryl), 1273 (vs, CF_3), 1117 (vs, CNH_2), 889 (s, CNH_2), 837 (m, 1,3,5-trisubsituted benzene). UV-vis (nm, EtOH, 12.0 °C (ε, $M^{-1}cm^{-1}$)): 269 (12800), 278 (10300), 351 (71.5), 459 (74.5).

Δ-$[Cr(en)_3]^{3+}$ $3BAr_f^-$. Δ-$[Cr(en)_3]^{3+}$ $3Cl^-\cdot 1.6H_2O$ (0.0228 g, 0.0620 mmol),[20] H_2O (15 mL), CH_2Cl_2 (15 mL), and Na^+ BAr_f^- (0.1650 g, 0.1861 mmol) were combined in a procedure analogous to that for Λ-$[Cr(en)_3]^{3+}$ $3BAr_f^-$. An identical workup gave Δ-$[Cr(en)_3]^{3+}$ $3BAr_f^-\cdot 14H_2O$ as a canary yellow solid (0.1742 g, 0.05667 mmol, 91%) that was stored at –35 °C to slow decomposition. Anal. Calcd. for $C_{102}H_{60}B_3CrF_{72}N_6\cdot 14H_2O$ (3074.17): C 39.85, H 2.89, N 2.73; found C 40.04, H 2.71, N 2.49. The thermal behavior and IR and UV-vis spectra were identical to those of the enantiomer.

Λ-$[Co(en)_3]^{3+}$ $3BAr_f^-$. A beaker was charged with Λ-$[Co(en)_3]^{3+}$ $3I^-\cdot H_2O$ (0.2267 g, 0.3554 mmol),[21] H_2O (15 mL), CH_2Cl_2 (15 mL), and Na^+ BAr_f^- (0.9447 g, 1.066 mmol, 3:1 mol ratio).[41] The biphasic mixture was vigorously stirred (10 min) and allowed to stand. The lower phase was separated and allowed to evaporate in a fume hood (several days) to give Λ-$[Co(en)_3]^{3+}$ $3BAr_f^-\cdot 14H_2O$ as an orange solid (0.9490 g, 0.3080 mmol, 87%). Anal. Calcd. for $C_{102}H_{60}B_3CoF_{72}N_6\cdot 14H_2O$ (3081.07): C, 39.76; H, 2.88; N, 2.73; found: C, 39.69; H, 2.85; N, 2.80. Capillary thermolysis, TGA, and DSC data: Table 2.1.

NMR (acetone-d_6, δ in ppm): ^{1}H (400 MHz), BAr_f^- at 7.78 (s, 24H, *o*), 7.67 (s, 12H, *p*); en at 5.69 (br s, 6H, N**H**H'), 5.29 (br s, 6H, NH**H'**), 3.41-3.24 (m, 12H, CH_2), 2.85 (br s, 33H, H_2O); $^{13}C\{^1H\}$ (100 MHz), BAr_f^- at 162.6 (q, $^1J_{BC}$ = 49.7 Hz, *i*), 135.5 (s, *o*), 130.0 (q, $^2J_{CF}$ = 31.4 Hz, *m*), 125.4 (q, $^1J_{CF}$ = 271.8 Hz, CF_3), 118.4 (s, *p*); en at 46.3 (s, CH_2). IR (powder film, cm^{-1}): 3246 (m, NH_2), 1613 (m, NH_2), 1355 (s, CF-aryl), 1274 (vs, CF_3), 1116 (vs, CNH_2), 891 (s, CNH_2), 837 (m, 1,3,5-trisubsituted benzene). UV-vis (nm, EtOH, 12.0 °C (ε, $M^{-1}cm^{-1}$)): 269 (13500), 278 (10700), 334 (255), 463 (170).

Δ-$[Co(en)_3]^{3+}$ 3BAr_f^-. A round bottom flask was charged with a colorless solution of Na^+ BAr_f^- (0.494 g, 0.557 mmol) in CH_2Cl_2 (25 mL). Then a solution of Δ-$[Co(en)_3]^{3+}$ 3$I^-\cdot H_2O$[21] (0.119 g, 0.186 mmol) in water (20 mL) was added. The heterogeneous mixture was vigorously stirred for 10 min. The now orange CH_2Cl_2 phase was separated from the aqueous phase and the CH_2Cl_2 was allowed to evaporate in a fume hood overnight to give Δ-$[Co(en)_3]^{3+}$ 3$BAr_f^-\cdot 14H_2O$ as an orange solid (0.501 g, 0.163 mmol, 87%). Anal. Calcd. for $C_{102}H_{60}B_3CoF_{72}N_6\cdot 14H_2O$ (3081.07): C, 39.76; H, 2.88; N, 2.73; found: C, 39.87; H, 2.77; N, 2.66. The thermal behavior and NMR (^{1}H, $^{13}C\{^1H\}$), IR, and UV-vis spectra were identical to those of the enantiomer.

Λ-$[Rh(en)_3]^{3+}$ 3BAr_f^-. A beaker was charged with Λ-$[Rh(en)_3]^{3+}$ 3$Cl^-\cdot 2.3H_2O$ (0.0204 g, 0.0473 mmol),[20b] H_2O (10 mL), CH_2Cl_2 (10 mL), and Na^+ BAr_f^- (0.1257 g, 0.1418 mmol, 3:1 mol ratio).[41] The biphasic mixture was vigorously stirred (10 min) and allowed to stand. The lower phase was separated and allowed to evaporate in a fume hood (several days) to give Λ-$[Rh(en)_3]^{3+}$ 3$BAr_f^-\cdot 11.5H_2O$ as an ivory solid (0.1420 g, 0.04610 mmol, 97%). Anal. Calcd. for $C_{102}H_{60}B_3F_{72}N_6Rh\cdot 11.5H_2O$ (3080.04): C 39.78, H 2.72, N 2.73; found C 39.23, H 2.77, N 2.70. Capillary thermolysis, TGA, and DSC data: Table 2.1.

NMR (acetone-d_6, δ in ppm): ^{1}H (400 MHz), BAr_f^- at 7.80 (s, 24H, *o*), 7.67 (s, 12H, *p*); en at 6.00 (br s, 6H, N**H**H'), 5.52 (br s, 6H, NH**H'**), 3.41-3.25 (m, 12H, CH_2), 3.20 (br s, 23H, H_2O); $^{13}C\{^1H\}$ (100 MHz), BAr_f^- at 162.6 (q, $^1J_{BC}$ = 49.9 Hz, *i*), 135.5 (s, *o*), 130.0 (q, $^2J_{CF}$ = 31.6 Hz, *m*), 125.4 (q, $^1J_{CF}$ = 271.8 Hz, CF_3), 118.4 (s, *p*); en at 47.0 (s, CH_2). IR (powder film, cm^{-1}): 3254 (m, NH_2), 1611 (m, NH_2), 1354 (s, CF-aryl), 1273 (vs, CF_3), 1107 (vs, CNH_2), 885 (s, CNH_2), 839 (m, 1,3,5-trisubsituted benzene). UV-vis (nm, EtOH, 12.0 °C (ε, $M^{-1}cm^{-1}$)): 269 (13000), 278 (10500), 304 (264).[43]

Δ-[Rh(en)$_3$]$^{3+}$ 3BAr$_f^-$. Δ-$[Rh(en)_3]^{3+}$ $3Cl^-\cdot 2.3H_2O$ (0.0204 g, 0.0473 mmol),[20b] H_2O (10 mL), CH_2Cl_2 (10 mL), and Na^+ BAr_f^- (0.1257 g, 0.1418 mmol) were combined in a procedure analogous to that for Λ-$[Rh(en)_3]^{3+}$ $3BAr_f^-$. An identical workup gave Δ-$[Rh(en)_3]^{3+}$ $3BAr_f^-\cdot 11.5H_2O$ as an ivory solid (0.1407 g, 0.04568 mmol, 97%), Anal. Calcd. for $C_{102}H_{60}B_3F_{72}N_6Rh\cdot 11.5H_2O$ (3080.04): C 39.78, H 2.72, N 2.73; found C 40.25, H 2.68, N 2.73. The thermal behavior and NMR (^{1}H, $^{13}C\{^1H\}$), IR, and UV-vis spectra were identical to those of the enantiomer.

Λ-[Ir(en)$_3$]$^{3+}$ 3BAr$_f^-$. A beaker was charged with Λ-$[Ir(en)_3]^{3+}$ $3Cl^-\cdot 2H_2O$ (0.0193 g, 0.0375 mmol),[22] H_2O (15 mL), CH_2Cl_2 (15 mL), and Na^+ BAr_f^- (0.0997 g, 0.113 mmol, 3:1 mol ratio).[41] The biphasic mixture was vigorously stirred (10 min) allowed to stand. The lower phase was separated and allowed to evaporate in a fume hood (several days) to give Λ-$[Ir(en)_3]^{3+}$ $3BAr_f^-\cdot 9H_2O$ as white solid (0.1125 g, 0.03601 mmol, 96%). Anal. Calcd. for $C_{102}H_{60}B_3F_{72}IrN_6\cdot 9H_2O$ (3124.31): C 39.21, H 2.52, N 2.69; found C 39.52, H 2.55, N 2.70. Capillary thermolysis, TGA, and DSC data: Table 2.1.

NMR (acetone-d_6, δ in ppm): ^{1}H (400 MHz), BAr_f^- at 7.79 (s, 24H, *o*), 7.67 (s, 12H, *p*); en at 6.42 (br s, 6H, N**H**H'), 5.92 (br s, 6H, NH**H'**), 3.28-3.12 (m, 12H, CH_2), 3.01 (br s, 30H, H_2O); $^{13}C\{^1H\}$ (100 MHz), BAr_f^- at 162.4 (q, $^1J_{BC}$ = 49.9 Hz, *i*), 135.4 (s, *o*), 129.9 (q, $^2J_{CF}$ = 31.4 Hz, *m*), 125.2 (q, $^1J_{CF}$ = 271.8 Hz, CF_3), 118.3 (s, *p*); en at

48.5 (s, CH_2). IR (powder film, cm^{-1}): 3254 (m, NH_2), 1611 (m, NH_2), 1356 (s, CF-aryl), 1273 (vs, CF_3), 1119 (vs, CNH_2), 889 (s, CNH_2), 837 (m, 1,3,5-trisubsituted benzene). UV-vis (nm, EtOH, 12.0 °C (ε, $M^{-1}cm^{-1}$)): 269 (10400), 278 (8380).[43]

Δ-[Ir(en)$_3$]$^{3+}$ 3BAr$_f^-$. Δ-$[Ir(en)_3]^{3+}$ $3Cl^-\cdot 2H_2O$ (0.0236 g, 0.0458 mmol),[22] H_2O (15 mL), CH_2Cl_2 (15 mL), and Na^+ BAr_f^- (0.1219 g, 0.1376 mmol) were combined in a procedure analogous to that for Λ-$[Ir(en)_3]^{3+}$ $3BAr_f^-$. An identical workup gave Δ-$[Ir(en)_3]^{3+}$ $3BAr_f^-\cdot 9H_2O$ as a white solid (0.1391 g, 0.04452 mmol, 97%). Anal. Calcd. for $C_{102}H_{60}B_3F_{72}IrN_6\cdot 9H_2O$ (3124.31): C 39.21, H 2.52, N 2.69; found C 39.10, H 2.53, N 2.72. The thermal behavior and NMR (^1H, $^{13}C\{^1H\}$), IR, and UV-vis spectra were identical to those of the enantiomer.

Λ-[Pt(en)$_3$]$^{4+}$ 4BAr$_f^-$. A beaker was charged with Λ-$[Pt(en)_3]^{4+}$ $4Cl^-\cdot 2H_2O$ (0.0186 g, 0.0336 mmol),[6,23] H_2O (10 mL), CH_2Cl_2 (10 mL), and Na^+ BAr_f^- (0.1192 g, 0.1345 mmol, 4:1 mol ratio).[41] The biphasic mixture was vigorously stirred (10 min) and allowed to stand. The pale yellow lower phase was separated and allowed to evaporate in a fume hood (several days) to give Λ-$[Pt(en)_3]^{4+}$ $4BAr_f^-\cdot 17H_2O$ as a pale yellow solid (0.1324 g, 0.03202 mmol, 95%). Anal. Calcd. for $C_{134}H_{72}B_4F_{96}N_6Pt\cdot 17H_2O$ (4134.52): C 38.93, H 2.58, N 2.03; found C 38.79, H 2.57, N 2.04. Capillary thermolysis, TGA, and DSC data: Table 2.1.

NMR (acetone-d_6, δ in ppm): ^1H (400 MHz), BAr_f^- at 7.79 (s, 32H, *o*), 7.67 (s, 16H, *p*); en at 8.48 (br s, 4H, N**H**H'),[44] 8.05 (br s, 4H, NH**H'**),[44] 3.94-3.62 (m, 12H, CH_2), 3.50 (br s, 36H, H_2O); $^{13}C\{^1H\}$ (100 MHz), BAr_f^- at 162.5 (q, $^1J_{BC}$ = 49.8 Hz, *i*), 135.6 (s, *o*), 130.0 (m, *m*), 125.4 (q, $^1J_{CF}$ = 271.8 Hz, CF_3), 118.4 (m, *p*); en at 50.7 (s, CH_2). IR (powder film, cm^{-1}): 3244 (m, NH_2), 1611 (m, NH_2), 1356 (s, CF-aryl), 1273 (vs, CF_3), 1117 (vs, CNH_2), 889 (s, CNH_2), 837 (m, 1,3,5-trisubsituted benzene). UV-vis (nm, EtOH, 12.0 °C (ε, $M^{-1}cm^{-1}$)): 269 (17000), 278 (13900), 318 (101).[43]

Δ-[Pt(en)$_3$]$^{4+}$ 4BAr$_f^-$. Δ-[Pt(en)$_3$]$^{4+}$ 4Cl$^-$·2H$_2$O (0.0180 g, 0.0325 mmol),[6,23] H$_2$O (10 mL), CH$_2$Cl$_2$ (10 mL), and Na$^+$ BAr$_f^-$ (0.1153 g, 0.1301 mmol) were combined in a procedure analogous to that for Λ-[Pt(en)$_3$]$^{4+}$ 4BAr$_f^-$. An identical workup gave Δ-[Pt(en)$_3$]$^{4+}$ 4BAr$_f^-$·17H$_2$O as a pale yellow solid (0.1280 g, 0.03096 mmol, 95%). Anal. Calcd. for C$_{134}$H$_{72}$B$_4$F$_{96}$N$_6$Pt·17H$_2$O (4134.52): C 38.93, H 2.58, N 2.03; found C 39.05, H 2.48, N 2.02. The thermal behavior and NMR (^{1}H, ^{13}C{^{1}H}), IR, and UV-vis spectra were identical to those of the enantiomer.

Thermal experiments (Table 2.1). A. An open capillary was charged with *ca.* 0.008 g of the salt and inserted into an OptiMelt MPA 100 instrument. The sample was heated from 30.0 °C to the temperature listed in column 3 of Table 2.1 at 10.0 °C/min, and then allowed to cool to room temperature before dissolution in acetone-d_6 for ^{1}H NMR analysis. **B**. The other experiments employed either a TA Instruments Q50 TGA, using 0.010-0.015 g samples that were heated from 30.0 to 500.0 °C at 10.0 °C/min, or a TA Instruments Q20 DSC, using 0.005-0.010 g samples that were heated from 25.0 °C to 50 °C beyond their liquefaction temperature at 10.0 °C/min.

Dimethyl 2-(2-nitro-1-phenylethyl)malonate (**1**; Figure 2.3). An authentic sample of this known compound was obtained as a colorless oil by a literature procedure.[13a] A 5 mm NMR tube was charged with a solution of *trans*-β-nitrostyrene (0.0054 g, 0.036 mmol, 1.0 equiv), catalyst (0.0036 mmol, 0.10 equiv), dimethyl malonate (0.0045 mL, 0.0052 g, 0.039 mmol, 1.1 equiv), and Ph$_2$SiMe$_2$ (0.0020 mL, internal standard) in CD$_3$CN (0.40 mL). A ^{1}H NMR spectrum was recorded to confirm the initial *trans*-β-nitrostyrene/standard ratio. A stir bar was added and the sample cooled to 0 °C. Then NMM (0.0040 mL, 0.0037 g, 0.036 mmol, 1.0 equiv) was added and the mixture stirred. After 24 h, the stir bar was removed and the yield of **1** assayed by ^{1}H NMR. The solvent was removed under reduced pressure to give an oil, which was added to a plug of

silica. The plug was eluted with hexanes/EtOAc (1:1 v/v). The solvent was removed from the product containing fraction under reduced pressure. The enantiomeric excess was determined by HPLC (Chiralpak AD column, 98:2 v/v hexanes/isopropanol, 1.0 mL/min, λ = 220 nm; for entry 5 t_R = 27.1 and 37.8 min (major and minor)).[45]

***N,N'*-Bis(t-butoxycarbonyl)-1-hydrazino-2-oxocyclopentanecarboxylic acid methyl ester** (**2**; Figure 2.4)**.** An authentic sample was obtained as a colorless oil by a literature procedure.[15a] A 5 mm NMR tube was charged with a solution of di-*tert*-butylazodicarboxylate (0.0083 g, 0.036 mmol, 1.0 equiv), catalyst (0.0036 mmol, 0.10 equiv), methyl 2-oxocyclopentanecarboxylate (0.0046 mL, 0.0053 g, 0.037 mmol, 1.0 equiv), and Ph_2SiMe_2 (0.0020 mL, internal standard) in CD_3CN (0.40 mL). A ^1H NMR spectrum was recorded to confirm the initial di-*tert*-butylazodicarboxylate/standard ratio. A stir bar was added and the sample cooled to 0 °C. Then NMM (0.0040 mL, 0.0037 g, 0.036 mmol, 1.0 equiv) was added and the mixture stirred. After 24 h, the stir bar was removed and the yield of **2** assayed by ^1H NMR. The solvent was removed under reduced pressure to give an oil, which was added to a plug of silica. The plug was eluted with hexanes/EtOAc (7:3 v/v). The solvent was removed from the product containing fractions under reduced pressure. The enantiomeric excess was determined by HPLC (Chiralpak AD column, 96:4 v/v hexanes/isopropanol, 1.0 mL/min, λ = 210 nm; for entry 5 t_R = 15.1 and 22.4 min (minor and major)).[46]

3-(Bis(isopropoxycarbonyl)methyl)cyclopentanone (**3**; Figure 2.5, entries 1-4, 6-11)**.** An authentic sample was obtained as a colorless oil by adapting a literature procedure.[10,47] A 5 mm NMR tube was charged with a solution of 2-cyclopenten-1-one (0.0030 mL, 0.0029 g, 0.036 mmol, 1.0 equiv), catalyst (0.0036 mmol, 0.10 equiv), diisopropyl malonate (0.0070 mL, 0.0070 g, 0.037 mmol, 1.0 equiv), and Ph_2SiMe_2 (0.0020 mL, standard) in CD_2Cl_2 (0.40 mL). A ^1H NMR spectrum was recorded to

confirm the initial 2-cyclopenten-1-one/standard ratio. A stir bar was added and the sample was cooled to –35 °C. Then Et_3N (0.0050 mL, 0.0036 g, 0.036 mmol, 1.0 equiv) was added and the mixture stirred. After 24 h, the stir bar was removed and the yield of **3** assayed by ^1H NMR. The solvent was removed under reduced pressure to give an oil, which was added to a plug of silica. The product was eluted with hexanes/acetone (9:1 v/v). The solvent was removed from the product containing fraction under reduced pressure. The enantiomeric excess was determined by HPLC (Chiralpak AD-H column, 95:5 v/v hexanes/isopropanol, 1.0 mL/ min, λ = 215 nm; for entry 5, t_R = 10.7 and 11.7 min (major and minor)).[47]

3-(Bis(methoxycarbonyl)methyl)cyclopentanone (Figure 2.5, entry 5)**.** An authentic sample was obtained as a colorless oil by adapting a literature procedure.[10,48] A round bottom flask was charged with a solution of 2-cyclopenten-1-one (0.034 mL, 0.033 g, 0.040 mmol, 1.0 equiv), Λ-$[Co(en)_3]^{3+}$ $3BAr_f^-\cdot 14H_2O$ (0.112 g, 0.0364 mmol, 0.09 equiv), and dimethyl malonate (0.046 mL, 0.053 g, 0.4 mmol, 1.0 equiv) in CH_2Cl_2 (5 mL). A stir bar was added and the sample was cooled to –40 °C. Then Et_3N (0.056 mL, 0.040 g, 0.40 mmol, 1.0 equiv) was added and the mixture stirred. After 8 h, the solvent was removed under reduced pressure to give an orange oil, which was added to a silica gel column that was eluted with hexanes/acetone (9:1 v/v). The solvent was removed from the product containing fractions under reduced pressure. to give 3-(bis(methoxycarbonyl)methyl)cyclopentanone as a colorless oil (0.067 g, 0.31 mmol, 78%). The enantiomeric excess was determined by HPLC analysis of the ketal derived from ethylene glycol (Daicel Chiralcel OD column, 97:3 v/v hexanes/isopropanol, 0.7 mL/min, λ = 225 nm; for entry 5, t_R = 22.0 and 24.8 min (major and minor)).[48]

$NMMH^+$ BAr_f^-. A beaker was charged with $NMMH^+$ Cl^- (0.0301 g, 0.219 mmol),[49] H_2O (15 mL), CH_2Cl_2 (15 mL), and Na^+ BAr_f^- (0.1938 g, 0.219 mmol).[41] The

biphasic mixture was vigorously stirred (10 min) and allowed to stand. The lower phase was separated, the solvent removed by rotary evaporation, and the residue dried by oil pump vacuum (room temperature, overnight) to give $NMMH^+$ BAr_f^- as an off white solid (0.1909 g, 0.1978 mmol, 90%). Thermolysis (open capillary): 178-190 °C (darkens, then liquefaction). Anal. Calcd. for $C_{37}H_{24}BF_{24}NO$ (965.36): C, 46.03; H, 2.51; N, 1.45; found: C, 45.89; H, 2.36; N, 1.46.

NMR (acetone-d_6, δ in ppm): ^1H (400 MHz), BAr_f^- at 7.79 (s, 8H, *o*), 7.67 (s, 4H, *p*); $NMMH^+$ at 4.19-3.90 (m, 4H, CH_2O), 3.79-3.47 (m, 4H, C**H**$_2N^+H$), 3.26 (s, 3H, CH_3); $^{13}C\{^1H\}$ (100 MHz), BAr_f^- at 162.6 (q, $^1J_{BC}$ = 49.8 Hz, *i*), 135.5 (s, *o*), 130.0 (q, $^2J_{CF}$ = 31.4 Hz, *m*), 125.4 (q, $^1J_{CF}$ = 271.7 Hz, CF_3), 118.4 (s, *p*); $NMMH^+$ at 64.7 (s, double intensity), 55.1 (s, double intensity), 44.6 (s).

2.5 References (All titles are given in the capitalization format of the original article)

(1) (a) Werner, A. Zur Kenntnis des asymmetrischen Kobaltatoms. I. *Ber. Dtsch. Chem. Ges.* **1911**, *44*, 1887-1898. King, V. L. is listed as an author for the experimental section. (b) Werner, A. Zur Kenntnis des asymmetrischen Kobaltatoms. II. *Ber. Dtsch. Chem. Ges.* **1911**, *44*, 2445-2455. (c) Werner, A. Zur Kenntnis des asymmetrischen Kobaltatoms. III. *Ber. Dtsch. Chem. Ges.* **1911**, *44*, 3272-3278. (d) Werner, A. Zur Kenntnis des asymmetrischen Kobaltatoms. IV. *Ber. Dtsch. Chem. Ges.* **1911**, *44*, 3279-3284. (e) Werner, A. Zur Kenntnis des asymmetrischen Kobaltatoms. V. *Ber. Dtsch. Chem. Ges.* **1912**, *45*, 121-130.

(2) (a) Morral, F. R. Alfred Werner and Cobalt Complexes. In *Werner Centennial*; Kauffman, G. B., Ed.; American Chemical Society: Washington, D. C., 1967; Vol. 62; pp. 70-77. (b) Kauffman, G. B. Alfred Werner's Research on Optically Active Coordination Compounds. *Coord. Chem. Rev.* **1974**, *12*, 105-149.

(3) (a) Pfeiffer, P. Über Chromiake. Abhandlung I. Trichlorotripyridinbrom und Triäthylenediaminchromisalze. *Z. Anorg. Allg. Chem.* **1900**, *24*, 279-304. (b) Werner, A. Über Spiegelbildisomerie bei Chromverbindungen. II. *Ber. Dtsch. Chem. Ges.* **1912**, *45*, 865-869.

(4) Werner, A. Über Spiegelbildisomerie bei Rhodium-Verbindungen. I. *Ber. Dtsch. Chem. Ges.* **1912**, *45*, 1228-1236.

(5) Werner, A.; Smirnoff, A. P. Über optisch-aktive Iridiumverbindungen. *Helv. Chim. Acta* **1920**, *3*, 472-486.

(6) Werner, A. Über Spiegelbildisomerie bei Platinverbindungen I. *Vierteljahresschr. Naturforsch. Ges. Zürich* **1917**, *62*, 553-564.

(7) (a) von Zelewsky, A. *Stereochemistry of Coordination Compounds*; John Wiley & Sons: Chichester, 1996. (b) *Chirality in Transition Metal Chemistry*; Amouri,

H.; Gruselle, M.; John Wiley & Sons: Chichester, 2008. (c) Ehnbom, A.; Ghosh, S. K.; Lewis, K. G.; Gladysz, J. A. Octahedral Werner complexes with substituted ethylenediamine ligands: a stereochemical primer for a historic series of compounds now emerging as a modern family of catalysts. *Chem. Soc. Rev.* **2016**, *45*, 6799-6811.

(8) (a) Taube, H. Rates and Mechanisms of Substitution in Inorganic Complexes in Solution. *Chem. Rev*. 1952, 50, 69-126. (b) Data for $[Co(en)_3]^{3+}$: Friend, J. A.; Nunn, E. K. Substitution Reactions in the Trisethylenediaminecobalt(III) Ion. *J. Chem. Soc.* **1958**, 1567-1571. (c) For an entry level rationale, see *Selected Topics in Inorganic Chemistry*; Malik, W. U.; Tuli, G. D.; Madan, R. D.; S. Chand & Company: New Delhi, 2002. Chapter 14.

(9) (a) Sen, D.; Fernelius, W. C. Catalytic racemization of optically active complexes: Tris(ethylenediamine)cobalt(III), -platinum(IV), and -rhodium(III) halides. *J. Inorg. Nucl. Chem.* **1959**, *10*, 269-274. (b) Douglas, B. D. Racemization of Tris-(ethylenediamine)-cobalt(III) Ion in the Presence of Decolorizing Carbon. *J. Am. Chem. Soc.* **1954**, *76*, 1020-1021. (c) Harnung, S. E.; Kallesøe, S.; Sargeson, A. M.; Schäffer, C. E. The Tris[(±)-1,2-propanediamine]cobalt(III) System. *Acta Chem. Scand.* **1974**, *A28*, 385-398; see especially the final paragraph of the experimental section.

(10) Ganzmann, C.; Gladysz, J. A. Phase Transfer of Enantiopure Werner Cations into Organic Solvents: An Overlooked Family of Chiral Hydrogen Bond Donors for Enantioselective Catalysis. *Chem. Eur. J.* **2008**, *14*, 5397-5400.

(11) Ghosh, S. K.; Ehnbom, A.; Lewis, K. G.; Gladysz, J. A. Hydrogen bonding motifs in structurally characterized salts of the tris(ethylenediamine) cobalt trication, $[Co(en)_3]^{3+}$; An interpretive review, including implications for catalysis. *Coord. Chem. Rev.* **2017**, *350*, 30-48.

(12) (a) Taylor, M. S.; Jacobsen, E. N. Asymmetric Catalysis by Chiral Hydrogen-Bond Donors. *Angew. Chem., Int. Ed.* **2006***, 45,* 1520-1543; Asymmetrische Katalyse durch chirale Wasserstoffbrückendonoren. *Angew. Chem.* **2006**, *118*, 1550-1573. (b) Doyle, A. G.; Jacobsen, E. N. Small-Molecule H-Bond Donors in Asymmetric Catalysis. *Chem. Rev.* **2007**, *107*, 5713-5743. (c) Yu, X.; Wang, W. Hydrogen-Bond-Mediated Asymmetric Catalysis. *Chem. Asian J.* **2008**, *3*, 516-532. (d) Takemoto, Y. Recognition and activation by ureas and thioureas: stereoselective reactions using ureas and thioureas as hydrogen-bonding donors. *Org. Biomol. Chem.* **2005**, *3*, 4299-4306. (e) Held, F. E.; Tsogoeva, S. B. Asymmetric cycloaddition reactions catalyzed by bifunctional thiourea and squaramide organocatalysts: recent advances. *Catal. Sci. Technol.* **2016**, *6*, 645-667.

(13) (a) Lewis, K. G.; Ghosh, S. K.; Bhuvanesh, N.; Gladysz, J. A. Cobalt(III) Werner Complexes with 1,2-Diphenylethylenediamine Ligands: Readily Available, Inexpensive, and Modular Chiral Hydrogen Bond Donor Catalysts for Enantioselective Organic Synthesis. *ACS Cent. Sci.* **2015**, *1*, 50-56. (b) Ghosh, S. K.; Lewis, K. G.; Kumar, A.; Gladysz, J. A. Syntheses of Families of Enantiopure and Diastereopure Cobalt Catalysts Derived from Trications of the Formula $[Co(NH_2CHArCHArNH_2)_3]^{3+}$. *Inorg. Chem.* **2017**, 56, 2304-2320.

(14) Ghosh, S. K.; Ganzmann, C.; Bhuvanesh, N.; Gladysz, J. A. Werner Complexes with ω-Dimethylaminoalkyl Substituted Ethylenediamine Ligands: Bifunctional Hydrogen-Bond-Donor Catalysts for Highly Enantioselective Michael Additions. *Angew. Chem., Int. Ed.* **2016**, *55*, 4356-4360; Werner-Komplexe mit ω-Dimethylaminoalkyl-substitutierten Ethylendiaminliganden: bifunktionale H-Brückendonor-Katalysatoren für hoch enantioselektive Michael-Additionen. *Angew. Chem.* **2016**, *128*, 4429-4433.

(15) (a) Kumar, A.; Ghosh, S. K.; Gladysz, J. A. Tris(1,2-diphenylethylenediamine)cobalt(III) Complexes: Chiral Hydrogen Bond Donor Catalysts for Enantioselective *α*-Aminations of 1,3-Dicarbonyl Compounds. *Org. Lett.* **2016**, *18*, 760-763. (b) Joshi, H.; Ghosh, S. K.; Gladysz, J. A. Enantioselective Additions of Stabilized Carbanions to Imines Generated from α-Amido Sulfones By Using Lipophilic Salts of Chiral Tris(1,2-diphenylethylenediamine) Cobalt(III) Trications as Hydrogen Bond Donor Catalysts. *Synthesis* **2017**, *49*, 3905-3915. (c) Maximuck, W. J.; Gladysz, J. A. Lipophilic Chiral Cobalt(III) Complexes of hexaamine ligands: Efficacies as enantioselective hydrogen bond donor catalysts. *Mol. Catal.* **2019**, *473*, 110360. (d) Kabes, C. Q.; Maximuck, W. J.; Ghosh, S. K.; Kumar, A.; Bhuvanesh, N.; Gladysz, J. A. Chiral Tricationic Tris(1,2-diphenylethylenediamine) Cobalt(III) Hydrogen Bond Donor Catalysts with Defined Carbon/Metal Configurations; Matched/Mismatched Effects upon Enantioselectivities with Enantiomeric Chiral Counter Anions. *ACS Catal.* **2020**, *10*, 3249-3263. (e) See also Luu, Q. H.; Lewis, K. G.; Banerjee, A.; Bhuvanesh, N.; Gladysz, J. A. The robust, readily available cobalt(III) trication $[Co(NH_2CHPhCHPhNH_2)_3]^{3+}$ is a progenitor of broadly applicable chirality and prochirality sensing agents. *Chem. Sci.* **2018**, *9*, 5087-5099.

(16) (a) Scherer, A.; Mukherjee, T.; Hampel, F.; Gladysz, J. A. Metal-Templated Hydrogen Bond Donors as 'Organocatalysts' for Carbon-Carbon Bond Forming Reactions: Syntheses, Structures, and Reactivities of 2-Guanidinobenzimidazole Cyclopentadienyl Ruthenium Complexes. *Organometallics* **2014**, *33*, 6709-6722. (b) Mukherjee, T.; Ganzmann, C.; Bhuvanesh, N.; Gladysz, J. A. Syntheses of Enantiopure Bifunctional 2-Guanidinobenzimidazole Cyclopentadienyl Ruthenium Complexes: Highly Enantioselective Organometallic Hydrogen Bond Donor Catalysts for Carbon-Carbon Bond Forming Reactions. *Organometallics* **2014**, *33*, 6723-6737. (c) Wititsuwannakul, T.;

Hall, M. B.; Gladysz, J. A. A Computational Study of Hydrogen Bonding Motifs in Halide, Tetrafluoroborate, Hexafluorophosphate, and Tetraarylborate Salts of Chiral Cationic Ruthenium and Cobalt Guanidinobenzimidazole Hydrogen Bond Donor Catalysts; Acceptor Properties of the "BArf" Anion. *Polyhedron* **2020**, *187*, 114618. (d) Wititsuwannakul, T.; Mukherjee, T.; Hall, M. B.; Gladysz, J. A. Computational Investigations of Enantioselection in Carbon-Carbon Bond Forming Reactions of Ruthenium Guanidinobenzimidazole Second Coordination Sphere Hydrogen Bond Donor Catalysts. *Organometallics* **2020**, *39*, 1149-1162. (e) Mukherjee, T.; Ghosh, S. K.; Wititsuwannakul, T.; Bhuvanesh, N.; Gladysz, J. A. Chiral-at-Metal Ruthenium Complexes with Guanidinobenzimidazole and Pentaphenylcyclopentadienyl Ligands: Synthesis, Resolution, and Preliminary Screening as Enantioselective Second Coordination Sphere Hydrogen Bond Donor Catalysts. *Organometallics* **2020**, *39*, 1163-1175.

(17) (a) Chen, L.-A.; Tang, X.; Xi, J.; Xu, W.; Gong, L.; Meggers, E. Chiral-at-Metal Octahedral Iridium Catalyst for the Asymmetric Construction of an All-Carbon Quaternary Stereocenter. *Angew. Chem., Int. Ed.* **2013**, *52*, 14021-14025 and *Angew. Chem.* **2013**, *125*, 14271-14275. (b) Huo, H.; Fu, C.; Wang, C.; Harms, K.; Meggers, E. Metal-templated enantioselective enamine/H-bonding dual activation catalysis. *Chem. Commun*. **2014**, *50*, 10409-10411. (c) Hu, Y.; Zhou, Z.; Gong, L.; Meggers, E. Asymmetric aza-Henry reaction to provide oxindoles with quaternary carbon stereocenter catalyzed by a metal-templated chiral Brønsted base. *Org. Chem. Front.* **2015**, *2*, 968-972. (d) Ding, X.; Lin, H.; Gong, L.; Meggers, E. Enantioselective Sulfa-Michael Addition to α,β-Unsaturated γ-Oxoesters Catalyzed by a Metal-Templated Chiral Brønsted Base. *Asian J. Org. Chem.* **2015**, *4*, 434-437. (e) Xu, W.; Arieno, M.; Löw, H.; Huang, K.; Xie, X.; Cruchter, T.; Ma, Q.; Xi, J.; Huang, B.; Wiest, O.; Gong, L.; Meggers, E. Metal-Temp-

lated Design: Enantioselective Hydrogen-Bond-Driven Catalysis Requiring Only Parts-per-Million Catalyst Loading. *J. Am. Chem. Soc.* **2016,** *138*, 8774-8780. (f) Xu, W.; Shen, X.; Ma, Q.; Gong, L.; Meggers, E. Restricted Conformation of a Hydrogen Bond Mediated Catalyst Enables the Highly Efficient Enantioselective Construction of an All-Carbon Quaternary Stereocenter. *ACS Catal.* **2016**, *6*, 7641-7646. (g) Ding, X.; Tian, C.; Hu, Y.; Gong, L.; Meggers, E. Tuning the Basicity of a Metal-Templated Brønsted Base to Facilitate the Enantioselective Sulfa-Michael Addition of Aliphatic Thiols to α,β-Unsaturated *N*-Acylpyrazoles. *Eur. J. Org. Chem.* **2016**, *2016*, 887-890.

(18) (a) Belokon, Y. N.; Maleev, V. I.; North, M.; Larionov, V. A.; Savel'yeva, T. F.; Nijland, A.; Nelyubina, Y. V. Chiral Octahedral Complexes of Co^{III} As a Family of Asymmetric Catalysts Operating under Phase Transfer Conditions. *ACS Catal.* **2013**, *3*, 1951-1955. (b) Maleev, V. I.; North, M.; Larionov, V. A.; Fedyanin, I. V.; Savel'yeva, T. F.; Moscalenko, M. A.; Smolyakov, A. F.; Belokon, Y. N. Chiral Octahedral Complexes of Cobalt(III) as "Organic Catalysts in Disguise" for the Asymmetric Addition of a Glycine Schiff Base Ester to Activated Olefins. *Adv. Synth. Catal.* **2014**, *356*, 1803-1810. (c) Larionov, V. A.; Markelova, E. P.; Smol'yakov, A. F.; Savel'yeva, T. F.; Maleev, V. I.; Belokon, Y. N. Chiral octahedral complexes of Co(III) as catalysts for asymmetric epoxidation of chalcones under phase transfer conditions. *RSC Adv.* **2015**, *5*, 72764-72771. (d) Rulev, Y. A.; Larionov, V. A.; Lokutova, A. V.; Moskalenko, M. A.; Lependina, O. L.; Maleev, V. I.; North, M.; Belokon, Y. N. Chiral Cobalt(III) Complexes as Bifunctional Brønsted Acid-Lewis Base Catalysts for the Preparation of Cyclic Organic Carbonate. *ChemSusChem* **2016**, *9*, 216-222.

(19) Skubi, K. L.; Kidd, J. B.; Jung, H.; Guzei, I. A.; Baik, M.-H.; Yoon, T. P. Enantioselective Excited-State Photoreactions Controlled by a Chiral Hydrogen-Bonding Iridium Sensitizer. *J. Am. Chem. Soc.* **2017**, *139*, 17186-17192.

(20) (a) Gillard, R. D.; Mitchell, P. R. Tris(diamine)chromium(III) Salts. *Inorg. Synth*. **1972**, *13*, 184-186. (b) Galsbøl, F. Resolution of Tris(ethylenediamine)-rhodium(III) and -chromium(III) Chloride by Means of (+)-Tartrate. *Inorg. Synth*. **1970**, *12*, 269-280.

(21) Broomhead, J. A.; Dwyer, F. P.; Hogarth, J. W. Resolution of the Tris(ethylenediamine)cobalt(III) Ion. *Inorg. Synth*. **1960**, *6,* 183-186.

(22) Galsbøl, F.; Rasmussen, B. S. The Preparation, Resolution, and Characterization of Tris(1,2-ethanediamine)iridium(III) Complexes. *Acta Chem. Scand.* **1982**, *A36*, 83-87.

(23) Giedt, D. C.; Nyman, C. J. Tris(ethylenediamine)platinum(IV) Chloride. *Inorg. Synth*. **1966**, *8*, 239-241.

(24) Ganzmann, C. Werner-type Cobalt Complexes and Ruthenium Complexes with substituted 2-Guanidinobenzimidazole Ligands as Catalysts for Michael and Friedel Crafts Reactions. Doctoral Thesis, Friedrich-Alexander-Universität Erlangen-Nürnberg: Erlangen, Germany, July 2010.

(25) Maximuck, W. J. Syntheses of Lipophilic Werner Complexes For Application as Chiral Hydrogen Bond Donors in Enantioselective Catalysis and Investigation of the Effect of Chloride on Fluid Catalytic Cracking Catalysts, Texas A&M University, College Station, TX, USA, May 2021.

(26) (a) Clark, R. J. H.; Greenfield, W. R. Ethylenediamine and Propylenediamine Complexes of Titanium (III), Vanadium (III), and Chromium (III). *J. Chem. Soc. A* **1967**, 409-414. (b) Schläfer, H. L.; Kling, O. Über die Zersetzung des Tris-äthylendiamin-chrom(III)-komplexions in wäßriger Lösung als Dunkel- und Lichtreaktion. *Z. Anorg. Allg. Chem.* **1956**, *287*, 296-312.

(27) (a) Sharma, R. K.; Fry, J. L. Instability of Anhydrous Tetra-*n*-alkylammonium Fluorides. *J. Org. Chem.* **1983**, *48*, 2112-2114. (b) Kanungo, S. B.; Mishra, S. K. Thermal dehydration and decomposition of $FeCl_3 \cdot xH_2O$. *J. Therm. Anal. Calorim.* **1996**, *46*, 1487-1500. (c) Felsche, J.; Luger, S. Phases and thermal decomposition characteristics of hydro-sodalites $Na_{6+x}[AlSiO_4]_6(OH)_x \cdot nH_2O$. *Thermochim. Acta* **1987**, *118*, 35-55.

(28) (a) Nishida, H.; Takada, N.; Yoshimura, M.; Sonoda, T.; Kobayashi, H. Tetrakis[3,5-bis(trifluoromethyl)phenyl]borate. Highly Lipophilic Stable Anionic Agent for Solvent-extraction of Cations. *Bull. Chem. Soc. Jpn.* **1984**, *57*, 2600-2604. (b) Yakelis, N. A.; Bergman, R. G. Safe Preparation of Sodium Tetrakis[3,5-(trifluoromethyl)phenyl]borate ($NaBArF_{24}$): Reliable and Sensitive Analysis of Water in Solutions of Fluorinated Tetraarylborates. *Organometallics* **2005**, *24*, 3579-3581. (c) Carreras, L.; Rovira, L.; Vaquero, M.; Mon, I.; Martin, E.; Buchholz-Benet, J.; Vidal-Ferran, A. Syntheses, characterisation and solid-state study of alkali and ammonium BArF salts. *RSC Adv.* **2017**, *7*, 32833-32841.

(29) (a) Takamizawa, S.; Akatsuka, T.; Ueda, T. Gas-Conforming Transformability of an Ionic Single-Crystal Host Consisting of Discrete Charged Components. *Angew. Chem., Int. Ed.* **2008**, *47*, 1689-1692; Gas-Conforming Transformability of an Ionic Single-Crystal Host Consisting of Discrete Charged Components. *Angew. Chem.* **2008**, *120*, 1713-1716. (b) Takamizawa, S.; Kohbara, M.; Akatsuka, T.; Miyake, R. Gas-adsorbing ability of tris-ethylenediamine metal complexes (M = Co(III), Cr(III), Rh(III), Ir(III)) as transformable ionic single crystal hosts. *New J. Chem.* **2008**, *32*, 1782-1787.

(30) Hoffmann, S. K.; Hodgson, D. J.; Hatfield, W. E. Crystal Structures and Magnetic and EPR Studies of Intradimer and Interdimer Exchange Coupling in

$[M(en)_3]_2[Cu_2Cl_8]Cl_2 \cdot 2H_2O$ (M = Co, Rh, Ir) Crystals. *Inorg. Chem.* **1985**, *24*, 1194-1201.

(31) Larsen, K. P.; Hazell, R. G.; Toftlund, H.; Andersen, P. R.; Bisgård, P.; Edlund, K.; Eliasen, M.; Herskind, C.; Laursen, T.; Pedersen, P. M. The crystal structure of *trans*-Dichlorobis(ethylenediamine)-platinum(IV) Tetrachlorocuprate(II) Monohydrate. *Acta Chem. Scand.* **1975**, *A29*, 499-504.

(32) Shannon, R. D. Revised Effective Ionic Radii and Systematic Studies of Interatomic Distances in Halides and Chalcogenides. *Acta Crystallogr.* **1976**, *A32*, 751-767.

(33) Palmer, J. W.; Basolo, F. Effect of Transition Metal Ion on Rates of Hydrogen Exchange in Metal Ammines. *J. Inorg. Nucl. Chem.* **1960**, *15*, 279-286. For the original determinations involving the cations $[M(en)_3]^{n+}$ in this reference, the counter anions were not specified.

(34) Grinberg, A. A.; Gil'dengershel, K. I. О Кислотных Свойствах Аммиакатов И Аминатов Четырехвалентной Платины (Acidic Properties of Ammoniates and Aminates of Quadrivalent Platinum). *Izv. Akad. Nauk SSSR, Ser. Khim.* **1948**, 479-492.

(35) Goodall, D. M.; Hardy, M. J. Conjugate Bases of Tris(ethylenediamine)cobalt(III) and Nitropenta-ammine-cobalt(III) in Aqueous Hydroxide-Dimethyl Sulphoxide Mixtures. *J. Chem. Soc., Chem. Commun.* **1975**, *72*, 919-921.

(36) Hall, H. K., Jr. Potentiometric Determination of the Base Strengths of Amines in Non-protolytic Solvents. *J. Phys. Chem.* **1956**, *60*, 63-70.

(37) House, J. E., Jr.; Tahir, F. M. Determination of Tris(ethylenediamine)nickel(II) Chloride and Tris(ethylenediamine)platinum(IV) Chloride. *Thermochim. Acta* **1987**, *118*, 191-197.

(38) (a) Lungwitz, R.; Spange, S. A hydrogen bond accepting (HBA) scale for anions, including room temperature ionic liquids. *New. J. Chem.* **2008**, *32*, 392-394. (b) Cláudio, A. F. M.; Swift, L.; Hallett, J. P.; Welton, T.; Coutinho, J. A. P.; Freire, M. G. Extended scale for the hydrogen-bond basicity of ionic liquids. *Phys. Chem. Chem. Phys.* **2014**, *16*, 6593-6601.

(39) Girolami, G. S.; Rauchfuss, T. B.; Angelici, R. J. *Synthesis and Technique in Inorganic Chemistry: A Laboratory Manual*, 3rd ed.; University Science Books: Sausalito, CA, 1999.

(40) (a) Parmar, D.; Sugiono, E.; Raja, S.; Rueping, M. Complete Field Guide to Asymmetric BINOL-Phosphate Derived Brønsted Acid and Metal Catalysis: History and Classification by Mode of Activation; Brønsted Acidity, Hydrogen Bonding, Ion Pairing, and Metal Phosphates. *Chem. Rev.* **2014**, *114*, 9047-9153. (b) Phipps, R. J.; Hamilton, G. L.; Toste, F. D. The progression of chiral anions from concepts to applications in asymmetric catalysis. *Nat. Chem.* **2012**, *4*, 603-614.

(41) The web pages of the vendor do not indicate that the Na^+ BAr_f^- is hydrated, but the bottles received are labeled Na^+ $BAr_f^- \cdot xH_2O$. Since excess BAr_f^- can be difficult to separate from certain salts, the samples were treated as anhydrous.

(42) Cammenga, H. K.; Epple, M. Basic Principles of Thermoanalytical Techniques and Their Applications in Preparative Chemistry. *Angew. Chem., Int. Ed. Engl.* **1995**, *34*, 1171-1187; Grundlagen der Thermischen Analysetechniken und ihre Anwendungen in der präparativen Chemie. *Angew. Chem.* **1995**, *107*, 1284-1301. The T_e values best represent the temperature of a phase transition.

(43) In this complex, UV absorptions associated with BAr_f^- mask electronic transitions expected for the cation $[M(en)_3]^{3+}$.

(44) The signal intensity was reduced due to NH/ND exchange with the solvent.

(45) (a) Andrés, J. M.; Manzano, R.; Pedrosa, R. Novel Bifunctional Chiral Urea and Thiourea Derivatives as Organocatalysts: Enantioselective Nitro-Michael Reaction of Malonates and Diketones. *Chem. Eur. J.* **2008**, *114*, 5116-5119. (b) Almaşi, D.; Alonso, D. A.; Gómez-Bengoa, E.; Nájera, C. Chiral 2-Aminobenzimidazoles as Recoverable Organocatalysts for the Addition of 1,3-Dicarbonyl Compounds to Nitroalkenes. *J. Org. Chem.* **2009**, *74*, 6163-6168.

(46) (a) Saaby, S.; Bella, M.; Jørgensen, K. A. Asymmetric Construction of Quaternary Stereocenters by Direct Organocatalytic Amination of α-Substituted α-Cyanoacetates and β-Dicarbonyl Compounds. *J. Am. Chem. Soc.* **2004**, *126*, 8120-8121. (b) The chiral HPLC column used to analyze **2** featured the same stationary phase but a different particle size from that in the preceding reference. It is presumed that the well separated enantiomers exhibit identical orders of elution. Configurations were assigned accordingly.

(47) Wu, L.-L.; Li, L.-P.; Xiang, Y; Guan, Z.; He, Y.-H. Enzyme-Promoted Direct Asymmetric Michael Reaction by Using Protease from *Streptomyces griseus*. *Catal. Lett.* **2017**, *147*, 2209-2214.

(48) Kim, Y. S.; Matsunaga, S.; Das, J.; Sekine, A.; Ohshima, T.; Shibasaki, M. Stable, Storable, and Reusable Asymmetric Catalyst: A Novel La-linked-BINOL Complex for the Catalytic Asymmetric Michael Reaction. *J. Am. Chem. Soc*. **2000**, *122*, 6506-6507.

(49) Chiappe, C.; Rajamani, S.; D'Andrea, F. A dramatic effect of the ionic liquid structure in esterification reactions in protic ionic media. *Green Chem.* **2013**, *15*, 137-143.

3. CHIRAL TRICATIONIC TRIS(1,2-DIPHENYLETHYLENEDIAMINE) COBALT(III) HYDROGEN BOND DONOR CATALYSTS WITH DEFINED CARBON/METAL CONFIGURATIONS; MATCHED/MISMATCHED EFFECTS UPON ENANTIOSELECTIVITIES WITH ENANTIOMERIC CHIRAL COUNTER ANIONS†

3.1 Introduction

There has been a marked increase in interest in enantioselective catalysis using chiral organic hydrogen bond donors over the last 20 years.[1] This derives in part from widespread needs to direct the configurations of carbon stereocenters in pharmaceutical and agricultural chemicals. Our research group has been interested in developing chiral transition metal containing hydrogen bond donors,[2-5] which can provide binding motifs and modes of action that greatly differ from their organic counterparts. Several other laboratories have had parallel interests.[6-8]

Werner developed his coordination chemistry in aqueous media. However, for our purposes it was first necessary to solubilize such cobalt salts in organic solvents, so that the NH donor groups would not be saturated by hydrogen bonded water molecules. This was accomplished using lipophilic anions such as tetrakis(3,5-bis(trifluoromethyl)phenyl)borate (BAr_f^- or $B(3,5\text{-}C_6H_3(CF_3)_2)_4^-$), which is depicted in Figure 3.2.[12] All $[Co(en)_3]^{3+}$ salts investigated have been highly active catalysts, but the enantioselectivities have been modest.[4c,12] Importantly, replacing a single en ligand by

†Reprinted with permission from "Chiral Tricationic Tris(1,2-diphenylethylenediamine) Cobalt(III) Hydrogen Bond Donor Catalysts with Defined Carbon/Metal Configurations; Matched/Mismatched Effects upon Enantioselectivities with Enantiomeric Chiral Counter Anions" by Kabes, C. Q.; Maximuck, W. J.; Ghosh, S. K.; Kumar, A.; Bhuvanesh, N.; Gladysz, J. A., 2020. *ACS Catal.*, 10, 3249-3263, Copyright 2020 by the American Chemical Society.

one with an appended $(CH_2)_3NMe_2$ unit – affording a bifunctional catalyst that obviates the need for an external base – gives a highly enantioselective catalyst for additions of malonate esters to aromatic and aliphatic nitroalkenes.[3]

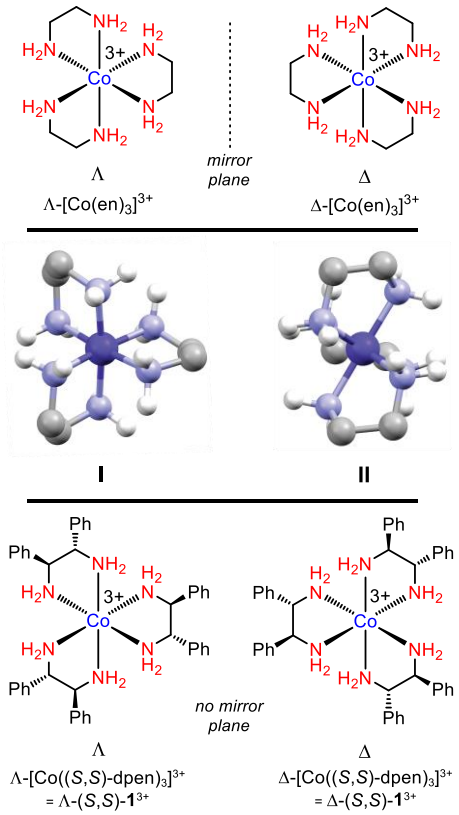

Figure 3.1. Relevant chiral cobalt tris(1,2-diamine) trications.

Highly enantioselective catalysts can also be obtained when all three en ligands are replaced by (*S*,*S*)- or (*R*,*R*)-1,2-diphenylethylenediamine, or dpen.[2,4a,b,13] Both enantiomers are commercially available at surprisingly low prices.[14] Given the greater lipophilicity of dpen versus en, salts with a single BAr_f^- anion generally have good solubilities in organic solvents.[15] An example, valid for any combination of cobalt and carbon configurations, would be $[Co(dpen)_3]^{3+}$ $2Cl^-BAr_f^-$. With this trication, it has been possible to prepare an extensive library of mixed (and non-mixed) anion salts,[15] all of

which afford slightly different enantioselectivities.[2,4a] The mechanisms of these condensations are not yet well understood. However, we have speculated that when hydrogen bond accepting anions are present, one may remain associated with the trication during the enantiomer determining step.[2,4a]

Over the last decade, there have been increasing applications of chiral anions and Brønsted acids in enantioselective catalysis.[16,17] In view of the dependence of the ee values of catalysts derived from $[Co(dpen)_3]^{3+}$ upon the counter anions, we anticipated that further optimization would be possible by incorporating chiral anions. It was thought that one enantiomer of an anion might be "matched" with respect to the cobalt/carbon configurations, leading to higher ee values, whereas the other enantiomer could be "mismatched", leading to lower ee values. Such phenomena are often observed in enantioselective transformations that involve diastereomeric combinations of two chiral reactants.[18]

In this report, we detail the syntheses of a variety of diastereomeric salts of the trication $[Co(dpen)_3]^{3+}$ – all featuring the cobalt and carbon configurations depicted in Figure 3.1 (bottom) – with the representative chiral anions in Figure 3.2.[19,20] These are subsequently evaluated as enantioselective catalysts in two typical addition reactions. Indeed, the ee values often show significant matched/mismatched relationships derived from the configurations of the anions (avg $\Delta_{\%ee} = 10$). Although these exceed those of the best catalysts with achiral anions in only a few cases, this study illustrates an underutilized approach to the optimization of "charged" enantioselective catalysts that to our knowledge has been rather infrequently investigated.[21-23]

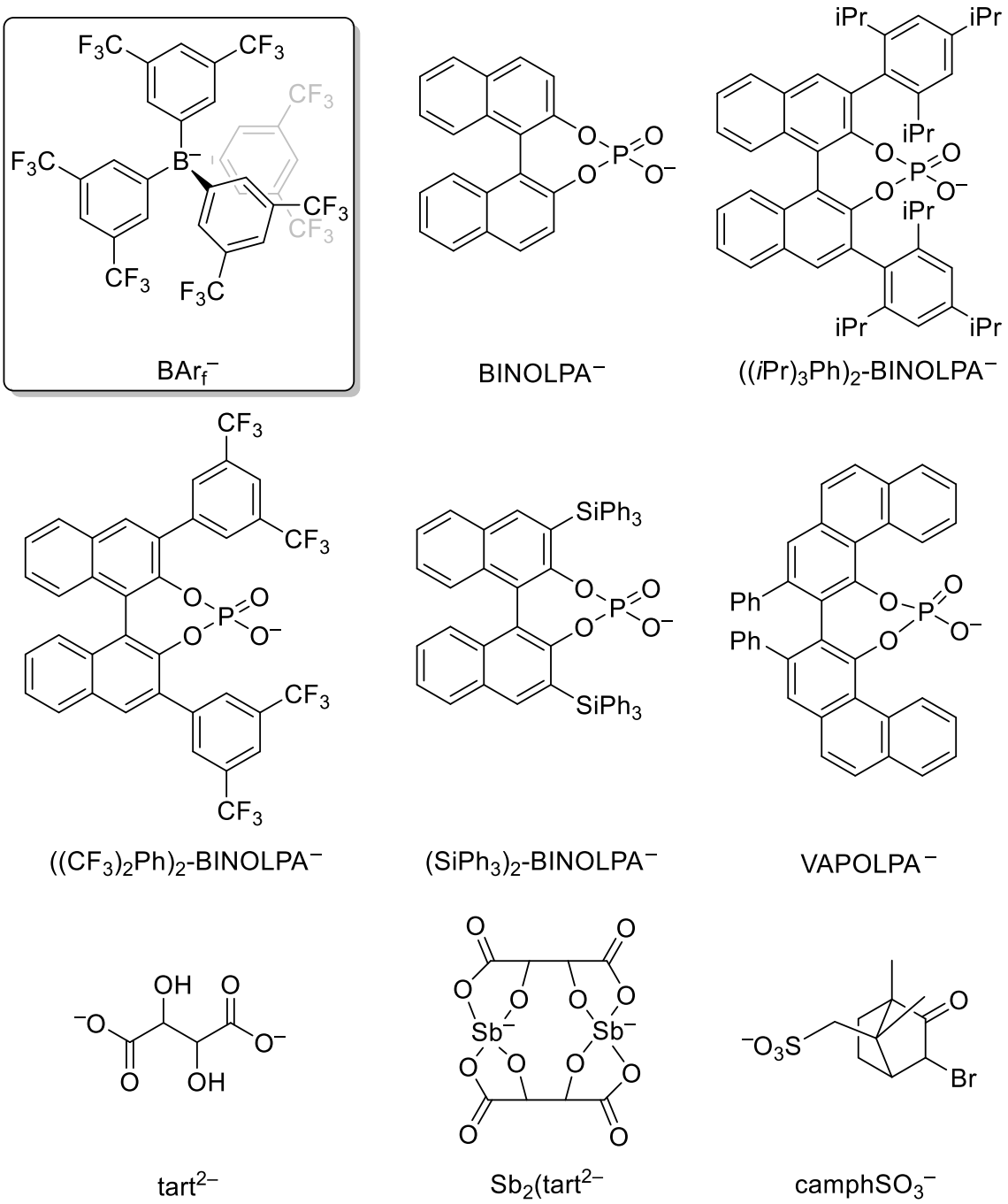

Figure 3.2. Structures of lipophilic or chiral anions used in this study and their dominant literature abbreviations. Specific configurations of the chiral anions are not depicted, as both enantiomers are generally used.

3.2 Results

3.2.1 Syntheses and characterization of catalysts

The diastereopure and enantiopure salts Λ-[Co((*S*,*S*)-dpen)$_3$]$^{3+}$ 3Cl$^-$ (Λ-(*S*,*S*)-**1**$^{3+}$ 3Cl$^-$), Λ-[Co((*S*,*S*)-dpen)$_3$]$^{3+}$ 2Cl$^-$BAr$_f$$^-$ (Λ-(*S*,*S*)-**1**$^{3+}$ 2Cl$^-$BAr$_f$$^-$), and Δ-[Co((*S*,*S*)-dpen)$_3$]$^{3+}$ 2Cl$^-$BAr$_f$$^-$ (Δ-(*S*,*S*)-**1**$^{3+}$ 2Cl$^-$BAr$_f$$^-$) were prepared according to previously reported procedures.[15] Note that the configurations of the dpen-based carbon stereocenters are kept constant (*S*,*S*), but those of the cobalt stereocenter are varied (Λ/Δ), such that both diastereomers are represented. The enantiomeric salts derived from (*R*,*R*)-dpen would be expected to give identical ee values.

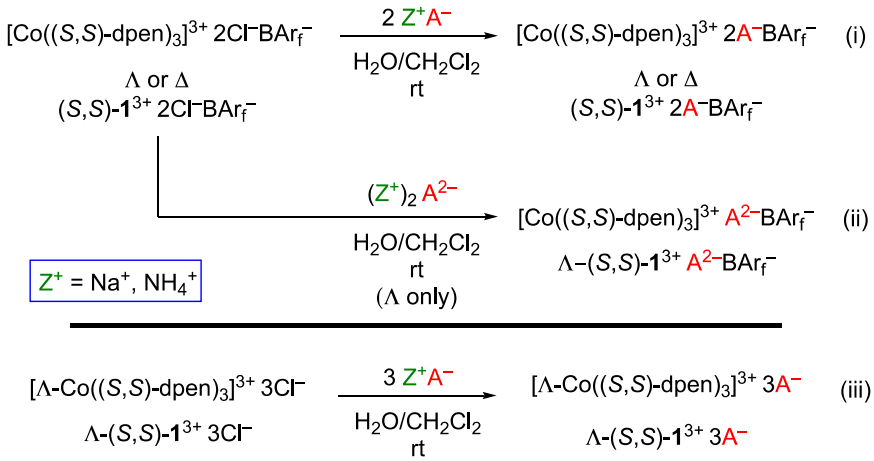

Figure 3.3. Syntheses of cobalt(III) catalysts with chiral anions (A$^-$) from Figure 3.1.

The new salts containing chiral anions were synthesized as summarized in Figure 3.3. As with other manipulations in this study, the reactions were carried out in air. In one series (eq i), Λ-(*S*,*S*)-**1**$^{3+}$ 2Cl$^-$BAr$_f$$^-$ was treated with 2.0-4.3 equiv of a sodium or ammonium salt of a chiral *mono*anion from Figure 3.2 (A$^-$; both enantiomers) in biphasic aqueous dichloromethane. Workups gave the target complexes Λ-(*S*,*S*)-**1**$^{3+}$ 2A$^-$BAr$_f$$^-$ depicted in Figure 3.5 in 44-99% yields. In several cases, diastereomeric salts with opposite cobalt configurations, Δ-(*S*,*S*)-**1**$^{3+}$ 2A$^-$BAr$_f$$^-$, were analogously prepared. With

the tartrate derived *di*anions, Λ-(*S*,*S*)-$\mathbf{1}^{3+}$ $2Cl^{-}BAr_f^{-}$ was similarly treated with 1.0-2.4 equiv of the respective salts to give Λ-(*S*,*S*)-$\mathbf{1}^{3+}$ $A^{2-}BAr_f^{-}$ in 94-99% yields (eq ii). Finally, some salts with *three* chiral monoanions, Λ-(*S*,*S*)-$\mathbf{1}^{3+}$ $3A^{-}$, were analogously prepared from Λ-(*S*,*S*)-$\mathbf{1}^{3+}$ $3Cl^{-}$ in 72-78% yields as shown in eq iii.

The new cobalt(III) salts, which are summarized in Figure 3.5 (entries 3-25), were characterized by microanalyses and NMR spectroscopy (^{1}H, ^{13}C) as detailed in the experimental section. All were soluble in dichloromethane, acetone, and acetonitrile. The camphorsulfonate salts were somewhat more lipophilic and also dissolved in THF. As also seen with salts of achiral anions (including the starting materials in Figure 3.3), the new species were isolated as hydrates. The ^{1}H NMR spectra exhibited broad OH signals, and the stoichiometry suggested by integration was usually close to that calculated from the microanalytical data. When these differed, microanalytical values were given precedence since NMR integrations can be enhanced by protic impurities. The water molecules are included in all stoichiometry and yield calculations, as given in the experimental section, but for simplicity are not represented in the graphics or main text.

As noted with salts of achiral anions earlier, the diastereotopic N**HH'** protons gave distinct NMR signals. As can be seen from **I** and **II** in Figure 3.1, one of these protons is associated with a C_3 face, and the other with a C_2 face. Earlier studies have shown that the Δδ values reflect, at least in part, the differential magnitudes of anion hydrogen bonding at the two sites (C_3 NH groups always favored as reflected by downfield chemical shifts).[2,15] Thus, one of the four diastereomers of the camphorsulfonate salts, Λ-(*S*,*S*)-$\mathbf{1}^{3+}$ 2(1*R*)-camph$SO_3^{-}BAr_f^{-}$, exhibited a much greater Δδ value than the other three (4.02 vs. 1.09-1.89 ppm). Larger differences were also found with Λ-(*S*,*S*)-$\mathbf{1}^{3+}$ (*R*,*R*)-$tart^{2-}BAr_f^{-}$ and Λ-(*S*,*S*)-$\mathbf{1}^{3+}$ (*S*,*S*)-$tart^{2-}BAr_f^{-}$, but here they were independent of the configuration of the dianion (both 3.03 ppm). The next largest differences were in the 2.54-2.42 ppm range

(two of the four diastereomeric BINOLPA$^-$ salts, and one of the VAPOLPA$^-$ salts).

Also of interest is the degree to which the other ^{1}H NMR signals differ in salts that are identical except for the configuration of the anion. To a first approximation, greater trication/anion association should yield greater differentiation. However, in most cases the Δδ values were less than 0.08 ppm (ignoring multiplets), even for the camphorsulfonate salts. Larger Δδ differences were found only with the downfield signals of the salts with enantiomeric $((CF_3)_2Ph)_2$-BINOLPA$^-$ anions (Δδ 0.17 ppm) and enantiomeric $(SiPh_3)_2$-BINOLPA$^-$ anions (Δδ 0.13 ppm).

In our experience, single crystals of $[Co(dpen)_3]^{3+}$ salts are much more difficult to obtain than for other types of metal complexes under study in our laboratory. Thus, it was a pleasant surprise when crystals of Δ-(*S*,*S*)-**1**$^{3+}$ 2(1*S*)-camphSO_3^-BAr$_f^-$ could be grown from dichloromethane. Data were collected using synchrotron radiation, and the structure was solved as outlined in Table 3.1 and the experimental section. An ORTEP representation and a partial structure that highlights hydrogen bonding interactions are provided in Figure 3.4. The latter constitutes a view down one of the idealized C_2 axes.

In the >150 published crystal structures of $[Co(en)_3]^{3+}$ salts[24] and six of $[Co(dpen)_3]^{3+}$ salts,[2,13,25] trication/anion hydrogen bonding has been of particular interest. As can be seen in Figure 3.4, each RSO_3^- moiety hydrogen bonds to an opposite C_3 face, with each of the three oxygen atoms associated with a unique N-H bond. The N<u>H</u>···<u>O</u> distances range from 1.97 to 2.13 Å (average 2.03 Å). The corresponding <u>N</u>(H)···<u>O</u> distances range from 2.865 to 3.010 Å (average 2.920 Å), with N-H···O angles of 162.0° to 169.2°. These atomic separations compare closely with those found in the corresponding ammonium salt (averages 1.94 and 2.850 Å),[26] which however exhibits a different hydrogen bonding motif (each oxygen atom associating with a different ammonium cation).

3.2.2 Enantioselective catalysis

As shown in Figure 3.5, the salts prepared in Scheme 1 were evaluated as catalysts for additions of dimethyl malonate to *trans*-β-nitrostyrene in the presence of Et_3N (1.0:1.1:1.0 mol ratio). Reactions were carried out in acetone-d_6 at 0 °C with 10 mol% of catalyst and an internal standard. After 24 h, the yield of the addition product (**2**) was determined by ^{1}H NMR versus the standard. After workup, the ee values were assayed by HPLC. As shown in entry 1, the principal starting cobalt(III) complex in Figure 3.4, Λ-(*S*,*S*)-**1**$^{3+}$ 2Cl$^-$BAr$_f^-$, gave (*R*)-**2** in 87% ee. The diastereomer Δ-(*S*,*S*)-**1**$^{3+}$ 2Cl$^-$BAr$_f^-$, which usually affords somewhat lower enantioselectivities in additions to nitroalkenes, yielded the opposite enantiomer (*S*)-**2** in 77% ee (entry 2). However, this diastereomer sometimes gives superior results for other addition reactions.[4a] Two additional salts with achiral bromide and iodide counter anions were also tested (Λ-(*S*,*S*)-**1**$^{3+}$ 2X$^-$BAr$_f^-$; entries 26-27), but these data are only analyzed in the discussion section.

Interestingly, the diastereomeric camphorsulfonate salts Λ-(*S*,*S*)-**1**$^{3+}$ 2(1*R*)-camphSO$_3^-$BAr$_f^-$ and Λ-(*S*,*S*)-**1**$^{3+}$ 2(1*S*)-camphSO$_3^-$BAr$_f^-$ (entries 3,5), which differ in the anion configuration, gave (*R*)-**2** with comparably high ee values (87%, 88%; $\Delta_{\%ee}$ = 1). When the cobalt configurations were inverted (Δ-(*S*,*S*)-**1**$^{3+}$ 2(1*R*)-camphSO$_3^-$BAr$_f^-$ or Δ-(*S*,*S*)-**1**$^{3+}$ 2(1*S*)-camphSO$_3^-$BAr$_f^-$; entries 4,6), the ee values dropped (50%, 56%; $\Delta_{\%ee}$ = 6) and the yields diminished somewhat (69-82% versus 94-84%). Also the dominant enantiomer was now (*S*)-**2**, showing that the cobalt configuration of the catalyst controls the carbon configuration of the product.

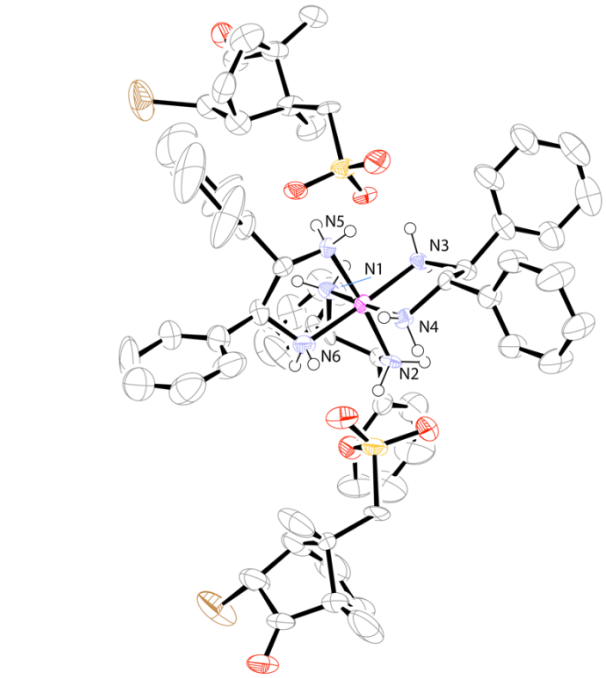

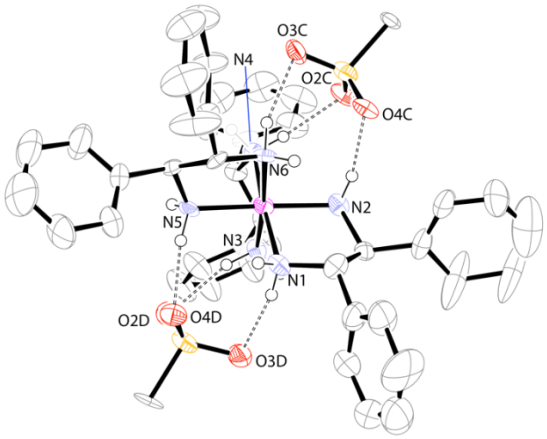

Figure 3.4. Top: Molecular structure of Δ-(*S*,*S*)-**1**$^{3+}$ 2(1*S*)-camphSO$_3^-$BAr$_f^-$ with the large BAr$_f^-$ anion omitted; the ellipsoids are depicted at the 50% probability level. Bottom: A view of hydrogen bonding between the NH and RSO$_3^-$ groups. Bond lengths (Å) and angles (°) about cobalt: Co(1)-N(1), 1.986(7); Co(1)-N(2), 1.985(5); Co(1)-N(3), 1.957(7); Co(1)-N(4), 1.976(7); Co(1)-N(5), 1.983(8); Co(1)-N(6), 1.986(8); N(1)-Co(1)-N(2), 83.0(3); N(1)-Co(1)-N(3), 92.2(3); N(1)-Co(1)-N(4), 174.2(3); N(1)-Co(1)-N(5), 93.9(3); N(1)-Co(1)-N(6), 90.8(3); N(2)-Co(1)-N(3), 92.2(3); N(2)-Co(1)-N(4), 92.9(3); N(2)-Co(1)-N(5), 174.5(3); N(3)-Co(1)-N(4), 83.7(3); N(3)-Co(1)-N(5), 92.5(3); N(3)-Co(1)-N(6), 175.1(3); N(4)-Co(1)-N(5), 90.5(3); N(4)-Co(1)-N(6), 93.6(3); N(5)-Co(1)-N(6), 83.5(3). Angles and distances relevant to hydrogen bonding: O(2C)···H(4B), 2.05; O(3C)···H(6B), 2.01; O(4C)···H(2B), 1.97; O(2D)···H(3B), 2.01; O(3D)···H(1B), 2.13; O(4D)···H(5B), 2.02; O(2C)···N(4), 2.936; O(3C)···N(6), 2.907; O(4C)···N(2), 2.865; O(2D)···N(3), 2.895; O(3D)···N(1), 3.010; O(4D)···N(5), 2.910; O(2C)···H(4B)-N(4), 162.8; O(3C)···H(6B)-N(6), 168.0; O(4C)···H(2B)-N(2), 169.2; O(2D)···H(3B)-N(3), 163.9; O(3D)···H(1B)-N(1), 162.0; O(4D)···H(5B)-N(5), 166.2.

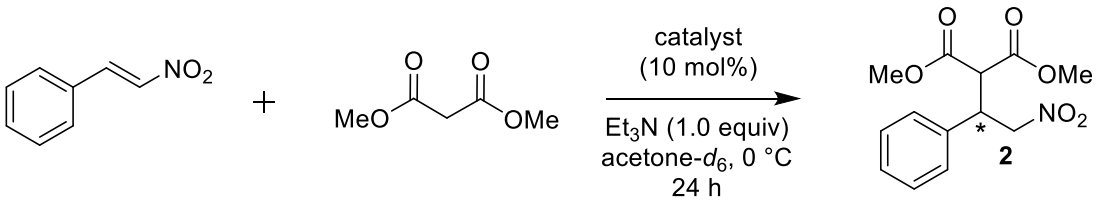

entry	catalyst	ee (%) (config)	yield (%)[a]
1[b]	Λ-(*S*,*S*)-**1**$^{3+}$ 2Cl^{-}BAr$_f^-$	87 (*R*)	93
2[c]	Δ-(*S*,*S*)-**1**$^{3+}$ 2Cl^{-}BAr$_f^-$	77 (*S*)	95
3	Λ-(*S*,*S*)-**1**$^{3+}$ 2(1*R*)-camphSO$_3^-$BAr$_f^-$	87 (*R*)	94
4	Δ-(*S*,*S*)-**1**$^{3+}$ 2(1*R*)-camphSO$_3^-$BAr$_f^-$	50 (*S*)	69
5	Λ-(*S*,*S*)-**1**$^{3+}$ 2(1*S*)-camphSO$_3^-$BAr$_f^-$	88 (*R*)	84
6	Δ-(*S*,*S*)-**1**$^{3+}$ 2(1*S*)-camphSO$_3^-$BAr$_f^-$	56 (*S*)	82
7	Λ-(*S*,*S*)-**1**$^{3+}$ 2(*R*)-BINOLPA$^-$BAr$_f^-$	88 (*R*)	73
8	Δ-(*S*,*S*)-**1**$^{3+}$ 2(*R*)-BINOLPA$^-$BAr$_f^-$	73 (*S*)	96
9	Λ-(*S*,*S*)-**1**$^{3+}$ 2(*S*)-BINOLPA$^-$BAr$_f^-$	85 (*R*)	75
10	Δ-(*S*,*S*)-**1**$^{3+}$ 2(*S*)-BINOLPA$^-$BAr$_f^-$	71 (*S*)	>99
11	Λ-(*S*,*S*)-**1**$^{3+}$ 2(*R*)-VAPOLPA$^-$BAr$_f^-$	87 (*R*)	>99
12	Λ-(*S*,*S*)-**1**$^{3+}$ 2(*S*)-VAPOLPA$^-$BAr$_f^-$	65 (*R*)	99
13	Λ-(*S*,*S*)-**1**$^{3+}$ 2(*R*)-((CF$_3$)$_2$Ph)$_2$-BINOLPA$^-$ BAr$_f^-$	88 (*R*)	>99
14	Λ-(*S*,*S*)-**1**$^{3+}$ 2(*S*)-((CF$_3$)$_2$Ph)$_2$-BINOLPA$^-$ BAr$_f^-$	84 (*R*)	>99
15	Λ-(*S*,*S*)-**1**$^{3+}$ 2(*R*)-(SiPh$_3$)$_2$-BINOLPA$^-$ BAr$_f^-$	75 (*R*)	>99
16	Λ-(*S*,*S*)-**1**$^{3+}$ 2(*S*)-(SiPh$_3$)$_2$-BINOLPA$^-$ BAr$_f^-$	79 (*R*)	>99
17	Λ-(*S*,*S*)-**1**$^{3+}$ 2(*S*)-((*i*Pr)$_3$Ph)$_2$-BINOLPA$^-$ BAr$_f^-$	78 (*R*)	>99
18	Λ-(*S*,*S*)-**1**$^{3+}$ (*R*,*R*)-tart^{2-}BAr$_f^-$	85 (*R*)	81
19	Λ-(*S*,*S*)-**1**$^{3+}$ (*S*,*S*)-tart^{2-}BAr$_f^-$	80 (*R*)	88
20	Λ-(*S*,*S*)-**1**$^{3+}$ (Sb$_2$((*R*,*R*)-tart')$_2$)$^{2-}$BAr$_f^-$	87 (*R*)	98
21	Λ-(*S*,*S*)-**1**$^{3+}$ (Sb$_2$((*S*,*S*)-tart')$_2$)$^{2-}$BAr$_f^-$	88 (*R*)	93
22	Λ-(*S*,*S*)-**1**$^{3+}$ 3(1*R*)-camphSO$_3^-$	67 (*R*)	72
23	Λ-(*S*,*S*)-**1**$^{3+}$ 3(1*S*)-camphSO$_3^-$	75 (*R*)[d]	78
24	Λ-(*S*,*S*)-**1**$^{3+}$ 3(*S*)-BINOLPA$^-$	79 (*R*)	86
25	Λ-(*S*,*S*)-**1**$^{3+}$ 3(*R*)-BINOLPA$^-$	75 (*R*)	87
26	Λ-(*S*,*S*)-**1**$^{3+}$ 2Br$^-$BAr$_f^-$	83 (*R*)	95
27	Λ-(*S*,*S*)-**1**$^{3+}$ 2I$^-$BAr$_f^-$	77 (*R*)	97

[a]Yields were determined by ^{1}H NMR relative to the internal standard Ph_2SiMe_2 per the experimental section. [b]These results agree with those reported earlier for an identical reaction (reference 2). [c]A 40% ee was found earlier for the corresponding reaction in CD_2Cl_2 (reference 2). [d]The ee values for analogous reactions in CD_2Cl_2 and CD_3CN were 70% and 73%, respectively.

Figure 3.5. Enantioselective additions of dimethyl malonate to *trans*-β-nitrostyrene.

Four diastereomeric BINOLPA$^-$ salts were analogously assayed as catalysts (entries 7-10). Again, the two Λ diastereomers gave similarly high ee values (88%, 85%). The two Δ diastereomers gave lower ee values (73%, 71%), but higher than those of the corresponding camphorsulfonate salts. These differences (entries 4,6 versus 8,10) underscore the important but still ill-defined role that the counter anions play in determining enantioselectivities. Furthermore, it is clear that *all* of the salts of the Δ diastereomers with chiral anions give ee values lower than that of the parent salt with achiral anions, Δ-(*S*,*S*)-**1**$^{3+}$ 2Cl$^-$BAr$_f^-$ (entries 2, 77% ee, versus 4,6,8,10, 50-73% ee). In other words, in the Δ-(*S*,*S*) series, all combinations of trication/anion configurations are "mismatched" relative to Δ-(*S*,*S*)-**1**$^{3+}$ 2Cl$^-$BAr$_f^-$.

Salts of three substituted BINOLPA$^-$ anions and VAPOLPA$^-$, a related biphenanthryl species (Figure 3.2), were also evaluated. However, in view of the data in entries 3-10, and the greater expense of these anions, efforts were restricted to Λ diastereomers. As shown in entries 13-14, the fluorinated BINOLPA$^-$ derivatives gave ee values very close to those of the parent BINOLPA$^-$ salts (88% and 84% versus 88% and 85% in entries 7,9). However, the others were not as effective. With the VAPOLA$^-$ salts, there was a particularly large difference in enantioselectivities between diastereomers with opposite anion configurations (entries 11-12, 87% versus 65% ee; $\Delta_{\%ee}$ 22).

Studies of salts of dianions or three chiral monoanions were also limited to Λ diastereomers. As shown in entries 18-21, the two types of tartrate containing catalysts gave ee values that only slightly depended upon the configuration of the anions ($\Delta_{\%ee}$ 1-5). Somewhat greater but still modest differences were found with the tris(camphorsulfonate) and tris(BINOLPA$^-$) salts in entries 22-25. Nonetheless, entries 22 and 23 provide the second highest $\Delta_{\%ee}$ among pairs of salts with opposite anion configurations (67% versus 75% ee). Throughout Figure 3.5, the anion configuration has

no effect on the dominant configuration of **2** (i.e., the product configuration is controlled by that of the trication).

As shown in Figure 3.6, the same cobalt(III) salts were evaluated as catalysts for additions of methyl 2-oxocyclopentanecarboxylate to di-*tert*-butylazodicarboxylate in the presence of N-methylmorpholine (NMM; 1.0:1.0:1.0 mol ratio). Reactions were carried out in CD_3CN at 0 °C with 10 mol% of catalyst and an internal standard. Yields and enantioselectivities of the addition product (**3**) were determined as in Figure 3.5. As shown in entry 1, the principal starting cobalt(III) complex in Scheme 1, Λ-(*S*,*S*)-$\mathbf{1}^{3+}$ $2Cl^-BAr_f^-$, gave (*S*)-**3** in 76% ee. The diastereomer Δ-(*S*,*S*)-$\mathbf{1}^{3+}$ $2Cl^-BAr_f^-$, which usually affords somewhat higher enantioselectivities in additions to di-*tert*-butylazodicarboxylate,[4a] gave the opposite enantiomer (*R*)-**3** in 92% ee (entry 2). Salts that feature the perfluorinated tetraarylborate $B(C_6F_5)_4^-$ in place of BAr_f^- can give slightly higher ee values.[4a] However, since our primary interest was in assaying the effects of counter anion configurations, we proceeded with BAr_f^- salts as in Figure 3.5.

The diastereomeric camphorsulfonate salts Λ-(*S*,*S*)-$\mathbf{1}^{3+}$ 2(1*R*)-camph$SO_3^-BAr_f^-$ and Λ-(*S*,*S*)-$\mathbf{1}^{3+}$ 2(1*S*)-camph$SO_3^-BAr_f^-$ (entries 3,5), which differ only in the anion configuration, gave (*S*)-**3** with comparable ee values (68%, 67%). When the cobalt configurations were inverted (Δ-(*S*,*S*)-$\mathbf{1}^{3+}$ 2(1*R*)-camph$SO_3^-BAr_f^-$ or Δ-(*S*,*S*)-$\mathbf{1}^{3+}$ 2(1*S*)-camph$SO_3^-BAr_f^-$; entries 4,6), the ee values dropped slightly (66%, 62%; (*R*)-**3** dominant), per the pattern in Figure 3.5. However, the lower enantioselectivities for the Δ diastereomers are opposite to the trend in entries 1-2 of Figure 3.6.

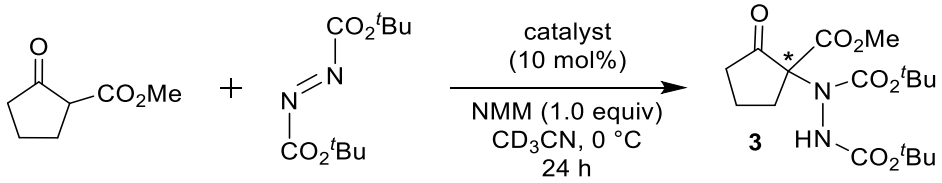

entry	catalyst	ee (%) (config)	yield (%)[a]
1[b]	Λ-(*S*,*S*)-**1**$^{3+}$ 2Cl^{-}BAr$_f^{-}$	76 (*S*)	98
2[c]	Δ-(*S*,*S*)-**1**$^{3+}$ 2Cl^{-}BAr$_f^{-}$	92 (*R*)	99
3	Λ-(*S*,*S*)-**1**$^{3+}$ 2(1*R*)-camphSO$_3^{-}$BAr$_f^{-}$	68 (*S*)	99
4	Δ-(*S*,*S*)-**1**$^{3+}$ 2(1*R*)-camphSO$_3^{-}$BAr$_f^{-}$	66 (*R*)	86
5	Λ-(*S*,*S*)-**1**$^{3+}$ 2(1*S*)-camphSO$_3^{-}$BAr$_f^{-}$	67 (*S*)	86
6	Δ-(*S*,*S*)-**1**$^{3+}$ 2(1*S*)-camphSO$_3^{-}$BAr$_f^{-}$	62 (*R*)	89
7	Λ-(*S*,*S*)-**1**$^{3+}$ 2(*R*)-BINOLPA^{-}BAr$_f^{-}$	57 (*S*)	89
8	Δ-(*S*,*S*)-**1**$^{3+}$ 2(*R*)-BINOLPA^{-}BAr$_f^{-}$	92 (*R*)	89
9	Λ-(*S*,*S*)-**1**$^{3+}$ 2(*S*)-BINOLPA^{-}BAr$_f^{-}$	64 (*S*)	90
10	Δ-(*S*,*S*)-**1**$^{3+}$ 2(*S*)-BINOLPA^{-}BAr$_f^{-}$	81 (*R*)	91
11	Λ-(*S*,*S*)-**1**$^{3+}$ 2(*R*)-VAPOLPA^{-}BAr$_f^{-}$	73 (*S*)	89
12	Λ-(*S*,*S*)-**1**$^{3+}$ 2(*S*)-VAPOLPA^{-}BAr$_f^{-}$	54 (*S*)	80
13	Λ-(*S*,*S*)-**1**$^{3+}$ 2(*R*)-((CF$_3$)$_2$Ph)$_2$-BINOLPA^{-}BAr$_f^{-}$	69 (*S*)	91
14	Λ-(*S*,*S*)-**1**$^{3+}$ 2(*S*)-((CF$_3$)$_2$Ph)$_2$-BINOLPA^{-}BAr$_f^{-}$	77 (*S*)	88
15	Λ-(*S*,*S*)-**1**$^{3+}$ 2(*R*)-(SiPh$_3$)$_2$-BINOLPA^{-}BAr$_f^{-}$	83 (*S*)	92
16	Λ-(*S*,*S*)-**1**$^{3+}$ 2(*S*)-(SiPh$_3$)$_2$-BINOLPA^{-}BAr$_f^{-}$	20 (*S*)	87
17	Λ-(*S*,*S*)-**1**$^{3+}$ 2(*S*)-((*i*Pr)$_3$Ph)$_2$-BINOLPA^{-}BAr$_f^{-}$	63 (*S*)	23
18	Λ-(*S*,*S*)-**1**$^{3+}$ (*R*,*R*)-tart^{2-}BAr$_f^{-}$	73 (*S*)	98
19	Λ-(*S*,*S*)-**1**$^{3+}$ (*S*,*S*)-tart^{2-}BAr$_f^{-}$	66 (*S*)	>99
20	Λ-(*S*,*S*)-**1**$^{3+}$ (Sb$_2$((*R*,*R*)-tart')$_2$)$^{2-}$BAr$_f^{-}$	70 (*S*)	89
21	Λ-(*S*,*S*)-**1**$^{3+}$ (Sb$_2$((*S*,*S*)-tart')$_2$)$^{2-}$BAr$_f^{-}$	67 (*S*)	92
22	Λ-(*S*,*S*)-**1**$^{3+}$ 3(1*R*)-camphSO$_3^{-}$	40 (*S*)	94
23	Λ-(*S*,*S*)-**1**$^{3+}$ 3(1*S*)-camphSO$_3^{-}$	48 (*S*)	91
24	Λ-(*S*,*S*)-**1**$^{3+}$ 3(*S*)-BINOLPA^{-}	58 (*S*)	94
25	Λ-(*S*,*S*)-**1**$^{3+}$ 3(*R*)-BINOLPA^{-}	25 (*S*)	95
26	Λ-(*S*,*S*)-**1**$^{3+}$ 2Br^{-}BAr$_f^{-}$	71 (*S*)	99
27	Λ-(*S*,*S*)-**1**$^{3+}$ 2I^{-}BAr$_f^{-}$	71 (*S*)	99

[a]Yields were determined by ^{1}H NMR relative to the internal standard Ph_2SiMe_2 per the experimental section. [b]A 76% ee was found earlier for the corresponding reaction in CD_2Cl_2 at room temperature (reference 4b). [c]A 91% ee was found earlier for the corresponding reaction with Δ-(*S*,*S*)-**1**$^{3+}$ 2Cl^{-}B(C$_6$F$_5$)$_4^{-}$.

Figure 3.6. Enantioselective additions of methyl 2-oxocyclopentane-1-carboxylate to di-*tert*-butyl azodicarboxylate.

The four diastereomeric BINOLPA$^-$ salts were analogously assayed as catalysts (entries 7-10). The two Λ diastereomers gave ee values of 57% and 64%. Now, in line with entries 1-2, the two Δ diastereomers afforded higher ee values, 92% and 81%. Furthermore, in both diastereomer series there is a significant dependence upon the anion configuration ($\Delta_{\%ee}$ 7-11).

The salts of the Λ diastereomers with substituted BINOLPA$^-$ anions and VAPOLPA$^-$ demonstrate the potential for matched and mismatched trication/anion chiralities. The difference between the ee values in entries 13-14 (69%, 77%; $\Delta_{\%ee}$ 8) is moderate, but that for entries 11-12 (73%, 54%; $\Delta_{\%ee}$ 19) is substantial and that for entries 15-16 (83%, 20%; $\Delta_{\%ee}$ 63) is huge. Also, in the last case the ee value significantly exceeds that of the benchmark catalyst with achiral chloride anions (83% versus 76% for entry 1).

As shown in entries 18-21, the two types of tartrate containing catalysts gave ee values that only moderately depended upon the configuration of the anions (73% versus 66% and 70% versus 67%; $\Delta_{\%ee}$ 7 and 3). However, the differences became large again for the tris(BINOLPA$^-$) salts (entries 24-25, 58% versus 25% ee; $\Delta_{\%ee}$ 33). In parallel to Figure 3.5, in no case did the anion configuration affect the dominant configuration of the addition product **3**.

3.3 Discussion

The syntheses of the new $[Co(dpen)_3]^{3+}$ salts (Figure 3.3) and their NMR properties generally parallel those of analogs with achiral anions reported earlier.[2,15] The complexes derived from tartrate or deprotonated tartrate[19a] (entries 18-21, Figures 3.5 and 3.6) represent the first $[Co(dpen)_3]^{3+}$ salts of dianions. However, Werner's original resolution of $[Co(en)_3]^{3+}$ also involved diastereomeric tartrate salts.[9e]

The crystal structure of Δ-(*S*,*S*)-**1**$^{3+}$ 2(1*S*)-camphSO$_3^-$BAr$_f^-$ (Figure 3.4)

represents the first for a "mixed salt" of $[Co(dpen)_3]^{3+}$. Trichloride,[2] triiodide,[13] and tris(nitrate) salts[25] have been crystallographically characterized previously. The new structure provides a welcome validation of our many earlier claims of mixed salts in this series of compounds.[2,15] Although our NMR and chromatographic evidence was compelling, there are cases where a species assigned as a mixed salt was later shown to be a mixture of two non-mixed salts.

The most striking feature of the crystal structure is the hydrogen bonding pattern. As noted above, the three roughly synperiplanar N-H units on each C_3 face hydrogen bond to separate oxygen atoms of the RSO_3^- moieties. According to a recent analysis, this can be classified as a $[C_3,C_3,C_3][3]$ trication/anion interaction.[24] In the arsenate salt $[Co(en)_3]^{3+}$ AsO_4^{3-}, three oxygen atoms of the tetrahedral trianion similarly bind a C_3 face.[27] The enhanced lipophilicities noted for all of the diastereomeric camphorsulfonate salts suggest that some RSO_3^-/H-N hydrogen bonding is maintained in solution. Although BAr_f^- is one of the feeblest hydrogen bond accepting anions,[28,29] there are a few F/HC and F/HN van der Waals contacts in the crystal (2.62, 2.65, 2.45 Å). However, the distances are much greater than those of the hydrogen bonds in Figure 3.4.

The trication also crystallizes in what is termed an ob_3 orientation.[11] When the structure is viewed down the C_3 axis (as in the graphical abstract), the three N**C**-**C**N bonds lie roughly in a perpendicular plane (that of the paper). As detailed elsewhere, this follows from the relative cobalt and dpen configurations (Δ/*S*,*S*).[11] In the case of the opposite diastereomer (e.g., Δ/*R*,*R*), the N**C**-**C**N bonds preferentially align parallel to the C_3 axis, in what is termed a lel_3 orientation.

The diastereomeric tartrate salts of $[Co(en)_3]^{3+}$ originally prepared by Werner have been extensively studied, and not surprisingly, their association constants differ.[20a,30] Analyses of the crystal structures, and those of the diastereomeric tris(*trans*-

1,2-cyclohexanediamine) analogs,[31] reveal a number of features that promote stronger hydrogen bonding and/or enhanced stabilities for certain chirality combinations. These phenomena can be viewed in the context of matched/mismatched trication/anion chiral recognition, and made us optimistic that there would be conceptually related rate driven effects on product enantioselectivities when similar species were used as asymmetric catalysts.

Indeed, the many pairs of diastereomeric catalysts in Figures 3.5 and 3.6 (entries 3-25) generally give different enantioselectivities. In a few cases, the differences are substantial (entries 11-12, Figures 3.5 and 3.6; entries 15-16, Figure 3.6), amounting to $\Delta_{\%ee}$ of 19-63, but most are moderate, in the range of $\Delta_{\%ee}$ of 3-8. From a statistical viewpoint, the average/high/median $\Delta_{\%ee}$ values in Figures 3.5 and 3.6 are 5/22/4 and 15/63/8, respectively, or in aggregate 10/63/6. Nonetheless, only in the case of Λ-(*S*,*S*)-$\mathbf{1}^{3+}$ 2(*R*)-$(SiPh_3)_2$-BINOLPA$^-$$BAr_f^-$ (entry 15, Figure 3.6) is there an appreciable improvement over the enantioselectivity of the benchmark catalyst with achiral anions, Λ-(*S*,*S*)-$\mathbf{1}^{3+}$ 2Cl$^-$$BAr_f^-$ (83% ee versus 76% ee).

In this context, it would be naive to expect or imply that the ee values for diastereomeric catalysts with different anion configurations should be symmetrically distributed about the ee value for any related catalyst with achiral anions. As shown in entries 26 and 27 of Figure 3.5, the bromide and iodide salts Λ-(*S*,*S*)-$\mathbf{1}^{3+}$ 2Br$^-$$BAr_f^-$ and Λ-(*S*,*S*)-$\mathbf{1}^{3+}$ 2I$^-$$BAr_f^-$ give lower enantioselectivities than the chloride salt (83% and 77% ee versus 87% ee). Relative to these values, one diastereomer of most of the salts with opposite anion configurations shows an improvement. A reviewer of the manuscript corresponding to this dissertation chapter[32] has also questioned whether (1) the chiral anions directly affect product formation, or (2) the differing levels of hydrogen bonding in the diastereomeric salts are largely responsible for the observed $\Delta_{\%ee}$ values.

Computational studies along these lines are in progress.[33,34]

Another approach to catalyst optimization would be to replace the phenyl groups of $[Co(dpen)_3]^{3+}$ with other types of aryl groups. Indeed, dozens of such species have been prepared in our laboratory and representative examples reported.[15] However, in a series of experiments conducted with $2Cl^{-}BAr_f^{-}$ salts and the test reaction in Figure 3.5, none of these afforded the addition product **2** with significantly higher enantioselectivities. In many cases, the ee values diminished. Thus, two independent approaches to catalyst optimization have not been very productive, although it remains possible that introducing chiral anions into catalysts with other types of aryl groups may still give substantial improvements.

In summary, this study has greatly expanded the range and numbers of chiral cobalt(III) hydrogen bond donor catalysts that can be applied in enantioselective synthesis, specifically by the incorporation of chiral anions. The motivating thesis regarding "matched" and "mismatched" pairings of trication and anion configurations could be successfully established, as reflected by the significant average/median $\Delta_{\%ee}$ values (10/6). However, the performance of the matched systems only occasionally exceeds those of a benchmark catalyst with achiral $2Cl^{-}BAr_f^{-}$ anions. Nonetheless, this illustrates a seldom employed approach to the optimization of enantioselective catalysts[21-23] – and one of a very few involving isolated salts[21] – that could be spectacularly successful in other cases. Additional strategies for optimizing and enhancing the efficacy of this catalyst family are under study and will be described in future reports.

3.4 Experimental section

General data. All operations were carried out under ambient (air) atmospheres. NMR spectra were recorded on standard FT spectrometers at ambient probe temperatures. Chemical shifts (δ/ppm) were referenced to solvent signals (^{1}H: acetone-d_5, 2.05;

CHD_2CN, 1.94; ^{13}C: acetone-d_6, 29.8; CD_3CN, 1.32). Microanalyses were conducted by Atlantic Microlab. HPLC analyses employed a Shimadzu instrument package (pump/autosampler/detector LC-20AD/SIL-20A /SPD-M20A). Reaction, HPLC, and deuterated solvents as well as the educts and bases in Figures 3.5 and 3.6 were used as received from common commercial sources (generally given in previous reports).[2,4a] Chiral anions or their precursors were used as received from the following sources: (1*R*)- and (1*S*)-ammonium 3-bromocamphor-8-sulfonate, 2 × Alfa Aesar (98%); (*R*)- and (*S*)-1,1'-binaphthyl-2,2'-diyl hydrogenphosphate, 2 × Chem-Impex International, Inc. (≥99%); (*R*)- and (*S*)-VAPOL hydrogenphosphate and (*R*)- and (*S*)-3,3'-bis(triphenylsilyl)-1,1'-binapthyl-2,2'-diyl hydrogenphosphate, 4 × Santa Cruz Biotechnology; (*S*)-3,3'-bis(triphenylsilyl)-1,1'-binapthyl-2,2'-diyl hydrogenphosphate, Sigma-Aldrich (96%); (*R*)- and (*S*)-3,3'-bis(3,5-trifluoromethyl)-1,1'-binapthyl-2,2'-diyl hydrogenphosphate and (*S*)-3,3'-bis(2,4,6-triisopropylphenyl)-1,1'-binapthyl-2,2'-diyl hydrogenphosphate, 3 × Strem (98%); (*R*,*R*)-tart$^{2-}\cdot 2H_2O$, Alfa Aesar (99%); (*S,S*)-tartaric acid, Sigma-Aldrich (99%). The catalysts or catalyst precursors Λ-(*S*,*S*)-**1**$^{3+}$ 2Cl$^-$BAr$_f^-\cdot 2H_2O$,[15] Δ-(*S*,*S*)-**1**$^{3+}$ 2Cl$^-$BAr$_f^-\cdot H_2O$,[15] Λ-(*S*,*S*)-**1**$^{3+}$ 3Cl$^-\cdot 3H_2O$,[15] and Λ-(*S*,*S*)-**1**$^{3+}$ 2I$^-$BAr$_f^-\cdot 0.5H_2O$[13] were prepared as described previously.

Λ-[Co((*S*,*S*)-dpen)$_3$]$^{3+}$ 2(1*R*)-camphSO$_3^-$BAr$_f^-$ (Λ-(*S*,*S*)-1^{3+} 2(1*R*)-camphSO$_3^-$BAr$_f^-$). A round bottom flask was charged with a solution of Λ-(*S*,*S*)-**1**$^{3+}$ 2Cl$^-$BAr$_f^-\cdot 2H_2O$ (0.0520 g, 0.0312 mmol) in CH_2Cl_2 (5 mL). A solution of (1*R*)-ammonium 3-bromocamphor-8-sulfonate (0.0420 g, 0.128 mmol, 4.3 equiv) in distilled H_2O (5 mL) was added. The biphasic mixture was vigorously stirred. After 1 h, the aqueous phase was removed and the orange organic phase was washed with distilled H_2O (2 × 5 mL). The solvent was removed by rotary evaporation. The residue was dried by oil pump vacuum (rt, overnight) to give Λ-(*S*,*S*)-**1**$^{3+}$ 2(1*R*)-camphSO$_3^-$BAr$_f^-\cdot H_2O$ as a bright

orange solid (0.0586 g, 0.0267 mmol, 87%), mp 151-155 °C (dec, open capillary). Anal. Calcd. for $C_{94}H_{88}BBr_2CoF_{24}N_6O_8S_2 \cdot H_2O$ (2197.40): C 51.38, H 4.13, N, 3.82; found C 51.10, H 4.25, N 3.75.

NMR (acetone-d_6, δ/ppm): ^{1}H (400 MHz) BAr_f^- at 7.79 (s, 8H, *o*), 7.67 (s, 4H, *p*); dpen at 7.60-7.56 (m, 12H, *o*-Ph), 7.40-7.26 (m, 24H, *m*-, *p*-Ph, N**H**H'), 5.42 (br s, 6H, NH**H'**), 5.10 (s, 6H, C**H**NH_2); 2.83 (s, 3H, $\mathbf{H}_2O$); camphSO_3^- at 4.82 (d, J = 4.3 Hz, 2H), 3.23 (d, J = 15.1 Hz, 2H), 3.13 (t, J = 4.2 Hz, 2H), 2.81-2.77 (m, 2H), 2.28-2.16 (m, 2H), 2.12-2.07 (m, 2H), 1.87-1.77 (m, 2H), 1.37 (ddd, J = 14.5, 9.4, 5.5 Hz, 2H), 1.29 (s, 6H), 0.95 (s, 6H); ^{13}C{^{1}H} (100 MHz) BAr_f^- at 162.6 (q, $^1J_{BC}$ = 49.8 Hz, *i*), 135.5 (s, *o*), 130.0 (m, *m*), 125.4 (q, $^1J_{CF}$ = 274.0 Hz, **C**F_3), 118.4 (s, *p*); dpen at 136.8 (s, *i*-Ph), 130.0, 129.7 (2 × s, *o*-, *m*-, *p*-Ph), 63.4 (s, **C**HNH_2); camphSO_3^- at 211.3, 60.0, 54.9, 54.5, 48.3, 47.9, 30.7, 22.9, 18.0, 10.0 (10 × s).

Δ-(*S*,*S*)-$\mathbf{1}^{3+}$ 2(1*R*)-camph$\mathbf{SO_3^-}$$\mathbf{BAr_f^-}$. Δ-(*S*,*S*)-$\mathbf{1}^{3+}$ $2Cl^-BAr_f^- \cdot H_2O$ (0.3295 g, 0.2002 mmol), CH_2Cl_2 (10 mL), (1*R*)-ammonium 3-bromocamphor-8-sulfonate (0.2624 g, 0.7987 mmol, 4.0 equiv), and distilled H_2O (10 mL) were combined in a procedure analogous to that for Λ-(*S*,*S*)-$\mathbf{1}^{3+}$ 2(1*R*)-camph$SO_3^-BAr_f^-$. An identical workup gave Δ-(*S*,*S*)-$\mathbf{1}^{3+}$ 2(1*R*)-camph$SO_3^-BAr_f^- \cdot H_2O$ as a bright orange solid (0.383 g, 0.174 mmol, 87%), mp 176-182 °C (dec, open capillary). Anal. Calcd. for $C_{94}H_{88}BBr_2CoF_{24}N_6O_8S_2 \cdot H_2O$ (2197.40): C 51.38, H 4.13, N, 3.82; found C 51.25, H 4.24, N 3.91.

NMR (acetone-d_6, δ/ppm): ^{1}H (500 MHz) BAr_f^- at 7.79 (s, 8H, *o*), 7.68 (s, 4H, *p*); dpen at 7.55-7.42 (m, 12H, *o*-Ph), 7.34-7.17 (m, 18H, *m*-, *p*-Ph), 7.04 (s, 6H, N**H**H'), 5.95 (d, $^3J_{HH}$ = 11.0 Hz, 6H, NH**H'**), 5.19 (br s, 6H, C**H**NH_2); 2.95 (br s, 6H, $\mathbf{H}_2O$); camphSO_3^- at 4.68 (d, $^3J_{HH}$ = 4.0 Hz, 2H), 3.11 (d, $^2J_{HH}$ = 14.5 Hz, 2H), 3.00-2.97 (m, 2H), 2.67 (d, $^2J_{HH}$ = 14.5 Hz, 2H), 2.29-2.19 (m, 2H), 2.13-2.07 (m, 2H), 1.87-1.75 (m,

2H), 1.42-1.33 (m, 2H), 1.29 (s, 6H), 0.99-0.82 (m, 6H); $^{13}C\{^{1}H\}$ (100 MHz) BAr_f^- at 162.5 (q, $^{1}J_{BC}$ = 50.0 Hz, *i*), 135.5 (s, *o*), 129.9 (m, *m*), 125.3 (q, $^{1}J_{CF}$ = 271.8 Hz, **C**F_3), 118.4 (m, *p*); dpen at 137.3 (s, *i*-Ph), 129.7 (s, *p*-Ph), 129.5, 129.4 (2 × s, *o*-, *m*-Ph), 66.1 (s, **C**HNH_2); camphSO_3^- at 211.3, 60.1, 54.8, 54.5, 48.3, 47.7, 30.6, 22.8, 17.9, 10.0 (10 × s).

Λ-(*S*,*S*)-$\mathbf{1}^{3+}$ 2(1*S*)-camph$\mathbf{SO_3^-}\mathbf{BAr_f^-}$. Λ-(*S*,*S*)-$\mathbf{1}^{3+}$ $2Cl^-BAr_f^-\cdot 2H_2O$ (0.108 g, 0.0648 mmol), CH_2Cl_2 (10 mL), (1*S*)-ammonium 3-bromocamphor-8-sulfonate (0.0892 g, 0.272 mmol, 4.2 equiv), and distilled H_2O (10 mL) were combined in a procedure analogous to that for Λ-(*S*,*S*)-$\mathbf{1}^{3+}$ 2(1*R*)-camph$SO_3^-BAr_f^-$. An identical workup gave Λ-(*S*,*S*)-$\mathbf{1}^{3+}$ 2(1*S*)-camph$SO_3^-BAr_f^-\cdot H_2O$ as a bright orange solid (0.122 g, 0.0555 mmol, 85%), mp 145-151 °C (dec, open capillary). Anal. Calcd. for $C_{94}H_{88}BBr_2CoF_{24}N_6O_8S_2\cdot H_2O$ (2197.40): C 51.38, H 4.13, N, 3.82; found C 51.55, H 4.40, N 3.70.

NMR (acetone-d_6, δ/ppm): ^{1}H (500 MHz) BAr_f^- at 7.79 (s, 8H, *o*), 7.68 (s, 4H, *p*); dpen at 7.55 (s, 12H, *o*-Ph), 7.31 (br s, 24H, *m*-, *p*-Ph, N**H**H'), 5.42 (s, 6H, NH**H'**), 5.11 (s, 6H, C**H**NH_2); 2.90 (br s, 6H, $\mathbf{H}_2O$); camphSO_3^- at 4.82 (s, 2H), 3.22 (d, $^{2}J_{HH}$ = 15.0 Hz, 2H), 3.15 (s, 2H), 2.81 (d, $^{2}J_{HH}$ = 14.0 Hz, 2H), 2.29-2.18 (m, 2H), 2.13-2.07 (m, 2H), 1.87-1.75 (m, 2H), 1.42-1.33 (m, 2H), 1.29 (s, 6H), 0.99-0.82 (m, 6H); $^{13}C\{^{1}H\}$ (125 MHz) BAr_f^- at 162.5 (q, $^{1}J_{BC}$ = 50.0 Hz, *i*), 135.5 (s, *o*), 129.9 (m, *m*), 125.3 (q, $^{1}J_{CF}$ = 271.8 Hz, **C**F_3), 118.4 (m, *p*); dpen at 136.8 (s, *i*-Ph), 129.9 (s, *p*-Ph), 129.8, 129.7 (2 × s, *o*-, *m*-Ph), 63.4 (s, **C**HNH_2); camphSO_3^- at 211.2, 60.0, 54.8, 54.4, 48.3, 47.8, 30.7, 22.8, 18.0, 10.0 (10 × s).

Δ-(*S*,*S*)-$\mathbf{1}^{3+}$ 2(1*S*)-camph$\mathbf{SO_3^-}\mathbf{BAr_f^-}$. Δ-(*S*,*S*)-$\mathbf{1}^{3+}$ $2Cl^-BAr_f^-\cdot H_2O$ (0.0250 g, 0.0152 mmol), CH_2Cl_2 (5 mL), (1*S*)-ammonium 3-bromocamphor-8-sulfonate (0.0105 g, 0.0319 mmol, 2.1 equiv), and distilled H_2O (5 mL) were combined in a procedure

analogous to that for Λ-(*S*,*S*)-$\mathbf{1}^{3+}$ 2(1*R*)-camph$SO_3^-BAr_f^-$ (3 h reaction time). An identical workup gave Δ-(*S*,*S*)-$\mathbf{1}^{3+}$ 2(1*S*)-camph$SO_3^-BAr_f^-$ as a bright orange solid (0.0322 g, 0.0148 mmol, 97%), mp 156-160 °C (dec, open capillary). Anal. Calcd. for $C_{94}H_{88}BBr_2CoF_{24}N_6O_8S_2$ (2179.41): C 51.80, H 4.07, N, 3.86; found C 51.95, H 4.27, N 3.92.

NMR (acetone-d_6, δ/ppm): ^{1}H (300 MHz) BAr_f^- at 7.80 (s, 8H, *o*), 7.68 (s, 4H, *p*); dpen at 7.51-7.45 (m, 12H, *o*-Ph), 7.28-7.22 (m, 18H, *m*-, *p*-Ph), 7.07 (s, 6H, N**H**H'), 5.91 (d, $^3J_{HH}$ = 11.1 Hz, 6H, NH**H'**), 5.17 (br s, 6H, C**H**NH_2); 2.90 (br s, 5H, $\mathbf{H}_2O$); camphSO_3^- at 4.74 (d, $^3J_{HH}$ = 3.8 Hz, 2H), 3.11 (d, $^2J_{HH}$ = 14.7 Hz, 2H), 3.04-2.98 (m, 2H), 2.70 (d, $^2J_{HH}$ = 14.4 Hz, 2H), 2.22-2.09 (m, 2H), 1.83-1.70 (m, 2H), 1.39-1.33 (m, 2H), 1.24 (s, 6H), 0.91 (s, 6H); ^{13}C {^{1}H} (75 MHz) BAr_f^- at 162.5 (q, $^1J_{BC}$ = 50.0 Hz, *i*), 135.5 (s, *o*), 129.9 (m, *m*), 125.3 (q, $^1J_{CF}$ = 270 Hz, **C**F_3), 118.4 (m, *p*); dpen at 137.4 (s, *i*-Ph), 129.6 (s, *p*-Ph), 129.4, 129.3 (2 × s, *o*-, *m*-Ph), 66.2 (s, **C**HNH_2); camphSO_3^- at 211.2, 60.0, 54.8, 54.4, 48.2, 47.7, 30.6, 22.7, 18.0, 10.0 (10 × s).

Λ-(*S*,*S*)-$\mathbf{1}^{3+}$ 2(*R*)-BINOLPA$^-BAr_f^-$. A round bottom flask was charged with a solution of Λ-(*S*,*S*)-$\mathbf{1}^{3+}$ $2Cl^-BAr_f^-\cdot 2H_2O$ (0.0250 g, 0.0152 mmol) in CH_2Cl_2 (5 mL), (*R*)-BINOLPAH (0.0111 g, 0.0319 mmol, 2.1 equiv), NaOH (0.0013 g, 0.033 mmol, 2.2 equiv), and distilled H_2O (5 mL). The biphasic mixture was vigorously stirred. After 1 h, the aqueous phase was removed. The solvent was removed from the orange organic phase by rotary evaporation. The residue was dried by oil pump vacuum (rt, overnight) to give Λ-(*S*,*S*)-$\mathbf{1}^{3+}$ 2(*R*)-BINOLPA$^-BAr_f^-\cdot 3H_2O$ as an orange solid (0.0307 g, 0.0133 mmol, 88%), mp 166-174 °C (dec, open capillary). Anal. Calcd. for $C_{114}H_{84}BCoF_{24}N_6O_8P_2\cdot 3H_2O$ (2307.66): C 59.34, H 3.93, N, 3.64; found C 59.26, H 3.99, N 3.65.

NMR (acetone-d_6, δ/ppm): ^{1}H (500 MHz) BAr_f^- at 7.80 (s, 8H, *o*), 7.68 (s, 4H, *p*);

dpen at 7.91 (br s, 6H, N**H**H'), 7.65-7.55 (m, 12H, *o*-Ph), 7.35-7.19 (m, 18H, *m*-, *p*-Ph), 5.37 (br s, 6H, NH**H'**), 5.19-5.09 (m, 6H, C**H**NH_2); 3.02 (br s, 9H, $\mathbf{H}_2O$); BINOLPA$^-$ at 8.18 (d, $^3J_{HH}$ = 8.5 Hz, 4H), 8.08 (d, $^3J_{HH}$ = 8.0 Hz, 4H), 7.55-7.50 (m, 4H), 7.46 (d, $^3J_{HH}$ = 8.5 Hz, 4H), 7.43-7.35 (m, 8H); $^{13}C\{^1H\}$ (125 MHz) BAr_f^- at 162.5 (q, $^1J_{BC}$ = 50.0 Hz, *i*), 135.5 (s, *o*), 129.9 (m, *m*), 125.3 (q, $^1J_{CF}$ = 270 Hz, **C**CF_3), 118.4 (m, *p*); dpen at 137.1 (s, *i*-Ph), 129.9 (s, *p*-Ph), 129.8, 129.7 (2 × s, *o*-, *m*-Ph), 63.6 (s, **C**HNH_2); BINOLPA$^-$ at 150.3 (d, $^2J_{CP}$ = 9.3 Hz), 133.4, 132.1, 131.2, 129.4, 127.4, 127.3, 125.9, 122.9, 122.6 (9 × s).

Δ-(*S*,*S*)-$\mathbf{1}^{3+}$ 2(*R*)-BINOLPA$^-$$BAr_f^-$. Δ-(*S*,*S*)-$\mathbf{1}^{3+}$ $2Cl^-BAr_f^-\cdot H_2O$ (0.0250 g, 0.0152 mmol), CH_2Cl_2 (5 mL), (*R*)-BINOLPAH (0.0111 g, 0.0319 mmol, 2.1 equiv), NaOH (0.0013 g, 0.033 mmol, 2.2 equiv), and distilled H_2O (5 mL) were combined in a procedure analogous to that for Λ-(*S*,*S*)-$\mathbf{1}^{3+}$ 2(*R*)-BINOLPA$^-$$BAr_f^-$. An identical workup gave Δ-(*S*,*S*)-$\mathbf{1}^{3+}$ 2(*R*)-BINOLPA$^-$$BAr_f^-\cdot H_2O$ as an orange solid (0.0295 g, 0.0129 mmol, 85%), mp 178-182 °C (open capillary). Anal. Calcd. for $C_{114}H_{84}BCoF_{24}N_6O_8P_2\cdot H_2O$ (2271.63): C 60.28, H 3.82, N, 3.70; found C 59.91, H 4.27, N 3.66.

NMR (acetone-d_6, δ/ppm): ^1H (500 MHz) BAr_f^- at 7.81 (m, 8H, *o*), 7.69 (s, 4H, *p*); dpen at 7.40-7.33 (m, 12H, *o*-Ph), 7.32-7.24 (m, 18H, *m*-, *p*-Ph), 7.20 (br s, 6H, N**H**H'), 6.04 (d, $^3J_{HH}$ = 11.0 Hz, 6H, NH**H'**), 5.17-5.08 (m, 6H, C**H**NH_2); 2.94 (br s, 8H, $\mathbf{H}_2O$); BINOLPA$^-$ at 8.11 (d, $^3J_{HH}$ = 9.0 Hz, 4H), 8.05 (d, $^3J_{HH}$ = 8.0 Hz, 4H), 7.58-7.52 (m, 12H), 7.52-7.47 (m, 4H); ^{13}C $\{^1H\}$ (125 MHz) BAr_f^- at 162.5 (q, $^1J_{BC}$ = 50.0 Hz, *i*), 135.5 (s, *o*), 129.9 (m, *m*), 125.3 (q, $^1J_{CF}$ = 270 Hz, **C**CF_3), 118.4 (m, *p*); dpen at 137.5 (s, *i*-Ph), 130.9 (s, *p*-Ph), 129.5, 129.2 (2 × s, *o*-, *m*-Ph), 66.1 (s, **C**HNH_2); BINOLPA$^-$ at 150.5 (d, $^2J_{CP}$ = 9.3 Hz), 133.3, 132.0, 129.7, 129.3, 127.4, 127.1, 125.8, 122.89, 122.87 (9 × s).

Λ-(*S*,*S*)-$\mathbf{1}^{3+}$ 2(*S*)-BINOLPA$^-$$BAr_f^-$. Λ-(*S*,*S*)-$\mathbf{1}^{3+}$ $2Cl^-BAr_f^-\cdot 2H_2O$ (0.0850 g,

0.051 mmol), CH_2Cl_2 (15 mL), (*S*)-BINOLPAH (0.0415 g, 0.112 mmol, 2.2 equiv), NaOH (0.0045 g, 0.11 mmol, 2.2 equiv) and distilled H_2O (15 mL) were combined in a procedure analogous to that for Λ-(*S*,*S*)-**1**$^{3+}$ 2(*R*)-BINOLPA$^-$BAr$_f^-$ (3 h reaction time). An identical workup gave Λ-(*S*,*S*)-**1**$^{3+}$ 2(*S*)-BINOLPA$^-$BAr$_f^-$·2H_2O as an orange solid (0.0944 g, 0.0407 mmol, 80%), mp 166-174 °C (dec, open capillary). Anal. Calcd. for $C_{114}H_{84}BCoF_{24}N_6O_8P_2$·2$H_2O$ (2307.62): C 59.80, H 3.87, N, 3.67; found C 60.06, H 4.00, N 3.63.

NMR (acetone-d_6, δ/ppm): ^{1}H (500 MHz) BAr$_f^-$ at 7.80 (s, 8H, *o*), 7.68 (s, 4H, *p*); dpen at 7.80 (br s, 6H, N**H**H') 7.61-7.54 (m, 12H, *o*-Ph), 7.33-7.27 (m, 18H, *m*-, *p*-Ph), 5.38 (br s, 6H, NH**H'**), 5.14 (s, 6H, C**H**NH_2); 2.96 (br s, 9H, $\mathbf{H}_2O$); BINOLPA$^-$ at 8.11-8.01 (m, 8H), 7.54-7.48 (m, 4H), 7.44-7.33 (m, 12H); ^{13}C{^{1}H} (125 MHz) BAr$_f^-$ at 162.5 (q, $^1J_{BC}$ = 50.0 Hz, *i*), 135.5 (s, *o*), 129.8 (m, *m*), 125.3 (q, $^1J_{CF}$ = 270 Hz, **C**F_3), 118.4 (m, *p*); dpen at 137.2 (s, *i*-Ph), 129.8 (s, *p*-Ph), 129.7 (s, *o*-, *m*-Ph), 63.4 (s, **C**HNH_2); BINOLPA$^-$ at 150.3 (d, $^2J_{CP}$ = 9.3 Hz), 133.3, 132.0, 131.1, 129.4, 127.4, 127.2, 125.8, 122.9, 122.7 (9 × s).

Δ-(*S*,*S*)-1^{3+} 2(*S*)-BINOLPA$^-$BAr$_f^-$. Δ-(*S*,*S*)-**1**$^{3+}$ 2Cl$^-$BAr$_f^-$·H_2O (0.0250 g, 0.0152 mmol), CH_2Cl_2 (5 mL), (*S*)-BINOLPAH (0.0111 g, 0.0319 mmol, 2.1 equiv), NaOH (0.0013 g, 0.033 mmol, 2.2 equiv), and distilled H_2O (5 mL) were combined in a procedure analogous to that for Λ-(*S*,*S*)-**1**$^{3+}$ 2(*R*)-BINOLPA$^-$BAr$_f^-$ (4 h reaction time). An identical workup gave Δ-(*S*,*S*)-**1**$^{3+}$ 2(*R*)-BINOLPA$^-$BAr$_f^-$·H_2O as an orange solid (0.0329 g, 0.0146 mmol, 96%), mp 178-182 °C (dec, open capillary). Anal. Calcd. for $C_{114}H_{84}BCoF_{24}N_6O_8P_2$·$H_2O$ (2271.63): C 60.28, H 3.82, N, 3.70; found C 60.83, H 4.37, N 3.67.

NMR (acetone-d_6, δ/ppm): ^{1}H (500 MHz) BAr$_f^-$ at 7.81 (m, 8H, *o*), 7.69 (s, 4H, *p*); dpen at 7.40-7.33 (m, 12H, *o*-Ph), 7.32-7.24 (m, 18H, *m*-, *p*-Ph), 7.20 (br s, 6H, N**H**H'),

6.04 (d, $^3J_{HH}$ = 11.0 Hz, 6H, NH**H'**), 5.17-5.08 (m, 6H, C**H**NH_2); 2.94 (br s, 8H, $\mathbf{H}_2O$); BINOLPA$^-$ at 8.11 (d, $^3J_{HH}$ = 9.0 Hz, 4H), 8.05 (d, $^3J_{HH}$ = 8.0 Hz, 4H), 7.58-7.52 (m, 12H), 7.52-7.47 (m, 4H); ^{13}C {^{1}H} (125 MHz) BAr_f^- at 162.5 (q, $^1J_{BC}$ = 50.0 Hz, *i*), 135.5 (s, *o*), 129.9 (m, *m*), 125.3 (q, $^1J_{CF}$ = 270 Hz, **C**F_3), 118.4 (m, *p*); dpen at 137.5 (s, *i*-Ph), 130.9 (s, *p*-Ph), 129.5, 129.2 (2 × s, *m*-Ph), 66.1 (s, **C**HNH_2); BINOLPA$^-$ at 150.5 (d, $^2J_{CP}$ = 9.3 Hz), 133.3, 132.0, 129.7, 129.3, 127.4, 127.1, 125.8, 122.97, 122.95 (9 × s).

Λ-(*S*,*S*)-$\mathbf{1}^{3+}$ 2(*R*)-VAPOLPA$^-$$BAr_f^-$. Crude Na^+ (*R*)-VAPOLPA$^-$ was prepared by charging a vial with (*R*)-VAPOLPAH (0.0850 g, 0.136 mmol), NaOH (0.0054 g, 0.14 mmol, 1.0 equiv), and MeOH/H_2O (10 mL, 1:1 v/v). The mixture was vigorously stirred (rt, overnight). The solvent was removed by rotary evaporation. To the white residue was added a solution of Λ-(*S*,*S*)-$\mathbf{1}^{3+}$ 2Cl$^-$$BAr_f^-$·2$H_2O$ (0.0532 g, 0.0319 mmol, 0.33 equiv) in CH_2Cl_2 (10 mL). The mixture was vigorously stirred (rt, overnight). The phases were allowed to separate and the orange organic phase washed with water (2 × 10 mL) and dried (Na_2SO_4). The solvent was removed by rotary evaporation. The residue was dried by oil pump vacuum (rt, overnight) to give Λ-(*S*,*S*)-$\mathbf{1}^{3+}$ 2(*R*)-VAPOLPA$^-$$BAr_f^-$·3$H_2O$ as a bright orange solid (0.0879 g, 0.0313 mmol, 98%), mp 160-172 °C (dec, open capillary). Anal. Calcd. for $C_{154}H_{108}BCoF_{24}N_6O_8P_2$·3$H_2O$ (2812.29): C 65.77, H 4.09, N 2.99; found C 65.70, H 4.14, N 2.79.

NMR (acetone-d_6, δ/ppm): ^{1}H (500 MHz) BAr_f^- at 7.79 (s, 8H, *o*), 7.69 (s, 4H, *p*); dpen at 7.52 (m, 6H, N**H**H'), 7.31-7.19 (m, 18H), 6.96-6.86 (m, 12H), 5.58 (br s, 6H, NH**H'**), 4.83 (s, 6H, C**H**NH_2); 2.97 (br s, 9H, $\mathbf{H}_2O$); VAPOLPA$^-$ at 10.01 (d, $^3J_{HH}$ = 7.9 Hz, 4H), 8.03 (d, $^3J_{HH}$ = 7.5 Hz, 4H), 7.94 (d, $^3J_{HH}$ = 8.8 Hz, 4H), 7.90 (d, $^3J_{HH}$ = 8.8 Hz, 4H), 7.64 (s, 4H), 7.14 (m, 12H), 6.98 (t, $^3J_{HH}$ = 7.7 Hz, 8H), 6.52 (d, $^3J_{HH}$ = 7.5 Hz, 8H); ^{13}C{^{1}H} (125 MHz) BAr_f^- at 162.6 (q, $^1J_{BC}$ = 49.7 Hz, *i*), 135.6 (s, *o*), 130.0 (m, *m*), 125.4 (q, $^1J_{CF}$ = 271.8 Hz, **C**F_3), 118.5 (m, *p*); dpen at 136.1 (s, *i*-Ph), 130.4 (s, *p*-Ph),

130.1, 129.8 (2 × s, *o*-, *m*-Ph), 64.2 (s, **C**$CHNH_2$); VAPOLPA$^-$ at 151.2 (d, $^2J_{CP}$ = 9.4 Hz), 142.4, 140.9, 135.4, 134.4, 130.0, 129.6, 129.5, 129.2, 128.6, 128.5, 128.2, 127.6, 127.5, 127.4, 127.2, 127.0, 122.7 (17 × s).

Λ-(*S*,*S*)-$\mathbf{1}^{3+}$ 2(*S*)-VAPOLPA$^-$$BAr_f^-$. Crude Na^+ (*S*)-VAPOLPA$^-$ was prepared by charging a vial with (*S*)-VAPOLPAH (0.0545 g, 0.0907 mmol), NaOH (0.0036 g, 0.091 mmol, 1.0 equiv), and MeOH/H_2O (5 mL, 1:1 v/v). The mixture was vigorously stirred (rt, overnight). The solvent was removed by rotary evaporation and the white residue dried by oil pump vacuum (rt, overnight). A vial was charged with Λ-(*S*,*S*)-$\mathbf{1}^{3+}$ $2Cl^-BAr_f^-$ $\cdot 2H_2O$ (0.0341 g, 0.0205 mmol), distilled H_2O (5 mL), CH_2Cl_2 (5 mL), and crude Na^+ (*S*)-VAPOLPA$^-$ (0.0255 g, 0.0410 mmol, 2.0 equiv). The biphasic mixture was vigorously stirred (rt, overnight). The orange organic phase was separated and the solvent removed by rotary evaporation. The residue was dried by oil pump vacuum (rt, overnight) to give Λ-(*S*,*S*)-$\mathbf{1}^{3+}$ 2(*S*)-VAPOLPA$^-$$BAr_f^-$$\cdot 4H_2O$ as a bright orange solid (0.0572 g, 0.0202 mmol, 99%), mp 171-180 °C (dec, open capillary). Anal. Calcd. for $C_{154}H_{108}BCoF_{24}N_6O_8P_2 \cdot 4H_2O$ (2830.31): C 65.35, H 4.13, N 2.97; found C 65.35, H 4.23, N 2.55.

NMR (acetone-d_6, δ/ppm): ^{1}H (500 MHz) BAr_f^- at 7.81 (s, 8H, *o*), 7.69 (s, 4H, *p*); dpen at 7.49 (br s, 6H, N**H**H'), 7.30 (t, $^3J_{HH}$ = 7.3 Hz, 6H, *p*-Ph), 7.22 (t, $^3J_{HH}$ = 7.5 Hz, 12H, *m*-Ph), 7.16 (d, $^3J_{HH}$ = 6.9 Hz, 12H, *o*-Ph), 5.04 (br s, 6H, NH**H'**), 4.60 (s, 6H, C**H**NH_2); 2.97 (br s, 15H, $\mathbf{H}_2O$); VAPOLPA$^-$ at 9.74 (d, $^3J_{HH}$ = 8.0 Hz, 4H), 8.04 (d, $^3J_{HH}$ = 7.5 Hz, 4H), 7.95 (d, $^3J_{HH}$ = 8.3 Hz, 4H), 7.90 (d, $^3J_{HH}$ = 8.3 Hz, 4H), 7.78-7.67 (m, 8H), 7.58 (s, 4H), 7.17-7.12 (m, 4H), 6.99 (t, $^3J_{HH}$ = 7.3 Hz, 8H), 6.60 (d, $^3J_{HH}$ = 7.3 Hz, 8H); $^{13}C\{^1H\}$ (125 MHz) BAr_f^- at 162.6 (q, $^1J_{BC}$ = 49.7 Hz, *i*), 135.6 (s, *o*), 130.0 (m, *m*), 125.4 (q, $^1J_{CF}$ = 271.8 Hz, **C**F_3), 118.5 (m, *p*); dpen at 136.1 (s, *i*-Ph), 130.4 (s, *p*-Ph), 130.1, 129.6 (2 × s, *o*-, *m*-Ph), 64.2 (s, **C**$CHNH_2$); VAPOLPA$^-$ at 151.2 (d, $^2J_{CP}$ = 9.5 Hz), 142.4, 140.9, 135.4, 134.4, 130.8, 129.8, 129.5, 129.2, 128.6, 128.5, 128.2, 127.6,

127.5, 127.4, 127.2, 127.0, 122.7 (17 × s).

Λ-(*S*,*S*)-1^{3+} 2(*R*)-((CF$_3$)$_2$Ph)$_2$-BINOLPA$^-$BAr$_f^-$. Crude Na$^+$ (*R*)-((CF$_3$)$_2$Ph)$_2$-BINOLPA$^-$ was prepared by charging a vial with (*R*)-((CF$_3$)$_2$Ph)$_2$-BINOLPAH (0.0850 g, 0.107 mmol), NaOH (0.0043 g, 0.11 mmol, 1.5 equiv), and MeOH/H$_2$O (10 mL, 1:1 v/v). The mixture was vigorously stirred (rt, overnight). The solvent was removed by rotary evaporation and the white residue dried by oil pump vacuum (rt, overnight). A solution of Λ-(*S*,*S*)-**1**$^{3+}$ 2Cl$^-$BAr$_f^-$·2H$_2$O (0.0594 g, 0.0357 mmol, 0.33 equiv) in CH$_2$Cl$_2$ (10 mL) was added. The biphasic mixture was vigorously stirred. After 1 h, the phases were allowed to separate. The orange organic phase was washed with water (2 × 10 mL) and dried (Na$_2$SO$_4$). The solvent was removed by rotary evaporation. The residue was dried by oil pump vacuum (rt, overnight) to give Λ-(*S*,*S*)-**1**$^{3+}$ 2(*R*)-((CF$_3$)$_2$Ph)$_2$-BINOLPA$^-$BAr$_f^-$·3H$_2$O as a bright orange solid (0.0497 g, 0.0157 mmol, 44%), mp 165-171 °C (dec, open capillary). Anal. Calcd. for C$_{146}$H$_{92}$BCoF$_{48}$N$_6$O$_8$P$_2$·3H$_2$O (3156.04): C 55.56, H 3.13, N 2.66; found C 55.75, H 3.32, N 2.47.

NMR (acetone-*d*$_6$, δ/ppm): ^{1}H (500 MHz) BAr$_f^-$ at 7.79 (s, 8H, *o*), 7.67 (s, 4H, *p*); dpen at 7.24 (t, $^3J_{HH}$ = 7.4 Hz, 6H, *p*-Ph), 7.14 (t, $^3J_{HH}$ = 7.7 Hz, 12H, *m*-Ph), 6.94 (d, $^3J_{HH}$ = 7.3 Hz, 12H, *o*-Ph), 7.00 (br s, 6H, N**H**H'), 5.12 (br s, 6H, NH**H'**), 4.42 (s, 6H, C**H**NH$_2$); 2.84 (br s, 8H, **H**$_2$O); ((CF$_3$)$_2$Ph)$_2$-BINOLPA$^-$ at 8.80 (s, 8H), 8.40 (s, 4H), 8.21 (d, $^3J_{HH}$ = 8.1 Hz, 4H), 8.03 (s, 4H), 7.57 (t, $^3J_{HH}$ = 7.5 Hz, 4H), 7.38 (t, $^3J_{HH}$ = 8.1 Hz, 4H), 7.19 (d, $^3J_{HH}$ = 8.5 Hz, 4H); ^{13}C{^{1}H} (125 MHz) BAr$_f^-$ at 162.6 (q, $^1J_{BC}$ = 50.0 Hz, *i*), 135.5 (s, *o*), 130.0 (m, *m*), 125.3 (q, $^1J_{CF}$ = 271.8 Hz, **C**F$_3$), 118.4 (m, *p*); dpen at 134.9 (s, *i*-Ph), 130.4 (s, *p*-Ph), 129.8, 128.9 (2 × s, *o*-, *m*-Ph), 63.5 (s, **C**HNH$_2$); ((CF$_3$)$_2$Ph)$_2$-BINOLPA$^-$ at 147.1 (d, $^2J_{CP}$ = 9.3 Hz), 140.9, 134.9, 133.2, 132.6 (4 × s), 132.1 (q, $^2J_{CF}$ = 33.5 Hz), 131.8 (d, $^2J_{CP}$ = 3.0 Hz), 131.6 (s), 129.4 (q, $^1J_{CF}$ = 272.0 Hz, **C**F$_3$) 128.3, 127.6, 127.3, 126.8 (4 × s), 123.6 (d, $^2J_{CP}$ = 2.0 Hz), 121.8 (s).

Λ-(*S*,*S*)-$\mathbf{1}^{3+}$ 2(*S*)-$((CF_3)_2Ph)_2$-BINOLPA$^-$$BAr_f^-$. Crude Na^+ (*S*)-$((CF_3)_2Ph)_2$-BINOLPA$^-$ was prepared by charging a vial with (*S*)-$((CF_3)_2Ph)_2$-BINOLPAH (0.0515 g, 0.0667 mmol), NaOH (0.0040 g, 0.10 mmol, 1.5 equiv), and MeOH/H_2O (5 mL, 1:1 v/v). The mixture was vigorously stirred (rt, overnight). The solvent was removed by rotary evaporation and the white residue dried by oil pump vacuum (rt, overnight). A vial was charged with Λ-(*S*,*S*)-$\mathbf{1}^{3+}$ $2Cl^-BAr_f^-\cdot 2H_2O$ (0.0567 g, 0.0340 mmol), distilled H_2O (5 mL), CH_2Cl_2 (5 mL), and crude Na^+ (*S*)-$((CF_3)_2Ph)_2$-BINOLPA$^-$ (0.0541 g, 0.0681 mmol, 2.0 equiv). The biphasic mixture was vigorously stirred (rt, overnight). The orange organic phase was separated and the solvent was removed by rotary evaporation. The residue was dried by oil pump vacuum (rt, overnight) to give Λ-(*S*,*S*)-$\mathbf{1}^{3+}$ 2(*S*)-$((CF_3)_2Ph)_2$-BINOLPA$^-$$BAr_f^-\cdot 3H_2O$ as a bright orange solid (0.1013 g, 0.03210 mmol, 94%), mp 159-164 °C (dec, open capillary). Anal. Calcd. for $C_{146}H_{92}BCoF_{48}N_6O_8P_2\cdot 3H_2O$ (3156.04): C 55.56, H 3.13, N 2.66; found C 55.60, H 3.15, N 2.53.

NMR (acetone-d_6, δ/ppm): ^1H (500 MHz) BAr_f^- at 7.81 (s, 8H, *o*), 7.69 (s, 4H, *p*); dpen at 7.29 (t, $^3J_{HH}$ = 7.4 Hz, 6H, *p*-Ph), 7.08 (t, $^3J_{HH}$ = 7.3 Hz, 12H, *m*-Ph), 6.98 (d, $^3J_{HH}$ = 6.5 Hz, 12H, *o*-Ph), 6.73 (br s, 6H, N**H**H'), 5.47 (br s, 6H, NH**H'**), 4.29 (s, 6H, C**H**NH_2); 3.04 (br s, 8H, $\mathbf{H}_2O$); $((CF_3)_2Ph)_2$-BINOLPA$^-$ at 8.97 (s, 8H), 8.38 (s, 4H), 8.25-8.12 (m, 4H), 8.00 (s, 4H), 7.65-7.51 (m, 4H), 7.46-7.33 (m, 4H), 7.27-7.21 (m, 4H); $^{13}C\{^1H\}$ (125 MHz) BAr_f^- at 162.6 (q, $^1J_{BC}$ = 50.0 Hz, *i*), 135.5 (s, *o*), 130.0 (m, *m*), 125.3 (q, $^1J_{CF}$ = 271.8 Hz, $\mathbf{C}F_3$), 118.4 (m, *p*); dpen at 134.9 (s, *i*-Ph), 130.4 (s, *p*-Ph), 129.8, 128.9 (2 × s, *o*-, *m*-Ph), 63.5 (s, **C**HNH_2); $((CF_3)_2Ph)_2$-BINOLPA$^-$ at 147.1 (d, $^2J_{CP}$ = 9.3 Hz), 140.9, 134.9, 133.2, 132.6 (4 × s), 132.1 (q, $^2J_{CF}$ = 33.5 Hz), 131.8 (d, $^2J_{CP}$ = 3.0 Hz), 131.6 (s), 129.4 (q, $^1J_{CF}$ = 272.0 Hz, $\mathbf{C}F_3$) 128.3, 127.6, 127.3, 126.8 (4 × s), 123.6 (d, $^2J_{CP}$ = 2.0 Hz), 121.8 (s).

Λ-(*S*,*S*)-$\mathbf{1}^{3+}$ 2(*R*)-$(SiPh_3)_2$-BINOLPA$^-$$BAr_f^-$. Crude Na^+ (*R*)-$(SiPh_3)_2$-

BINOLPA$^-$ was prepared by the charging a vial with (*R*)-(SiPh$_3$)$_2$-BINOLPAH (0.0515 g, 0.0667 mmol), NaOH (0.0040 g, 1.0 mmol, 1.5 equiv), and MeOH/H$_2$O (5 mL, 1:1 v/v). The mixture was vigorously stirred (rt. overnight). The solvent was removed by rotary evaporation and the white residue dried by oil pump vacuum (rt, 17 h). A vial was charged with Λ-(*S*,*S*)-**1**$^{3+}$ 2Cl$^-$BAr$_f^-$·2H$_2$O (0.0545 g, 0.0327 mmol), distilled H$_2$O (5 mL), CH$_2$Cl$_2$ (5 mL), and crude Na$^+$ (*R*)-(SiPh$_3$)$_2$-BINOLPA$^-$ (0.0580 g, 0.0654 mmol, 2.0 equiv). The biphasic mixture was vigorously stirred (rt, overnight). The orange organic phase was separated and the solvent removed by rotary evaporation. The residue was dried by oil pump vacuum (rt, overnight) to give Λ-(*S*,*S*)-**1**$^{3+}$ 2(*R*)-(SiPh$_3$)$_2$-BINOLPA$^-$BAr$_f^-$ ·6H$_2$O as a bright yellow solid (0.1040 g, 0.03063 mmol, 94%), mp 149-157 °C (dec, open capillary). Anal. Calcd. for C$_{186}$H$_{140}$BCoF$_{24}$N$_6$O$_8$P$_2$Si$_4$·6H$_2$O (3395.28): C 65.80, H 4.51, N 2.48; found C 65.72, H 4.53, N 2.45.

NMR (acetone-d_6, δ/ppm): ^{1}H (500 MHz) BAr$_f^-$ at 7.81 (s, 8H, *o*), 7.69 (s, 4H, *p*); dpen at 7.29-7.23 (m, 18H, *m*-, *p*-Ph), 7.12-7.06 (m, 12H, *o*-Ph), 6.50 (br s, 6H, N**H**H'), 4.88 (br s, 6H, NH**H'**), 4.12 (s, 6H, C**H**NH$_2$); 3.12 (br s, 10H, **H**$_2$O); (SiPh$_3$)$_2$-BINOLPA$^-$ at 8.17 (s, 4H), 7.90 (d, $^3J_{HH}$ = 8.1 Hz, 4H), 7.58-7.54 (m, 24H), 7.44 (t, $^3J_{HH}$ = 7.5 Hz, 4H), 7.34-7.27 (m, 20H), 7.20 (t, $^3J_{HH}$ = 7.5 Hz, 20H), 7.16 (d, $^3J_{HH}$ = 8.6 Hz, 4H); ^{13}C{^{1}H} (125 MHz) BAr$_f^-$ at 162.6 (q, $^1J_{BC}$ = 49.8 Hz, *i*), 135.6 (s, *o*), 130.1 (m, *m*), 125.4 (q, $^1J_{CF}$ = 272.9 Hz, **C**F$_3$), 118.5 (m, *p*); dpen at 135.6 (s, *i*-Ph), 130.8 (s, *p*-Ph), 130.1, 129.6 (2 × s, *o*-, *m*-Ph), 63.9 (s, **C**HNH$_2$); (SiPh$_3$)$_2$-BINOLPA$^-$ at 155.6 (d, $^2J_{CP}$ = 9.3 Hz), 142.0, 137.8, 135.9, 135.1, 131.0, 130.2, 128.4, 128.1, 127.3, 127.2, 125.8, 122.6 (12 × s).

Λ-(*S*,*S*)-1^{3+} 2(*S*)-(SiPh$_3$)$_2$-BINOLPA$^-$BAr$_f^-$. (*S*)-(SiPh$_3$)$_2$-BINOLPAH (0.0538 g, 0.0714 mmol), NaOH (0.0057 g, 0.14 mmol, 2.0 equiv), MeOH/H$_2$O (5 mL, 1:1 v/v), Λ-(*S*,*S*)-**1**$^{3+}$ 2Cl$^-$BAr$_f^-$·2H$_2$O (0.0512 g, 0.0307 mmol), distilled H$_2$O (5 mL), CH$_2$Cl$_2$ (5

mL), and crude Na^+ (*S*)-$(SiPh_3)_2$-BINOLPA$^-$ (0.0600 g, 0.0676 mmol, 2.2 equiv) were combined in a procedure analogous to that for Λ-(*S*,*S*)-**1**$^{3+}$ 2(*R*)-$(SiPh_3)_2$-BINOLPA$^-$ BAr_f^-. An identical workup gave Λ-(*S*,*S*)-**1**$^{3+}$ 2(*S*)-$(SiPh_3)_2$-BINOLPA$^-$$BAr_f^-$·$6H_2O$ as a bright orange solid (0.1028 g, 0.03028 mmol, 99%), mp 149-157 °C (dec, open capillary). Anal. Calcd. for $C_{186}H_{140}BCoF_{24}N_6O_8P_2Si_4$·$6H_2O$ (3395.28): C 65.80, H 4.51, N 2.48; found C 65.76, H 4.51, N 2.35.

NMR (acetone-d_6, δ/ppm): ^{1}H (500 MHz) BAr_f^- at 7.80 (s, 8H, *o*), 7.68 (s, 4H, *p*); dpen at 7.35-7.23 (m, 18H, Ph), 6.67 (br s, 6H, N**H**H'), 5.22 (br s, 6H, NH**H'**), 4.71 (s, 6H, C**H**NH_2); 3.18 (br s, 12H, $\mathbf{H}_2O$); $(SiPh_3)_2$-BINOLPA$^-$ at 8.04 (s, 4H), 7.80-7.77 (m, 4H), 7.65-7.59 (m, 24H), 7.39 (t, $^3J_{HH}$ = 7.6 Hz, 4H), 7.35-7.28 (m, 20H), 7.21 (t, $^3J_{HH}$ = 7.4 Hz, 20H), 7.21-7.18 (m, 4H); $^{13}C\{^1H\}$ (125 MHz) BAr_f^- at 162.6 (q, $^1J_{BC}$ = 49.8 Hz, *i*), 135.6 (s, *o*), 130.1 (m, *m*), 125.4 (q, $^1J_{CF}$ = 271.4 Hz, **C**F_3), 118.5 (m, *p*); dpen at 135.6 (s, *i*-Ph), 130.8 (s, *p*-Ph), 129.9, 129.4 (2 × s, *o*-, *m*-Ph), 63.7 (s, **C**HNH_2); $(SiPh_3)_2$-BINOLPA$^-$ at 155.2 (d, $^2J_{CP}$ = 9.3 Hz), 142.0, 137.8, 135.9, 135.2, 131.0, 130.2, 128.4, 128.0, 127.11, 127.06, 125.6, 122.9 (12 × s).

Λ-(*S*,*S*)-1^{3+} 2(*S*)-((*i*Pr)$_3$Ph)$_2$-BINOLPA$^-$$BAr_f^-$. Crude Na^+ (*S*)-((*i*Pr)$_3$Ph)$_2$-BINOLPA$^-$ was prepared by charging a vial with (*S*)-((*i*Pr)$_3$Ph)$_2$-BINOLPAH (0.0538 g, 0.0714 mmol), NaOH (0.0057 g, 0.14 mmol, 2.0 equiv), and MeOH/H_2O (5 mL, 1:1 v/v). The mixture was vigorously stirred (rt, overnight). The solvent was removed by rotary evaporation and the white residue dried by oil pump vacuum (rt, overnight). A vial was charged with Λ-(*S*,*S*)-**1**$^{3+}$ 2Cl$^-$$BAr_f^-$·$2H_2O$ (0.0640 g, 0.0384 mmol), distilled H_2O (5 mL), CH_2Cl_2 (5 mL), and crude Na^+ (*S*)-((*i*Pr)$_3$Ph)$_2$-BINOLPA$^-$ (0.0665 g, 0.0858 mmol, 2.2 equiv). The biphasic mixture was vigorously stirred (rt, overnight). The orange organic phase was separated and the solvent was removed by rotary evaporation. The residue was dried by oil pump vacuum (rt, overnight) to give Λ-(*S*,*S*)-**1**$^{3+}$ 2(*S*)-((*i*Pr)$_3$Ph)$_2$-BINOLPA$^-$

$BAr_f^-·6H_2O$ as a bright orange solid (0.1123 g, 0.03541 mmol, 92%), mp 150-160 °C (dec, open capillary). Anal. Calcd. for $C_{174}H_{172}BCoF_{24}N_6O_8P_2·6H_2O$ (3171.07): C 65.91, H 5.85, N 2.65; found C 65.69, H 5.62, N 2.63.

NMR (acetone-d_6, δ/ppm): ^{1}H (500 MHz) BAr_f^- at 7.81 (s, 8H, *o*), 7.69 (s, 4H, *p*); dpen at 7.25-7.19 (m, 18H, Ph), 7.15-7.10 (m, 12H, Ph), 6.25 (br s, 6H, N**H**H'), 5.67 (br s, 6H, NH**H'**), 4.81 (s, 6H, C**H**NH_2); 3.31 (br s, 11H, $\mathbf{H}_2O$); ((*i*Pr)$_3$Ph)$_2$-BINOLPA$^-$ at 8.01 (d, $^3J_{HH}$ = 8.1 Hz, 4H), 7.80 (s, 4H), 7.45 (t, $^3J_{HH}$ = 7.5 Hz, 4H), 7.27 (t, $^3J_{HH}$ = 7.6 Hz, 4H), 7.25-7.19 (m, 4H), 7.18 (s, 4H), 7.13 (s, 4H), 3.26-3.09 (m, 4H), 3.08-2.92 (m, 4H), 2.85-2.76 (m, 4H), 1.19-1.14 (m, 24H), 1.10 (t. $^3J_{HH}$ = 6.8 Hz, 24H), 1.08-1.03 (m, 12H), 0.93 (d, $^3J_{HH}$ = 6.8 Hz, 12H); ^{13}C {^{1}H} (125 MHz) BAr_f^- at 162.2 (q, $^1J_{BC}$ = 51.9 Hz, *i*), 135.5 (s, *o*), 130.0 (m, *m*), 125.4 (q, $^1J_{CF}$ = 272.9 Hz, **C**F_3), 118.4 (m, *p*); dpen at 135.8 (s, *i*-Ph), 130.2 (s, *p*-Ph), 130.0, 128.9 (2 × s, *o*-, *m*-Ph), 63.6 (s, **C**HNH_2); ((*i*Pr)$_3$Ph)$_2$-BINOLPA$^-$ at 149.8 (d, $^2J_{CP}$ = 9.3 Hz), 148.6, 148.5, 147.8, 134.8, 133.9, 133.7, 132.6, 132.61, 132.55, 131.2, 128.9, 127.4, 126.5, 125.5, 123.8, 122.0, 120.8, 35.1, 31.7, 31.6, 26.3, 25.0, 24.9, 24.5, 24.4, 23.9 (25 × s).

Λ-(*S*,*S*)-$\mathbf{1}^{3+}$ (*R*,*R*)-tart^{2-}$\mathbf{BAr_f^-}$. A vial was charged with Λ-(*S*,*S*)-$\mathbf{1}^{3+}$ $2Cl^-BAr_f^-$ $·2H_2O$ (0.0673 g, 0.0404 mmol), distilled H_2O (5 mL), CH_2Cl_2 (5 mL), and $2Na^+$ (*R*,*R*)-tart$^{2-}·2H_2O$ (0.0093 g, 0.040 mmol, 1.0 equiv). The biphasic mixture was vigorously stirred (rt, overnight). The orange organic phase was separated and the solvent removed by rotary evaporation. The residue was dried by oil pump vacuum (rt, overnight) to give Λ-(*S*,*S*)-$\mathbf{1}^{3+}$ (*R*,*R*)-tart^{2-}$BAr_f^-·2H_2O$ as a bright orange solid (0.0693 g, 0.0398 mmol, 98%), mp 115-122 °C (dec, open capillary). Anal. Calcd. for $C_{78}H_{64}BCoF_{24}N_6O_6·2H_2O$ (1743.14): C 53.75, H 3.93, N 4.82; found C 53.86, H 4.17, N 4.47.

NMR (acetone-d_6, δ/ppm): ^{1}H (500 MHz) BAr_f^- at 7.80 (s, 8H, *o*), 7.68 (s, 4H, *p*); dpen at 8.27 (br s, 6H, N**H**H'), 7.58-7.52 (m, 12H, *o*-Ph), 7.35-7.27 (m, 18H, *m*-, *p*-Ph),

5.24 (br s, 6H, NH**H'**), 5.10 (s, 6H, C**H**NH_2); 2.95 (br s, 9H, $\mathbf{H}_2O$); $tart^{2-}$ at 4.27 (s, 2H), 3.88 (s, 2H); $^{13}C\{^1H\}$ (125 MHz) BAr_f^- at 162.6 (q, $^1J_{BC}$ = 50.0 Hz, *i*), 135.5 (s, *o*), 130.0 (m, *m*), 125.4 (q, $^1J_{CF}$ = 271.7 Hz, **C**F_3), 118.4 (m, *p*); dpen at 137.4 (s, *i*-Ph), 130.1 (s, *p*-Ph), 129.8, 129.6 (2 × s, *o*-, *m*-Ph), 63.5 (s, **C**HNH_2); $tart^{2-}$ at 176.5, 74.9 (2 × s).

Λ-(*S*,*S*)-$\mathbf{1}^{3+}$ (*S*,*S*)-$\mathbf{tart^{2-}BAr_f^-}$. Crude $2Na^+$ (*S*,*S*)-$tart^{2-}$ was prepared by charging a vial with (*S*,*S*)-tartaric acid (1.0000 g, 6.6628 mmol), NaOH (0.5330 g, 13.33 mmol, 2.0 equiv), and distilled H_2O (4 mL). The mixture was vigorously stirred (30 min), and the solvent was removed by rotary evaporation. The white residue was dried by oil pump vacuum (rt, overnight). A vial was charged with Λ-(*S*,*S*)-$\mathbf{1}^{3+}$ $2Cl^-BAr_f^-\cdot 2H_2O$ (0.0605 g, 0.0363 mmol), distilled H_2O (5 mL), CH_2Cl_2 (5 mL), and crude $2Na^+$ (*S*,*S*)-$tart^{2-}$ (0.0167 g, 0.0861 mmol, 2.4 equiv). The biphasic mixture was vigorously stirred (rt, overnight). The orange organic phase was separated and the solvent was removed by rotary evaporation. The residue was dried by oil pump vacuum (rt, overnight) to give Λ-(*S*,*S*)-$\mathbf{1}^{3+}$ (*S*,*S*)-$tart^{2-}BAr_f^-\cdot 2H_2O$ as a bright orange solid (0.0611 g, 0.0351 mmol, 97%), mp 112-121 °C (dec, open capillary). Anal. Calcd. for $C_{78}H_{64}BCoF_{24}N_6O_6\cdot 2H_2O$ (1743.14): C 53.75, H 3.93, N 4.82; found C 53.53, H 3.93, N 4.57.

NMR (acetone-d_6, δ/ppm): ^1H (500 MHz) BAr_f^- at 7.80 (s, 8H, *o*), 7.68 (s, 4H, *p*); dpen at 8.30 (br s, 6H, N**H**H'), 7.58-7.52 (m, 12H, *o*-Ph), 7.36-7.27 (m, 18H, *m*-, *p*-Ph), 5.27 (br s, 6H, NH**H'**), 5.09 (s, 6H, C**H**NH_2); 3.02 (br s, 7H, $\mathbf{H}_2O$); $tart^{2-}$ at 4.30 (s, 2H), 3.86 (s, 2H); $^{13}C\{^1H\}$ (125 MHz) BAr_f^- at 162.6 (q, $^1J_{BC}$ = 49.9 Hz, *i*), 135.5 (s, *o*), 130.0 (m, *m*), 125.4 (q, $^1J_{CF}$ = 272.6 Hz, **C**F_3), 118.4 (m, *p*); dpen at 137.4 (s, *i*-Ph), 129.8 (s, *p*-Ph), 129.73, 129.66 (2 × s, *o*-, *m*-Ph), 63.4 (s, **C**HNH_2); $tart^{2-}$ at 176.5, 74.9 (2 × s).

Λ-(*S*,*S*)-$\mathbf{1}^{3+}$ $\mathbf{(Sb_2((\mathit{R},\mathit{R})\text{-}tart')_2)^{2-}BAr_f^-}$. A vial was charged with Λ-(*S*,*S*)-$\mathbf{1}^{3+}$ $2Cl^-BAr_f^-\cdot 2H_2O$ (0.0781 g, 0.0469 mmol), distilled H_2O (5 mL), CH_2Cl_2 (5 mL), and $2Na^+$ $(Sb_2((R,R)\text{-tart}')_2)^{2-}\cdot 5H_2O$ (0.0317 g, 0.0469 mmol, 1.0 equiv).[20b] The biphasic

mixture was vigorously stirred (rt, overnight). The orange organic phase was separated and the solvent was removed by rotary evaporation. The residue was dried by oil pump vacuum (rt, overnight) to give Λ-(*S*,*S*)-**1**$^{3+}$ $(Sb_2((R,R)\text{-tart}')_2)^{2-}BAr_f^-\cdot 0.5H_2O$ as a bright orange solid (0.0923 g, 0.0439 mmol, 94%), mp 170-185 °C (dec, open capillary). Anal. Calcd. for $C_{82}H_{64}BCoF_{24}N_6O_{12}Sb_2\cdot 0.5H_2O$ (2103.68): C 46.82, H 3.11, N 4.00; found C 47.25, H 3.15, N 3.77.

NMR (acetone-d_6, δ/ppm): ^{1}H (500 MHz) BAr_f^- at 7.80 (s, 8H, *o*), 7.68 (s, 4H, *p*); dpen at 7.64-7.56 (m, 12H, *o*-Ph), 7.31-7.24 (m, 18H, *m*-, *p*-Ph), 6.24 (br s, 6H, N**H**H'), 5.56 (br s, 6H, NH**H'**), 5.15 (s, 6H, C**H**NH_2); 3.45 (br s, 6H, $\mathbf{H}_2O$); $(Sb_2(tart')_2)^{2-}$ at 3.92 (s, 4H); $^{13}C\{^1H\}$ (125 MHz) BAr_f^- at 162.6 (q, $^1J_{BC}$ = 49.8 Hz, *i*), 135.5 (s, *o*), 130.0 (m, *m*), 125.4 (q, $^1J_{CF}$ = 271.9 Hz, **C**F_3), 118.4 (m, *p*); dpen at 136.8 (s, *i*-Ph), 130.0 (s, *p*-Ph), 129.9, 129.6 (2 × s, *o*-, *m*-Ph), 64.9 (s, **C**HNH_2); $(Sb_2(tart')_2)^{2-}$ at 181.8, 78.2 (2 × s).

Λ-(*S*,*S*)-1^{3+} $(Sb_2((S,S)\text{-tart}')_2)^{2-}BAr_f^-$. Λ-(*S*,*S*)-**1**$^{3+}$ $2Cl^-BAr_f^-\cdot 2H_2O$ (0.0518 g, 0.0311 mmol), distilled H_2O (5 mL), CH_2Cl_2 (5 mL), and $2Na^+$ $(Sb_2((S,S)\text{-tart}')_2)^{2-}\cdot 5H_2O$ (0.0210 g, 0.0331 mmol, 1.1 equiv; prepared analogously to the enantiomer[20b]) were combined in a procedure analogous to that for Λ-(*S*,*S*)-**1**$^{3+}$ $(Sb_2((R,R)\text{-tart}')_2)^{2-}BAr_f^-\cdot 0.5H_2O$. An identical workup gave Λ-(*S*,*S*)-**1**$^{3+}$ $(Sb_2((S,S)\text{-tart}')_2)^{2-}BAr_f^-\cdot 0.5H_2O$ as a bright orange solid (0.0654 g, 0.0311 mmol, 99%), mp 174-185 °C (dec, open capillary). Anal. Calcd. for $C_{82}H_{64}BCoF_{24}N_6O_{12}Sb_2\cdot 0.5H_2O$ (2103.68): C 46.82, H 3.11, N 4.00; found C 47.19, H 3.18, N 3.86.

NMR (acetone-d_6, δ/ppm): ^{1}H (500 MHz) BAr_f^- at 7.79 (s, 8H, *o*), 7.68 (s, 4H, *p*); dpen at 7.74-7.64 (m, 12H, *o*-Ph), 7.32-7.22 (m, 18H, *m*-, *p*-Ph), 6.45 (br s, 6H, N**H**H'), 5.74 (br s, 6H, NH**H'**), 4.98 (s, 6H, C**H**NH_2); 3.58 (br s, 6H, $\mathbf{H}_2O$); $(Sb_2(tart')_2)^{2-}$ at 4.64 (s, 4H); $^{13}C\{^1H\}$ (125 MHz) BAr_f^- at 162.6 (q, $^1J_{BC}$ = 49.9 Hz, *i*), 135.5 (s, *o*), 130.0 (m, *m*), 125.4 (q, $^1J_{CF}$ = 271.9 Hz, **C**F_3), 118.5 (m, *p*); dpen at 136.6 (s, *i*-Ph), 130.5 (s, *p*-Ph),

129.7, 129.6 (2 × s, *o*-, *m*-Ph), 65.3 (s, **C**HNH$_2$); (Sb$_2$(tart')$_2$)$^{2-}$ at 181.8, 78.4 (2 × s).

Λ-(*S*,*S*)-1^{3+} 3(1*R*)-camphSO$_3^-$. A suspension of Λ-(*S*,*S*)-**1**$^{3+}$ 3Cl$^-$·3H$_2$O (0.0200 g, 0.0237 mmol) in CH$_2$Cl$_2$ (5 mL) and a solution of (1*R*)-ammonium 3-bromocamphor-8-sulfonate (0.0260 g, 0.0792 mmol, 3.3 equiv) in distilled H$_2$O (5 mL) were combined. The biphasic mixture was rapidly stirred. After 1 h, the phases were allowed to separate. The orange organic phase was washed with distilled H$_2$O (2 × 5 mL) and dried (Na$_2$SO$_4$). The solvent was removed by rotary evaporation. The residue was dried by oil pump vacuum (rt, overnight) to give Λ-(*S*,*S*)-**1**$^{3+}$ 3(1*R*)-camphSO$_3^-$·2H$_2$O as an orange solid (0.0304 g, 0.0183 mmol, 76%), mp 203-210 °C (dec, open capillary), Anal. Calcd. for C$_{72}$H$_{90}$Br$_3$CoN$_6$O$_{12}$S$_3$·2H$_2$O (1662.40): C 52.02, H 5.70, N, 5.06, found C 51.99, H, 5.75, N 4.84.

NMR (acetone-d_6, δ/ppm): ^{1}H (500 MHz) dpen at 7.68 (m, 12H, *o*-Ph), 7.26 (m, 18H, *m*-, *p*-Ph), 7.07 (br s, 6H, N**H**H'), 5.67 (br s, 6H, NH**H'**), 5.05 (m, 6H, C**H**NH$_2$); 2.90 (br s, 6H, **H**$_2$O); camphSO$_3^-$ at 4.78 (d, J = 3.8 Hz, 3H), 3.16 (t, J = 4.3 Hz, 3H), 3.02 (d, J = 14.2 Hz, 3H), 2.40 (d, J = 14.2 Hz, 3H), 2.29-2.15 (m, 3H), 2.01 (ddd, J = 13.2, 9.6, 3.8 Hz, 3H), 1.84-1.76 (m, 3H), 1.29 (ddd, J = 14.4, 9.4, 5.4 Hz, 3H), 1.18 (s, 9H), 0.86 (s, 9H); ^{13}C{^{1}H} (125 MHz) dpen at 136.2 (s, *i*-Ph), 129.6 (s, *p*-Ph), 128.7, 128.6 (2 × s, *o*-, *m*-Ph), 62.6 (s, **C**HNH$_2$); camphSO$_3^-$ at 211.7, 60.0, 54.9, 54.7, 48.2, 47.9, 30.7, 22.8, 18.0, 10.2 (10 × s).

Λ-(*S*,*S*)-1^{3+} 3(1*S*)-camphSO$_3^-$. Λ-(*S*,*S*)-**1**$^{3+}$ 3Cl$^-$·3H$_2$O (0.0200 g, 0.0234 mmol), CH$_2$Cl$_2$ (5 mL), (1*S*)-ammonium 3-bromocamphor-8-sulfonate (0.0260 g, 0.0792 mmol, 3.3 equiv), and distilled H$_2$O (5 mL) were combined in a procedure analogous to that for Λ-(*S*,*S*)-**1**$^{3+}$ 3(1*R*)-camphSO$_3^-$. An identical workup gave Λ-(*S*,*S*)-**1**$^{3+}$ 3(1*S*)-camphSO$_3^-$·3H$_2$O as an orange solid (0.0286 g, 0.0170 mmol, 73%), mp 129 °C (dec, open capillary), Anal. Calcd. for C$_{72}$H$_{90}$Br$_3$CoN$_6$O$_{12}$S$_3$·3H$_2$O (1680.41): C 51.46, H

5.76, N, 5.00; found C 51.54, H, 5.84, N 4.82.

NMR (acetone-d_6, δ/ppm): ^{1}H (500 MHz) dpen at 7.68 (m, 12H, *o*-Ph), 7.26 (m, 18H, *m*-, *p*-Ph), 7.07 (br s, 6H, N**H**H'), 5.67 (br s, 6H, NH**H'**), 5.05 (m, 6H, C**H**NH_2); 2.92 (br s, 4H, $\mathbf{H}_2O$); camphSO_3^- at 4.78 (d, J = 3.8 Hz, 3H), 3.13 (t, J = 4.3 Hz, 3H), 2.94-2.88 (m, 3H), 2.56 (d, J = 14.2 Hz, 3H), 2.25-2.15 (m, 3H), 1.98 (ddd, J = 13.2, 9.6, 3.7 Hz, 3H), 1.69 (ddd, J = 15.0, 12.2, 3.8 Hz, 3H), 1.27 (ddd, J = 14.4, 9.4, 5.4 Hz, 3H), 1.22 (s, 9H), 0.88 (s, 9H); ^{13}C{^{1}H} (125 MHz) dpen at 137.1 (s, *i*-Ph), 130.4 (s, *p*-Ph), 129.5, 129.4 (2 × s, *o*-, *m*-Ph), 63.5 (s, **C**HNH_2); camphSO_3^- at 211.7, 60.0, 54.9, 54.7, 48.2, 47.9, 30.7, 22.8, 18.0, 10.2 (10 × s).

Λ-(*S*,*S*)-$\mathbf{1}^{3+}$ 3*(R)*-BINOLPA$^-$. A vial was charged with a suspension of Λ-(*S*,*S*)-$\mathbf{1}^{3+}$ $3Cl^-\cdot 3H_2O$ (0.0500 g, 0.0598 mmol) in CH_2Cl_2 (10 mL), (*R*)-BINOLPAH (0.0630 g, 0.181 mmol, 3.0 equiv), NaOH (0.0072 g, 0.18 mmol, 3.0 equiv) and distilled H_2O (10 mL). The biphasic mixture was vigorously stirred. After 4 h, the phases were allowed to separate. The orange organic phase was washed with distilled H_2O (2 × 10 mL) and dried (Na_2SO_4). The solvent was removed by rotary evaporation. The residue was dried by oil pump vacuum (rt, overnight) to give Λ-(*S*,*S*)-$\mathbf{1}^+$ 3(*R*)-BINOLPA$^-\cdot 3H_2O$ as an orange solid (0.0855 g, 0.0468 mmol, 78%), mp 237-249 °C (dec, open capillary), Anal. Calcd. for $C_{102}H_{84}CoN_6O_{12}P_3\cdot 3H_2O$ (1827.76): C 67.03, H 5.18, N, 4.60, found C 66.84, H, 4.79, N 4.33.

NMR (acetone-d_6, δ/ppm): ^{1}H (500 MHz) 8.09 (d, $^3J_{HH}$ = 8.8 Hz, 6H), 7.91 (d, $^3J_{HH}$ = 8.2 Hz, 6H), 7.71-7.59 (m, 6H, N**H**H'), 7.51-7.40 (m, 18H), 7.40-7.24 (m, 18H), 7.20-7.06 (m, 18H), 5.92 (br s, 6H, NH**H'**), 4.86 (br s, 6H, C**H**NH_2); 3.02 (br s, 6H, $\mathbf{H}_2O$); ^{13}C{^{1}H} (125 MHz) dpen at 137.1 (s, *i*-Ph), 130.0 (s, *p*-Ph), 129.4, 129.1 (2 × s, *o*-, *m*-Ph), 63.6 (s, **C**HNH_2); BINOLPA$^-$ at 150.5 (d, $^2J_{CP}$ = 9.2 Hz) 133.3, 132.0, 131.3, 129.4, 127.4, 126.9, 125.5, 123.0, 122.9 (9 × s).

Λ-(*S*,*S*)-$\mathbf{1}^{+}$ 3(*S*)-BINOLPA^{-}. Λ-(*S*,*S*)-$\mathbf{1}^{3+}$ $3Cl^{-}\cdot 3H_2O$ (0.0500 g, 0.0598 mmol), CH_2Cl_2 (10 mL), (*S*)-BINOLPAH (0.0630 g, 0.181 mmol, 3.0 equiv), NaOH (0.0072 g, 0.18 mmol, 3.0 equiv), and distilled H_2O (10 mL) were combined in a procedure analogous to that for Λ-(*S*,*S*)-$\mathbf{1}^{3+}$ 3*(R)*-BINOLPA^{-}. An identical workup gave Λ-(*S*,*S*)-$\mathbf{1}^{+}$ 3(*S*)-BINOLPA$^{-}\cdot 4H_2O$ as an orange solid (0.0777 g, 0.0429 mmol, 72%), mp 234-240 °C (dec, open capillary), Anal. Calcd. for $C_{102}H_{84}CoN_6O_{12}P_3\cdot 4H_2O$ (1809.74): C 67.70, H 5.12, N, 4.64, found C 67.84, H, 5.12, N 4.22.

NMR (acetone-d_6, δ/ppm): ^{1}H (500 MHz) dpen at 7.65-7.53 (m, 12H, *o*-Ph), 7.44-7.32 (m, 18H, *m*-, *p*-Ph), 7.17 (br s, 6H, N**H**H'), 5.92 (s, 6H, NH**H'**), 5.19-5.09 (br s, 6H, C**H**NH_2); 3.02 (br s, 6H, $\mathbf{H}_2O$); BINOLPA^{-} at 7.98 (d, $^{3}J_{HH}$ = 8.8 Hz, 6H), 7.91 (d, $^{3}J_{HH}$ = 8.2 Hz, 6H), 7.34-7.23 (m, 6H), 7.10-6.98 (m, 18H); $^{13}C\{^{1}H\}$ (125 MHz) dpen at 137.1 (s, *i*-Ph), 129.9 (s, *p*-Ph), 129.4, 129.3 (2 × s, *o*-, *m*-Ph), 64.1 (s, **C**HNH_2); BINOLPA^{-} at 150.4 (d, $^{2}J_{CP}$ = 9.2 Hz), 133.3, 132.0, 131.3, 129.2, 127.4, 126.9, 125.5, 123.0, 122.9 (9 × s).

Λ-(*S*,*S*)-$\mathbf{1}^{3+}$ 2Br^{-}BAr$_f^{-}$. A gas-circulating flask[15] was charged with $Co(OAc)_2\cdot 4H_2O$ (0.1255 g, 0.5039 mmol), activated charcoal (0.1000 g), (*S*,*S*)-dpen (0.4250 g, 2.002 mmol, 4.0 equiv), and CH_3OH (50 mL). The mixture was vigorously stirred. After 30 h, the sample was filtered through Celite. Aqueous HBr (1.0 mL, 8.9 M) was added to the orange filtrate. The dark yellow solution was concentrated via rotary evaporation, and H_2O (50 mL) was added. The suspension was filtered. The filter cake was washed with H_2O (50 mL) and dried by oil pump vacuum (rt, overnight) to give crude Λ-(*S*,*S*)-$\mathbf{1}^{3+}$ $3Br^{-}$ as a dark yellow solid (0.4456 g, 0.4503 mmol if pure sample). A portion of this solid (0.1024 g, 0.1035 mmol if pure), Na^{+} BAr_f^{-} (0.0916 g, 0.103 mmol, 1.0 equiv), and CH_2Cl_2 (5 mL) were added to a round-bottom flask. The mixture was sonicated (5 min) and filtered. The filtrate was chromatographed (2.0 × 10 cm silica gel

column), eluting with CH_2Cl_2/CH_3OH (100:0 to 97:3 (v/v)). The solvent was removed from the main yellow band by rotary evaporation. The residue was dried by oil pump vacuum (rt, overnight) to give Λ-(*S*,*S*)-**1**$^{3+}$ 2Br$^-$BAr$_f^-$·H_2O as a yellow solid (0.1356 g, 0.07807 mmol, 75% from Λ-(*S*,*S*)-**1**$^{3+}$ 3Br$^-$), mp 112-130 °C (dec, open capillary). Anal. Calcd. for $C_{74}H_{60}BBr_2CoF_{24}N_6·H_2O$ (1736.86): C 51.17, H 3.60, N 4.84; found C 51.37, H 3.80, N 4.52.

NMR (acetone-d_6, δ/ppm): ^{1}H (500 MHz) BAr$_f^-$ at 7.79 (s, 8H, *o*), 7.68 (s, 4H, *p*); dpen at 8.04 (br s, 6H, N**H**H'), 7.53-7.48 (m, 12H, *o*-Ph), 7.34-7.30 (m, 18H, *m*-, *p*-Ph), 5.35 (br s, 6H, NH**H'**), 5.13 (s, 6H, C**H**NH_2); 2.88 (br s, 11H, $\mathbf{H}_2O$); $^{13}C\{^1H\}$ NMR (125 MHz): BAr$_f^-$ at 162.6 (q, $^1J_{BC}$ = 50.3 Hz, *i*), 135.6 (s, *o*), 130.0 (m, *m*), 125.4 (q, $^1J_{CF}$ = 271.6 Hz, **C**F_3), 118.5 (m, *p*); dpen at 137.1 (s, *i*-Ph), 130.1 (s, *p*-Ph), 130.0, 129.6 (2 × s, *o*-, *m*-Ph), 63.3 (s, **C**HNH_2).

Dimethyl 2-(2-nitro-1-phenylethyl)malonate (**2**; Figure 3.5)**.** An authentic sample of this known compound was obtained as a colorless oil by a literature procedure.[2] A 5 mm NMR tube was charged with a solution of *trans*-β-nitrostyrene (0.0054 g, 0.036 mmol, 1.0 equiv), catalyst (0.0036 mmol, 0.10 equiv), dimethyl malonate (0.0045 mL, 0.0052 g, 0.039 mmol, 1.1 equiv), and Ph_2SiMe_2 (0.0020 mL, internal standard) in acetone-d_6 (0.40 mL). A ^{1}H NMR spectrum was recorded to confirm the initial *trans*-β-nitrostyrene/standard ratio. A stir bar was added and the sample was cooled to 0 °C. Then Et_3N (0.0050 mL, 0.0036 g, 0.036 mmol, 1.0 equiv) was added and the mixture stirred. After 24 h, the stir bar was removed and the yield of **2** was assayed by ^{1}H NMR. The solvent was removed under reduced pressure to give an orange oil, which was added to a plug of silica. The plug was eluted with hexanes/EtOAc (1:1 v/v). The solvent was removed from the fraction containing the product under reduced pressure. The enantiomeric excess was determined by HPLC (Chiralpak AD column, 98:2 v/v hexanes/isopropanol,

1.0 mL/min, λ = 220 nm; for entry 20 t_R = 35.0 and 44.8 min (major and minor)).[35]

***N,N'*-bis(t-butoxycarbonyl)-1-hydrazino-2-oxocyclopentanecarboxylic acid methyl ester** (**3**; Figure 3.6)**.** This known compound was obtained as a colorless oil by a literature procedure.[4a] A 5 mm NMR tube was charged with a solution of di-*tert*-butylazodicarboxylate (0.0083 g, 0.036 mmol, 1.0 equiv), catalyst (0.0036 mmol, 0.10 equiv), methyl 2-oxocyclopentanecarboxylate (0.0046 mL, 0.0053 g, 0.037 mmol, 1.0 equiv), and Ph_2SiMe_2 (0.0020 mL, internal standard) in CD_3CN (0.40 mL). A ^1H NMR spectrum was recorded to confirm the initial di-*tert*-butylazodicarboxylate/standard ratio. A stir bar was added and the sample was cooled to 0 °C. Then NMM (0.0040 mL, 0.0037 g, 0.036 mmol, 1.0 equiv) was added and the mixture stirred. After 24 h, the stir bar was removed and the yield of **3** was assayed by ^1H NMR. The solvent was removed under reduced pressure to give an orange oil, which was added to a plug of silica. The plug was eluted with hexanes/EtOAc (7:3 v/v). The solvent was removed from the fraction containing the product under reduced pressure. The enantiomeric excess was determined by HPLC (Chiralpak AD column, 96:4 v/v hexanes/isopropanol, 1.0 mL/min, λ = 210 nm; for entry 20 t_R = 14.0 and 20.2 min (minor and major).[36]

Crystallography. A solution of Δ-(*S*,*S*)-$\mathbf{1}^{3+}$ 2(1*S*)-camph$SO_3^-BAr_f^-$ (0.189 g, 0.0865 mmol) in CH_2Cl_2 (10 mL) was kept in a closed container at room temperature. After 2 d, brown block crystals were collected. Synchrotron radiation (see Acknowledgements) was employed for crystal screening, unit cell determination, and data collection on a D8 goniostat equipped with PHOTON detector at Beamline 11.3.1 (λ = 0.8857 Å). Integrated intensity information for each reflection was obtained by reduction of the data frames with the program APEX2.[37] All data were corrected for Lorentz and polarization factors, as well as for crystal decay effects. The program SADABS[38] was employed to correct for absorption effects. Additional data are provided in Table 3.1.

Systematic reflection conditions and statistical tests suggested the space group $P2_12_12_1$. A solution was readily obtained using SHELXTL (XS).[39] No reflections were observed above 1.0 Å resolution, possibly suggesting significant disorder. The absence of additional symmetry or voids was confirmed using PLATON (ADDSYM).[40] All non-hydrogen atoms were refined with anisotropic thermal parameters. Hydrogen atoms were placed in idealized positions and refined using a riding model. Elongated anisotropic displacement ellipsoids were noted for a phenyl group and several fluorine atoms. Efforts to model this disorder not only increased the number of restraints and/or constraints, but also did not improve the reliability factors. Consequently, RIGU and SIMU restraints were used to keep the ellipsoids reasonable. Also, difference Fourier maps indicated electron densities suggesting disordered and/or partially occupied solvent molecules; these could not be modeled and were eventually removed by MASK using OLEX2.[41] The structure was refined (weighted least squares on F^2) to convergence.[39,40] The Flack parameter (0.004(5)) confirmed the absolute configuration.[42]

Table 3.1. Summary of crystallographic data for Δ-(*S*,*S*)-$\mathbf{1}^{3+}$ 2(1*S*)-camphSO_3^-BAr$_f^-$.[a]

empirical formula	$C_{94}H_{88}BBr_2CoF_{24}N_6O_8S_2$
formula weight	2179.38
temperature of collection [K]	110.15
diffractometer	Bruker D8
wavelength [Å]	0.8857
crystal system	orthorhombic
space group	$P2_12_12_1$
unit cell dimensions:	
a [Å]	18.4403(12)
b [Å]	25.0680(17)
c [Å]	25.5947(17)
α [°]	90
β [°]	90
γ [°]	90
V [Å^3]	11831.4(14)
Z	4
ρ_{calc} [Mg/m^3]	1.224
absorption coefficient [mm^{-1}]	1.680
F(000)	4432
Crystal size [mm^3]	0.04 × 0.03 × 0.01
Θ [deg]	2.227 to 25.202
range / indices (*h*, *k*, *l*)	–17,17; 0,24; 0,24
reflections collected	10970
independent reflections	10970 [R(int) = 0.0898]
completeness to Θ = 25.202°	99.7%
absorption correction	semi-empirical from equivalents
max. and min. transmission	0.7454 and 0.6109
refinement method	full-matrix least-squares on F^2
data / restraints / parameters	10970 / 1388 / 1241
goodness-of-fit on F^2	1.016
final R indices [I>2σ(I)]	$R1$ = 0.0572, w$R2$ = 0.1477
R indices (all data)	$R1$ = 0.0777, w$R2$ = 0.1593
absolute structure (Flack) parameter	0.004(5)
largest diff. peak and hole [e.Å^{-3}]	0.489 / –0.374

[a] The solvent molecules associated with this structure were removed using MASK as detailed in the experimental section. Thus, the formula weight and density are underestimated.

3.5 References (All titles are given in the capitalization format of the original article)

(1) (a) Taylor, M. S.; Jacobsen, E. N. Asymmetric Catalysis by Chiral Hydrogen-Bond Donors. *Angew. Chem., Int. Ed.* **2006***, 45,* 1520-1543; Asymmetrische Katalyse durch chirale Wasserstoffbrückendonoren. *Angew. Chem.* **2006**, *118*, 1550-1573. (b) Doyle, A. G.; Jacobsen, E. N. Small-Molecule H-Bond Donors in Asymmetric Catalysis. *Chem. Rev.* **2007**, *107*, 5713-5743. (c) Yu, X.; Wang, W. Hydrogen-Bond-Mediated Asymmetric Catalysis. *Chem. Asian J.* **2008**, *3*, 516-532. (d) Takemoto, Y. Recognition and Activation by Ureas and Thioureas: Stereoselective Reactions using Ureas and Thioureas as Hydrogen-Bonding Donors. *Org. Biomol. Chem.* **2005**, *3*, 4299-4306. (e) Held, F. E.; Tsogoeva, S. B. Asymmetric Cycloaddition Reactions Catalyzed by Bifunctional Thiourea and Squaramide Organocatalysts: Recent Advances. *Catal. Sci. Technol.* **2016**, *6*, 645-667.

(2) Lewis, K. G.; Ghosh, S. K.; Bhuvanesh, N.; Gladysz, J. A. Cobalt(III) Werner Complexes with 1,2-Diphenylethylenediamine Ligands: Readily Available, Inexpensive, and Modular Chiral Hydrogen Bond Donor Catalysts for Enantioselective Organic Synthesis. *ACS Cent. Sci.* **2015**, *1*, 50-56.

(3) Ghosh, S. K.; Ganzmann, C.; Bhuvanesh, N.; Gladysz, J. A. Werner Complexes with ω-Dimethylaminoalkyl Substituted Ethylenediamine Ligands: Bifunctional Hydrogen-Bond-Donor Catalysts for Highly Enantioselective Michael Additions. *Angew. Chem., Int. Ed.* **2016**, *55*, 4356-4360; Werner-Komplexe mit ω-Dimethylaminoalkyl-substitutierten Ethylendiaminliganden: bifunktionale H-Brückendonor-Katalysatoren für hoch enantioselektive Michael-Additionen. *Angew. Chem.* **2016**, *128*, 4429-4433.

(4) (a) Kumar, A.; Ghosh, S. K.; Gladysz, J. A. Tris(1,2-diphenylethylenediamine)cobalt(III) Complexes: Chiral Hydrogen Bond Donor Catalysts for Enantioselective *α*-Aminations of 1,3-Dicarbonyl Compounds. *Org. Lett.* **2016**, *18*, 760-763. (b) Joshi, H.; Ghosh, S. K.; Gladysz, J. A. Enantioselective Additions of

Stabilized Carbanions to Imines Generated from α-Amido Sulfones By Using Lipophilic Salts of Chiral Tris(1,2-diphenylethylenediamine) Cobalt(III) Trications as Hydrogen Bond Donor Catalysts. *Synthesis* **2017**, *49*, 3905-3915. (c) Maximuck, W. J.; Gladysz, J. A. Lipophilic chiral cobalt(III) complexes of hexaamine ligands; Efficacies as enantioselective hydrogen bond donor catalysts. *Mol. Catal.* **2019**, *473*, 110360.

(5) (a) Scherer, A.; Mukherjee, T.; Hampel, F.; Gladysz, J. A. Metal Templated Hydrogen Bond Donors as 'Organocatalysts' for Carbon-Carbon Bond Forming Reactions: Syntheses, Structures, and Reactivities of 2-Guanidinobenzimidazole Cyclopentadienyl Ruthenium Complexes. *Organometallics* **2014**, *33*, 6709-6722. (b) Mukherjee, T.; Ganzmann, C.; Bhuvanesh, N.; Gladysz, J. A. Syntheses of Enantiopure Bifunctional 2-Guanidinobenzimidazole Cyclopentadienyl Ruthenium Complexes: Highly Enantioselective Organometallic Hydrogen Bond Donor Catalysts for Carbon-Carbon Bond Forming Reactions. *Organometallics* **2014**, *33*, 6723-6737.

(6) (a) Chen, L.-A.; Tang, X.; Xi, J.; Xu, W.; Gong, L.; Meggers, E. Chiral-at-Metal Octahedral Iridium Catalyst for the Asymmetric Construction of an All-Carbon Quaternary Stereocenter. *Angew. Chem., Int. Ed.* **2013**, *52*, 14021-14025 and *Angew. Chem.* **2013**, *125*, 14271-14275. (b) Huo, H.; Fu, C.; Wang, C.; Harms, K.; Meggers, E. Metal-templated Enantioselective Enamine/H-bonding Dual Activation Catalysis. *Chem. Commun*. **2014**, *50*, 10409-10411. (c) Hu, Y.; Zhou, Z.; Gong, L.; Meggers, E. Asymmetric aza-Henry reaction to provide oxindoles with quaternary carbon stereocenter catalyzed by a metal-templated chiral Bronsted base. *Org. Chem. Front.* **2015**, *2*, 968-972. (d) Ding, X.; Lin, H.; Gong, L.; Meggers, E. Enantioselective Sulfa-Michael Addition to α,β-Unsaturated γ-Oxoesters Catalyzed by a Metal-Templated Chiral Brønsted Base. *Asian J. Org. Chem.* **2015**, *4*, 434-437. (e) Xu, W.; Arieno, M.; Löw, H.; Huang, K.; Xie, X.; Cruchter, T.; Ma, Q.; Xi, J.; Huang, B.; Wiest, O.; Gong, L.; Meggers, E. Metal-

Templated Design: Enantioselective Hydrogen-Bond-Driven Catalysis Requiring Only Parts-per-Million Catalyst Loading. *J. Am. Chem. Soc.* **2016,** *138*, 8774-8780. (f) Ding, X.; Tian, C.; Hu, Y.; Gong, L.; Meggers, E. Tuning the Basicity of a Metal-Templated Brønsted Base to Facilitate the Enantioselective Sulfa-Michael Addition of Aliphatic Thiols to α,β-Unsaturated *N*-Acylpyrazoles. *Eur. J. Org. Chem.* **2016**, *2016*, 887-890.

(7) (a) Belokon, Y. N.; Maleev, V. I.; North, M.; Larionov, V. A.; Savel'yeva, T. F.; Nijland, A.; Nelyubina, Y. V. Chiral Octahedral Complexes of Co^{III} As a Family of Asymmetric Catalysts Operating under Phase Transfer Conditions. *ACS Catal.* **2013**, *3*, 1951-1955. (b) Maleev, V. I.; North, M.; Larionov, V. A.; Fedyanin, I. V.; Savel'yeva, T. F.; Moscalenko, M. A.; Smolyakov, A. F.; Belokon, Y. N. Chiral Octahedral Complexes of Cobalt(III) as "Organic Catalysts in Disguise" for the Asymmetric Addition of a Glycine Schiff Base Ester to Activated Olefins. *Adv. Synth. Catal.* **2014**, *356*, 1803-1810. (c) Larionov, V. A.; Markelova, E. P.; Smol'yakov, A. F.; Savel'yeva, T. F.; Maleev, V. I.; Belokon, Y. N. Chiral octahedral complexes of Co(III) as catalysts for asymmetric epoxidation of chalcones under phase transfer conditions. *RSC Adv.* **2015**, *5*, 72764-72771. (d) Rulev, Y. A.; Larionov, V. A.; Lokutova, A. V.; Moscalenko, M. A.; Lependina, O. L.; Maleev, V. I.; North, M.; Belokon, Y. N. Chiral Cobalt(III) Complexes as Bifunctional Brønsted Acid-Lewis Base Catalysts for the Preparation of Cyclic Organic Carbonate. *ChemSusChem* **2016**, *9*, 216-222.

(8) (a) Pardo, P.; Carmona, D.; Lamata, P.; Rodríguez, R.; Lahoz, F. J.; García-Orduña, P.; Oro, L. A. Reactivity of the Chiral Metallic Brønsted Acid [(η^6-*p*-MeC_6H_4*i*Pr)Ru(κ^3*P*,*O*,*O*′-POH)][SbF_6]$_2$ (POH = S_{C1},R_{C2})-$Ph_2PC(Ph)HC(OH)HCH_2OMe$) toward Aldimines. *Organometallics* **2014**, *33*, 6927-6936. (b) Skubi, K. L.; Kidd, J. B.; Jung, H.; Guzei, I. A.; Baik, M.-H.; Yoon, T. P. Enantioselective Excited-State Photoreactions Controlled by a Chiral Hydrogen-Bonding Iridium Sensitizer. *J. Am. Chem. Soc.* **2017**, *139*, 17186-17192. (c) For relevant achiral

catalysts, see Nickerson, D. M.; Angeles, V. V.; Auvil, T. J.; So, S. S.; Mattson, A. E. Internal Lewis Acid Assisted Ureas: Tunable Hydrogen Bond Donor Catalysts. *Chem. Commun*. **2013**, *49*, 4289-4291 and earlier work cited therein.

(9) (a) Werner, A. Zur Kenntnis des asymmetrischen Kobaltatoms. I. *Ber. Dtsch. Chem. Ges.* **1911**, *44*, 1887-1898. King, V. L. is listed as an author for the experimental section. (b) Werner, A. Zur Kenntnis des asymmetrischen Kobaltatoms. II. *Ber. Dtsch. Chem. Ges.* **1911**, *44*, 2445-2455. (c) Werner, A. Zur Kenntnis des asymmetrischen Kobaltatoms. III. *Ber. Dtsch. Chem. Ges.* **1911**, *44*, 3272-3278. (d) Werner, A. Zur Kenntnis des asymmetrischen Kobaltatoms. IV. *Ber. Dtsch. Chem. Ges.* **1911**, *44*, 3279-3284. (e) Werner, A. Zur Kenntnis des asymmetrischen Kobaltatoms. V. *Ber. Dtsch. Chem. Ges.* **1912**, *45*, 121-130.

(10) (a) Morral, F. R. Alfred Werner and Cobalt Complexes. In *Werner Centennial*; Kauffman, G. B., Ed.; American Chemical Society: Washington, D. C., 1967; Vol. 62; pp. 70-77. (b) Kauffman, G. B. Alfred Werner's Research on Optically Active Coordination Compounds. *Coord. Chem. Rev.* **1974**, *12*, 105-149.

(11) Ehnbom, A.; Ghosh, S. K.; Lewis, K. G.; Gladysz, J. A. Octahedral Werner complexes with substituted ethylenediamine ligands: a stereochemical primer for a historic series of compounds now emerging as a modern family of catalysts. *Chem. Soc. Rev.* **2016**, *45*, 6799-6811.

(12) Ganzmann, C.; Gladysz, J. A. Phase Transfer of Enantiopure Werner Cations into Organic Solvents: An Overlooked Family of Chiral Hydrogen Bond Donors for Enantioselective Catalysis. *Chem. Eur. J.* **2008**, *14*, 5397-5400.

(13) See also Luu, Q. H.; Lewis, K. G.; Banerjee. A.; Bhuvanesh, N.; Gladysz, J. A. The robust, readily available cobalt(III) trication $[Co(NH_2CHPhCHPhNH_2)_3]^{3+}$ is a progenitor of broadly applicable chirality and prochirality sensing agents. *Chem. Sci.* **2018**, *9*, 5087-5099.

(14) As of the submission date of this manuscript, the best prices are (*R*,*R*)-dpen, $348/ 100 g and (*S*,*S*)-dpen, $358/100 g (https:// www.ambeed.com, accessed 24 September 2019).

(15) Ghosh, S. K.; Lewis, K. G.; Kumar, A.; Gladysz, J. A. Syntheses of Families of Enantiopure and Diastereopure Cobalt Catalysts Derived from Trications of the Formula $[Co(NH_2CHArCHArNH_2)_3]^{3+}$. *Inorg. Chem.* **2017**, *56*, 2304-2320.

(16) Reviews: (a) Parmar, D.; Sugiono, E.; Raja, S.; Rueping, M. Complete Field Guide to Asymmetric BINOL-Phosphate Derived Brønsted Acid and Metal Catalysis: History and Classification by Mode of Activation; Brønsted Acidity, Hydrogen Bonding, Ion Pairing, and Metal Phosphates. *Chem. Rev.* **2014**, *114*, 9047-9153. (b) Phipps, R. J.; Hamilton, G. L.; Toste, F. D. The progression of chiral anions from concepts to applications in asymmetric catalysis. *Nat. Chem.* **2012**, *4*, 603-614.

(17) See, *inter alia* (a) Rueping, M.; Antonchick, A. P.; Theissman, T. A Highly Enantioselective Brønsted Acid Catalyzed Cascade Reaction: Organocatalytic Transfer Hydrogenation of Quinolines and their Application in the Synthesis of Alkaloids. *Angew. Chem., Int. Ed.* **2006**, *45*, 3683-3686; Eine hoch enantioselektive Brønsted-Säure-katalysierte Kaskadenreaktion: organokatalytische Transferhydrierung von Chiolinen und deren Anwendung in der Synthese von Alkaloiden. *Angew. Chem.* **2006**, *118*, 3765-3768. (b) Rueping, M.; Koenigs, R. M.; Atodiresei, I. Unifying Metal and Brønsted Acid Catalysis–Concepts, Mechanisms, and Classifications. *Chem. Eur. J.* **2010**, *16*, 9350-9365 (c) Kwon, Y.; Li, J.; Reid, J. P.; Crawford, J. M.; Jacob, R.; Sigman, M. S.; Toste, F. D.; Miller, S. J. Disparate Catalytic Scaffolds for Atroposelective Cyclodehydration. *J. Am. Chem. Soc.* **2019**, *141*, 6698-6705. (d) Ouyang, J.; Kennemur, J. L.; De, C. K.; Farès, C.; List, B. Strong and Confined Acids Enable a Catalytic Asymmetric Nazarov Cyclization of Simple Divinyl Ketones. *J. Am. Chem. Soc.* **2019**, *141*, 3414-3418.

(18) Masamune, S.; Choy, W.; Peterson, J. S.; Sita, L. R. Double Asymmetric

Synthesis and a New Strategy for Stereochemical Control in Organic Synthesis. *Angew. Chem., Int. Ed.* **1985**, *24*, 1-30; Doppelte Stereodifferenzierung und eine neue Strategie zur Stereokontrolle in der Organischen Synthese. *Angew. Chem.* **1985**, *97*, 1-31.

(19) (a) For the antimony compound in Figure 3.2, the abbreviation $Sb_2(tart)_2^{2-}$ dominates in the literature.[20] However the structure depicted does not feature the entity generally accepted as "tartrate", but rather two doubly deprotonated tartrates (quadruply deprotonated tartaric acids). To help resolve this inconsistency while keeping close to the commonly used name, the primed abbreviation $Sb_2(tart')_2^{2-}$ is employed herein. (b) The "old school" authors regard Ph as an abbreviation for C_6H_5, and therefore consider $(i\text{Pr})_3\text{Ph}$ and $(CF_3)_2\text{Ph}$ to be "failed nomenclature". These designations are nonetheless employed for consistency with the literature.

(20) (a) Nakazawa, H.; Yoneda, H. Chromatographic Study of Optical Resolution II. Separation of Optically Active Cobalt(III) Complexes Using Potassium Antimony d-Tartrate as Eluent. *J. Chromatog.* **1978**, *160*, 89-99. (b) Bernhardt, P. V.; Dyahningtyas, T. E.; Harrowfield, J. M.; Kim, J.-Y.; Kim, Y.; Rukmini, E. Chiral Resolution of Hexaamine Cobalt(III) Cages: Substituent Effects on Chiral Discrimination. *Aust. J. Chem.* **2003**, *56*, 1187-1191. (c) Clark, I. J.; Crispini, A.; Donnelly, P. S.; Engelhardt, L. M.; Harrowfield, J. M.; Jeong, S.-H.; Kim, Y.; Koutsantonis, G. A.; Lee, Y. H.; Lengkeek, N. A.; Mocerino, M.; Nealon, G. L.; Ogden, M. I.: Park, Y. C.; Pettinari, C.; Polanzan, L.; Rukmini, E.; Sargeson, A. M.; Skelton, B. W.; Sobolev, A. N.; Thuéry, P.; White, A. H. Variations on a Cage Theme: Some Complexes of Bicyclic Polyamines as Supramolecular Synthons. *Aust. J. Chem.* **2009**, *62*, 1246-1260.

(21) It is difficult to systematically retrieve this literature via the usual search methods, and hits are scarce in reviews of chiral anions in enantioselective catalysis.[16] For a study involving a poorly coordinating chiral anion where the isolated diastereomeric catalysts give identical ee values, see Lacour, J.; Monchaud, D.; Marsol, C. Effect of the

medium on the oxaziridinium-catalyzed enantioselective epoxidation. *Tetrahedron Lett.* **2002**, *43*, 8257-8260.

(22) Studies involving diastereomeric combinations of chiral anions and chiral ligands in the presence of achiral metal cations have been reported. These undoubtedly entail the generation of catalytically active salts comprised of chiral cations and chiral anions. Although the anion/ligand combinations have not been extensive, one exhibits a pronounced matched/mismatched effect. See (a) Llewellyn, D. B.; Adamson, D.; Arndtsen, B. A. A Novel Example of Chiral Counteranion Induced Enantioselective Metal Catalysis: The Importance of Ion-Pairing in Copper Catalyzed Olefin Aziridination and Cyclopropanation. *Org. Lett.* **2000**, *2*, 4165-4168. (b) Hamilton, G. L.; Kang, E. J.; Mba, M.; Toste, F. D. A Powerful Chiral Counterion Strategy for Asymmetric Transition Metal Catalysis. *Science* **2007**, *317*, 496-499.

(23) There are studies in which the addition of a chiral Brønsted acid to a neutral chiral metal complex or a silver salt of a chiral anion to a neutral chiral metal chloride complex would logically generate salts comprised of chiral cations and chiral anions. Some of the limited number of combinations reported exhibit pronounced matched/mismatched effects. See (a) Li, C.; Wang, C.; Villa-Marcos, B.; Xiao, J. Chiral Counteranion-Aided Asymmetric Hydrogenation of Acyclic Imines. *J. Am. Chem. Soc.* **2008**, *130*, 14450-14451. (b) Aikawa, K.; Kojima, M.; Mikami, K. Synergistic Effect: Hydroalkoxylation of Allenes through Combination of Enantiopure BIPHEP-Gold Complexes and Chiral Anions. *Adv. Synth. Catal.* **2010**, *352*, 3131-3135.

(24) Ghosh, S. K.; Ehnbom, A.; Lewis, K. G.; Gladysz, J. A. Hydrogen bonding motifs in structurally characterized salts of the tris(ethylenediamine) cobalt trication, $[Co(en)_3]^{3+}$; An interpretive review, including implications for catalysis. *Coord. Chem. Rev.* **2017**, *350*, 30-48.

(25) (a) Kuroda, R.; Mason, S. F. Crystal Structure and Absolute Configuration of

(+)-Tris[(–)-1,2-diphenylethylenediamine]cobalt(III) Nitrate Monohydrate. *J. Chem. Soc., Dalton Trans.* **1977**, 1016-1020. (b) De los Santos, Z. A.; Lynch, C. C.; Wolf, C. Optical Chirality Sensing with an Auxiliary-Free Earth-Abundant Cobalt Probe. *Angew. Chem., Int. Ed.* **2019**, *58*, 1198-1202; Optische Chiralitätssensorik mit ligandenfreien, weit verbreiteten Cobaltsalzen. *Angew. Chem.* **2019**, *131*, 1211-1215.

(26) Abbasi, M. A.; "Aziz-ur-Rehman"; Akkurt, M.; Jahangir, M.; Ng, S. W.; Khan, I. U. Ammonium [(1*S*)-(*endo,anti*)]-(–)-3-bromocamphor-8-sulfonate. *Acta Crystallogr.* **2010**, *E66*, o1707-o1708. The authors are uncertain how to format the fully hyphenated name highlighted by quote marks for publication.

(27) Rius, J.; Gali, S. Tris(ethylenediamine) Cobalt(III) Arseniate Trihydrate, $[Co(C_2H_8N_2)_3]$ $AsO_4 \cdot 3H_2O$. *Cryst. Struct. Commun.* **1982**, *11*, 829-831.

(28) (a) Lungwitz, R.; Spange, S. A hydrogen bond accepting (HBA) scale for anions, including room temperature ionic liquids. *New. J. Chem.* **2008**, *32*, 392-394. (b) Cláudio, A. F. M.; Swift, L.; Hallett, J. P.; Welton, T.; Coutinho, J. A. P.; Freire, M. G. Extended scale for the hydrogen-bond basicity of ionic liquids. *Phys. Chem. Chem. Phys.* **2014**, *16*, 6593-6601.

(29) Wititsuwannakul, T.; Hall, M. B.; Gladysz, J. A. A Computational Study of Hydrogen Bonding Motifs in Halide, Tetrafluoroborate, Hexafluorophosphate, and Tetraarylborate Salts of Chiral Cationic Ruthenium and Cobalt Guanidinobenzimidazole Hydrogen Bond Donor Catalysts; Acceptor Properties of the "BArf" Anion. *Polyhedron* **2020**, *187*, 114618.

(30) (a) Ogino, K.; Saito, U. Association Involving Optically Active Ions. I. Association Constants of Tris(ethylenediamine)cobalt(III) and Tartrate Ions. *Bull. Chem. Soc. Jpn.* **1967**, *40*, 826-829. (b) Yoneda, H.; Taura, T. Stereoselectivity in Ion-Pair Formation. I. Association Constants of Λ- and Δ-$[Co(en)_3]^{3+}$ with L- and *meso*-Tartrates from CD Measurements. *Chem. Lett.* **1977**, *6*, 63-66.

(31) Mizuta, T.; Toshitani, K.; Miyoshi, K.; Yoneda, H. Structural Study of Optical Resolution. 14. Highly Efficient Chiral Discrimination of the *lel*$_3$-Tris(*trans*-1,2-cyclohexanediamine)cobalt(III) Ion Attained with the *d*-(*R*,*R*)-Tartrate Ion Assuming an Anomalous Conformation. *Inorg. Chem.* **1990**, *29*, 3020-3026.

(32) Kabes, C. Q.; Maximuck, W. J.; Ghosh, S. K.; Kumar, A.; Bhuvanesh, N.; Gladysz, J. A. Chiral Tricationic Tris(1,2-diphenylethylenediamine) Cobalt(III) Hydrogen Bond Donor Catalysts with Defined Carbon/Metal Configurations; Matched/Mismatched Effects upon Enantioselectivities with Enantiomeric Chiral Counter Anions. *ACS Catal.* **2020**, *10*, 3249-3263.

(33) We have so far completed DFT investigations of (1) ion pairing in halide, BF_4^-, PF_6^-, and BAr_f^- salts of chiral ruthenium monocations and cobalt trications related to the systems in this paper,[29] and (2) the mechanism of enantioselection for the reaction in Figure 3.5 with salts of chiral ruthenium monocations as catalysts: Wititsuwannakul, T.; Mukherjee, T.; Hall, M. B.; Gladysz, J. A. Computational Investigations of Enantioselection in Carbon-Carbon Bond Forming Reactions of Ruthenium Guanidinobenzimidazole Second Coordination Sphere Hydrogen Bond Donor Catalysts. *Organometallics* **2020**, *39*, 1149-1162.

(34) The same reviewer has asked about the possible influence of solvent polarity. Data given in entries 2 and 23 of Figure 3.5 show that the less polar solvent CD_2Cl_2 gives (at least in two cases) lower ee values than acetone-d_6. The catalysts are not soluble in still less polar solvents such at toluene.

(35) (a) Andrés, J. M.; Manzano, R.; Pedrosa, R. Novel Bifunctional Chiral Urea and Thiourea Derivatives as Organocatalysts: Enantioselective Nitro-Michael Reaction of Malonates and Diketones. *Chem. Eur. J.* **2008**, *114*, 5116-5119. (b) Almaşi, D.; Alonso, D. A.; Gómez-Bengoa, E.; Nájera, C. Chiral 2-Aminobenzimidazoles as Recoverable Organocatalysts for the Addition of 1,3-Dicarbonyl Compounds to Nitroalkenes. *J. Org.*

Chem. **2009**, *74*, 6163-6168.

(36) Saaby, S.; Bella, M.; Jørgensen, K. A. Asymmetric Construction of Quaternary Stereocenters by Direct Organocatalytic Amination of α-Cyanoacetates and β-Dicarbonyl Compounds. *J. Am. Chem. Soc.* **2004**, *126*, 8120-8121. The chiral HPLC column employed with the addition product featured the same stationary phase but a different particle size from that used earlier in the literature. It is presumed that the well separated enantiomers exhibit identical orders of elution. Configurations were assigned accordingly.

(37) APEX2 "Program for Data Collection on Area Detectors" BRUKER AXS Inc., 5465 East Cheryl Parkway, Madison, WI 53711-5373 USA.

(38) SADABS, Sheldrick, G. M. "Program for Absorption Correction of Area Detector Frames", BRUKER AXS Inc., 5465 East Cheryl Parkway, Madison, WI 53711-5373 USA.

(39) Sheldrick, G. M. A Short History of SHELX. *Acta Crystallogr.* **2008**, *A64*, 112-122.

(40) Spek, A. L. Single-crystal structure validation with the program *PLATON*. *J. Appl. Crystallogr.* **2003**, *36*, 7-13.

(41) Dolomanov, O. V.; Bourhis, L. J.; Gildea, R. J.; Howard, J. A. K.; Puschmann, H. OLEX2: A Complete Structure Solution, Refinement and Analysis Program. *J. Appl. Crystallogr.* **2009**, *42*, 339-341.

(42) Flack, H. D. On Enantiomorph-Polarity Estimation. *Acta Crystallogr.* **1983**, *A39*, 876-881.

4. LIPOPHILIC CHIRAL COBALT(III) COMPLEXES OF HEXAAMINE LIGANDS: EFFICACIES AS ENANTIOSELECTIVE HYDROGEN BOND DONOR CATALYSTS†

4.1 Introduction

The last twenty years have seen the extensive development of chiral hydrogen bond donor catalysts for enantioselective organic synthesis.[1] Nearly all of these were metal-free (organic) species prior to our report of the use of a lipophilic salt of a classical enantiopure Werner trication, Δ-$[Co(en)_3]^{3+}$ $3BAr_f^-$ (**I**; en = 1,2-ethylenediamine; BAr_f = $B(3,5\text{-}C_6H_3(CF_3)_2)_4$) or the enantiomer.[2] This strong NH hydrogen bond donor[3] is depicted in Figure 4.1. Since then, we have continued to develop a range of cobalt(III) tris(diprimary 1,2-diamine) catalysts[4-7] such as Λ-$[Co((S,S)\text{-dpen})_3]^{3+}$ $2Cl^-BAr_f^-$ (**II**; dpen = 1,2-diphenylethylenediamine)[7] and the bifunctional species **III**,[5-8] as well as much different systems such as the ruthenium adducts **IV**, which feature NH hydrogen bond donors remote from the metal.[9,10] Others,[11-13] especially the Meggers group,[13] have explored complementary motifs, usually with NH donor groups remote from the metal as exemplified by **V**.

Since Werner's time, the coordination chemistry of cobalt(III) has expanded beyond diprimary 1,2-diamines to include a number of macrobicyclic hexadentate ligands featuring secondary amine moieties. Prominent classes include the sepulchrates (sep) and sarcophagines (sar), illustrated by **VIa** and **VIb** in Figure 4.1.[14] These ligands, which have been applied to a variety of other transition metal ions,[14-18] confer inherently greater thermodynamic stabilities compared to hexa(monoamine) or tris(diamine) analogs.[14-19]

†Reprinted with permission from "Lipophilic chiral cobalt (III) complexes of hexaamine ligands: Efficacies as enantioselective hydrogen bond donor catalysts" by Maximuck, W. J.; Gladysz, J. A., 2019. *Mol. Catal.*, 473, 110360, Copyright 2019 by Elsevier.

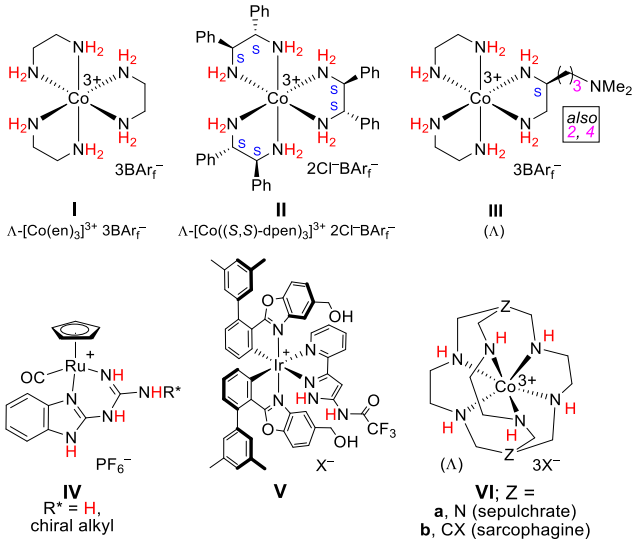

Figure 4.1. Some types of chiral enantiopure metal-containing hydrogen bond donors.

Many of these complexes can be synthesized from $[Co(en)_3]^{3+}$ $3X^-$ using inexpensive reagents such as formaldehyde, ammonium hydroxide, and nitromethane.[15,18,20,21] Like their precursor, they possess metal centered chirality and idealized D_3 symmetry, as represented by the partial structures in Figure 4.2. The Δ enantiomer can be viewed as a right handed helix, as the chelates extend in a clockwise direction when bridging from the front to the rear trigonal coordination planes; for the Λ enantiomer, the chelates extend in a counter-clockwise direction.[22] In most cases, the enantiomers can be resolved by fractional crystallization of their diastereomeric tartrate salts.[14,23-25] Alternatively, enantiopure adducts can be accessed from enantiopure $[Co(en)_3]^{3+}$ $3X^-$.[15,20,21]

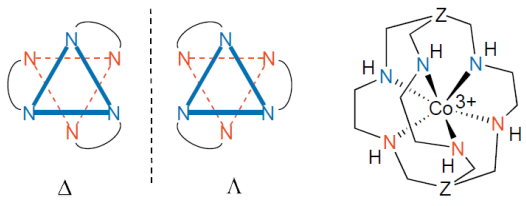

Figure 4.2. Λ/Δ configurations of metal stereocenters in octahedral complexes with three chelating ligands.

In this paper, we report that cobalt(III) complexes of the types **VIa**,**b** can in fact serve as hydrogen bond donor catalysts for various carbon-carbon and carbon-nitrogen bond forming reactions. The specific systems investigated are depicted in Figure 4.3. However, the enantioselectivities are much lower than those obtained with **II** and **III**. Nonetheless, close relatives yield significant enantioselectivities, and the data provide insight that should aid future catalyst design and optimization.

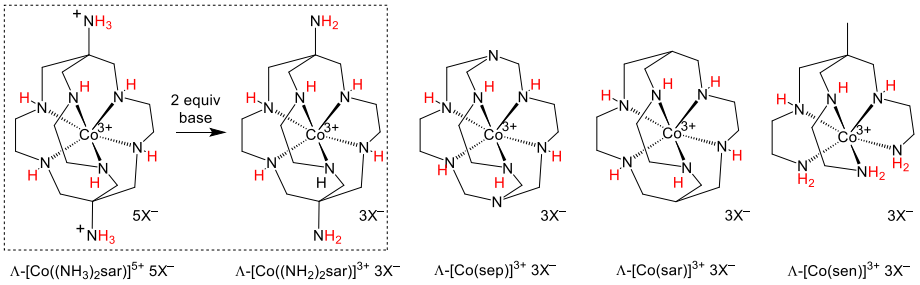

Figure 4.3. Some enantiopure catalysts investigated (X = BAr_f) and their precursors (X = Cl).

4.2 Results

4.2.1 Catalyst synthesis

The enantiopure chloride salts Λ-$[Co((NH_3)_2sar)]^{5+}$ $5Cl^-$,[18] Λ-$[Co(sep)]^{3+}$ $3Cl^-$, Δ-$[Co(sep)]^{3+}$ $3Cl^-$,[26] Λ-$[Co(sar)]^{3+}$ $3Cl^-$,[15,27] and Λ-$[Co(sen)]^{3+}$ $3Cl^-$,[23,28] the cations of which are depicted in Figure 4.3, were prepared according to previously reported procedures. The hexadentate ligand in Λ-$[Co(sen)]^{3+}$ $3Cl^-$ is acyclic. Hence, the complex is of lower symmetry than the others (C_3 vs. D_3), and possesses a trigonal coordination plane with three primary amine donor groups (-NH_2).

These complexes were dissolved in water, and in the case of the pentacation Λ-$[Co((NH_3)_2sar)]^{5+}$ $5Cl^-$, NaOH was added to deprotonate the alkylammonium groups and generate a trication. Then CH_2Cl_2 solutions of Na^+ BAr_f^- (3.0 equiv) were added. The characteristic orange color of the cobalt(III) cations transferred from the upper aqueous to the lower CH_2Cl_2 phases, as depicted in Figure 4.4.

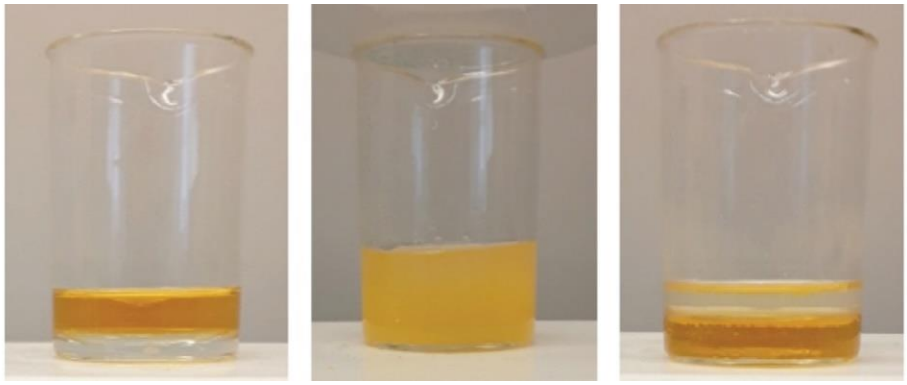

$$[Co(L)]^{3+}\ 3Cl^{-}\ (aq)\ +\ 3\ Na^{+}\ BAr_f^{-}\ (CH_2Cl_2) \xrightarrow[H_2O/CH_2Cl_2]{\text{biphasic conditions}} [Co(L)]^{3+}\ 3BAr_f^{-}\ (CH_2Cl_2)\ +\ 3\ Na^{+}\ Cl^{-}\ (aq)$$

L = $(NH_2)_2$sar, sep, sar, sen

Figure 4.4. Syntheses of the cobalt(III) catalysts shown in Figure 4.3. The photograph in the left panel depicts the reactants in the above equation (L = sep), that in the middle the stirred reaction, and that in the right the products.

Workups of the CH_2Cl_2 phases gave the corresponding tris(tetraarylborate) or $3BAr_f^-$ salts in 89-98% yields as bright orange solids. These contained 4-15 water molecules per cobalt, as estimated from ^{1}H NMR and microanalytical data. The water molecules are accounted for in all the molar quantities and yields reported herein, but for simplicity are only represented in the experimental section. To our knowledge, these represent the first lipophilic salts of the trications in Figure 4.3.

The ^{1}H and ^{13}C{^{1}H} NMR spectra of the new salts were recorded in acetone-d_6, and data for all C**H**$_n$ and carbon signals closely matched those reported for the trichloride salts in D_2O. Separate ^{1}H NMR signals were found for the NH and NH_2 protons of Λ-$[Co((NH_2)_2sar)]^{3+}$ $3BAr_f^-$, and the NH and diastereotopic NHH' protons of Λ-$[Co(sen)]^{3+}$ $3BAr_f^-$. However, these peaks were not observed in D_2O, presumably due to H/D exchange. All of the salts were soluble in other moderately polar organic solvents, such as acetonitrile.

Analogous anion metatheses were attempted with the trichloride salts Λ-$[Co(Cl_2sar)]^{3+}$ $3Cl^-$[27] and Λ-$[Co((NO_2)_2sar)]^{3+}$ $3Cl^-$,[15,27] in which more electron

withdrawing substituents have replaced the apical amino groups of Λ-[Co($(NH_2)_2$sar)]$^{3+}$ 3Cl^-. These groups render the secondary NH units more acidic; pK_a values of 8.85 (NO_2), [15] 10.36 (Cl),[29] and 12.0 (NH_2, chromium(III) analog)[16] have been reported. Interestingly, the initially formed bright orange CH_2Cl_2 solutions turned deep violet. The same color change occurs when the analogous trichloride or tris(perchlorate) salts are monodeprotonated, a process noted to happen (at least to some extent) spontaneously in the presence of organic solvents (or upon vacuum dessication).[15]

4.2.2. Catalyst screening

Figure 4.5 depicts the addition of a malonate ester to *trans*-β-nitrostyrene in the presence of a tertiary amine base. This reaction could be catalyzed with high enantioselectivities by the tris(1,2-diphenylethylenediamine) complex **II** (Figure 4.1) and related salts with 2$BF_4^-$$BAr_f^-$ and 3BF_4^- anion sets.[4] As summarized in entries 2-6 for additions in CD_2Cl_2 in the presence of Et_3N, all of the cobalt(III) cage complexes were effective catalysts. Over the course of 2 h at 0 °C, >99% conversions were realized, as assayed by NMR versus an internal standard.

Unfortunately, significant enantioselectivities were not achieved, as assayed by HPLC (see Appendix). The top performer was Λ-[Co(sen)]$^{3+}$ 3BAr_f^- with only a 10% ee (entry 6). The ee values for the hexadentate secondary amine complexes (entries 2-5) were also surpassed by that of Λ-[Co($en)_3$]$^{3+}$ 3BAr_f^- (**I**; entry 1). The dominant product configurations were determined by HPLC elution orders established previously, always with the same type of chiral column.[4,30,31] The catalyst in entry 2 features two NH_2 groups, but when the experiment was repeated without added Et_3N, no reaction occurred. No background reactions were detected in the absence of catalyst.

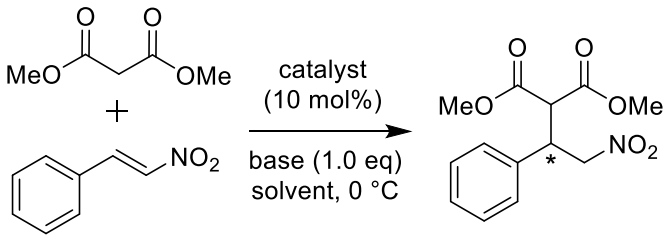

entry	catalyst	yield (%)[b]	ee (%) (config)[c]
A. Et_3N, CD_2Cl_2, 2 h			
1	Λ-$[Co(en)_3]^{3+}$ $3BAr_f^-$ (**I**)	>99	6 (*R*)
2	Λ-$[Co((NH_2)_2sar)]^{3+}$ $3BAr_f^-$	>99	0
3	Λ-$[Co(sep)]^{3+}$ $3BAr_f^-$	>99	4 (*R*)
4	Δ-$[Co(sep)]^{3+}$ $3BAr_f^-$	>99	4 (*S*)
5	Λ-$[Co(sar)]^{3+}$ $3BAr_f^-$	>99	0
6	Λ-$[Co(sen)]^{3+}$ $3BAr_f^-$	>99	10 (*R*)
B. *N*-methylmorpholine (NMM), CD_3CN, 24 h			
7	Λ-$[Co(en)_3]^{3+}$ $3BAr_f^-$ (**I**)	95	27 (*R*)
8	Λ-$[Co(sen)]^{3+}$ $3BAr_f^-$	87	30 (*R*)

[a]Reaction scale: 0.036 mmol alkene, 0.039 mmol malonate. [b]The yield was determined by integration of the C*H*$(CO_2Me)_2$ ^{1}H NMR signal of the product versus the methyl signal of internal standard Ph_2SiMe_2. [c]Enantioselectivities and configurations were determined by chiral HPLC analyses.[4,30,31]

Figure 4.5. Additions of dimethyl malonate to *trans*-β-nitrostyrene catalyzed by the cobalt(III) complexes in Figure 4.3.[a]

Analogous experiments were also conducted in CD_3CN using *N*-methylmorpholine as the base. Reactions became slower, but the ee values obtained with Λ-$[Co(en)_3]^{3+}$ $3BAr_f^-$ and Λ-$[Co(sen)]^{3+}$ $3BAr_f^-$ increased significantly (Figure 4.5, entries 7 and 8). Those for the other catalysts remained very low. Hence, the presence of a trigonal coordination plane with three primary amine donor groups appears to enhance enantioselectivities.

Figure 4.6 depicts a different type of base promoted malonate addition that we studied earlier with Δ-$[Co(en)_3]^{3+}$ $3BAr_f^-$ (**I**), but could never achieve an ee value of over 33%.[2] Under the conditions of Figure 4.6, the ee with **I** was 20% (entry 1). All of the cobalt(III) cage complexes were competent catalysts (entries 2-6), but reactions were

slower than those in Figure 4.5. All of the hexadentate secondary amine complexes (entries 2-5) again gave very low enantioselectivities. However, Λ-$[Co(sen)]^{3+}$ $3BAr_f^-$, the best performing catalyst in Figure 4.5, afforded a significant enantioselectivity of 57% ee (entry 6).

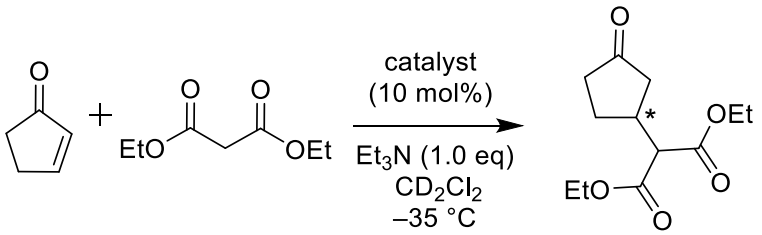

entry	catalyst	yield (%) (time)[b]	ee (%) (config)[c]
1	Λ-$[Co(en)_3]^{3+}$ $3BAr_f^-$ (**I**)	94 (21 h)	20 (*S*)
2	Λ-$[Co((NH_2)_2sar)]^{3+}$ $3BAr_f^-$	93 (144 h)	5 (*S*)
3	Λ-$[Co(sep)]^{3+}$ $3BAr_f^-$	49 (96 h)	9 (*S*)
4	Δ-$[Co(sep)]^{3+}$ $3BAr_f^-$	55 (96 h)	9 (*R*)
5	Λ-$[Co(sar)]^{3+}$ $3BAr_f^-$	70 (192 h)	5 (*S*)
6	Λ-$[Co(sen)]^{3+}$ $3BAr_f^-$	>99 (21 h)	57 (*S*)

[a]Reaction scale: 0.036 mmol enone, 0.037 mmol malonate. [b]The yield was determined by integration of the $CH(CO_2Et)_2$ ^1H NMR signal of the product versus the methyl signal of internal standard Ph_2SiMe_2. [c]Enantioselectivities and configurations were determined by chiral HPLC analyses.[32,33]

Figure 4.6. Additions of diethyl malonate to 2-cyclopenten-1-one catalyzed by the cobalt(III) complexes in Figure 4.3.[a]

Figure 4.7 depicts a base promoted addition of a 1,3-dicarbonyl compound to an azo linkage. This transformation is catalyzed by the tris(1,2-diphenylethylenediamine) complex **II**, and an enantioselectivity of 76% ee was obtained using *N*-methylmorpholine as the base; ee values of >90% could be realized with other solvents, anion sets, or the Δ diastereomer.[6a] All cobalt(III) cage complexes were again competent catalysts, with rates generally similar to those in Figure 4.5 (entries 2-6). As in Figures 4.5 and 4.6, Λ-$[Co(sen)]^{3+}$ $3BAr_f^-$ was again the clear "winner", with an ee of 40%.

Finally, some data on relative catalyst rates were sought. The malonate addition in Figure 4.5 was repeated, but with lower loadings of catalyst and base so as to slow the reaction and allow more precise comparisons. As shown in Figure 4.8, Λ-$[Co(en)_3]^{3+}$ $3BAr_f^-$ (**I**) was the most active catalyst, followed by Λ-$[Co(sen)]^{3+}$ $3BAr_f^-$ and Λ-$[Co(sar)]^{3+}$ $3BAr_f^-$. Some possible rationales are suggested in the discussion section.

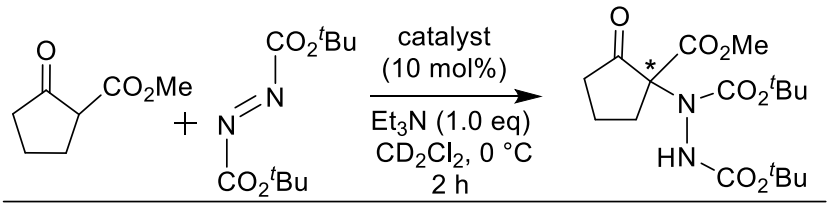

entry	catalyst	yield (%)[b]	ee (%) (config)[c]
1	Λ-$[Co(en)_3]^{3+}$ $3BAr_f^-$ (**I**)	>99	27 (*S*)
2	Λ-$[Co((NH_2)_2sar)]^{3+}$ $3BAr_f^-$	>99	6 (*S*)
3	Λ-$[Co(sep)]^{3+}$ $3BAr_f^-$	>99	6 (*S*)
4	Δ-$[Co(sep)]^{3+}$ $3BAr_f^-$	>99	6 (*R*)
5	Λ-$[Co(sar)]^{3+}$ $3BAr_f^-$	>99	5 (*S*)
6	Λ-$[Co(sen)]^{3+}$ $3BAr_f^-$	>99	40 (*S*)

[a]Reaction scale: 0.036 mmol azo compound, 0.037 mmol 1,3-dicarbonyl compound.
[b]The yield was determined by integration of the two $C(CH_3)_3$ ^1H NMR signals of the product versus the methyl signal of the internal standard Ph_2SiMe_2.
[c]Enantioselectivities and configurations were determined by chiral HPLC analyses.[6a,34]

Figure 4.7. Additions of methyl 2-oxocyclopentanecarboxylate to di(*t*-butyl) azodicarboxylate catalyzed by the cobalt(III) complexes in Figure 4.3.[a]

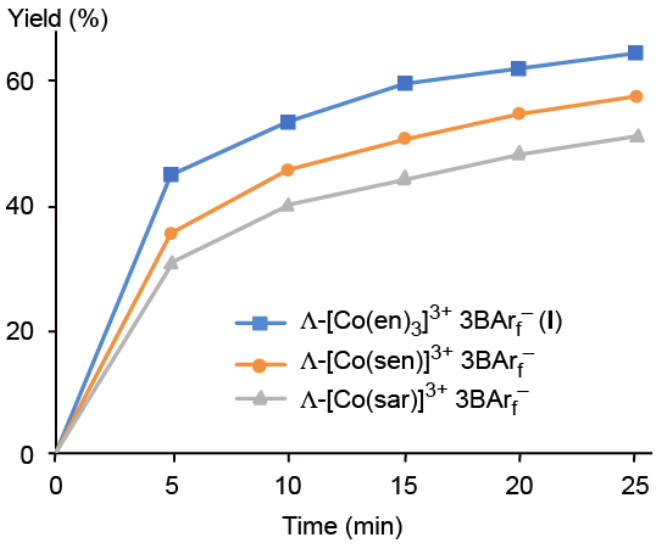

Figure 4.8. Rate profiles for the addition in Figure 4.5 with three catalysts under conditions modified to give slower reactions (2 mol% cat, 0.36 equiv Et_3N, CD_2Cl_2, rt).

Inspired by these results, we decided to produce additional cage compounds for follow-up studies. In the Gladysz group, certain bifunctional ligands have proved to be very effective in enantioselective catalysis. The most effective bifunctional ligands are composed of a traditional ethylenediamine backbone with an additional alkyl chain of varying lengths boasting a pendant secondary or tertiary amine.[8,35] The advantage that these ligands feature is that they can be used in our traditional catalytic reactions without the requirement for the addition of an external base.[5] Not only is this more economical, but the use of these catalysts can often result in high product enantioselectivities, perhaps due to lower entropic cost as the deprotonation occurs at the catalyst. This leads to considerably less distance and time for the enolate to experience before its addition to the alkene. Fortunately, these catalysts only need one of these bifunctional ligands to perform very effectively. In fact, all reported cases in the group possess one bifunctional ligand and two ethylenediamine ligands, which lead to ee values of >90% when the length of the alkyl chain to which the pendant tertiary amine is bonded is appropriate.[5] In contrast,

$[Co(en)_3]^{3+}$ results in catalysts with much more modest ee values (30-60%) as reported in this dissertation (Section 2).[2,36]

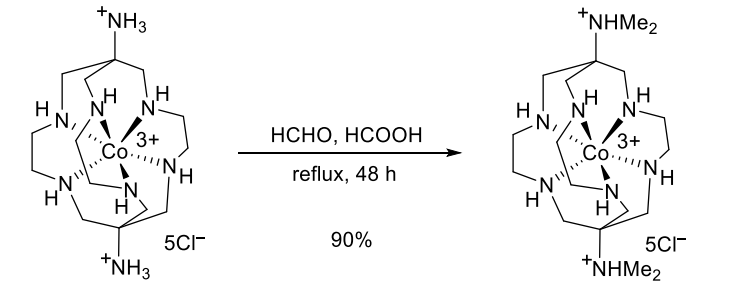

Figure 4.9. Synthesis of Λ-$[Co((NHMe_2)_2sar)]^{5+}$ $5Cl^-$.

Thankfully, we already had the complex Λ-$[Co((NH_3)_2sar)]^{5+}$ $5Cl^-$ in hand from the studies derived from Figure 4.3. The conversion of this complex to Λ-$[Co((NHMe_2)_2sar)]^{5+}$ $5Cl^-$ was achievable through a Eschweiler-Clarke reaction by refluxing Λ-$[Co((NH_3)_2sar)]^{5+}$ $5Cl^-$ in formic acid and an aqueous formaldehyde solution for 48 h (Figure 4.9).[37] Deprotonation with sodium hydroxide, and anion metathesis with Na^+ BAr_f^- provided the desired bifunctional catalyst Λ-$[Co((NMe_2)_2sar)]^{3+}$ $3BAr_f^-$.

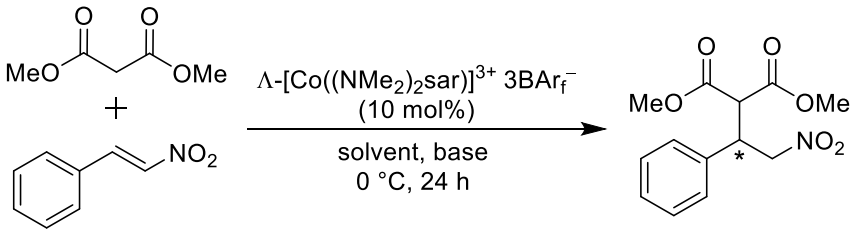

entry	solvent	base	yield (%)[a]	ee (%) (config)
1	CD_3CN	----	10	4 (*R*)
2	CD_2Cl_2	----	21	2 (*R*)
3	CD_2Cl_2	Et_3N	>99	0

[a]Yields were determined by ^1H NMR relative to the internal standard Ph_2SiMe_2 (experimental section).

Figure 4.10. Additions of dimethyl malonate to *trans*-β-nitrostyrene catalyzed by Λ-$[Co((NMe_2)_2sar)]^{3+}$ $3BAr_f^-$.

The catalyst was tested on the nitrostyrene-dimethyl malonate Michael addition reaction. The first attempt was made in the absence of an external base in CD_3CN. This gave a 10% yield of the addition product with 4% ee (*R* dominant) (Figure 4.10, entry 1). It is important to note that no conversion occurs in the absence of base when using $[Co(en)_3]^{3+}$ $3BAr_f^-$ as a catalyst for this reaction. When the solvent CD_2Cl_2 was used, the yield increased to 21% and the enantioselectivity decreased to 2% ee (*R* dominant) (entry 2). As the product yield was very low through the 24 h reaction time period, Et_3N was added as a base to speed up the reaction. This resulted in >99% yield, but a racemic addition product (entry 3).

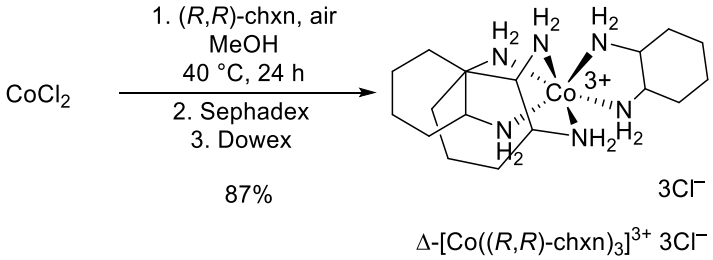

Figure 4.11. Synthesis of Δ-$[Co((R,R)\text{-chxn})_3]^{3+}$ $3Cl^-$.

The commercial availability of *trans*-(*R*,*R*)-1,2-cyclohexanediamine ((*R*,*R*)-chxn) prompted attempts of employing these enantiopure compounds as ligands in cobalt(III) catalysts. Thankfully, there is a well-established procedure to synthesize the trichloride salt Δ-$[Co((R,R)\text{-chxn})_3]^{3+}$ $3Cl^-$ (Figure 4.11) and separate it from small amounts of the Λ diastereomer (97:3 Δ/Λ) using Sephadex column chromatography.[38a] Anion metathesis with 3.0 equiv of Na^+ BAr_f^- provided the tris(tetraarylborate) salt Δ-$[Co((R,R)\text{-chxn})_3]^{3+}$ $3BAr_f^-$. We envisioned the additional steric bulk of the cyclohexane rings would provide a tighter chiral pocket, in turn increasing enantioselectivity. The catalyst Δ-$[Co((R,R)\text{-chxn})_3]^{3+}$ $3BAr_f^-$ gave admirable rates, but did not offer the enantioselectivity enhancements that were desired as summarized in entry 1 of Figures 4.12-4.14.

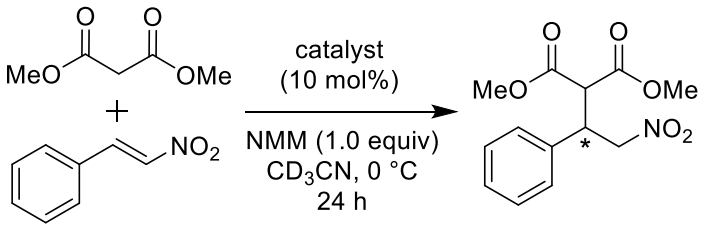

entry	catalyst	yield (%)[a]	ee (%) (config)
1	Δ-[Co((*R*,*R*)-chxn)$_3$]$^{3+}$ 3BAr$_f^-$	83	37 (*S*)
2	Λ-[Co(CO_2Et-oxosen–H)]$^{2+}$ 2BAr$_f^-$	61	17 (*R*)
3	Λ-[Co(taetacn)]$^{3+}$ 3BAr$_f^-$	>99	25 (*R*)

[a]Yields were determined by ^{1}H NMR relative to the internal standard Ph_2SiMe_2 (experimental section).

Figure 4.12. Additions of dimethyl malonate to *trans*-β-nitrostyrene catalyzed by BAr$_f^-$ salts of the cobalt(III) complexes in Figures 4.11, 4.15, and 4.16.

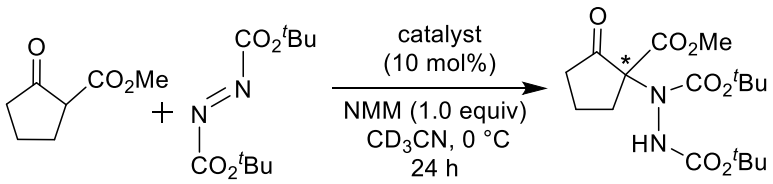

entry	catalyst	yield (%)[a]	ee (%) (config)
1	Δ-[Co((*R*,*R*)-chxn)$_3$]$^{3+}$ 3BAr$_f^-$	88	51 (*R*)
2	Λ-[Co(CO_2Et-oxosen–H)]$^{2+}$ 2BAr$_f^-$	31	51 (*S*)
3	Λ-[Co(taetacn)]$^{3+}$ 3BAr$_f^-$	99	59 (*S*)

[a]Yields were determined by ^{1}H NMR relative to the internal standard Ph_2SiMe_2 (experimental section).

Figure 4.13. Additions of methyl 2-oxocyclopentanecarboxylate to di-*tert*-butylazodicarboxylate catalyzed by BAr$_f^-$ salts of the cobalt(III) complexes in Figures 4.11, 4.15, and 4.16.

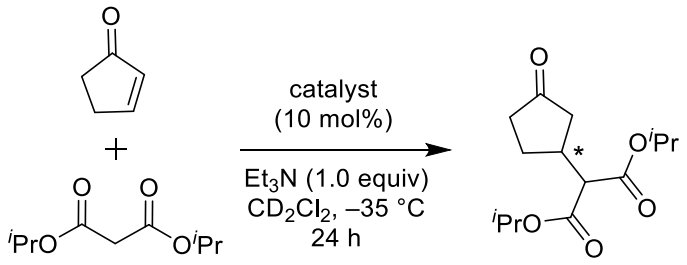

entry	catalyst	yield (%)[a]	ee (%) (config)
1	Δ-[Co((*R*,*R*)-chxn)$_3$]$^{3+}$ 3BAr$_f^-$	99	17 (*R*)
2	Λ-[Co(CO$_2$Et-oxosen–H)]$^{2+}$ 2BAr$_f^-$	54	14 (*S*)
3	Λ-[Co(taetacn)]$^{3+}$ 3BAr$_f^-$	98	13 (*S*)

[a]Yields were determined by ^{1}H NMR relative to the internal standard Ph_2SiMe_2 (experimental section).

Figure 4.14. Additions of diisopropyl malonate to 2-cyclopenten-1-one catalyzed by BAr$_f^-$ salts of the cobalt(III) complexes in Figures 4.11, 4.15, and 4.16.

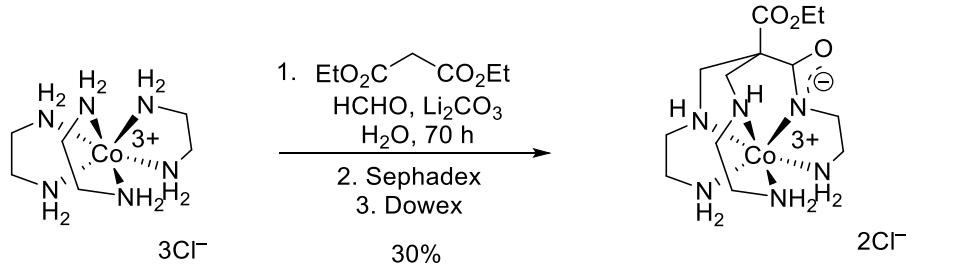

Figure 4.15. Synthesis of Λ-[Co(CO$_2$Et-oxosen–H)]$^{2+}$ 2Cl$^-$.

Given the results with Λ-[Co(sen)]$^{3+}$ 3BAr$_f^-$ in Figures 4.5-4.7, the performance of the half-cage or monocapped cobalt(III) complexes warranted further investigation. A promising and facile synthetic strategy came from the literature in the form of Λ-[Co(CO$_2$Et-oxosen–H)]$^{2+}$ 2Cl$^-$.[39] As shown in Figure 4.15, this complex could be synthesized seamlessly in its enantiopure form from Λ-[Co(en)$_3$]$^{3+}$ 3Cl$^-$ with the addition of formaldehyde, diethyl malonate, and lithium carbonate. This presents a rare example of a dicationic complex in this dissertation. The bis(chloride) (2Cl$^-$) salt (Figure 4.15) was a vibrant red and was soluble in methanol. The bis(tetraarylborate) (2BAr$_f^-$) salt was

prepared; however attempts to prepare the mixed $Cl^{-}BAr_f^{-}$ salt were unsuccessful. Due to the amide and ester functionalities, the complex surrendered some symmetry relative to those described above. This resulted in an ^1H NMR spectrum that featured 8 individual NH peaks. This lipophilic Werner complex was a satisfactory catalyst, but did not provide an improvement over similar catalysts (Figures 4.12-4.14, entry 2). The diminished product conversion might be connected to an increase in NH bond acidity due to the electron withdrawing carbonyl and ester groups.

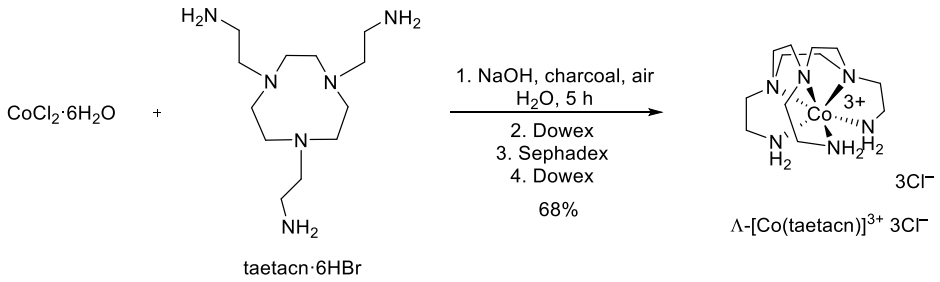

Figure 4.16. Synthesis of Λ-$[Co(taetacn)]^{3+}$ $3Cl^{-}$.

Finally, the monocapped complex $[Co(taetacn)]^{3+}$ $3X^{-}$ was also investigated. The synthesis of the trichloride salt is given in Figure 4.16,[40] which was then converted to the lipophilic salt $[Co(taetacn)]^{3+}$ $3BAr_f^{-}$. The ligand synthesis was considerably more involved than in the previous cases.[40b] The taetacn complex features a mixture of primary and tertiary amines that are coordinated to the metal center, which would suggest catalysis could only occur on one "side" of the complex with "open" NH_2 groups. Similar to the other cage compounds with a single accessible C_3 face, $[Co(taetacn)]^{3+}$ $3BAr_f^{-}$ often produced addition products with appreciable enantioselectivities (Figures 4.12-4.14, entry 3).

4.3 Discussion

One of the most obvious conclusions from Figures 4.5-4.7 is that all of the cobalt(III) catalysts derived from bicyclic hexaamine ligands (and which have D_3

symmetry) afford dismal enantioselectivities. Apparently the secondary NH moieties are effective enough hydrogen bond donors to give active catalysts, but the diastereomeric transition states leading to the different product enantiomers seem to be very close in energy. Both Λ-$[Co((NH_2)_2sar)]^{3+}$ $3BAr_f^-$ and Λ-$[Co(sep)]^{3+}$ $3BAr_f^-$, which also contain RNH_2 and NR_3 moieties, are potentially bifunctional catalysts. However, a single run *without* the Et_3N base (*vide supra*) gave no reaction, and we were discouraged from attempting additional experiments by the very low ee values.

The bifunctional catalyst Λ-$[Co((NMe_2)_2sar)]^{3+}$ $3BAr_f^-$ represents a considerably different structure than those we have used in the past.[5] This is a hexadentate ligand that is capped on both C_3 faces and features two dimethyl amino groups. The catalyst Λ-$[Co((NMe_2)_2sar)]^{3+}$ $3BAr_f^-$ followed the enantioselectivity trend of its demethylated analogue. The low conversion is likely due to unsatisfactory basicity of the tertiary amine. The cobalt(III) ion exerts an electron withdrawing effect over the tertiary amine based on their proximity,[14] reducing its potency to efficiently deprotonate dimethyl malonate. The less polar solvent CD_2Cl_2 lessens the competition between NH active sites between substrates and solvent relative to CD_3CN.

There is perhaps still some basis for cautious optimism regarding the D_3 catalysts. For certain complexes, the modes of hydrogen bonding to enantiomeric tartrate anions have been studied in detail, and it has been possible to demonstrate that one diastereomer can be substantially more favored than the other[24] – in other words, an appreciable level of chiral recognition. When high diastereoselectivities can be established for ground states, it becomes more plausible that significant selectivities can be achieved for competing transition states.

Regardless, the most interesting leads that emerge from this work are the less symmetric (C_3) catalysts containing an acyclic hexaamine ligand, Λ-$[Co(sen)]^{3+}$ $3BAr_f^-$

and Λ-[Co(taetacn)]$^{3+}$ 3BAr$_f^-$. The first species can be formally derived from the corresponding D_3 sarcophagine (**VIb**, X = CH_3) by removing one of the two $CH_3C(CH_2)_3$ apices, thereby exposing a C_3 face that features three NH_2 moieties. This motif can also be found (twice) in the tris(1,2-ethylenediamine) complex **I** and the tris(1,2-diphenylethylenediamine) complex **II** (Figure 4.1), with the latter being an enantioselective catalyst of wide applicability. The catalyst prepared via Figure 4.11, Δ-[Co((*R*,*R*)-chxn)$_3$]$^{3+}$ 3BAr$_f^-$ also features two C_3 faces, although it gives enantioselectivity level similar to those of single C_3 faced Λ-[Co(taetacn)]$^{3+}$ 3BAr$_f^-$. For at least some reactions, there is good evidence that the C_3 face of **II** is the "active site".[4] Also, note that the rate trends in Figure 4.8 correlate to the number of C_3 faces in the catalysts. Thus, we view Λ-[Co(sen)]$^{3+}$ 3BAr$_f^-$ and Λ-[Co(taetacn)]$^{3+}$ 3BAr$_f^-$ as deserving of follow-up studies.

This recommendation is bolstered by unpublished results. For example, for the addition in Figure 4.6 (entry 6), Λ-[Co(sen)]$^{3+}$ 3BAr$_f^-$ actually outperforms the tris(1,2-diphenylethylenediamine) complex Λ-[Co((*S*,*S*)-dpen)$_3$]$^{3+}$ 3BAr$_f^-$,[7] which gives a 47% ee under analogous conditions. Furthermore, other solvents, bases, and anion sets – at least those investigated to date – afford lower ee values. This includes the mixed salt catalyst **II**, which features two strongly hydrogen bonding chloride anions and gives a very sluggish reaction.

Finally, we note that some of the complexes in Figures 4.3 and 4.10 have demonstrated proficiencies as oxidative catalysts,[41] electron transfer mediators,[42] and photosensitizers.[43] With this work, the large class of complexes represented,[14] many of which are readily available in enantiopure form, are shown to have new relevancy as potential enantioselective catalysts. Although the ee values in Figures 4.5-4.7 and 4.12-4.14 are often modest, there are innumerable ways to build upon or augment the hydrogen

bonding interactions that underlie the reactions. Efforts along these lines will be reported in due course.

4.4 Experimental section

General data. All reactions were conducted under aerobic conditions. Solvents for NMR (Cambridge Isotopes), HPLC (hexanes, Fisher; isopropanol, JT Baker), and reactions (CH_2Cl_2 (anhydrous, ≥99.8%), acetone and ethyl acetate (2 × ACS grade, ≥99.5%), hexanes (ACS reagent, ≥98.5%), 4 × Aldrich) were used as received. Other chemicals were used as received from the following sources: NaOH (ACS grade), VWR; Na^+ BAr_f^- (97%), Ark Pharm (BAr_f = B(3,5-$C_6H_3(CF_3)_2)_4$); *trans*-β-nitrostyrene (98%), dimethyl malonate (98%), diethyl malonate (99%), Et_3N (98%), and *N*-methylmorpholine (99%), 5 × Alfa Aesar; 2-cyclopenten-1-one (≥98%), Acros; di-*t*-butyl azodicarboxylate (98%), Aldrich; methyl 2-oxocyclopentanecarboxylate (>97%), TCI; Ph_2SiMe_2 (≥97%), TCI; silica gel (SiliaFlash® F60), Silicycle.

NMR spectra were recorded on a 500 MHz spectrometer at ambient probe temperatures and referenced (δ in ppm) to solvent signals (^{1}H: residual acetone-d_5, 2.05, $CHDCl_2$, 5.32, or CHD_2CN, 1.94; ^{13}C: acetone-d_6, 206.3). HPLC analyses were carried out with a Shimadzu instrument package (pump/autosampler/detector LC-20AD/SIL-20A/SPD-M20A). Melting points were determined using an OptiMelt MPA100 instrument. Microanalyses were conducted by Atlantic Microlab.

Λ-[Co((NH$_2$)$_2$sar)]$^{3+}$ 3BAr$_f^-$. A beaker was charged with Λ-[Co((NH$_3$)$_2$sar)]$^{5+}$ $5Cl^-\cdot H_2O$ (0.0533 g, 0.0934 mmol;[18] Figure 4.3) and distilled H_2O (15 mL). Then NaOH (aq, 2% w/w) was added until a pH of *ca.* 8 was attained, followed by CH_2Cl_2 (15 mL) and Na^+ BAr_f^- (0.2480 g, 0.2798 mmol, 3.0 equiv). The biphasic mixture was vigorously stirred (10 min) and allowed to stand. The lower bright orange phase was separated and the solvent removed by passive evaporation (fume hood) to give Λ-[Co((NH$_2$)$_2$sar)]$^{3+}$

$3BAr_f^-\cdot 7H_2O$ as a bright orange solid (0.2562 g, 0.0829 mmol, 89%), mp (open capillary) 70 °C (dec). Anal. Calcd. for $C_{110}H_{70}B_3CoF_{72}N_8\cdot 7H_2O$ (3089.18): C 42.77, H 2.74, N 3.63; found C 42.69, H 2.50, N 3.39.

NMR (acetone-d_6, δ in ppm): ^{1}H (500 MHz), BAr_f^- at 7.82 (s, 24H, *o*), 7.68 (s, 12H, *p*); $(NH_2)_2$sar at 6.85 (br s, 6H, N**H**), 3.80-3.71 (m, 6H, NCC**H**H'N), 3.60-3.42 (m, 6H, NCCH**H'**N, overlapping with H_2O), 3.54 (br s, 14H, $\mathbf{H}_2O$), 3.25-3.17 (m, 6H, NC**H**H'C**H**H'N), 2.90-2.80 (m, 6H, NCH**H'**CH**H'**N). 2.01-1.93 (m, 4H, N$\mathbf{H}_2$); $^{13}C\{^1H\}$ (126 MHz), BAr_f^- at 162.2 (q, $^1J_{BC}$ = 49.9 Hz, *i*), 135.1 (s, *o*), 129.6 (m, *m*), 125.0 (q, $^1J_{CF}$ = 271.8 Hz, **C**F_3), 118.0 (m, *p*); $(NH_2)_2$sar at 57.9 (s, **C**NHC'), 56.8 (s, CNH**C'**), 56.0 (s, **C**NH_2).

Λ- and Δ-[Co(sep)]$^{3+}$ 3BAr$_f^-$. Λ-$[Co(sep)]^{3+}$ $3Cl^-\cdot 3H_2O$ (0.0205 g, 0.0453 mmol ;[26] Figure 4.3), distilled H_2O (15 mL), CH_2Cl_2 (15 mL), and Na^+ BAr_f^- (0.1204 g, 0.1359 mmol, 3.0 equiv) were combined in a procedure analogous to that for Λ-$[Co((NH_2)_2sar)]^{3+}$ $3BAr_f^-$ (but without NaOH). An identical workup gave Λ-$[Co(sep)]^{3+}$ $3BAr_f^-\cdot 7H_2O$ as a bright orange solid (0.1365 g, 0.0446 mmol, 98%), mp (open capillary) 122-133 °C (dec). Anal. Calcd. for $C_{108}H_{64}B_3CoF_{72}N_8\cdot 7H_2O$ (3061.13): C 42.38, H 2.63, N 3.66; found C 42.30, H 2.68, N 3.61. The enantiomer was analogously prepared from Δ-$[Co(sep)]^{3+}$ $3Cl^-\cdot 3H_2O$ (0.0166 g, 0.0367 mmol);[26] found C 42.27, H 2.61, N 3.44.

NMR (acetone-d_6, δ in ppm): ^{1}H (500 MHz), BAr_f^- at 7.79 (s, 24H, *o*), 7.67 (s, 12H, *p*); sep at 6.91 (br s, 6H, N**H**), 4.81-4.69 (m, 6H, NC**H**H'N), 4.14-4.07 (m, 6H, NCH**H'**N), 3.85-3.72 (m, 6H, NC**H**H'C**H**H'N), 3.40-3.26 (m, 6H, NCH**H'**CH**H'**N), 3.01 (br s, 17H, $\mathbf{H}_2O$). $^{13}C\{^1H\}$ (126 MHz), BAr_f^- at 162.6 (q, $^1J_{BC}$ = 49.8 Hz, *i*), 135.6 (s, *o*), 130.0 (m, *m*), 125.4 (q, $^1J_{CF}$ = 272.0 Hz, **C**F_3), 118.5 (m, *p*); sep at 68.7 (s, N**C**H_2N), 54.9 (s, N**C**H_2**C**H_2N).

Λ-[Co(sar)]$^{3+}$ 3BAr$_f^-$. Λ-[Co(sar)]$^{3+}$ 3Cl$^-$·1.5H$_2$O (0.0083 g, 0.017 mmol;[15,27] Figure 4.3), distilled H$_2$O (15 mL), CH$_2$Cl$_2$ (15 mL), and Na$^+$ BAr$_f^-$ (0.0462 g, 0.0521 mmol, 3.0 equiv) were combined in a procedure analogous to that for [Co(sep)]$^{3+}$ 3BAr$_f^-$. An identical workup gave Λ-[Co(sar)]$^{3+}$ 3BAr$_f^-$·4H$_2$O as a bright orange solid (0.0489 g, 0.0163 mmol, 96%), mp (open capillary) 120-131 °C (dec). Anal. Calcd. for C$_{110}$H$_{68}$B$_3$CoF$_{72}$N$_6$·4H$_2$O (3005.11): C 43.97, H 2.55, N 2.80; found C 44.24, H 2.62, N 2.82.

NMR (acetone-d_6, δ in ppm): ^{1}H (500 MHz), BAr$_f^-$ at 7.79 (s, 24H, *o*), 7.68 (s, 12H, *p*); sar at 6.70 (br s, 6H, N**H**), 3.79-3.72 (m, 6H, NC**H**H'C**H**H'N), 3.69-3.62 (m, 6H, NCH**H'**CH**H'**N), 3.60 (br s, 15H, **H**$_2$O), 3.25-3.15 (m, 6H, NC**H**H'CH), 3.09-3.02 (m, 6H, NCH**H'**CH), 2.83-2.79 (m, 2H, C**H**). ^{13}C{^{1}H} (126 MHz), BAr$_f^-$ at 162.6 (q, $^1J_{BC}$ = 50.0 Hz, *i*), 135.6 (s, *o*), 130.0 (m, *m*), 125.4 (q, $^1J_{CF}$ = 271.8 Hz, **C**F$_3$), 118.5 (m, *p*); sar at 55.9 (s, N**C**H$_2$**C**H$_2$N), 51.0 (s, N**C**H$_2$CH), 40.8 (s, **C**H).

Λ-[Co(sen)]$^{3+}$ 3BAr$_f^-$. Λ-[Co(sen)]$^{3+}$ 3Cl$^-$·3H$_2$O (0.0364 g, 0.0782 mmol;[23,28] Figure 4.3), distilled H$_2$O (15 mL), CH$_2$Cl$_2$ (15 mL), and Na$^+$ BAr$_f^-$ (0.2078 g, 0.2345 mmol, 3.0 equiv) were combined in a procedure analogous to that for [Co(sep)]$^{3+}$ 3BAr$_f^-$. An identical workup gave Λ-[Co(sen)]$^{3+}$ 3BAr$_f^-$·15H$_2$O as a bright orange solid (0.2226 g, 0.07033 mmol, 90%), mp (open capillary) 143-147 °C (dec). Anal. Calcd. for C$_{107}$H$_{66}$B$_3$CoF$_{72}$N$_6$·15H$_2$O (3165.22): C 40.60, H 3.06, N 2.66; found C 40.15, H 2.78, N 2.65.

NMR (acetone-d_6, δ in ppm): ^{1}H (500 MHz), BAr$_f^-$ at 7.79 (s, 24H, *o*), 7.67 (s, 12H, *p*); sen at 6.90 (br s, 3H, N**H**), 5.46 (br s, 3H, N**H**H'), 5.37 (br s, 3H, NH**H'**), 3.70-3.62 (m, 3H), 3.51-3.43 (m, 6H), 3.28-3.19 (m, 6H, overlapping with H$_2$O), 3.19 (br s, 29H, **H**$_2$O), 2.94-2.88 (m, 3H), 1.09 (s, 3H, C**H**$_3$). ^{13}C{^{1}H} (126 MHz), BAr$_f^-$ at 162.6 (q, $^1J_{BC}$ = 49.8 Hz, *i*), 135.4 (s, *o*), 129.9 (m, *m*), 125.2 (q, $^1J_{CF}$ = 271.9 Hz, **C**F$_3$), 118.3

(m, *p*); sen at 57.8 and 55.8 (2 s, NH**C**H_2**C**$H_2$$NH_2$), 46.2 (s, **C**$CH_3$), 44.2 (s, N**C**$H_2$$CCH_3$), 20.4 (s, **C**$H_3$).

Λ-[Co((NMe$_2$)$_2$sar)]$^{3+}$ 3BAr$_f^-$. A beaker was charged with Λ-[Co((NHMe$_2$)$_2$sar)]$^{5+}$ 5Cl$^-$·5H_2O (0.0500 g, 0.0715 mmol;[37] Figure 4.9) and distilled H_2O (10 mL). Then NaOH (aq, 2% w/w) was added until a pH of *ca.* 8 was attained, followed by CH_2Cl_2 (15 mL) and Na^+ BAr$_f^-$ (0.1924 g, 0.2171 mmol, 3.04 equiv). The biphasic mixture was vigorously stirred (10 min) and allowed to stand. The lower bright orange phase was separated and the solvent removed by passive evaporation (fume hood) to give Λ-[Co((NMe$_2$)$_2$sar)]$^{3+}$ 3BAr$_f^-$·4H_2O as a bright orange solid (0.2208 g, 0.07143 mmol, >99%), mp (open capillary) 141-146 °C (dec). Anal. Calcd. for $C_{114}H_{78}B_3CoF_{72}N_8$·4$H_2O$ (3091.24): C 44.29, H 2.80, N 3.62; found C 44.01, H 2.80, N 3.63.

NMR (acetone-d_6, δ in ppm): ^{1}H (400 MHz), BAr$_f^-$ at 7.79 (s, 24H, *o*), 7.67 (s, 12H, *p*); (NMe$_2$)$_2$sar at 6.55 (br s, 6H, NH), 4.11-3.98 (m, 6H), 3.51-3.39 (m, 12H), 3.29-3.19 (m, 6H), 2.94 (br s, 14H, H_2O), 2.31 (s, 12H, N(CH_3)$_2$); ^{13}C{^{1}H} (100 MHz), BAr$_f^-$ at 162.6 (q, $^1J_{BC}$ = 49.8 Hz, *i*), 135.5 (s, *o*), 130.0 (m, *m*), 125.4 (q, $^1J_{CF}$ = 271.7 Hz, **C**F_3), 118.4 (s, *p*); (NMe$_2$)$_2$sar at 64.7 (s), 52.1 (m), 51.5 (m), 38.9 (s, N(CH_3)$_2$).

Δ-[Co((*R*,*R*)-chxn)$_3$]$^{3+}$ 3BAr$_f^-$. Δ-[Co((*R*,*R*)-chxn)$_3$]$^{3+}$ 3Cl$^-$·4H_2O (0.0487 g, 0.0840 mmol;[38a] Figure 4.11), distilled H_2O (15 mL), CH_2Cl_2 (15 mL), and Na^+ BAr$_f^-$ (0.2233 g, 0.2520 mmol, 3.00 equiv) were combined in a procedure analogous to that for [Co(sep)]$^{3+}$ 3BAr$_f^-$. An identical workup gave Δ-[Co((*R*,*R*)-chxn)$_3$]$^{3+}$ 3BAr$_f^-$·10H_2O as a bright orange solid (0.2404 g, 0.07581 mmol, 90%), mp (open capillary) 129-158 °C (dec). Anal. Calcd. for $C_{114}H_{78}B_3CoF_{72}N_6$·10$H_2O$ (3171.28): C 43.18, H 3.11, N 2.65; found C 43.25, H 3.00, N 2.76.

NMR (acetone-d_6, δ in ppm): ^{1}H (400 MHz), BAr_f^- at 7.78 (s, 24H, *o*), 7.67 (s, 12H, *p*); chxn at 5.54 (br s, 6H, N**H**H'), 5.16 (br s, 6H, NH**H'**), 3.03-2.94 (m, 6H), 2.92 (br s, 25H, H_2O), 2.39-2.31 (m, 6H), 1.77-1.70 (m, 6H), 1.68-1.57 (m, 6H), 1.29-1.16 (m, 6H); $^{13}C\{^1H\}$ (100 MHz), BAr_f^- at 162.6 (q, $^1J_{BC}$ = 49.9 Hz, *i*), 135.5 (s, *o*), 130.0 (q, $^2J_{CF}$ = 31.5 Hz, *m*), 125.4 (q, $^1J_{CF}$ = 271.8 Hz, CF_3), 118.4 (s, *p*); chxn at 61.6 (s, NCH), 33.6 (s, CH_2), 24.6 (s, CH_2).

Λ-[Co(CO$_2$Et-oxosen–H)]$^{2+}$ 2BAr$_f^-$. Λ-[Co(CO_2Et-oxosen–H)]$^{2+}$ $2Cl^-\cdot 3H_2O$ (0.0271 g, 0.0541 mmol;[39] Figure 4.15), distilled H_2O (10 mL), CH_2Cl_2 (10 mL), and Na^+ BAr_f^- (0.0958 g, 0.108 mmol, 2.00 equiv) were combined in a procedure analogous to that for [Co(sep)]$^{3+}$ $3BAr_f^-$. An identical workup gave Λ-[Co(CO_2Et-oxosen–H)]$^{2+}$ $2BAr_f^-\cdot 5H_2O$ as a red solid (0.0906 g, 0.0413 mmol, 76%), mp (open capillary) 67-86 °C (dec). Anal. Calcd. for $C_{77}H_{53}B_2CoF_{48}N_6O_3\cdot 5H_2O$ (2192.86): C, 42.18; H, 2.90; N, 3.83; found: C, 42.16; H, 2.65; N, 3.79.

NMR (acetone-d_6, δ in ppm): ^{1}H (400 MHz), BAr_f^- at 7.79 (s, 16H, *o*), 7.68 (s, 8H, *p*); CO_2Et-oxosen–H at 6.10 (br s, 1H, NH), 5.75 (br s, 1H, NH), 5.42 (br s, 1H, NH), 5.27 (br s, 1H, NH), 4.91 (br s, 1H, NH), 4.69 (br s, 1H, NH), 4.47 (br s, 1H, NH), 5.54 (br s, 1H, NH), 4.16 (q, $^3J_{HH}$ = 6.9 Hz, 2H), 3.05 (br s, 25H, H_2O), 2.39-2.31 (m, 6H), 1.77-1.70 (m, 6H), 1.68-1.57 (m, 6H), 1.29-1.16 (m, 6H), 1.22 (t, $^3J_{HH}$ = 7.1 Hz, 3H); $^{13}C\{^1H\}$ (100 MHz), BAr_f^- at 162.6 (q, $^1J_{BC}$ = 49.8 Hz, *i*), 135.5 (s, *o*), 130.0 (q, $^2J_{CF}$ = 31.6 Hz, *m*), 125.4 (q, $^1J_{CF}$ = 271.8 Hz, CF_3), 118.4 (s, *p*); CO_2Et-oxosen–H at 174.2 (C(=O)N), 168.7 (**C**O_2Et), 62.0 (OCH_2), 60.5, 57.1, 55.6, 53.9, 53.2, 47.4, 45.9, 44.9, 44.2, 14.3 (CH_3) (13 × s).

Λ- and Δ-[Co(taetacn)]$^{3+}$ 3BAr$_f^-$. Λ-[Co(taetacn)]$^{3+}$ $3Cl^-\cdot H_2O$ (0.0225 g, 0.0509 mmol;[40] Figure 4.16), distilled H_2O (10 mL), CH_2Cl_2 (10 mL), and Na^+ BAr_f^- (0.1354 g, 0.1528 mmol, 3.00 equiv) were combined in a procedure analogous to that for

[Co(sep)]$^{3+}$ 3BAr$_f^-$. An identical workup gave Λ-[Co(taetacn)]$^{3+}$ 3BAr$_f^-$·6H$_2$O as an orange solid (0.1444 g, 0.04789 mmol, 94%), mp (open capillary) 148-154 °C (dec). Anal. Calcd. for $C_{108}H_{66}B_3CoF_{72}N_6 \cdot 6H_2O$ (3015.10): C, 43.02; H, 2.61; N, 2.79; found: C, 42.76; H, 2.40; N, 2.64. The enantiomer was analogously prepared from Δ-[Co(taetacn)]$^{3+}$ 3Cl$^-$·H$_2$O (0.0225 g, 0.0509 mmol);[40] found C 43.04, H 2.51, N 2.64.

NMR[44] (acetone-d_6, δ in ppm): ^{1}H (400 MHz), BAr$_f^-$ at 7.82 (s, 24H, *o*), 7.68 (s, 12H, *p*); taetacn at 6.14 (br s, 3H, N**H**H'), 5.12 (br s, 3H, NH**H'**), 4.68 (m, 3H), 4.20-4.07 (m, 9H), 3.96 (m, 3H), 3.70 (m, 3H), 3.65-3.56 (m, 6H), 3.30 (br s, 24H, **H**$_2$O); ^{13}C{^{1}H} (100 MHz), BAr$_f^-$ at 162.7 (q, $^1J_{BC}$ = 49.8 Hz, *i*), 135.6 (s, *o*), 130.0 (m, *m*), 125.4 (q, $^1J_{CF}$ = 271.8 Hz, **C**F$_3$), 118.5 (s, *p*); taetacn at 65.7, 65.1, 64.0, 46.9 (4 × s).

Dimethyl 2-(2-nitro-1-phenylethyl)malonate; catalyst screening (Figures 4.5 and 4.12)**.** An authentic sample of the racemate (colorless oil) was obtained by adapting a literature procedure.[4] A 5 mm NMR tube was charged with a solution of *trans*-β-nitrostyrene (0.0054 g, 0.036 mmol, 1.0 equiv), catalyst (0.0036 mmol, 0.10 equiv), dimethyl malonate (0.0045 mL, 0.0052 g, 0.039 mmol, 1.1 equiv), and a solution of Ph$_2$SiMe$_2$ (0.0020 mL, standard) in CD$_2$Cl$_2$ or CD$_3$CN (0.40 mL). A stir bar was added and the sample was cooled to 0 °C. Then Et$_3$N (0.0050 mL, 0.0036 g, 0.036 mmol) or *N*-methylmorpholine (0.0040 mL, 0.0037 g, 0.036 mmol) was added and the mixture stirred. After 2 h, the stir bar was removed and a ^{1}H NMR spectrum recorded. The product yield was assayed by integrating the C*H*(CO$_2$Me)$_2$ signal versus the CH$_3$ signal of the standard. The solvent was removed under reduced pressure to give an orange oil, which was added to a plug of silica. The product was eluted with hexanes/EtOAc (1:1 v/v). The solvent was removed from the product containing fraction under reduced pressure. The enantiomeric excess was determined by HPLC with a Chiralpak AD column (98:2 v/v

hexanes/isopropanol, 1.0 mL/min, λ = 220 nm); for entry 6, t_R = 31.0 min (major), 41.0 min (minor).[4,30,31]

3-(Bis(ethoxycarbonyl)methyl)cyclopentanone; catalyst screening (Figure 4.6)**.** An authentic sample of the racemate (colorless oil) was obtained by adapting a literature procedure.[2,32,33] A 5 mm NMR tube was charged with 2-cyclopenten-1-one (0.0030 mL, 0.0029 g, 0.036 mmol, 1.0 equiv), catalyst (0.0036 mmol, 0.10 equiv), diethyl malonate (0.0056 mL, 0.0059 g, 0.037 mmol, 1.0 equiv), and a solution of Ph_2SiMe_2 (0.0020 mL, standard) in CD_2Cl_2 (0.40 mL). A stir bar was added and the sample was cooled to –35 °C. Then Et_3N (0.0050 mL, 0.0036 g, 0.036 mmol, 1.0 equiv) was added and the mixture stirred. After the specified time (Figure 4.6), the stir bar was removed and a ^1H NMR spectrum recorded. The product yield was assayed by integrating the C*H*$(CO_2Et)_2$ signal versus the CH_3 signal of the standard. The solvent was removed under reduced pressure to give an orange oil, which was added to a plug of silica. The product was eluted with hexanes/acetone (9:1 v/v). The solvent was removed from the product containing fraction under reduced pressure. The enantiomeric excess was determined by HPLC with a Chiralpak AS-H column (97.5:2.5 v/v hexanes/isopropanol, 0.8 mL/min, λ = 220 nm); for entry 6, t_R = 45.1 min (major), 51.3 min (minor).[32,33]

***N,N*'-Bis(t-butoxycarbonyl)-1-hydrazino-2-oxocyclopentanecarboxylic acid methyl ester; catalyst screening** (Figures 4.7 and 4.13)**.** An authentic sample of the racemate (colorless oil) was obtained by adapting a literature procedure.[6a] A 5 mm NMR tube was charged with di-*t*-butyl azodicarboxylate (0.0083 g, 0.036 mmol, 1.0 equiv), catalyst (0.0036 mmol, 0.10 equiv), methyl 2-oxocyclopentanecarboxylate (0.0046 mL, 0.0053 g, 0.037 mmol, 1.0 equiv), and a solution of Ph_2SiMe_2 (0.0020 mL, standard) in CD_2Cl_2 (0.40 mL). A stir bar was added and the sample was cooled to 0 °C. Then Et_3N (0.0050 mL, 0.0036 g, 0.036 mmol, 1.0 equiv) was added and the mixture stirred. After 2

h, the stir bar was removed and a ^{1}H NMR spectrum recorded. The product yield was assayed by integrating the C(CH_3)$_3$ and C'(C'H_3)$_3$ signals versus the CH_3 signal of the standard. The solvent was removed under reduced pressure to give an orange oil, which was added to a plug of silica. The product was eluted with hexanes/EtOAc (7:3 v/v). The solvent was removed from the product containing fraction under reduced pressure. The enantiomeric excess was determined by HPLC with a Chiralpak AD column (96:4 v/v hexanes/isopropanol, 1.0 mL/min, λ = 210 nm); for entry 6, t_R = 13.6 min (minor), 20.3 min (major).[6a,34.]

Rate Profiles (Figure 4.8)**.** A 5 mm NMR tube was charged with a solution of *trans*-β-nitrostyrene (0.0075 g, 0.050 mmol, 1.0 equiv), catalyst (0.001 mmol, 0.02 equiv), dimethyl malonate (0.0063 mL, 0.0072 g, 0.055 mmol, 1.1 equiv), and Ph_2SiMe_2 (0.0020 mL, standard) in CD_2Cl_2 (0.50 mL). Et_3N (0.0025 mL, 0.0018 g, 0.018 mmol, 0.36 equiv) was added. The tube was inverted once (mixing) and placed in a NMR probe. The product yield was assayed by ^{1}H NMR as for the corresponding reaction in Figure 4.5.

3-(Bis(isopropoxycarbonyl)methyl)cyclopentanone (Figure 4.14). An authentic sample was obtained as a colorless oil by adapting a literature procedure.[2,45] A 5 mm NMR tube was charged with a solution of 2-cyclopenten-1-one (0.0030 mL, 0.0029 g, 0.036 mmol, 1.0 equiv), catalyst (0.0036 mmol, 0.10 equiv), diisopropyl malonate (0.0070 mL, 0.0070 g, 0.037 mmol, 1.0 equiv), and Ph_2SiMe_2 (0.0020 mL, standard) in CD_2Cl_2 (0.40 mL). A ^{1}H NMR spectrum was recorded to confirm the initial 2-cyclopenten-1-one/standard ratio. A stir bar was added and the sample was cooled to –35 °C. Then Et_3N (0.0050 mL, 0.0036 g, 0.036 mmol, 1.0 equiv) was added and the mixture stirred. After 24 h, the stir bar was removed and the yield assayed by ^{1}H NMR. The solvent was

removed under reduced pressure to give an oil, which was added to a plug of silica. The product was eluted with hexanes/acetone (9:1 v/v). The solvent was removed from the product containing fraction under reduced pressure. The enantiomeric excess was determined by HPLC (Chiralpak AD-H column, 95:5 v/v hexanes/isopropanol, 1.0 mL/ min, λ = 215 nm; for entry 3, t_R = 10.5 and 11.5 min (major and minor)).[45]

4.5 References (All titles are given in the capitalization format of the original article)

(1) (a) Taylor, M. S.; Jacobsen, E. N. Asymmetric Catalysis by Chiral Hydrogen-Bond Donors. *Angew. Chem., Int. Ed.* **2006***, 45,* 1520-1543; Asymmetrische Katalyse durch chirale Wasserstoffbrückendonoren. *Angew. Chem.* **2006**, *118*, 1550-1573. (b) Doyle, A. G.; Jacobsen, E. N. Small-Molecule H-Bond Donors in Asymmetric Catalysis. *Chem. Rev.* **2007**, *107*, 5713-5743. (c) Yu, X.; Wang, W. Hydrogen-Bond-Mediated Asymmetric Catalysis. *Chem. Asian J.* **2008**, *3*, 516-532. (d) Takemoto, Y. Recognition and Activation by Ureas and Thioureas: Stereoselective Reactions using Ureas and Thioureas as Hydrogen-Bonding Donors. *Org. Biomol. Chem.* **2005**, *3*, 4299-4306. I Held, F. E.; Tsogoeva, S. B. Asymmetric Cycloaddition Reactions Catalyzed by Bifunctional Thiourea and Squaramide Organocatalysts: Recent Advances. *Catal. Sci. Technol.* **2016**, *6*, 645-667.

(2) Ganzmann, C.; Gladysz, J. A. Phase Transfer of Enantiopure Werner Cations into Organic Solvents: An Overlooked Family of Chiral Hydrogen Bond Donors for Enantioselective Catalysis. *Chem. Eur. J.* **2008**, *14*, 5397-5400.

(3) Ghosh, S. K.; Ehnbom, A.; Lewis, K. G.; Gladysz, J. A. Hydrogen bonding motifs in structurally characterized salts of the tris(ethylenediamine) cobalt trication, $[Co(en)_3]^{3+}$; An interpretive review, including implications for catalysis. *Coord. Chem. Rev.* **2017**, *350*, 30-48.

(4) Lewis, K. G.; Ghosh, S., K.; Bhuvanesh, N.; Gladysz, J. A. Cobalt(III) Werner Complexes with 1,2-Diphenylethylenediamine Ligands: Readily Available, Inexpensive, and Modular Chiral Hydrogen Bond Donor Catalysts for Enantioselective Organic Synthesis. *ACS Cent. Sci.* **2015**, *1*, 50-56.

(5) Ghosh, S. K.; Ganzmann, C.; Bhuvanesh, N.; Gladysz, J. A. Werner Complexes with ω-Dimethylaminoalkyl Substituted Ethylenediamine Ligands: Bifunctional

Hydrogen-Bond-Donor Catalysts for Highly Enantioselective Michael Additions. *Angew. Chem., Int. Ed.* **2016**, *55*, 4356-4360; Werner-Komplexe mit ω-Dimethylaminoalkyl-substitutierten Ethylendiaminliganden: bifunktionale H-Brückendonor-Katalysatoren für hoch enantioselective Michael-Additionen. *Angew. Chem.* **2016**, *128*, 4429-4433.

(6) (a) Kumar, A.; Ghosh, S. K.; Gladysz, J. A. Tris(1,2-diphenylethylenediamine)cobalt(III) Complexes: Chiral Hydrogen Bond Donor Catalysts for Enantioselective α-Aminations of 1,3-Dicarbonyl Compounds. *Org. Lett.* **2016**, *18*, 760-763. (b) Joshi, H.; Ghosh, S. K.; Gladysz, J. A. Enantioselective Additions of Stabilized Carbanions to Imines Generated from α-Amido Sulfones By Using Lipophilic Salts of Chiral Tris(1,2-diphenylethylenediamine) Cobalt(III) Trications as Hydrogen Bond Donor Catalysts. *Synthesis* **2017**, *49*, 3905-3915.

(7) Ghosh, S. K.; Lewis, K. G.; Kumar, A.; Gladysz, J. A. Syntheses of Families of Enantiopure and Diastereopure Cobalt Catalysts Derived from Trications of the Formula $[Co(NH_2CHArCHArNH_2)_3]^{3+}$. *Inorg. Chem.* **2017**, 56, 2304-2320.

(8) Ghosh, S. K.; Ganzmann, C.; Gladysz, J. A. Synthesis of a series of ω-dimethylaminoalkyl substituted ethylenediamine ligands for use in enantioselective catalysis. *Tetrahedron: Asymmetry* **2015**, *26*, 1273-1280.

(9) Mukherjee, T.; Ganzmann, C.; Bhuvanesh, N.; Gladysz, J. A. Syntheses of Enantiopure Bifunctional 2-Guanidinobenzimidazole Cyclopentadienyl Ruthenium Complexes: Highly Enantioselective Organometallic Hydrogen Bond Donor Catalysts for Carbon-Carbon Bond Forming Reactions. *Organometallics* **2014**, *33*, 6723-6737.

(10) See also: Thomas, C.; Gladysz, J. A. Highly Active Families of Catalysts for the Ring Opening Polymerization of Lactide: Metal Templated Organic Hydrogen Bond Donors Derived from 2-Guanidinobenzimidazole. *ACS Catal.* **2014**, *4*, 1134-1138.

(11) (a) Maleev, V. I.; North, M.; Larionov, V. A.; Fedyanin, I. V.; Savel'yeva, T. F.; Moscalenko, M. A.; Smolyakov, A. F.; Belokon, Y. N. Chiral Octahedral Complexes of Cobalt(III) as "Organic Catalysts in Disguise" for the Asymmetric Addition of a Glycine Schiff Base Ester to Activated Olefins. *Adv. Synth. Catal.* **2014**, *356*, 1803-1810. (b) Pardo, P.; Carmona, D.; Lamata, P.; Rodríguez, R.; Lahoz, F. J.; García-Orduña, P.; Oro, L. A. Reactivity of the Chiral Metallic Brønsted Acid [(η^6-*p*-MeC_6H_4*i*Pr)Ru(κ^3*P*,*O*,*O*'-POH)][SbF_6]$_2$ (POH = S_{C1},R_{C2})-Ph_2P-C(Ph)HC(OH)HCH_2OMe) toward Aldimines. *Organometallics* **2014**, *33*, 6927-6936. (c) Skubi, K. L.; Kidd, J. B.; Jung, H.; Guzei, I. A.; Baik, M.-H.; Yoon, T. P. Enantioselective Excited-State Photoreactions Controlled by a Chiral Hydrogen-Bonding Iridium Sensitizer. *J. Am. Chem. Soc.* **2017**, *139*, 17186-17192.

(12) (a) Nickerson, D. M.; Mattson, A. E. Transition Metal and Hydrogen Bond Donor Hybrids: Catalysts for the Activation of Alkylidene Malonates. *Chem. Eur. J.* **2012**, *18*, 8310-8314. (b) Nickerson, D. M.; Angeles, V. V.; Auvil, T. J.; So, S. S.; Mattson, A. E. Internal Lewis Acid Assisted Ureas: Tunable Hydrogen Bond Donor Catalysts. *Chem. Commun*. **2013**, *49*, 4289-4291.

(13) (a) Huo, H.; Fu, C.; Wang, C.; Harms, K.; Meggers, E. Metal-templated Enantioselective Enamine/H-bonding Dual Activation Catalysis. *Chem. Commun*. **2014**, *50*, 10409-10411. (b) Hu, Y.; Zhou, Z.; Gong, L.; Meggers, E. Asymmetric aza-Henry reaction to provide oxindoles with quaternary carbon stereocenter catalyzed by a metal-templated chiral Brønsted base. *Org. Chem. Front.* **2015**, *2*, 968-972. (c) Ding, X.; Lin, H.; Gong, L.; Meggers, E. Enantioselective Sulfa-Michael Addition to α,β-Unsaturated γ-Oxoesters catalyzed by a Metal-Templated Chiral Brønsted Base. *Asian J. Org. Chem.* **2015**, *4*, 434-437. (d) Xu, W.; Arieno, M.; Löw, H.; Huang, K.; Xie, X.; Cruchter, T.; Ma, Q.; Xi, J.; Huang, B.; Wiest, O.; Gong, L.; Meggers, E. Metal-Templated Design:

Enantioselective Hydrogen-Bond-Driven Catalysis Requiring Only Parts-per-Million Catalyst Loading. *J. Am. Chem. Soc.* **2016,** *138*, 8774-8780. I Ding, X.; Tian, C.; Hu, Y.; Gong, L.; Meggers, E. Tuning the Basicity of a Metal-Templated Brønsted Base to Facilitate the Enantioselective Sulfa-Michael Addition of Aliphatic Thiols to α,β-Unsaturated *N*-Acylpyrazoles. *Eur. J. Org. Chem.* **2016**, *2016*, 887-890.

(14) Gahan, L. R.; Harrowfield, J. M. *Sepulchrate*: Four decades on. *Polyhedron* **2015**, *94*, 1-51.

(15) Geue, R. J.; Hambley, T. W.; Harrowfield, J. M.; Sargeson, A. M.; Snow, M. R. Metal Ion Encapsulation: Cobalt Cages Derived from Polyamines, Formaldehyde, and Nitromethane. *J. Am. Chem. Soc.* **1984**, *106*, 5478-5488.

(16) Comba, P.; Creaser, I. I.; Gahan, L. R.; Harrowfield, J. M.; Lawrance, G. A.; Martin, L. L.; Mau, A. W. H.; Sargeson, A. M.; Sasse, W. H. F.; Snow, M. R. Macrobicyclic Chromium(III) Hexaamine Complexes. *Inorg. Chem.* **1986**, *25*, 384-389.

(17) Boucher, H. A.; Lawrance, G. A.; Lay, P. A.; Sargeson, A. M.; Bond, A. M.; Sangster, D. F.; Sullivan, J. C. Macrobicyclic (Hexaamine)platinum(IV) Complexes: Synthesis, Characterization, and Electrochemistry. *J. Am. Chem. Soc.* **1983**, *105*, 4652-4661.

(18) Cai, H.; Fissekis, J.; Conti, P. S. Synthesis of a novel bifunctional chelator AmBaSar based on sarcophagine for peptide conjugation and ^{64}Cu radiolabelling. *Dalton Trans.* **2009**, *27*, 5395-5400.

(19) Martell, A. E.; Hancock, R. D.; Motekaitis, R. J. Factors affecting stabilities of chelate, macrocyclic, and macrobicyclic complexes in solution. *Coord. Chem. Rev.* **1994**, *133*, 39-65.

(20) Creaser, I. I.; Harrowfield, J. M.; Herlt, A. J.; Sargeson, A. M.; Springborg, J.; Geue, R. J.; Snow, M. R. Sepulchrate: A Macrobicyclic Nitrogen Cage for Metal Ions. *J. Am. Chem. Soc.* **1977**, *99*, 3181-3182.

(21) Creaser, I. I.; Geue, R. J.; Harrowfield, J. M.; Herlt, A. J.; Sargeson, A. M.; Snow, M. R.; Springborg, J. Synthesis and Reactivity of Aza-Capped Encapsulated Co(III) Ions. *J. Am. Chem. Soc.* **1982**, *104*, 6016-6025.

(22) Review of stereoisomerism in salts of the trication $[Co(en)_3]^{3+}$, and homologs with substituted 1,2-diamine ligands: Ehnbom, A.; Ghosh, S. K.; Lewis, K. G.; Gladysz, J. A. Octahedral Werner complexes with substituted ethylenediamine ligands: a stereochemical primer for a historic series of compounds now emerging as a modern family of catalysts. *Chem. Soc. Rev.* **2016**, *45*, 6799-6811.

(23) Sarneski, J. E.; Urbach, F. L. A Model for the Circular Dichroism Perturbations Which Arise upon Ion Pairing between Tris(diamine)-Metal Chelates and Certain Polyoxyanions. *J. Am. Chem. Soc.* **1971**, *93*, 884-888.

(24) Bernhardt, P. V.; Dyahningtyas, T. E.; Harrowfield, J. M.; Kim, J.-Y.; Kim, Y.; Rukmini, E. Chiral Resolution of Hexaamine Cobalt(III) Cages: Substituent Effects on Chiral Discrimination. *Aust. J. Chem.* **2003**, *56*, 1187-1191.

(25) Walker, G. W.; Geue, R. J.; Sargeson, A. M.; Behm, C. A. Surface-active cobalt cage complexes: synthesis, surface chemistry, biological activity, and redox properties. *Dalton Trans.* **2003**, *15*, 2992-3001.

(26) Gahan, L. R; Healy, P. C.; Patch, G. J. Synthesis of Cobalt (III) "Cage" Complexes: A Twist on an Old Theme in the Inorganic Laboratory. *J. Chem. Educ.* **1989**, *66*, 445-446.

(27) Bottomley, G. A; Clark, I. J.; Creaser, I. I.; Engelhardt, L. M.; Geue, R. J.; Hagen, K. S.; Harrowfield, J. M.; Lawrance, G. A.; Lay, P. A.; Sargeson, A. M.; See, A.

J.; Skelton, B. W.; White, A. H.; Wilner, F. R. The Synthesis and Structure of Encapsulating Ligands: Properties of Bicyclic Hexamines. *Aust. J. Chem.* **1994**, *47*, 143-179.

(28) Geue, R. J.; Searle, G. H. Cation-Exchange Chromatography and Selective Complexation in the Isolation of Branched Acyclic Polyamines: Syntheses of Ethylidynetris(methanamine) [tame], 2,2-Bis(aminomethyl)propan-1-ol [hmmp], 4,4',4"-Ethylidynetris(3-azabutan-1-amine) [sen] and 5,5',5"-Ethylidynetris(4-azapentan-1-amine) [stn]. *Aust. J. Chem.* **1983**, *36*, 927-935.

(29) Comba, P.; Sargeson, A. M. Is the *E*2 Mechanism required to explain Base Hydrolysis of Cobalt(III) Amine Complexes in the Limit of General Base Catalysis? *J. Chem. Soc., Chem. Commun.* **1985**, 51-52.

(30) Andrés, J. M.; Manzano, R.; Pedrosa, R. Novel Bifunctional Chiral Urea and Thiourea Derivatives as Organocatalysts: Enantioselective Nitro-Michael Reaction of Malonates and Diketones. *Chem. Eur. J.* **2008**, *114*, 5116-5119.

(31) Almaşi, D.; Alonso, D. A.; Gómez-Bengoa, E.; Nájera, C. Chiral 2-Aminobenzimidazoles as Recoverable Organocatalysts for the Addition of 1,3-Dicarbonyl Compounds to Nitroalkenes. *J. Org. Chem.* **2009**, *74*, 6163-6168.

(32) Li, P.; Wen, S.; Yu, F.; Liu, Q.; Li, W.; Wang, Y.; Liang, X.; Ye, J. Enantioselective Organocatalytic Michael Addition of Malonates to *α*,β-Unsaturated Ketones. *Org. Lett.* **2009**, *11*, 753-756.

(33) Wascholowski, V.; Knudsen, K. R.; Mitchell, C. E. T.; Ley, S. V. A General Organocatalytic Enantioselective Malonate Addition to α,β-Unsaturated Enones. *Chem. Eur. J.* **2008**, *114*, 6155-6165.

(34) Saaby, S.; Bella, M.; Jørgensen, K. A. Asymmetric Construction of Quaternary Stereocenters by Direct Organocatalytic Amination of α-Substituted α-

Cyanoacetates and β-Dicarbonyl Compounds. *J. Am. Chem. Soc.* **2004**, *126*, 8120-8121. The chiral HPLC column employed with the addition product featured the same stationary phase but a different particle size from that used earlier in the literature. It is presumed that the well separated enantiomers exhibit identical orders of elution. Configurations were assigned accordingly.

(35) (a) Kabes, C. Q.; Gunn, J. H.; Selbst, M. A.; Lucas, R. F.; Gladysz, J. A. Syntheses of Enantiopure 1,2-Ethylenediamines with Appended Secondary Amines of the Formula $NH_2CH_2CH((CH_2)_nNHMe)NH_2$ (n = 1-4) from α-Amino Acids: New Chiral Chelating Ligands for Asymmetric Catalysis. *Synthesis* **2020**, *52*, 3277-3285.

(36) Maximuck, W. J.; Ganzmann, C.; Alvi, S.; Hooda, K. R.; Gladysz, J. A. Rendering classical hydrophilic enantiopure Werner salts $[M(en)_3]^{n+}$ nX^- lipophilic (M/n = Cr/3, Co/3, Rh/3, Ir/3, Pt/4); New chiral hydrogen bond donor catalysts and enantioselectivities as a function of metal and charge. *Dalton Trans.* **2020**, *49*, 3680-3691.

(37) Bernhardt, P. V.; Bygott, A. M. T.; Geue, R. J.; Hendry, A. J.; Korybut-Daszkiewicz, B. R.; Lay, P. A.; Pladziewicz, J. R.; Sargeson, A. M.; Willis, A. C. Stabilization of Cobalt Cage Conformers in the Solid State and Solution. *Inorg. Chem.* **1994**, *33*, 4553-4561.

(38) (a) Geue, R. J.; McCarthy, M. G.; Sargeson, A. M. Synthesis, Chiroptical Properties, and Electron Self-Exchange Reactivity of a Rigid Pentacyclic Metal Ion Cage System with D_3 Symmetry. *J. Am. Chem. Soc.* **1984**, *106*, 8282-8291. (b) Walker, G. W.; Geue, R. J.; Haller, K. J.; Rae, A. D.; Sargeson, A. M. New synthetic routes to hexa-aza cages using cobalt(III) tris(1,2-diamine) templates. *Dalton Trans.* **2003**, 279-281.

(39) Geue, R. J.; Petri, W. R.; Sargeson, A. M.; Snow, M. R. Metal Ion Cages: Capping Reactions with Bifunctional Methylene Compounds and Formaldehyde. *Aust. J. Chem.* **1992**, *45*, 1681-1703.

(40) (a) Mikuriya, M.; Hamagawa, M.; Tomioka, N.; Fujimori, R.; Yoshioka, D.; Hori, S.; Kuriyama, T.; Sakiyama, H.; Handa, M.; Mitsuhashi, R. Nickel(II) complex with 1,4,7-tris(2-aminoethyl)-1,4,7-triazacyclononane. *Chem. Pap.* **2016**, *70*, 69-74. (b) Hammershøi, A.; Sargeson, A. M. Macrotricyclic Hexaamine Cage Complexes of Cobalt(III): Synthesis, Characterization, and Properties. *Inorg. Chem.* **1983**, *22*, 3554-3561.

(41) Ribeiro, S.; Cunha-Silva, L.; Balula, S. S.; Gago, S. Cobalt(III) sepulchrate complexes: application as sustainable oxidative catalysts. *New J. Chem.* **2014**, *38*, 2500-2507.

(42) He, F. M. C.; Bernhardt, P. V. Cobalt cage complexes as mediators of protein electron transfer. *J. Biol. Inorg. Chem.* **2017**, *22*, 775-788.

(43) Pina, F.; Mulazzani, Q. G.; Venturi, M.; Ciano, M.; Balzani, V. Photochemistry of $Co(sep)^{3+}$-Oxalate Ion Pairs: A Novel System for Dihydrogen Evolution from Aqueous Solutions. *Inorg. Chem.* **1985**, *24*, 848-851.

(44) In the previous literature report of $[Co(taetacn)]^{3+}$ $3ClO_4^-$,[40b] only $^{13}C\{^1H\}$ NMR spectra were reported (D_2O with 1,4-dioxane reference).

(45) Wu, L.-L.; Li, L.-P.; Xiang, Y; Guan, Z.; He, Y.-H. Enzyme-Promoted Direct Asymmetric Michael Reaction by Using Protease from *Streptomyces griseus*. *Catal. Lett.* **2017**, *147*, 2209-2214.

5. EXPLORATORY STUDIES OF FUNCTIONALIZED (*S*,*S*)-DIAMINE LIGANDS, CATALYST ANION COMBINATIONS, AND PLATINUM DIPHENYLETHYLENEDIAMINE COMPOUNDS

5.1 Introduction

We have learned quite a bit in the first decade and a half of working with lipophilic Werner complexes. Based on previous results, we were compelled to develop a few projects that fall under the category of curiosity-driven, exploratory research. Sometimes these efforts were met with puzzling and/or underwhelming findings. Among the projects, we focused on functionalizing the diamine ligands to produce catalysts with more steric bulk or differing electronics from our standard dpen ligand. A second project outlined in this section focuses on a variety of anion combinations with the Λ-$[Co((S,S)\text{-dpen})_3]^{3+}$ $3X^-$ (Λ-(*S*,*S*)-$\mathbf{1}^{3+}$ $3X^-$) system and the final portion details various synthetic attempts targeting the salts $[Pt(dpen)_n]^{n'+}$ $n'X^-$ (n/n' = 2/2, 3/4).

5.2 Functionalized (*S*,*S*)-diamine ligands

Following thorough development of the cobalt complexes comprised of classical (*S*,*S*)-dpen ligands, a logical catalyst optimization approach would involve functionalization of the phenyl rings.[1] The template for the stereospecific syntheses of these ligands has been developed for a considerable number of moieties by Jik Chin at the University of Toronto.[2]

The ligand variations enable tuning of the chiral pocket. Not only can the sterics be altered with the functionalities themselves, but the Brønsted acidities of the NH units can also be increased with the installation of electron withdrawing groups on the aromatic rings. This bump in acidity is thought to pull substrates deeper into the chiral pocket where the selectivity could be elevated.[1]

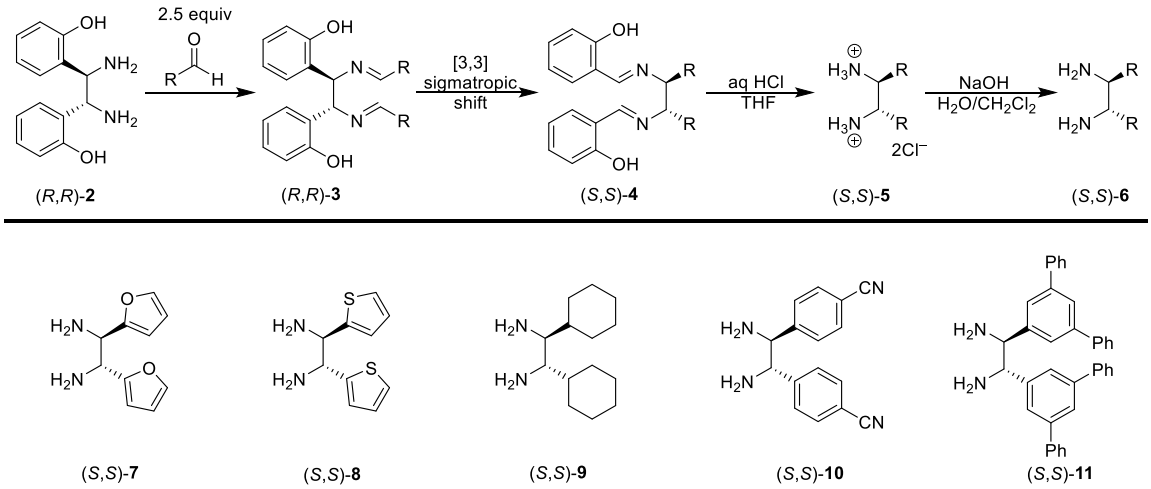

Figure 5.1. Synthetic scheme for the production of functionalized (*S*,*S*)-1,2-diamine ligands (top) and the specific ligands produced (bottom).

These ligand transformations are made possible by first condensing the commercially available so-called "mother diamine," (*R*,*R*)-bis(*o*-hydroxy)-1,2-diphenylethylenediamine, or (*R*,*R*)-**2**, with an appropriate aryl or cyclohexyl aldehyde to form di-Schiff bases, (*R*,*R*)-**3**.[2] Both stereocenters are inverted as a result of a stereospecific [3,3] sigmatropic rearrangement, (*S*,*S*)-**4**. This rearrangement is energetically favorable and the stereospecificity is due to the steric effects of the chair-like transition state. The imines can be hydrolyzed using HCl to yield dihydrochloride diammonium salts, (*S*,*S*)-**5**, which are subsequently deprotonated under basic conditions to form the desired "daughter diamine", (*S*,*S*)-**6**.[2] These sequences afforded the 2-furyl, 2-thiophenyl, cyclohexyl, 4-cyanophenyl, and terphenyl substituted diamines (*S*,*S*)-**7**-**11** shown in Figure 5.1.

Installation of the newly minted (*S*,*S*)-diamine ligands on the cobalt(III) metal center was carried out via procedures analogous to the syntheses of Λ- and Δ-(*S*,*S*)-$\mathbf{1}^{3+}$ $3X^-$ as summarized in Figure 5.2.[1] In the top of the figure, the tris(chloride) salt Λ-(*S*,*S*)-$\mathbf{14}^{3+}$ $3Cl^-$ was impure, but exhibited CH_2Cl_2 solubility, whereas other tris(chloride) complexes were generally only soluble in highly polar solvents such as CH_3OH or DMSO.

The purification process included treating the tris(chloride) salt Λ-(*S*,*S*)-**14**$^{3+}$ 3Cl^{-} with 1.0 equivalent of Na^{+} BAr$_f^{-}$ and the resulting reaction mixture was chromatographed on silica gel to give Λ-(*S*,*S*)-**14**$^{3+}$ 2Cl^{-}BAr$_f^{-}$ in a meager 10% yield (procedure **A**). Surprisingly, under analogous conditions Λ-(*S*,*S*)-**12**$^{3+}$ 3Cl^{-} was converted to the monochloride salt Λ-(*S*,*S*)-**12**$^{3+}$ Cl^{-}2BAr$_f^{-}$ in 37% yield. This was unusual given the reaction stoichiometry, but the composition was supported by (1) microanalysis and (2) integration of the ^{1}H NMR signals associated with the trication Λ-(*S*,*S*)-**12**$^{3+}$ and the anion BAr$_f^{-}$. Additionally, we have observed this oddity earlier in the synthesis of Λ-[Co((*S*,*S*)-$H_2NCH(3,5\text{-}C_6H_3(CF_3)_2)CH(3,5\text{-}C_6H_3(CF_3)_2)NH_2)_3]^{3+}$ Cl^{-}2BAr$_f^{-}$. Like Λ-(*S*,*S*)-**12**$^{3+}$ Cl^{-}2BAr$_f^{-}$, this compound was also obtained as a dark brown solid.[1a]

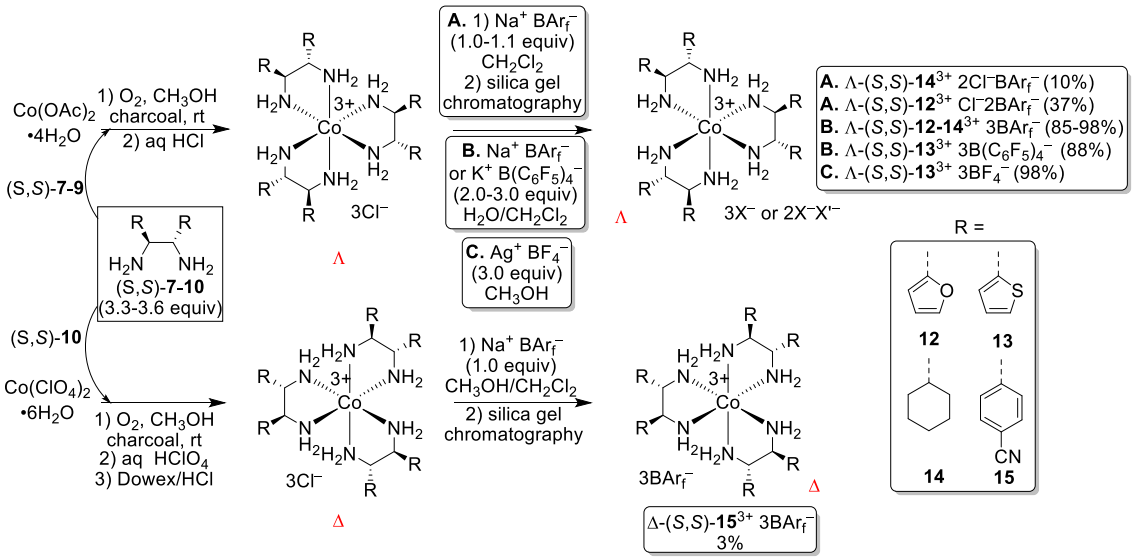

Figure 5.2. Syntheses of (*S*,*S*)-**12**-**15**$^{3+}$ 3Cl^{-} and subsequent anion metathesis.

The lipophilic salts Λ-(*S*,*S*)-**12**-**13**$^{3+}$ 3BAr$_f^{-}$ were synthesized via the addition of 3.0 equivalents of Na^{+} BAr$_f^{-}$ to the tris(chloride) precursors in biphasic H_2O/CH_2Cl_2 reaction conditions with isolated yields of 85-98% (procedure **B**). The tris(tetraarylborate) salt Λ-(*S*,*S*)-**13**$^{3+}$ 3B(C$_6$F$_5$)$_4^{-}$ was synthesized in an analogous manner using 3.0

equivalents of K^+ $B(C_6F_5)_4^-$. The mixed salt Λ-(*S*,*S*)-**14**$^{3+}$ 2$Cl^-$$BAr_f^-$ could be converted to the "nonmixed" salt Λ-(*S*,*S*)-**14**$^{3+}$ 3BAr_f^- with 2.0 equivalents of Na^+ BAr_f^- using identical reaction conditions. Alternatively, the tris(tetrafluoroborate) salt Λ-(*S*,*S*)-**13**$^{3+}$ 3BF_4^- was prepared by reacting the tris(chloride) precursor with 3.0 equivalents of Ag^+ BF_4^- in CH_3OH and filtration to remove Ag^+ Cl^- (procedure **C**).

Synthesis of the salt Δ-(*S*,*S*)-**15**$^{3+}$ 3BAr_f^- was carried out using a perchlorate salt precursor that normally leads to a Δ diastereomer (Figure 5.2, bottom).[1] Earlier synthetic attempts at the opposite diastereomer Λ-(*S*,*S*)-**15**$^{3+}$ 3Cl^- and subsequent anion metathesis were thwarted by the failure to substitute the acetate anions for chloride anions, a step necessary to facilitate further lipophilic anion metathesis. We presumed that this may be a result of the strong hydrogen bond accepting acetate anions refusing to easily break their hydrogen bonds from the NH units, which should have enhanced acidities due to the cyano substituents. Perchlorate is a weaker coordinating anion than acetate and the complex can be converted to the tris(chloride) salt via washing with HCl on a Dowex ion-exchange column.[1] The final product collected after anion metathesis with 1.0 equivalent of Na^+ BAr_f^- was of the tris(BAr_f^-) variety. This is possibly due to the elevated polarity of the ligand, making less lipophilic anion combinations too polar to traverse through the silica gel column, even with increased polarity of solvent mixtures.

This work has proven that the Werner complex ligand framework can be expanded to include aromatic heterocycles, electron withdrawing groups, as well as cyclohexane rings. Unfortunately, these ligands have not resulted in catalysts providing greater enantioselectivities than the tris(tetraarylborate) salt Λ-(*S*,*S*)-**1**$^{3+}$ 3BAr_f^- (Figure 5.3).[1b] The phenyl ring size, as well as favorable π-π interactions between ligand and substrate, may be the "sweet spot" with the lipophilic Λ-(*S*,*S*)-**1**$^{3+}$ system to achieve high enantioselectivities. It is also evident that the ligand not only affects the

enantioselectivities of the catalytic reactions, but also the turnover frequencies. With the catalysts Λ- and Δ-(*S*,*S*)-**12-15**$^{3+}$ 3BAr$_f^-$, the rates still pale in comparison to the salt Λ-(*S*,*S*)-**1**$^{3+}$ 3BAr$_f^-$.[1b] Both the catalyst [Pt(en)$_3$]$^{4+}$ 4BAr$_f^-$ and electron withdrawing (*S*,*S*)-**10** ligand result in poorer enantioselectivity despite presumed increased hydrogen bonding strength.[3]

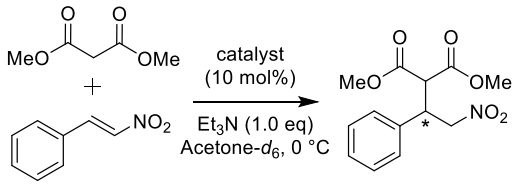

entry	catalyst	conversion (%) (time)[a]	ee (%) (config)[b]
1	Λ-(*S*,*S*)-**12**$^{3+}$ 3BAr$_f^-$	60 (23 h)	21 (*R*)
2	Λ-(*S*,*S*)-**12**$^{3+}$ Cl$^-$2BAr$_f^-$	76 (93 h)	25 (*R*)
3	Λ-(*S*,*S*)-**13**$^{3+}$ 3BAr$_f^-$	54 (53 h)	55 (*R*)
4	Λ-(*S*,*S*)-**13**$^{3+}$ 3BF$_4^-$	88 (46 h)	62 (*R*)
5	Λ-(*S*,*S*)-**13**$^{3+}$ 3B(C$_6$F$_5$)$_4^-$	>99 (21 h)	56 (*R*)
6	Λ-(*S*,*S*)-**14**$^{3+}$ 2Cl$^-$BAr$_f^-$	34 (52 h)	---
7	Λ-(*S*,*S*)-**14**$^{3+}$ 3BAr$_f^-$	58 (24 h)	27 (*R*)
8	Δ-(*S*,*S*)-**15**$^{3+}$ 3BAr$_f^-$	45 (24 h)	0

[a]The conversion was determined by ^{1}H NMR integration of the product C*H*(CO$_2$Me)$_2$ signal versus the internal standard Ph$_2$SiMe$_2$.
[b]Enantioselectivities were determined by chiral HPLC analyses.

Figure 5.3. Enantioselective additions of dimethyl malonate to *trans*-β-nitrostyrene with catalysts from Figure 5.2.

After analyzing this work, one may infer that mimicking a ligand similar to dpen, with subtle modifications, may be the best avenue to explore in enhancing catalytic enantioselectivities. One future possibility may include an anthracene ligand, which would extend the conjugated π system. Another possible improvement may come from the installation of a *para*-isopropyl group on the phenyl ring which may serve as a gate to the chiral pocket for incoming substrates.

Despite these promising hypotheses, the synthesis of diamines from aldehydes that lack polar groups can cause problems. Specifically, the diammonium salt of the terphenyl substituted ligand, (*S*,*S*)-H$_2$NCH(3,5-C$_5$H$_3$Ph$_2$)CH(3,5-C$_5$H$_3$Ph$_2$)NH$_2$·2HCl, ((*S*,*S*)-

11·2HCl), does not precipitate after hydrolysis. In preliminary efforts not represented in Figure 5.1, the same is true with diamines derived from 2-methylbenzaldehyde and cinnamaldehyde, among others. A strategic way to isolate these less polar molecules[4] involves the addition of diethyl ether to aid in the aqueous extraction of the dihydrochloride salt. This salt can be transformed into the free base by the addition of NaOH. This is the method utilized for the isolation of (*S*,*S*)-**11**.

Unfortunately, an attempt at synthesizing the desired complex Λ-[Co((*S*,*S*)-**11**$)_3$]$^{3+}$ 3Cl$^-$ under analogous reaction conditions as the tris(chloride) salt Λ-(*S*,*S*)-**1**$^{3+}$ 3Cl$^-$ was unsuccessful (Figure 5.4). The product was dark green in color and was provisionally assigned as *trans*-[Co((*S*,*S*)-**11**$)_2$(Cl$)_2$]$^+$ Cl$^-$ without additional spectroscopy. The same color is a distinct indicator of *trans*-[Co(dpen$)_2$(Cl$)_2$]$^+$ Cl$^-$.[1]

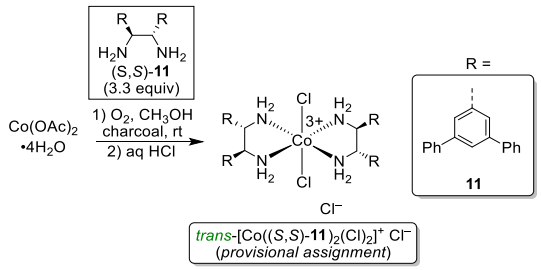

Figure 5.4. Attempted synthesis of Λ-[Co((*S*,*S*)-**11**$)_3$]$^{3+}$ 3Cl$^-$.

5.3 Anion combinations in salts of the trication Λ-(*S*,*S*)-**1**$^{3+}$

It has been well-established that the identities of the anions affect the kinetics and enantioselectivities of the cobalt(III) catalysts.[1b,5] Thanks to the bountiful supply of sodium and silver salts at our disposal from our stockroom, a synthetic undertaking was launched (Figure 5.5). In cases involving silver salts, an appropriate amount (1.0-3.0 equivalents) of the salt was reacted with the precursors Λ-(*S*,*S*)-**1**$^{3+}$ 3Cl$^-$ or Λ-(*S*,*S*)-**1**$^{3+}$ 2Cl$^-$BAr$_f^-$ in CH_3OH or CH_2Cl_2 and the reaction mixture filtered to remove Ag^+ Cl$^-$ from the desired lipophilic salt. The dodecyl sulfate (DS) containing complexes were prepared

from biphasic H_2O/CH_2Cl_2 reaction mixtures where the aqueous phase was employed to remove Na^+ Cl^- and the lower organic layer contained the desired product.

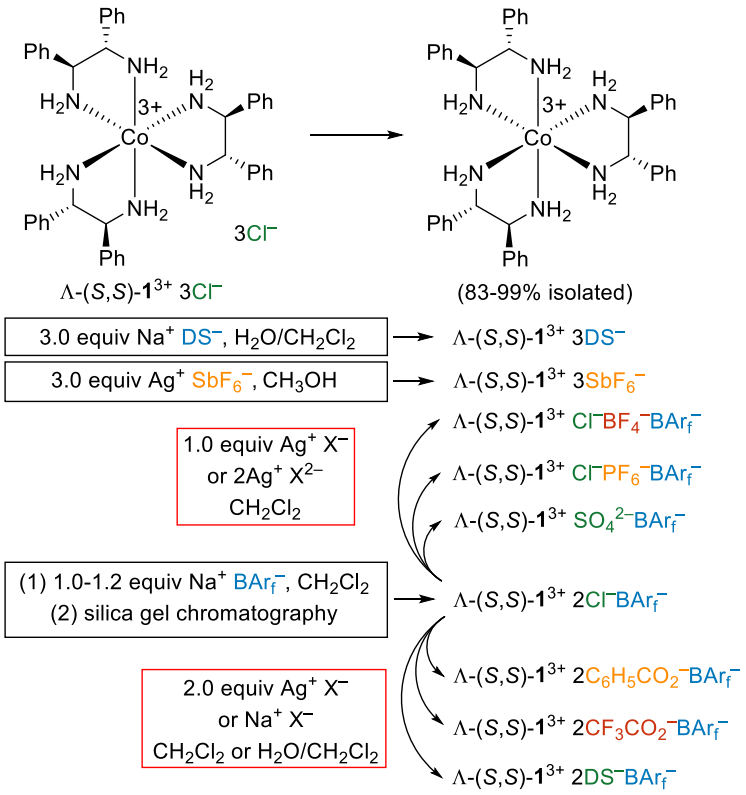

Figure 5.5. Anion metatheses involving the trication Λ-(*S*,*S*)-$\mathbf{1}^{3+}$ performed in section 5.3.

These catalysts did exhibit some interesting properties. Notably, the ^{1}H NMR spectrum of the catalyst Λ-(*S*,*S*)-$\mathbf{1}^{3+}$ $2C_6H_5CO_2^-BAr_f^-$ featured diastereotopic NH peaks with a large difference in chemical shift (Δδ) of 3.82 ppm in acetone-d_6 (8.94 and 5.12 ppm). The peak at 8.94 ppm represents one of the furthest downfield shifted C_3 NH peaks that we have observed with the Λ-(*S*,*S*)-$\mathbf{1}^{3+}$ cation under such conditions.[1] The Λ-(*S*,*S*)-$\mathbf{1}^{3+}$ $3SbF_6^-$ catalyst was among the most poorly soluble catalysts in acetone-d_6, which was juxtaposed by the DS containing catalysts which offered excellent organic solubility. These new catalysts were screened on the Michael addition of dimethyl malonate to nitrostyrene (see Figure 5.6), featuring ee values ranging from 78-86%. However, there

was not a catalyst that outperformed the benchmark salt Λ-(*S*,*S*)-**1**$^{3+}$ 2Cl^{-}BAr$_f^{-}$ (87% ee).[1b]

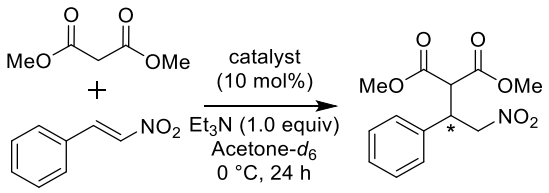

entry	catalyst	yield (%)[a]	ee (%) (config)[b]
1	Λ-(*S*,*S*)-**1**$^{3+}$ 2C$_6$H$_5$CO$_2^{-}$BAr$_f^{-}$	>99	78 (*R*)
2	Λ-(*S*,*S*)-**1**$^{3+}$ 2CF$_3$CO$_2^{-}$BAr$_f^{-}$	96	84 (*R*)
3	Λ-(*S*,*S*)-**1**$^{3+}$ SO$_4^{2-}$BAr$_f^{-}$	89	76 (*R*)
4	Λ-(*S*,*S*)-**1**$^{3+}$ 3SbF$_6^{-}$	67	80 (*R*)
5	Λ-(*S*,*S*)-**1**$^{3+}$ 2DS^{-}BAr$_f^{-}$	91	86 (*R*)
6	Λ-(*S*,*S*)-**1**$^{3+}$ 3DS^{-}	92	83 (*R*)
7	Λ-(*S*,*S*)-**1**$^{3+}$ Cl^{-}BF$_4^{-}$BAr$_f^{-}$	>99	82 (*R*)
8	Λ-(*S*,*S*)-**1**$^{3+}$ Cl^{-}PF$_6^{-}$BAr$_f^{-}$	96	79 (*R*)

[a]The conversion was determined by ^{1}H NMR integration of the product C*H*(CO$_2$Me)$_2$ signal versus the internal standard Ph$_2$SiMe$_2$. [b]Enantioselectivities and configurations were determined by chiral HPLC analyses.

Figure 5.6. Enantioselective additions of dimethyl malonate to *trans*-β-nitrostyrene with catalysts from Figure 5.5.

Mixed salts have earned a checkered reputation for their potentially deceptive possibility of existing as a proportional combination of "nonmixed" salts. We have conventionally dispelled these fears through multiple observations. Among them, strong evidence for these mixed salts is that they survive silica gel chromatography with the ^{1}H NMR signal integration ratio between anion and cation remaining constant. Most recently, in Section 3, a rare crystal structure (Figure 3.4) has also served as proof to silence doubters.[5]

Up to this point, all mixed salts in the group consisted of anions of two different identities. This inspired us to muse about the possibility of mixed salts with anions of three different identities (Figure 5.6, entries 7-8). These salts were synthesized using protocols illustrated in Figure 5.5. The triply mixed salts were confirmed by ratios amongst cations

and anions in ^{1}H and ^{19}F NMR spectroscopy. The ^{19}F NMR of the salts Λ-(*S*,*S*)-**1**$^{3+}$ Cl^{-} $BF_4^{-}BAr_f^{-}$ and Λ-(*S*,*S*)-**1**$^{3+}$ $Cl^{-}PF_6^{-}BAr_f^{-}$ featured peak integration ratios of 4:24 and 6:24, an expected agreement between the smaller fluorine-containing anions and the larger BAr_f^{-}. To our dismay, none of these anion combinations resulted in catalysts with greater enantioselectivities than the current pack in our repertoire (Figure 5.6).

The salts Λ-(*S*,*S*)-**1**$^{3+}$ $2Cl^{-}BAr_f^{-}$ and Λ-(*S*,*S*)-**1**$^{3+}$ $2I^{-}BAr_f^{-}$ have been established in the literature as robust, economical catalysts and chiral solvating agents.[1,6] This sparked the desire to complete the series and roll out the Λ-(*S*,*S*)-**1**$^{3+}$ $2Br^{-}BAr_f^{-}$ variant.[5] Attempts at converting Λ-(*S*,*S*)-**1**$^{3+}$ $2Cl^{-}BAr_f^{-}$ to Λ-(*S*,*S*)-**1**$^{3+}$ $2Br^{-}BAr_f^{-}$ under vigorous stirring with KBr in acetone proved unsuccessful, though an analogous method was viable for the complex Λ-(*S*,*S*)-**1**$^{3+}$ $2I^{-}BAr_f^{-}$.[6] The most effective method for the synthesis of the salt Λ-(*S*,*S*)-**1**$^{3+}$ $2Br^{-}BAr_f^{-}$ mirrored that of Λ-(*S*,*S*)-**1**$^{3+}$ $2Cl^{-}BAr_f^{-}$, but replacing the HCl addition with HBr. The Λ-(*S*,*S*)-**1**$^{3+}$ $3Br^{-}$ intermediate was impure, with unaccounted peaks in the ^{1}H NMR spectrum. This issue could be circumvented via anion metathesis with 1.0 equivalent of Na^{+} BAr_f^{-}, followed by silica gel chromatography (Figure 5.7, left panel). The faster-moving green band was eluted with CH_2Cl_2 and is possibly a lipophilic derivative of *trans*-$[Co((S,S)\text{-dpen})_2(Br)_2]^{+}$ Br^{-} (provisionally assigned solely by its similarity in color with *trans*-$[Co(dpen)_2(Cl)_2]^{+}$ Cl^{-}).[1] The slower-moving, dark yellow band could be eluted from the silica gel column with a small proportion of CH_3OH in CH_2Cl_2 to give the bis(bromide) salt Λ-(*S*,*S*)-**1**$^{3+}$ $2Br^{-}BAr_f^{-}$ as a yellow solid. The series of salts Λ-(*S*,*S*)-**1**$^{3+}$ $2X^{-}BAr_f^{-}$ are shown in NMR tubes in the right panel of Figure 5.7 below from left to right, where X = Cl, Br, and I. The ^{1}H NMR spectra of these complexes were compared in CD_2Cl_2 at equimolar concentrations (0.0169 M) resulting in Δδ values for the diastereotopic NH peaks of 4.14, 4.33, and 3.59 ppm for Cl, Br, and I respectively.

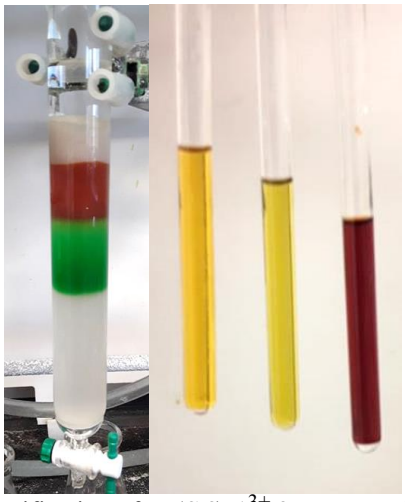

Figure 5.7. Silica gel column for the purification of Λ-(*S*,*S*)-**1**$^{3+}$ 2Br^{-}BAr$_f^{-}$ (left panel). 0.0169 M CD_2Cl_2 solutions of Λ-(*S*,*S*)-**1**$^{3+}$ 2Cl^{-}BAr$_f^{-}$, Λ-(*S*,*S*)-**1**$^{3+}$ 2Br^{-}BAr$_f^{-}$, and Λ-(*S*,*S*)-**1**$^{3+}$ 2I^{-}BAr$_f^{-}$ in NMR tubes (right panel, left to right).

5.4 Synthetic attempts at platinum tris(diphenylethylenediamine)

We have long hypothesized that more acidic NH units would be one of the keys to enhancing the enantioselectivities of our Werner catalysts.[1] To this end, we have pursued the installation of electron withdrawing functionalities on the aromatic rings of our dpen-like ligands. With so much focus on the development of these ligands due to their direct involvement in the catalytic mechanism, perhaps another opportunity was overlooked. Though the metal is not directly involved in the mechanism, it serves as an anchor for the ligands to bind and is directly adjacent to the NH active sites. Interestingly, the identity of the metal has a great deal of influence on the acidity of the coordinated NH groups. In fact, in the tris(ethylenediamine) series, NH bonds of the salt $[Pt(en)_3]^{4+}$ 4Cl^{-} are much more acidic (pK_a^1/K_a^1 = 5.5/3.2 × 10^{-6})[7,8] than those of the $[Co(en)_3]^{3+}$ 3Cl^{-} analogue (pK_a^1/K_a^1 = 14.9/1.3 × 10^{-15}).[9] The steric bulk of the dpen ligands in conjunction with acidity advantage of Pt(IV) over Co(III) could be the "magic bullet" that we have been chasing.

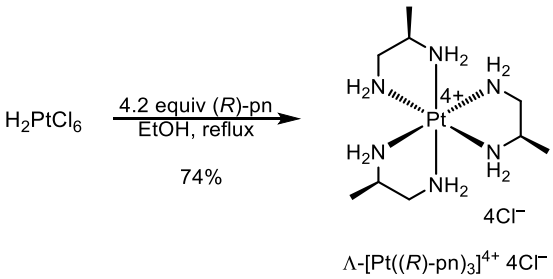

Figure 5.8. Literature synthesis of Λ-$[Pt((R)\text{-pn})_3]^{4+}$ $4Cl^-$.

Accordingly, salts of the tetracation $[Pt(dpen)_3]^{4+}$ were selected as synthetic targets, and several routes were explored. For comparison, H_2PtCl_6 was reacted with excess ethylenediamine in refluxing ethanol for 2 h and filtered to yield the pure salt $[Pt(en)_3]^{4+}$ $4Cl^-$ after three recrystallization cycles from HCl in a 66% isolated yield.[10] This complex served as an intermediate in section 2 (see Figure 2.2). As shown in Figure 5.8, a nearly identical procedure was used for synthesis of the more sterically demanding Λ-$[Pt((R)\text{-pn})_3]^{4+}$ $4Cl^-$ complex (pn = 1,2-propylenediamine).[11]

Disappointingly, these methods proved ineffective for the salt $[Pt(dpen)_3]^{4+}$ $4Cl^-$. In contrast to the situation with $[Pt(en)_3]^{4+}$ $4Cl^-$, the NMR spectra were very complex. Discouraged by these results, $PtCl_4$ was used as the platinum source. This variation provided cleaner NMR spectra. Altering solvent to allow for increased refluxing temperatures, led to the exploration of DMSO, *n*-propanol, and *n*-pentanol. The utilization of $PtCl_2$ and later adding H_2O_2 to oxidize the Pt(II) to Pt(IV) was also investigated.

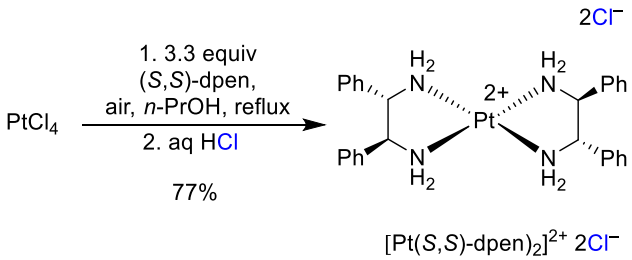

Figure 5.9. Synthesis of $[Pt((S,S)\text{-dpen})_2]^{2+}$ $2Cl^-$.

Only the combination of $PtCl_4$ reacting with 3.3 equiv of dpen in *n*-propanol (Figure 5.9) provided an NMR spectrum that held promise for the tetrachloride salt $[Pt(dpen)_3]^{4+}$ $4Cl^-$, mirroring the same features found in the trichloride salt Λ-(*S*,*S*)-**1**$^{3+}$ $3Cl^-$. The elemental analysis fit $[Pt(dpen)_3]^{4+}$ $4Cl^-\cdot 7H_2O$. The additional hydrate value, in comparison to Λ-(*S*,*S*)-**1**$^{3+}$ $3Cl^-\cdot 3H_2O$, intuitively fit the increased acidity of Pt(IV) versus Co(III). What we failed to consider for some time was the possibility that these analytical methods did not account for the potential that the isolated compound was the square planar complex $[Pt(dpen)_2]^{2+}$ $2Cl^-\cdot 2.5H_2O$. Unfortunately, the elemental analysis data also fit this dicationic compound and it was not until vibrational circular dichroism (VCD) was implemented and the X-ray crystal structure solved (Figure 5.10, Tables 5.1 and A-2) that this oversight was realized.

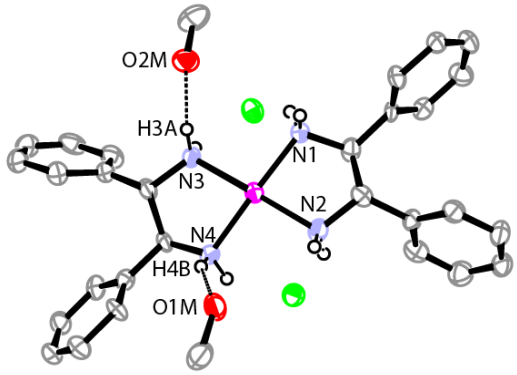

Figure 5.10. Molecular structure of $[Pt((S,S)\text{-dpen})_2]^{2+}$ $2Cl^-\cdot 2CH_3OH$; thermal ellipsoids are depicted at the 50% probability level. Bond lengths (Å) and angles (°) about platinum: Pt(1)-N(1), 2.034(6); Pt(1)-N(2), 2.036(6); Pt(1)-N(3), 2.036(6); Pt(1)-N(4), 2.053(6); N(1)-Pt(1)-N(2), 83.4(3); N(1)-Pt(1)-N(3), 97.4(2); N(1)-Pt(1)-N(4), 174.4(3); N(2)-Pt(1)-N(3), 177.7(3); N(2)-Pt(1)-N(4), 96.2(2); N(3)-Pt(1)-N(4), 82.7(1). Distances (Å) and angles (°) relevant to hydrogen bonding: O(1M)···H(4B), 2.08; O(2M)···H(3A), 1.96; O(1M)···N(4), 2.925; O(2M)···N(3), 2.854; O(1M)···H(4B)-N(4), 153.2; O(2M)···H(3A)-N(3), 167.0.

The structure in Figure 5.10 is chiral because of the (*S*,*S*) carbon configurations on the dpen ligands. The complex has average Pt-N bond lengths of 2.040(6) Å. The N1-Pt-N4 and N2-Pt-N3 bond angles are 174.4(3)° and 177.7(3)°, respectively. All compare

nicely to the average Pt-N bond lengths (2.038(9) Å) and equivalent bond angles (both 177.7(4)°) of the cation $[Pt(en)_2]^{2+}$ found in the literature.[12] It is also a promising sign for our catalysis, that the NH units hydrogen bond with the CH_3OH solvent molecules with relevant distances and angles listed in the caption.

We conjectured that the alcohol used in the synthesis may be responsible for reducing the Pt(IV) starting material to Pt(II), even under aerobic conditions. However, synthetic attempts with *t*-butanol as the solvent, which should eliminate the possibility of the solvent acting as a H_2 source, yielded identical results to *n*-propanol.

The complex $[Pt((S,S)\text{-dpen})_2]^{2+}$ $2Cl^-$ underwent anion metathesis to produce the lipophilic bis(tetraarylborate) salt $[Pt((S,S)\text{-dpen})_2]^{2+}$ $2BAr_f^-$. The resulting catalyst was tested in the nitrostyrene-dimethyl malonate addition under optimal conditions for Λ-(*S*,*S*)-**1**$^{3+}$ $3BAr_f^-$ (see Figure 5.3) using the solvent acetone-d_6 and the base Et_3N, this gave the (*R*) addition product in 48% ee and >99% yield after 24 h at 0 °C. This demonstrates the effectiveness of the ligands in these catalytic systems as there is no chirality at the metal center in this example.

5.5 Experimental section

General data. Reactions were conducted under aerobic atmospheres. NMR solvents (Cambridge Isotopes), HPLC grade solvents (hexanes, Fischer; isopropanol, JT Baker), and reaction solvents (CH_2Cl_2, Sigma-Aldrich, anhydrous, ≥99.8%; acetone and ethyl acetate, Sigma-Aldrich, ACS reagent, ≥99.5%; hexanes, Sigma-Aldrich, ACS reagent, ≥98.5%), *n*-propanol (Millipore Sigma, ≥98.0%), THF (Sigma-Aldrich, ≥99.0%), diethyl ether (anhydrous, Sigma-Aldrich, ACS reagent, ≥99.0%), DMSO (EMD Millipore, ACS grade), and CH_3OH (Sigma-Aldrich, ≥99.8%) were used as received.

Other chemicals were used as received from the following sources: Λ-$[Co((S,S)\text{-dpen})_3]^{3+}$ $2Cl^-BAr_f^-\cdot 2H_2O$ (Λ-(*S*,*S*)-**1**$^{3+}$ $2Cl^-BAr_f^-$) (prepared by author,[1a] but can be

purchased from Strem), NaOH (VWR, ACS), HCl (VWR, 36.5-38.0%, ACS), $HClO_4$ (Macron, 70%, ACS), Na^+ BAr_f^- (97%, Ark Pharm (BAr_f^- = $B(3,5\text{-}C_6H_3(CF_3)_2)_4^-$)), K^+ $B(C_6F_5)_4^-$ (Boulder Scientific), Ag^+ BF_4^-, (Oakwood Chemical, ≥97%), Ag^+ PF_6^- (Beantown, 98%), sodium dodecyl sulfate (SDS) (Sigma-Aldrich, 98%), Ag^+ $C_6H_5CO_2^-$ (Acros, 99%), Ag^+ $CF_3CO_2^-$ (Aldrich, 99.99%), $2Ag^+$ SO_4^{2-} (Alfa Aesar, 98%), Ag^+ SbF_6^- (Strem, ≥98%), *trans*-β-nitrostyrene (Alfa Aesar, 98%), dimethyl malonate (Acros, ≥97%), Et_3N (Alfa Aesar, 98%), Ph_2SiMe_2, (TCI, ≥97%), furfural (Alfa Aesar, 98%), 2-thiophenecarboxaldehyde (Alfa Aesar, 98+%), (1*R*,2*R*)-1,2-bis(2-hydroxyphenyl)ethylenediamine ((*R*,*R*)-**2**) (Sigma-Aldrich, 95%), $Co(OAc)_2{\cdot}4H_2O$ (Alfa Aesar, 98%), $Co(ClO_4)_2{\cdot}6H_2O$ (Alfa Aesar, reagent grade), $PtCl_4$ (Pressure Chemical), silica gel (Silicycle SiliaFlash®), Dowex 50WX2 (200-400 mesh, Aldrich), Celite 545 (Aldrich), Na_2SO_4 (EMD Millipore), activated charcoal (Acros, Norit SX 4).

NMR spectra were recorded on Mercury 300 MHz, Bruker 400 MHz, and Varian NMRS 500 MHz spectrometers at ambient probe temperatures and referenced (δ in ppm) to residual solvent signals (^{1}H: CHD_2CN, 1.94; acetone-d_5, 2.05; DMSO-d_5, 2.50; CHD_2OD, 3.31; $CHDCl_2$, 5.32; $CHCl_3$, 7.26; ^{13}C: CD_3CN, 1.32; acetone-d_6, 29.8; DMSO-d_6, 39.5; CD_3OD, 49.0; CD_2Cl_2, 54.0; $CDCl_3$, 77.2). HPLC analyses were carried out with a Shimadzu instrument package (pump/autosampler/detector LC-20AD/SIL-20A/SPD-M20A). Melting points were determined using an OptiMelt MPA100 instrument. Microanalyses were conducted by Atlantic Microlab. IR spectra were recorded on a Shimadzu IRAffinity-1 spectrometer (Pike MIRacle ATR system, diamond/ZnSe crystal).

(*S*,*S*)-H_2NCH(2-furyl)CH(2-furyl)NH_2 ((*S*,*S*)-7). A round bottom flask was charged with (*R*,*R*)-**2** (1.2231 g, 5.0068 mmol) and DMSO (25 mL). Then furfural (1.08 mL, 1.255 g, 13.06 mmol, 2.609 equiv) was added with stirring. After 20 h, the mixture

was poured into H_2O (150 mL), which was extracted with diethyl ether (3 × 100 mL). The combined extracts were washed with H_2O and dried (Na_2SO_4). The solvent was removed by rotary evaporation and then oil pump vacuum (overnight). The yellow oil was dissolved in THF (25 mL), and aqueous HCl (1.5 mL, 12.0 M) was added with stirring. After 3 h, a white precipitate had formed, which was isolated by filtration and washed with THF. The sample was dissolved in H_2O (40 mL) and aqueous NaOH (3.0 M) was added with stirring until the pH reached 11-12. The mixture was extracted with CH_2Cl_2 (1 × 75 mL) and diethyl ether (2 × 75 mL) and the combined extracts were dried (Na_2SO_4). The solvent was removed by rotary evaporation and then oil pump vacuum (overnight) to give (*S*,*S*)-**7** as a yellow/brown oil (0.5360 g, 2.788 mmol, 56%).

NMR ($CDCl_3$, δ in ppm): ^{1}H (300 MHz), 7.33-7.26 (m, 2H), 6.28-6.21 (m, 2H), 6.14-6.07 (m, 2H), 4.23 (s, 2H, C**H**NH_2), 1.68 (br s, 4H, NH_2). $^{13}C\{^1H\}$ (75 MHz), 153.2 (s, CH**C**O), 142.0 (s), 110.2 (s), 106.8 (s), 61.4 (s, $CHNH_2$).

Λ-[Co((*S*,*S*)-H_2NCH(2-furyl)CH(2-furyl)NH_2)$_3$]$^{3+}$ 3Cl$^-$ (Λ-(*S*,*S*)-12^{3+} 3Cl$^-$).

A gas-circulating flask[1a] was charged with a solution of $Co(OAc)_2 \cdot 4H_2O$ (0.2960 g, 1.188 mmol) in CH_3OH (75 mL). Activated charcoal (0.1000 g) and (*S*,*S*)-**7** (0.8207 g, 4.270 mmol, 3.594 equiv) were added with vigorous stirring. After 22 h, the mixture was filtered through Celite and aqueous HCl (1.5 mL, 12.0 M) was added. The solvent was removed by rotary evaporation to give an orange/brown solid. Then H_2O (100 mL) was added. The suspension was filtered. The filter cake was washed with H_2O (25 mL) and the remaining solid dried by oil pump vacuum (overnight) to give Λ-(*S*,*S*)-**12**$^{3+}$ 3Cl$^-$ $\cdot 3H_2O$ as an orange/brown solid (0.3942 g, 0.4952 mmol, 42%), mp 161-168 °C (dec, open capillary). Anal. Calcd. for $C_{30}H_{36}Cl_3CoN_6O_6 \cdot 3H_2O$ (795.98): C 45.27, H 5.32, N 10.56; found C 45.28 H 5.02, N 10.40.

NMR (DMSO-d_6, δ in ppm): ^{1}H (500 MHz), 7.73-7.71 (m, 6H), 6.75-6.69 (m, 6H, N**H**H'), 6.48-6.46 (m, 6H), 5.97 (m, 6H, NH**H'**), 4.48-4.41 (m, 6H, C**H**NH_2), 3.35 (br s, 11H, H_2O). ^{13}C{^{1}H} (CD_3OD, 126 MHz), 148.1 (s, CH**C**O), 143.9 (s), 111.3 (s), 110.0 (s), 55.9 (s, $CHNH_2$).

Λ-[Co((*S*,*S*)-H_2NCH(2-furyl)CH(2-furyl)NH_2)$_3$]$^{3+}$ 3BAr_f^- (Λ-(*S*,*S*)-12^{3+} 3BAr_f^-). A beaker was charged with Λ-(*S*,*S*)-**7**$^{3+}$ 3$Cl^-\cdot 3H_2O$ (0.0174 g, 0.0219 mmol), H_2O (15 mL), CH_2Cl_2 (15 mL), and Na^+ BAr_f^- (0.0581 g, 0.0656 mmol, 3.00 equiv). The biphasic mixture was vigorously stirred for 10 min, and then allowed to stand. The lower bright orange phase was separated and allowed to evaporate in the back of a fume hood to give Λ-(*S*,*S*)-**12**$^{3+}$ 3$BAr_f^-\cdot 10H_2O$ as an orange solid (0.0633 g, 0.0186 mmol, 85%), mp 85-92 °C (dec, open capillary). Anal. Calcd. for $C_{126}H_{72}B_3CoF_{72}N_6O_6\cdot 10H_2O$ (3405.40): C 44.44, H 2.72, N 2.47; found C 44.42, H 2.68, N 2.15.

NMR (acetone-d_6, δ in ppm): ^{1}H (300 MHz), BAr_f^- at 7.79 (s, 24H, *o*), 7.68 (s, 12H, *p*); (*S*,*S*)-**7** ligand at 7.67-7.64 (m, 6H), 6.55-6.51 (m, 6H), 6.44-6.39 (m, 6H), 6.37-6.27 (m, 6H, N**H**H'), 5.27-5.15 (m, 6H, NH**H'**), 5.00-4.93 (m, 6H, C**H**NH_2); 3.60 (br s, 25H, H_2O). ^{13}C{^{1}H} (75 MHz), BAr_f^- at 162.5 (q, $^1J_{BC}$ = 49.7 Hz, *i*), 135.4 (s, *o*), 129.7 (m, *m*), 125.2 (q, $^1J_{CF}$ = 271.8 Hz, CF_3), 118.3 (m, *p*); (*S*,*S*)-**7** ligand at 149.7 (s, CH**C**O), 144.6 (s), 111.7 (s), 110.4 (s), 57.2 (s, $CHNH_2$).

Λ-[Co((*S*,*S*)-H_2NCH(2-furyl)CH(2-furyl)NH_2)$_3$]$^{3+}$ Cl^-2BAr_f^- (Λ-(*S*,*S*)-12^{3+} Cl^-2BAr_f^-). A round-bottom flask was charged with Λ-(*S*,*S*)-**12**$^{3+}$ 3$Cl^-\cdot 3H_2O$ (0.1887 g, 0.2371 mmol), CH_2Cl_2 (10 mL), and Na^+ BAr_f^- (0.2311 g, 0.2608 mmol, 1.100 equiv). The mixture was sonicated for 10 min, during which time it became dark brown. The mixture was filtered to remove NaCl. The filtrate was loaded onto a silica gel column (1.5 × 16 cm), which was eluted with CH_2Cl_2/CH_3OH (100:0 to 90:10 v/v). The solvent was removed from the darkly colored fraction and dried by oil pump vacuum (overnight) to

give Λ-(*S*,*S*)-**12**$^{3+}$ $Cl^{-}2BAr_f^{-}\cdot 6H_2O$ as a dark brown/orange solid (0.1758 g, 0.07016 mmol, 37%), mp 185-194 °C (dec, open capillary). Anal. Calcd. for $C_{94}H_{60}B_2ClCoF_{48}N_6O_6\cdot 6H_2O$ (2505.57): C 45.06, H 2.90, N 3.35; found C 45.11, H 2.76, N 3.10.

NMR (CD_2Cl_2, δ in ppm): ^{1}H (500 MHz), BAr_f^{-} at 7.71 (s, 16H, *o*), 7.54 (s, 8H, *p*); (*S*,*S*)-**7** ligand at 7.51-7.50 (m, 6H), 6.40-6.29 (m, 6H, N**H**H'), 6.37-6.35 (m, 6H), 6.34-6.32 (m, 6H), 4.97-4.89 (m, 6H, C**H**NH_2), 4.83-4.73 (m, 6H, NH**H'**); 2.99 (br s, 26H, H_2O). $^{13}C\{^1H\}$ (126 MHz), BAr_f^{-} at 162.2 (q, $^1J_{BC}$ = 49.9 Hz, *i*), 135.2 (s, *o*), 129.1 (m, *m*), 125.0 (q, $^1J_{CF}$ = 272.5 Hz, CF_3), 117.9 (m, *p*); (*S*,*S*)-**7** at 146.7 (s, CH**C**O), 144.9 (s), 111.6 (s), 111.3 (s), 57.1 (s, $CHNH_2$).

(*S*,*S*)-H_2NCH(2-thiophenyl)CH(2-thiophenyl)NH_2 ((*S*,*S*)-8). A round bottom flask was charged with (*R*,*R*)-**2** (2.2149 g, 9.0667 mmol) and DMSO (50 mL). Then 2-thiophenecarboxaldehyde (2.1183 mL, 2.5420 g, 22.667 mmol, 2.4999 equiv) was added with stirring. After 18 h, the mixture was poured into H_2O (150 mL), which was extracted with diethyl ether (3 × 100 mL). The combined extracts were washed with H_2O and dried (Na_2SO_4). The solvent was removed by rotary evaporation and then oil pump vacuum (overnight). The yellow oil was dissolved in THF (50 mL), and aqueous HCl (3.0 mL, 12.0 M) was added with stirring. After 3 h, a white precipitate had formed, which was isolated by filtration and washed with THF. The sample was dissolved in H_2O (50 mL) and aqueous NaOH (6.0 M) was added with stirring until the pH reached 11-12. The mixture was extracted with CH_2Cl_2 (4 × 75 mL) and the combined extracts were dried (Na_2SO_4). The solvent was removed by rotary evaporation and then oil pump vacuum (overnight) to give (*S*,*S*)-**8** as a yellow/brown oil (1.0818 g, 4.8221 mmol, 53%).

NMR ($CDCl_3$, δ in ppm): ^{1}H (300 MHz), 7.21-7.19 (m, 2H), 6.96-6.93 (m, 2H), 6.91-6.88 (m, 2H), 4.44 (s, 2H, C**H**NH_2), 1.83 (br s, 4H, NH_2). $^{13}C\{^1H\}$ (75 MHz), 147.4 (s, CH**C**S), 126.7 (s), 124.1 (s), 123.8 (s), 58.4 (s, $CHNH_2$).

Λ-[Co((*S*,*S*)-H_2NCH(2-thiophenyl)CH(2-thiophenyl)NH_2)$_3$]$^{3+}$ 3Cl$^-$ (Λ-(*S*,*S*)-13^{3+} 3Cl$^-$). A gas-circulating flask[1a] was charged with a solution of $Co(OAc)_2{\cdot}4H_2O$ (0.2960 g, 1.188 mmol) in CH_3OH (75 mL). Activated charcoal (0.1000 g) and (*S*,*S*)-**8** (0.8974 g, 4.000 mmol, 3.367 equiv) were added with vigorous stirring. After 22 h, the mixture was filtered through Celite and aqueous HCl (1.5 mL, 12.0 M) was added. The solvent was removed by rotary evaporation to give a dark yellow solid. Then H_2O (100 mL) was added. The suspension was filtered. The filter cake was washed with H_2O (100 mL) and the remaining solid dried via oil pump vacuum (overnight) to give Λ-(*S*,*S*)-**13**$^{3+}$ 3Cl$^-{\cdot}3H_2O$ as a bronze solid (0.5032 g, 0.5639 mmol, 47%), mp 184-188 °C (dec, open capillary). Anal. Calcd. for $C_{30}H_{36}Cl_3CoN_6S_6{\cdot}3H_2O$ (892.35): C 40.38, H 4.74, N 9.42; found C 40.38 H 4.75, N 8.95.

NMR (DMSO-d_6, δ in ppm): ^{1}H (500 MHz), 7.54-7.48 (m, 6H), 7.46-7.40 (m, 6H), 7.09-7.03 (m, 6H), 6.93-6.84 (m, 6H, N**H**H'), 5.72-5.60 (m, 6H, NH**H'**), 5.17 (s, 6H, C**H**NH_2), 3.39 (br s, 9H, **H**$_2$O). $^{13}C\{^1H\}$ (126 MHz), 137.8 (s, CH**C**S), 128.1 (s), 127.4 (s), 126.8 (s), 57.2 (s, $CHNH_2$).

Λ-[Co((*S*,*S*)-H_2NCH(2-thiophenyl)CH(2-thiophenyl)NH_2)$_3$]$^{3+}$ 3BAr$_f^-$ (Λ-(*S*,*S*)-13^{3+} 3BAr$_f^-$). A beaker was charged with Λ-(*S*,*S*)-**13**$^{3+}$ 3Cl$^-{\cdot}3H_2O$ (0.0518 g, 0.0580 mmol), H_2O (15 mL), CH_2Cl_2 (15 mL), and Na^+ BAr$_f^-$ (0.1543 g, 0.1741 mmol, 3.00 equiv). The biphasic mixture was vigorously stirred for 10 min, and then allowed to stand. The lower bright yellow phase was separated and allowed to evaporate in the back of a fume hood to give Λ-(*S*,*S*)-**13**$^{3+}$ 3BAr$_f^-{\cdot}9H_2O$ as a yellow solid (0.1977 g, 0.05675 mmol, 98%), mp 95 °C (dec, open capillary). Anal. Calcd. for

$C_{126}H_{72}B_3CoF_{72}N_6S_6 \cdot 9H_2O$ (3483.75): C 43.44, H 2.60, N 2.41; found C 43.60, H 2.43, N 2.17.

NMR (acetone-d_6, δ in ppm): ^{1}H (500 MHz), BAr_f^- at 7.81 (s, 24H, *o*), 7.68 (s, 12H, *p*); (*S*,*S*)-**8** ligand at 7.60-7.54 (m, 6H), 7.27-7.21 (m, 6H), 7.07-7.02 (m, 6H), 6.51 (br s, 6H, N**H**H'), 6.32 (br s, 6H, NH**H'**), 5.42 (s, 6H, C**H**NH_2); 3.26 (br s, 22H, H_2O). $^{13}C\{^1H\}$ (126 MHz), BAr_f^- at 162.3 (q, $^1J_{BC}$ = 49.8 Hz, *i*), 135.2 (s, *o*), 129.7 (m, *m*), 125.0 (q, $^1J_{CF}$ = 271.8 Hz, CF_3), 118.1 (m, *p*); (*S*,*S*)-**8** ligand at 137.3 (s, CH**C**S), 129.4 (s), 128.7 (s), 128.1 (s), 59.9 (s, $CHNH_2$).

Λ-[Co((*S*,*S*)-H_2NCH(2-thiophenyl)CH(2-thiophenyl)NH_2)$_3$]$^{3+}$ 3BF_4^- (Λ-(*S*,*S*)-13^{3+} 3BF_4^-). A vial was charged with a solution of Λ-(*S*,*S*)-**13**$^{3+}$ 3$Cl^-\cdot 3H_2O$ (0.0346 g, 0.0388 mmol) in CH_3OH (5 mL) and Ag^+ BF_4^- (0.0227 g, 0.117 mmol, 3.00 equiv) was added. The mixture was sonicated for 5 min and filtered through Celite to remove AgCl. The solvent was removed from the filtrate by rotary evaporation. The residue was dried by oil pump vacuum (overnight) to give Λ-(*S*,*S*)-**13**$^{3+}$ 3$BF_4^-\cdot 2H_2O$ as a bright yellow solid (0.0392 g, 0.0381 mmol, 98%), mp 169-172 °C (dec, open capillary). Anal. Calcd. for $C_{30}H_{36}B_3CoF_{12}N_6S_6 \cdot 2H_2O$ (1028.39): C 35.04, H 3.92, N 8.17; found C 35.30, H 4.05, N 7.95.

NMR (acetone-d_6, δ in ppm): ^{1}H (500 MHz), 7.60-7.48 (m, 6H), 7.42-7.31 (m, 6H), 7.07-6.97 (m, 6H), 5.97 (br s, 12H, NH_2), 5.37 (s, 6H, C**H**NH_2) 2.98 (br s, 10H, H_2O). $^{13}C\{^1H\}$ (126 MHz), 137.8 (s, CH**C**S), 129.9 (s), 128.4 (s), 128.1 (s), 59.7 (s, $CHNH_2$).

Λ-[Co((*S*,*S*)-H_2NCH(2-thiophenyl)CH(2-thiophenyl)NH_2)$_3$]$^{3+}$ 3$B(C_6F_5)_4^-$ (Λ-(*S*,*S*)-13^{3+} 3$B(C_6F_5)_4^-$). A beaker was charged with Λ-(*S*,*S*)-**13**$^{3+}$ 3$Cl^-\cdot 3H_2O$ (0.0454 g, 0.0509 mmol), H_2O (15 mL), CH_2Cl_2 (15 mL), and K^+ $B(C_6F_5)_4^-$ (0.1094 g, 0.1523 mmol, 3.00 equiv). The biphasic mixture was vigorously stirred for 10 min, and then

allowed to stand. The lower bright yellow phase was separated and allowed to evaporate in the back of a fume hood to give Λ-(*S*,*S*)-**13**$^{3+}$ 3B$(C_6F_5)_4^-$·9H_2O a yellow solid (0.1314 g, 0.0448 mmol, 88%), mp 268-275 °C (dec, open capillary). Anal. Calcd. for $C_{102}H_{36}B_3CoF_{60}N_6S_6$·9$H_2O$ (2931.22): C 41.80, H 1.86, N 2.87; found C 41.88, H 1.92, N 2.94.

NMR (acetone-d_6, δ in ppm): ^{1}H (500 MHz), 7.59-7.55 (m, 6H), 7.25-7.21 (m, 6H), 7.07-7.03 (m, 6H), 6.51 (br s, 6H, N**H**H'), 6.33 (br s, 6H, NH**H'**), 5.47-5.37 (s, 6H, C**H**NH_2), 3.20 (br s, 20H, H_2O). ^{13}C{^{1}H} (126 MHz), B$(C_6F_5)_4^-$ at 148.6 (d, $^1J_{CF}$ = 239.0 Hz, *o*), 138.6 (d, $^1J_{CF}$ = 245.8 Hz, *p*), 136.5 (d, $^1J_{CF}$ = 247.4 Hz, *m*), 125.5-123.5 (m, *i*); (*S*,*S*)-**8** ligand at 137.3 (s, CH**C**S), 129.3 (s), 128.6 (s), 128.0 (s), 59.8 (s, $CHNH_2$).

Λ-[Co((*S*,*S*)-H_2NCH(cyclohexyl)CH(cyclohexyl)NH_2)$_3$]$^{3+}$ 2Cl$^-$BAr$_f^-$ (Λ-(*S*,*S*)-14^{3+} 2Cl$^-$BAr$_f^-$). A gas-circulating flask[1a] was charged with a solution of Co$(OAc)_2$·4H_2O (0.2061 g, 0.8274 mmol) in CH_3OH (50 mL). Activated charcoal (0.1000 g) and (*S*,*S*)-**9**[2b] (0.6127 g, 2.731 mmol, 3.300 equiv) with vigorous stirring. After 24 h, the mixture was filtered through Celite and aqueous HCl (1.0 mL, 12.1 M) was added. The solvent was removed by rotary evaporation and H_2O (100 mL) was added. The suspension was filtered. The filter cake was washed with H_2O (100 mL) and dried by oil pump vacuum (17 h) to give crude Λ-(*S*,*S*)-**14**$^{3+}$ 3Cl$^-$ as a brown/green solid (0.2345 g, 0.2627 mmol assuming a pure product). Then CH_2Cl_2 (10 mL) and Na$^+$ BAr$_f^-$ (0.2328 g, 0.2627 mmol, 1.000 equiv) were added. The mixture was sonicated for 10 min, during which time the solvent became dark yellow/brown. The mixture was filtered to remove NaCl. The filtrate was loaded onto a silica gel column (1.5 × 16 cm), which was eluted with CH_2Cl_2/CH_3OH (100:0 to 97:3 v/v). The solvent was removed from the main orange band by rotary evaporation and oil pump vacuum (overnight) to give Λ-(*S*,*S*)-**14**$^{3+}$ 2Cl$^-$ BAr$_f^-$·0.5H_2O as a yellow/orange solid (0.1426 g, 0.08512 mmol, 10%), mp 153-160 °C

(dec, open capillary). Anal. Calcd. for $C_{74}H_{96}BCl_2CoF_{24}N_6 \cdot 0.5H_2O$ (1675.24): C 53.06, H 5.84, N 5.02; found C 53.33, H 6.03, N 4.72.

NMR (acetone-d_6, δ in ppm): ^{1}H (500 MHz), BAr_f^- at 7.79 (s, 8H, *o*), 7.68 (s, 4H, *p*); (*S*,*S*)-**9** ligand at 7.60 (br s, 6H, N**H**H'), 3.35 (br s, 6H, NH**H'**), 3.03 (s, 6H, C**H**NH_2), 2.90 1.92-0.98 (m, 66H, cyclohexyl); (br s, 4H, H_2O); $^{13}C\{^1H\}$ (126 MHz), BAr_f^- at 162.7 (q, $^1J_{BC}$ = 49.8 Hz, *i*), 135.6 (s, *o*), 130.1 (m, *m*), 125.5 (q, $^1J_{CF}$ = 271.7 Hz, CF_3), 118.5 (m, *p*); (*S*,*S*)-**9** ligand at 63.4 (s, $CHNH_2$), 38.7 (s), 30.9 (s), 27.1 (s), 26.7 (2 × intensity), 24.7 (s).

Λ-[Co((*S*,*S*)-H_2NCH(cyclohexyl)CH(cyclohexyl)NH_2)$_3$]$^{3+}$ 3BAr_f^- (Λ-(*S*,*S*)-14^{3+} 3BAr_f^-). A beaker was charged with Λ-(*S*,*S*)-**14**$^{3+}$ 2$Cl^-BAr_f^- \cdot 0.5H_2O$ (0.0136 g, 0.00812 mmol), H_2O (15 mL), CH_2Cl_2 (15 mL), and Na^+ BAr_f^- (0.0144 g, 0.0162 mmol, 2.00 equiv). The biphasic mixture was vigorously stirred for 10 min, and then allowed to stand. The lower bright yellow phase was separated and the solvent evaporated in the back of a fume hood to give Λ-(*S*,*S*)-**14**$^{3+}$ 3$BAr_f^- \cdot 5H_2O$ as a bright orange solid (0.0262 g, 0.00768 mmol, 95%), mp 108-117 °C (dec, open capillary). Anal. Calcd. for $C_{138}H_{120}B_3CoF_{72}N_6 \cdot 5H_2O$ (3411.84): C 48.58, H 3.84, N 2.46; found C 48.60, H 3.85, N 2.45.

NMR (acetone-d_6, δ in ppm): ^{1}H (500 MHz), BAr_f^- at 7.78 (s, 24H, *o*), 7.68 (s, 12H, *p*); (*S*,*S*)-**9** ligand at 5.46 (br s, 6H, N**H**H'), 4.18 (br s, 6H, NH**H'**), 3.44 (s, 6H, C**H**NH_2), 1.89-0.81 (m, 66H, cyclohexyl); 2.87 (br s, 26H, H_2O); $^{13}C\{^1H\}$ (126 MHz), BAr_f^- at 162.7 (q, $^1J_{BC}$ = 50.7 Hz, *i*), 135.6 (s, *o*), 130.1 (m, *m*), 125.5 (q, $^1J_{CF}$ = 271.0 Hz, CF_3), 118.5 (m, *p*); (*S*,*S*)-**9** ligand at 64.6 (s, $CHNH_2$), 38.2 (s), 26.6 (s), 26.5 (s), 26.2 (s), 24.8 (s).

Δ-[Co((*S*,*S*)-H_2NCH(4-C_6H_4CN)CH(4-C_6H_4CN)NH_2)$_3$]$^{3+}$ 3BAr_f^- (Δ-(*S*,*S*)-15^{3+} 3BAr_f^-). ***Caution!*** *This procedure involves perchlorate salts that are potentially*

explosive. Although it has been carried out repeatedly without mishap, special care and protection are always required when working with perchlorate salts or $HClO_4$ solutions. A gas-circulating flask[1a] was charged with a solution of $Co(ClO_4)_2 \cdot 6H_2O$ (0.1782 g, 0.4870 mmol) in CH_3OH (50 mL). Activated charcoal (0.1000 g) and (*S*,*S*)-**10**[2a] (0.4225 g, 1.611 mmol, 3.308 equiv) were added with vigorous stirring. After 30 h, the mixture was filtered through Celite, and $HClO_4$ (2.0 mL, 35% in H_2O) was added. The solution was added onto a Dowex 50WX2 (200-400 mesh) cation exchange column (2.0 × 25 cm), which was washed with H_2O/CH_3OH (1:1 (v/v), 100 mL) and eluted with increasing concentrations of aqueous HCl in CH_3OH (CH_3OH/HCl 9:1 v/v (100 mL), 8:2 v/v (100 mL), 7:3 v/v (100 mL), 6:4 v/v until product elution). An orange band was collected. The solvents were removed by rotary evaporation (60 °C bath; base trap to scavenge HCl) to give crude Δ-(*S*,*S*)-**15**$^{3+}$ $3Cl^-$ (0.1172 g, 0.1165 mmol assuming a pure product). This was suspended in CH_2Cl_2/CH_3OH (1:1 v/v, 10 mL) and Na^+ BAr_f^- (0.1032 g, 0.1165 mmol, 1.000 equiv) was added. The mixture was sonicated for 5 min. The solvent was removed by rotary evaporation. Acetone (10 mL) was added and the green/yellow mixture was filtered to remove NaCl. The solvent was removed from the filtrate by rotary evaporation, dissolved in a minimum of CH_2Cl_2, and loaded onto a silica gel column (1.5 × 15 cm) that was eluted with CH_2Cl_2/CH_3OH (100:0 to 95:5 v/v). The solvent was removed from the main yellow band by rotary evaporation and oil pump vacuum (overnight) to give Δ-(*S*,*S*)-**15**$^{3+}$ $3BAr_f^- \cdot 13H_2O$ as a bright yellow solid (0.0571 g, 0.0156 mmol, 3%), mp 117-121 °C (dec, open capillary). Anal. Calcd. for $C_{144}H_{78}B_3CoF_{72}N_{12} \cdot 13H_2O$ (3669.74): C 47.13, H 2.86, N 4.58; found C 47.16, H 2.92, N 4.10. IR (powder film, cm^{-1}): 3312 (m, ν_{NH}), 2237 (m, ν_{CN}), 1613 (m, δ_{NH}), 1354 (s, $\nu_{Ar\text{-}CF3}$), 1275 (vs, ν_{CF}), 1119 (vs, δ_{CCN}).

NMR (acetone-d_6, δ in ppm): ^1H (500 MHz), BAr_f^- at 7.79 (s, 24H, *o*), 7.68 (s, 12H, *p*); (*S,S*)-**10** ligand at 7.80 (d, $^3J_{HH}$ = 8.5 Hz, 12H), 7.70 (d, $^3J_{HH}$ = 8.5 Hz, 12H),

6.61-6.54 (m, 6H, N**H**H'), 5.51-5.44 (m, 6H, NH**H'**), 5.08-4.99 (m, 6H, C**H**NH_2); 3.31 (br s, 30H, H_2O). $^{13}C\{^1H\}$ (126 MHz), BAr_f^- at 162.6 (q, $^1J_{BC}$ = 49.7 Hz, *i*), 135.5 (s, *o*), 130.0 (m, *m*), 125.4 (q, $^1J_{CF}$ = 271.7 Hz, CF_3), 118.5 (m, *p*); (*S,S*)-**10** ligand at 142.5 (s), 134.0 (s), 129.7 (s), 118.6 (s), 114.0 (s), 65.9 (s, $CHNH_2$).

(*S*,*S*)-$H_2NCH(3,5\text{-}C_5H_3Ph_2)CH(3,5\text{-}C_5H_3Ph_2)NH_2$ ((*S*,*S*)-11). A round bottom flask was charged with (*R*,*R*)-**2** (0.5825 g, 2.384 mmol) and DMSO (15 mL). Then [1,1':3,1"-terphenyl]-5'-carbaldehyde, O=CH(3,5-C_5H_3Ph),[14] (1.5403 g, 5.963 mmol, 2.501 equiv) was added with stirring. After 24 h, the mixture was poured into H_2O (50 mL), which was extracted with diethyl ether (3 × 100 mL). The combined extracts were washed with H_2O and dried (Na_2SO_4). The solvent was removed by rotary evaporation and then oil pump vacuum (overnight). The yellow oil was dissolved in THF (15 mL), and aqueous HCl (0.87 mL, 12.0 M) was added with stirring. After 24 h, diethyl ether (150 mL) was added to produce a gelatinous white precipitate. The sample was dissolved in H_2O (50 mL) and aqueous NaOH (6.0 M) was added with stirring until the pH reached 11-12. The mixture was extracted with CH_2Cl_2 (3 × 75 mL) and the combined extracts were dried (Na_2SO_4). The solvent was removed by rotary evaporation and then oil pump vacuum (overnight) to give (*S*,*S*)-**11** as a yellow solid (0.3597 g, 0.6962 mmol, 29%) mp 75-81 °C (dec, open capillary). Anal. Calcd. for $C_{38}H_{32}N_2 \cdot 0.5H_2O$ (525.70): C 86.82, H 6.33, N 5.33; found C 86.53, H 6.38, N 5.28.

NMR ($CDCl_3$, δ in ppm): ^1H (500 MHz), 7.73 (s, 2H), 7.64 (d, $^3J_{HH}$ = 7.4 Hz, 8H), 7.56 (s, 4H), 7.48 (t, $^3J_{HH}$ = 7.4 Hz, 8H), 7.40 (t, $^3J_{HH}$ = 7.1 Hz, 4H), 4.35 (s, 2H, C**H**NH_2), 1.89 (br s, 5H, N$\mathbf{H}_2$/$\mathbf{H}_2$O). $^{13}C\{^1H\}$ (126 MHz), 144.5 (s), 141.8 (s), 141.2 (s), 128.8 (s), 127.5 (s), 127.4 (s), 125.1 (2 × s), 62.6 (s, $CHNH_2$).

Λ-(*S*,*S*)-1^{3+} $2C_6H_5CO_2^-BAr_f^-$. A vial was charged with a solution of Λ-(*S*,*S*)-$\mathbf{1}^{3+}$ $2Cl^-BAr_f^- \cdot 2H_2O$ (0.0500 g, 0.0300 mmol) in CH_2Cl_2 (5 mL). Then Ag^+ $C_6H_5CO_2^-$

(0.0137 g, 0.0600 mmol, 2.00 equiv) was added. The mixture was sonicated for 5 min and filtered through Celite to remove AgCl. The solvent was removed from the filtrate by rotary evaporation. The residue was dried by oil pump vacuum (overnight) to give Λ-(*S*,*S*)-**1**$^{3+}$ $2C_6H_5CO_2^-BAr_f^-\cdot 2H_2O$ as an orange solid (0.0497 g, 0.0271 mmol, 90%), mp 103-111 °C (dec, open capillary). Anal. Calcd. for $C_{88}H_{70}BCoF_{24}N_6O_4\cdot 2H_2O$ (1837.30): C 57.33, H 4.06, N 4.57; found C 57.22, H 4.05, N 4.30.

NMR (acetone-d_6, δ in ppm): ^{1}H (400 MHz), BAr_f^- at 7.79 (s, 8H, *o*), 7.67 (s, 4H, *p*); $C_6H_5CO_2^-$ at 8.08 (apparent dd, $^3J_{HH}$ = 6.9, $^2J_{HH}$ = 1.6 Hz, 4H, *o*-Ph), 7.45 (apparent tt, $^3J_{HH}$ = 7.3, $^2J_{HH}$ = 2.3 Hz, 2H, *p*-Ph), 7.39 (apparent tt, $^3J_{HH}$ = 7.0 Hz, $^2J_{HH}$ = 1.1, 4H, *m*-Ph); (*S*,*S*)-dpen ligand at 8.94 (br s, 6H, N**H**H'), 7.57-7.53 (m, 12H, *o*-Ph), 7.28-7.23 (m, 18H, *m*-, *p*-Ph), 5.12 (2 × br s, 12H, NH**H'**, C**H**NH_2); 2.84 (br s, 10H, H_2O); $^{13}C\{^1H\}$ (100 MHz), BAr_f^- at 162.6 (q, $^1J_{BC}$ = 50.2 Hz, *i*), 135.5 (s, *o*), 130.0 (m, *m*), 125.4 (q, $^1J_{CF}$ = 271.8 Hz, CF_3), 118.4 (s, *p*); $C_6H_5CO_2^-$ and (*S*,*S*)-dpen ligand at 174.1 (s, C=O), 137.9 (s), 131.1 (s), 129.7 (s), 129.63 (2 × s), 129.60 (s), 128.4 (s), 129.5 (s), 63.5 (s, $CHNH_2$).

Λ-(*S*,*S*)-1^{3+} 2$CF_3CO_2^-BAr_f^-$. A vial was charged with a solution of Λ-(*S*,*S*)-**1**$^{3+}$ $2Cl^-BAr_f^-\cdot 2H_2O$ (0.0791 g, 0.0475 mmol) in CH_2Cl_2 (5 mL). Then Ag^+ $CF_3CO_2^-$ (0.0210 g, 0.0951 mmol, 2.00 equiv) was added. The mixture was sonicated for 5 min and filtered through Celite to remove AgCl. The solvent was removed from the filtrate by rotary evaporation. The residue was dried by oil pump vacuum (overnight) to give Λ-(*S*,*S*)-**1**$^{3+}$ $2CF_3CO_2^-BAr_f^-\cdot 2H_2O$ as an orange solid (0.0713 g, 0.0392 mmol, 83%), mp 107-120 °C (dec, open capillary). Anal. Calcd. for $C_{78}H_{60}BCoF_{30}N_6O_4\cdot 2H_2O$ (1821.10): C 51.44, H 3.54, N 4.61; found C 51.17, H 3.46, N 4.43.

NMR (acetone-d_6, δ in ppm): ^{1}H (400 MHz), BAr_f^- at 7.79 (s, 8H, *o*), 7.67 (s, 4H, *p*); (*S*,*S*)-dpen ligand at 7.51-7.44 (m, 18H, *o*-Ph, N**H**H'), 7.32-7.25 (m, 18H, *m*-, *p*-Ph),

5.54 (br s, 6H, NH**H'**), 5.17-5.11 (m, 6H, C**H**NH_2); 2.84 (br s, 16H, H_2O); $^{13}C\{^1H\}$ (100 MHz), BAr_f^- at 162.6 (q, $^1J_{BC}$ = 49.7 Hz, *i*), 135.5 (s, *o*), 130.0 (m, *m*), 125.4 (q, $^1J_{CF}$ = 271.8 Hz, CF_3), 118.4 (s, *p*); $CF_3CO_2^-$ at 161.8 (s, C=O), 125.4 (q, $^1J_{CF}$ = 271.8 Hz, CF_3); (*S*,*S*)-dpen ligand at 137.1 (s, *i*-Ph), 129.9 (s, *p*-Ph), 129.8 (s), 129.5 (s), 63.5 (s, $CHNH_2$).

Λ-(*S*,*S*)-$\mathbf{1}^{3+}$ $\mathbf{SO_4^{2-}BAr_f^-}$. A vial was charged with a solution of Λ-(*S*,*S*)-$\mathbf{1}^{3+}$ $2Cl^-$ $BAr_f^-\cdot 2H_2O$ (0.0500 g, 0.0300 mmol) in CH_2Cl_2 (5 mL). Then $2Ag^+$ SO_4^{2-} (0.0094 g, 0.0301 mmol, 1.00 equiv) was added. The mixture was sonicated for 5 min and filtered through Celite to remove AgCl. The solvent was removed from the filtrate by rotary evaporation. The residue was dried by oil pump vacuum (overnight) to give Λ-(*S*,*S*)-$\mathbf{1}^{3+}$ $SO_4^{2-}BAr_f^-\cdot H_2O$ as an orange solid (0.0423 g, 0.0253 mmol, 84%), mp 119-125 °C (dec, open capillary). Anal. Calcd. for $C_{74}H_{60}BCoF_{24}N_6O_4S\cdot H_2O$ (1673.11): C 53.12, H 3.74, N 5.02; found C 53.55, H 3.71, N 4.77.

NMR (acetone-d_6, δ in ppm): ^1H (400 MHz), BAr_f^- at 7.79 (s, 8H, *o*), 7.67 (s, 4H, *p*); (*S*,*S*)-dpen ligand at 8.28 (br s, 6H, N**H**H'), 7.51-7.47 (m, 12H, *o*-Ph), 7.34-7.30 (m, 18H, *m*-, *p*-Ph), 5.19 (br s, 6H, NH**H'**), 5.14-5.08 (m, 6H, C**H**NH_2); 2.85 (br s, 7H, H_2O); $^{13}C\{^1H\}$ (100 MHz), BAr_f^- at 162.6 (q, $^1J_{BC}$ = 49.9 Hz, *i*), 135.5 (s, *o*), 130.0 (m, *m*), 125.4 (q, $^1J_{CF}$ = 271.7 Hz, CF_3), 118.4 (s, *p*); (*S*,*S*)-dpen ligand at 137.3 (s, *i*-Ph), 130.0 (s, *p*-Ph), 129.9 (s), 129.4 (s), 63.4 (s, $CHNH_2$).

Λ-(*S*,*S*)-$\mathbf{1}^{3+}$ $\mathbf{3SbF_6^-}$. A vial was charged with a solution of Λ-(*S*,*S*)-$\mathbf{1}^{3+}$ $3Cl^-\cdot 3H_2O$ (0.0190 g, 0.0222 mmol) in CH_3OH (5 mL). Then Ag^+ SbF_6^- (0.0229 g, 0.0666 mmol, 3.00 equiv) was added. The mixture was sonicated for 5 min and filtered through Celite to remove AgCl. The solvent was removed from the filtrate by rotary evaporation. The residue was dried by oil pump vacuum (overnight) to give Λ-(*S*,*S*)-$\mathbf{1}^{3+}$ $3SbF_6^-\cdot 5H_2O$ as an orange solid (0.0314 g, 0.0210 mmol, 95%), mp 191-210 °C (dec, open capillary).

Anal. Calcd. For $C_{42}H_{48}CoF_{18}N_6Sb_3 \cdot 5H_2O$ (1493.15): C 33.79, H 3.92, N 5.63; found C 33.67, H 3.92, N 5.44.

NMR (acetone-d_6, δ in ppm): ^{1}H (400 MHz), 7.61-7.56 (m, 12H, *o*-Ph), 7.35-7.26 (m, 18H, *m*-, *p*-Ph), 6.22 (br s, 6H, N**H**H'), 5.78 (br s, 6H, NH**H'**), 5.21-5.10 (m, 6H, C**H**NH_2), 3.00 (br s, 13H, H_2O); ^{13}C{^{1}H} (100 MHz), 137.4 (s, *i*-Ph), 129.3 (s, *p*-Ph), 129.0 (2 × s), 63.4 (s, $CHNH_2$).

Λ-(*S*,*S*)-1^{3+} 2DS$^-$BAr$_f^-$. A beaker was charged with Λ-(*S*,*S*)-**1**$^{3+}$ 2Cl$^-$BAr$_f^-$ $\cdot 2H_2O$ (0.0500 g, 0.0300 mmol), H_2O (5 mL), CH_2Cl_2 (5 mL), and SDS (0.0173 g, 0.0600 mmol, 2.00 equiv). The biphasic mixture was vigorously stirred for 10 min, and then allowed to stand. The lower bright orange phase was separated and allowed to evaporate in the back of a fume hood to give Λ-(*S*,*S*)-**1**$^{3+}$ 2DS$^-$BAr$_f^-\cdot 2H_2O$ as an orange solid (0.0627 g, 0.0295 mmol, 98%), mp 144-152 °C (dec, open capillary). Anal. Calcd. for $C_{98}H_{110}BCoF_{24}N_6O_8S_2 \cdot 2H_2O$ (2125.85): C 55.37, H 5.41, N 3.80; found C 55.20, H 5.24, N 3.80.

NMR (CD_3CN, δ in ppm): ^{1}H (400 MHz), BAr$_f^-$ at 7.70 (s, 8H, *o*), 7.67 (s, 4H, *p*); (*S*,*S*)-dpen ligand at 7.51-7.46 (m, 12H, *o*-Ph), 7.39-7.34 (m, 18H, *m*-, *p*-Ph), 6.45 (br s, 6H, N**H**H'), 4.67-4.62 (m, 6H, C**H**NH_2), 4.43 (br s, 6H, NH**H'**); 2.16 (br s, 9H, H_2O); DS$^-$ at 3.84 (t, $^3J_{HH}$ = 6.8 Hz, 4H, $CH_2SO_3^-$), 1.52 (quint, $^3J_{HH}$ = 6.5 Hz, 4H, C**H**$_2CH_2SO_3^-$), 1.32-1.24 (m, 36H, (C**H**$_2)_9CH_2CH_2SO_3^-$), 0.88 (t, $^3J_{HH}$ = 7.0 Hz, 6H, CH_3); ^{13}C{^{1}H} (100 MHz), BAr$_f^-$ at 162.6 (q, $^1J_{BC}$ = 49.8 Hz, *i*), 135.6 (s, *o*), 130.0 (m, *m*), 125.4 (q, $^1J_{CF}$ = 271.7 Hz, CF_3), 118.5 (s, *p*); (*S*,*S*)-dpen ligand at 135.8 (s, *i*-Ph), 130.6 (s, *p*-Ph), 130.0 (s), 129.7 (s), 63.9 (s, $CHNH_2$); DS$^-$ at 69.2, 32.6, 30.41, 30.37 (2 × intensity), 30.35, 30.32, 30.1, 30.0, 26.5, 23.4, 14.3 (11 × s).

Λ-(*S*,*S*)-1^{3+} 3DS$^-$. A beaker was charged with Λ-(*S*,*S*)-**1**$^{3+}$ $3Cl \cdot 3H_2O$ (0.0250 g, 0.0292 mmol), H_2O (5 mL), CH_2Cl_2 (5 mL), and SDS (0.0252 g, 0.0874 mmol, 2.99

equiv). The biphasic mixture was vigorously stirred for 10 min and allowed to stand. The lower bright orange phase was separated and allowed to evaporate in the back of a fume hood to give Λ-(*S*,*S*)-**1**$^{3+}$ 3DS^{-}·2H_2O as an orange solid (0.0426 g, 0.0279 mmol, 95%), mp 162-173 °C (dec, open capillary). Anal. Calcd. for $C_{78}H_{123}CoN_6O_{12}S_3$·2$H_2O$ (1528.02): C 61.31, H 8.38, N 5.50; found C 61.59, H 8.45, N 5.44.

NMR (CD_3CN, δ in ppm): ^{1}H (400 MHz), (*S*,*S*)-dpen ligand at 7.54-7.48 (m, 12H, *o*-Ph), 7.36-7.30 (m, 18H, *m*-, *p*-Ph), 6.42 (br s, 6H, N**H**H'), 4.69-4.54 (m, 12H, C**H**NH_2, NH**H'**); 2.16 (br s, 28H, H_2O); DS$^-$ at 3.80-3.74 (m, 6H, $CH_2SO_3^-$), 1.49 (quint, $^3J_{HH}$ = 6.7 Hz, 6H, C**H**$_2CH_2SO_3^-$), 1.32-1.24 (m, 54H, (C**H**$_2)_9CH_2CH_2SO_3^-$), 0.88 (t, $^3J_{HH}$ = 7.0 Hz, 9H, CH_3); ^{13}C{^{1}H} (100 MHz), (*S*,*S*)-dpen ligand at 136.1 (s, *i*-Ph), 130.3 (s, *p*-Ph), 129.9 (s), 129.8 (s), 64.1 (s, $CHNH_2$); DS$^-$ at 68.6, 32.6, 30.42, 30.38, 30.37, 30.34, 30.13, 30.10 (2 × intensity), 26.5, 23.4, 14.4 (11 × s).

Λ-(*S*,*S*)-1^{3+} Cl$^-$BF$_4^-$BAr$_f^-$. A vial was charged with a solution of Λ-(*S*,*S*)-**1**$^{3+}$ 2Cl$^-$BAr$_f^-$·2H_2O (0.1164 g, 0.06987 mmol) in CH_2Cl_2 (5 mL). Then Ag^+ BF_4^- (0.0136 g, 0.0699 mmol, 1.00 equiv) was added. The mixture was sonicated for 5 min and filtered through Celite to remove AgCl. The solvent was removed from the filtrate by rotary evaporation. The residue was dried by oil pump vacuum (overnight) to give Λ-(*S*,*S*)-**1**$^{3+}$ Cl$^-$BF$_4^-$BAr$_f^-$·3H_2O as a bright orange solid (0.1201 g, 0.06921 mmol, 99%), mp 97-125 °C (dec, open capillary). Anal. Calcd. for $C_{74}H_{60}B_2ClCoF_{28}N_6$·3$H_2O$ (1735.34): C 51.22, H 3.83, N 4.84; found C 51.20, H 3.71, N 4.51.

NMR (acetone-d_6, δ in ppm): ^{1}H (500 MHz), BAr$_f^-$ at 7.80 (s, 8H, *o*), 7.68 (s, 4H, *p*); (*S*,*S*)-dpen ligand at 7.52-7.49 (m, 12H, *o*-Ph), 7.34-7.30 (m, 18H, *m*/*p*-Ph), 5.57 (br s, 6H, N**H**H'), 5.15 (s, 6H, C**H**NH_2), 2.99 (br s, 13H, NH**H'**/**H**$_2$O); ^{13}C{^{1}H} (126 MHz), BAr$_f^-$ at 162.5 (q, $^1J_{BC}$ = 50.1 Hz, *i*), 135.5 (s, *o*), 129.9 (m, *m*), 125.3 (q, $^1J_{CF}$ = 271.9

Hz, CF_3), 118.3 (s, *p*); (*S*,*S*)-dpen ligand at 136.6 (s, *i*-Ph), 130.1 (s, *p*-Ph), 130.0 (s), 129.5 (s), 63.5 (s, $CHNH_2$); ^{19}F (470 MHz), BAr_f^- at –60.8 (s, 24F); BF_4^- at –162.0 (s, 4F).

Λ-(*S*,*S*)-$\mathbf{1}^{3+}$ $\mathbf{Cl^-PF_6^-BAr_f^-}$. A vial was charged with a solution of Λ-(*S*,*S*)-$\mathbf{1}^{3+}$ $2Cl^-BAr_f^-\cdot 2H_2O$ (0.0422 g, 0.0253 mmol) in CH_2Cl_2 (5 mL). Then Ag^+ PF_6^- (0.0064 g, 0.025 mmol, 1.0 equiv) was added. The mixture was sonicated for 5 min and filtered through Celite to remove AgCl. The solvent was removed from the filtrate by rotary evaporation. The residue was dried by oil pump vacuum (overnight) to give Λ-(*S*,*S*)-$\mathbf{1}^{3+}$ $Cl^-PF_6^-BAr_f^-\cdot 4H_2O$ as a bright orange solid (0.0405 g, 0.0224 mmol, 88%), mp 75-86 °C (dec, open capillary). Anal. Calcd. for $C_{74}H_{60}BClCoF_{30}N_6P\cdot 4H_2O$ (1811.52): C 49.06, H 3.78, N 4.64; found C 49.27, H 3.65, N 4.38.

NMR (acetone-d_6, δ in ppm): ^1H (500 MHz), BAr_f^- at 7.79 (s, 8H, *o*), 7.67 (s, 4H, *p*); (*S*,*S*)-dpen ligand at 7.51-7.46 (m, 12H, *o*-Ph), 7.37-7.30 (m, 18H, *m*/*p*-Ph), 5.68 (br s, 6H, N**H**H'), 5.18 (s, 6H, C**H**NH_2), 2.90 (br s, 24H, NH**H'**/$\mathbf{H_2}$O); $^{13}C\{^1H\}$ (126 MHz), BAr_f^- at 162.6 (q, $^1J_{BC}$ = 50.0 Hz, *i*), 135.6 (s, *o*), 130.0 (m, *m*), 125.3 (q, $^1J_{CF}$ = 271.9 Hz, CF_3), 118.5 (s, *p*); (*S*,*S*)-dpen ligand at 136.6 (s, *i*-Ph), 130.1 (s, *p*-Ph), 130.0 (s), 129.5 (s), 63.7 (s, $CHNH_2$); ^{19}F (470 MHz), BAr_f^- at –60.7 (s, 24F); PF_6^- at –69.0 (d, $^1J_{FP}$ = 709.1 Hz, 6F).

[Pt((*S*,*S*)-dpen)$_2$]$^{2+}$ $\mathbf{2Cl^-}$. A round-bottom flask was charged with $PtCl_4$ (0.1064 g, 0.3158 mmol), (*S*,*S*)-dpen (0.2213 g, 1.042 mmol, 3.3 equiv), and *n*-propanol (30 mL) with stirring. The mixture was refluxed (18 h). The solvent was removed from the yellow solution by rotary evaporation. Then, HCl (25 mL, 2.0 M) was added to remove excess water-soluble reactants, the protonated diamine, and $PtCl_4$. The suspension was filtered to collect the product, which was washed with HCl (25 mL, 2.0 M). The filter cake was dissolved in CH_3OH. The solvent was removed by rotary evaporation and dried by oil pump vacuum (overnight) to give $[Pt((S,S)\text{-dpen})_2]^{2+}$ $2Cl^-\cdot 2.5H_2O$ as a pale yellow solid

(0.1794 g, 0.2439 mmol, 77%), mp 340 °C (dec, open capillary). Anal. Calcd. for $C_{28}H_{32}Cl_2N_4Pt \cdot 2.5H_2O$ (735.61): C 45.72, H 5.07, N 7.62; found C 45.83, H 5.35, N 7.60.

NMR (DMSO-d_6, δ in ppm): ^{1}H (500 MHz), 7.37 (d, $^3J_{HH}$ = 7.3 Hz, 8H, *o*-Ph), 7.32-7.20 (m, 12H, *m*/*p*-Ph), 6.85-6.75 (m, 4H, N**H**H'), 5.89 (br s, 4H, NH**H'**), 4.21-4.14 (m, 4H, C**H**NH_2), 3.34 (br s, 12H, H_2O); $^{13}C\{^1H\}$ (126 MHz), 137.0 (s, *i*-Ph), 128.53 (s) 128.48 (s, *p*-Ph), 128.1 (s), 65.7 (s, $CHNH_2$).

$[Pt((R,R)\text{-dpen})_2]^{2+}$ $2Cl^-$. $PtCl_4$ (0.0983 g, 0.292 mmol), (*R*,*R*)-dpen (0.2316 g, 1.091 mmol, 3.7 equiv), and *n*-propanol (30 mL) were combined in a procedure analogous to that for $[Pt((S,S)\text{-dpen})_2]^{2+}$ $2Cl^-$. An identical workup gave $[Pt((R,R)\text{-dpen})_2]^{2+}$ $2Cl^- \cdot 2.5H_2O$ as a pale yellow solid (0.1665 g, 0.2263 mmol, 78%), mp 340 °C (dec, open capillary). Anal. Calcd. for $C_{28}H_{32}Cl_2N_4Pt \cdot 2.5H_2O$ (735.61): C 45.72, H 5.07, N 7.62; found C 45.90, H 5.41, N 7.29. The ^{1}H and $^{13}C\{^1H\}$ NMR spectra were identical to those of the enantiomer.

$[Pt((S,S)\text{-dpen})_2]^{2+}$ $2BAr_f^-$. A beaker was charged with $[Pt((S,S)\text{-dpen})_2]^{2+}$ $2Cl^- \cdot 2.5H_2O$ (0.0073 g, 0.0099 mmol), H_2O (10 mL), CH_2Cl_2 (10 mL), and Na^+ BAr_f^- (0.0176 g, 0.0199 mmol, 2.0 equiv). The biphasic mixture was vigorously stirred for 10 min, and then allowed to stand. The lower bright orange phase was separated and allowed to evaporate in the back of a fume hood to give $[Pt((S,S)\text{-dpen})_2]^{2+}$ $2BAr_f^- \cdot H_2O$ as a pale yellow solid (0.0174 g, 0.00736 mmol, 74%), mp 140-144 °C (dec, open capillary). Anal. Calcd. for $C_{92}H_{56}B_2F_{48}N_4Pt \cdot H_2O$ (2364.13): C, 46.74; H, 2.47; N, 2.37; found: C, 47.21; H, 2.47; N, 2.42.

NMR (acetone-d_6, δ in ppm): ^{1}H (400 MHz), BAr_f^- at 7.79 (s, 16H, *o*), 7.67 (s, 8H, *p*); (*S*,*S*)-dpen ligand at 7.51-7.46 (m, 8H, *o*-Ph), 7.35-7.28 (m, 12H, *m*-, *p*-Ph), 6.68-6.57 (m, 4H, N**H**H'), 5.94-5.92 (m, 4H, NH**H'**), 4.77-4.70 (m, 4H, C**H**NH_2); 2.86 (br s,

12H, H_2O); $^{13}C\{^1H\}$ (100 MHz), BAr_f^- at 162.6 (q, $^1J_{BC}$ = 50.1 Hz, *i*), 135.5 (s, *o*), 130.0 (m, *m*), 125.4 (q, $^1J_{CF}$ = 271.9 Hz, CF_3), 118.4 (s, *p*); (*S*,*S*)-dpen ligand at 136.8 (s, *i*-Ph), 130.3 (s, *p*-Ph), 130.0 (s), 128.7 (s), 67.3 (s, $CHNH_2$).

Dimethyl 2-(2-nitro-1-phenylethyl)malonate; catalyst screening (Figures 5.3 and 5.6). An authentic sample of this known compound was obtained as a colorless oil by a literature procedure.[1b] A 5 mm NMR tube was charged with a solution of *trans*-β-nitrostyrene (0.0054 g, 0.036 mmol, 1.0 equiv), catalyst (0.0036 mmol, 0.10 equiv), dimethyl malonate (0.0045 mL, 0.0052 g, 0.039 mmol, 1.1 equiv), and Ph_2SiMe_2 (0.0020 mL, internal standard) in acetone-d_6 (0.40 mL). A ^1H NMR spectrum was recorded to confirm the initial *trans*-β-nitrostyrene/standard ratio. A stir bar was added and the sample was cooled to 0 °C. Then Et_3N (0.0050 mL, 0.0036 g, 0.036 mmol, 1.0 equiv) was added and the mixture stirred. After 24 h, the stir bar was removed and the yield was assayed by ^1H NMR. The solvent was removed under reduced pressure to give an orange oil, which was added to a plug of silica. The plug was eluted with hexanes/EtOAc (1:1 v/v). The solvent was removed from the fraction containing the product under reduced pressure. The enantiomeric excess was determined by HPLC (Chiralpak AD column, 98:2 v/v hexanes/isopropanol, 1.0 mL/min, λ = 220 nm; for $[Pt((S,S)\text{-dpen})_2]^{2+}$ $2BAr_f^-$, t_R = 34.3 min (major), t_R = 44.4 min (minor).[15]

Crystallography. A vial was charged a solution of $[Pt((S,S)\text{-dpen})_2]^{2+}$ $2Cl^-$ (0.0300 g, 0.0865 mmol) in CH_3OH (3 mL) and H_2O (3 mL) was added. After 3 d, one of the colorless needles was mounted for data collection as outlined in Table 5.1. Cell parameters were obtained from 5245 frames using ω and φ scans and refined with 5594 reflections. Integrated intensify information for each reflection was obtained by reduction of the data frames with SAINT (V8.38A).[16] The program SADABS (2016/2) was used for absorption corrections.[17] The space group was determined from systematic reflection

conditions and statistical tests. Using Olex2,[18] the structure was solved with the ShelXT structure solution program[19] applying intrinsic phasing and refined with the XL refinement package[20] using least squares minimization. Non-hydrogen atoms were refined with anisotropic thermal parameters. Hydrogen atoms were placed in idealized positions and refined using a riding model. The parameters were refined by weighted least squares refinement on F^2 to convergence.[20] For each platinum atom, two molecules of CH_3OH were located. The Flack parameter (0.0135(16)) confirmed the absolute configuration.[21]

Table 5.1. Summary of crystallographic data for $[Pt((S,S)\text{-dpen})_2]^{2+}\ 2Cl^{-}\cdot 2CH_3OH$.

Empirical formula	$C_{30}H_{40}Cl_2N_4O_2Pt$
formula weight	754.65
temperature of collection [K]	110
diffractometer	Bruker APEX-II CCD
wavelength [Å]	1.54178
crystal system	orthorhombic
space group	$P2_12_12_1$
unit cell dimensions:	
a [Å]	5.8038(13)
b [Å]	14.237(3)
c [Å]	38.208(8)
α [°]	90
β [°]	90
γ [°]	90
V [Å^3]	3157.1(12)
Z	4
ρ_{calc} [Mg/m^3]	1.588
absorption coefficient [mm^{-1}]	10.124
F(000)	1504.0
Crystal size [mm^3]	0.1 × 0.02 × 0.02
Θ [deg]	2.313 to 68.705
range / indices (*h*, *k*, *l*)	–5,6; –17,14; –46,46
reflections collected	24207
independent reflections	5594 [R(int) = 0.0367]
completeness to Θ = 68.705°	96%
absorption correction	semi-empirical from equivalents
max. and min. transmission	0.167 and 0.036
refinement method	full-matrix least-squares on F^2
data / restraints / parameters	5594 / 0 / 357
goodness-of-fit on F^2	1.038
final R indices [I>2σ(I)]	$R1$ = 0.0316, w$R2$ = 0.1115
R indices (all data)	$R1$ = 0.0317, w$R2$ = 0.1115
absolute structure (Flack) parameter	0.135(16)
largest diff. peak and hole [e.Å^{-3}]	1.54 / –1.75

5.6 References (All titles are given in the capitalization format of the original article)

(1) (a) Ghosh, S. K.; Lewis, K. G.; Kumar, A.; Gladysz, J. A. Syntheses of Families of Enantiopure and Diastereopure Cobalt Catalysts Derived from Trications of the Formula $[Co(NH_2CHArCHArNH_2)_3]^{3+}$. *Inorg. Chem.* **2017**, *56*, 2304-2320. (b) Lewis, K. G.; Ghosh, S., K.; Bhuvanesh, N.; Gladysz, J. A. Cobalt(III) Werner Complexes with 1,2-Diphenylethylenediamine Ligands: Readily Available, Inexpensive, and Modular Chiral Hydrogen Bond Donor Catalysts for Enantioselective Organic Synthesis. *ACS. Cent. Sci.* **2015**, *1*, 50-56.

(2) (a) Kim, H.; Nguyen, Y.; Yen, C. P.-H.; Chagal, L.; Lough, A. J.; Kim, B. M.; Chin, J. Stereospecific Synthesis of C_2 Symmetric Diamines from the Mother Diamine by Resonance-Assisted Hydrogen-Bond Directed Diaza-Cope Rearrangement. *J. Am. Chem. Soc.* **2008**, *130*, 12184-12191. (b) Kim, H.; Staikova, M.; Lough, A. J.; Chin, J. Stereospecific Synthesis of Alkyl-Substituted Vicinal Diamines from the Mother Diamine: Overcoming the "Intrinsic Barrier" to the Diaza-Cope Rearrangement Reaction. *Org. Lett.* **2009**, *11*, 157-160. (c) Kim, H.; Chin, J. Stereospecific Synthesis of α-Substituted syn-α,β-Diamino Acids by the Diaza-Cope Rearrangement. *Org. Lett.* **2009**, *11*, 5258-5260. (d) Lee, D.-N.; Kim, H.; Mui, L.; Myung, S.-W.; Chin, J.; Kim, H. J. Electronic Effect on the Kinetics of the Diaza-Cope Rearrangement. *J. Org. Chem.* **2009**, *74*, 3330-3334. I So, S. M.; Kim, H.; Mui, L.; Chin, J. Mimicking Nature to Make Unnatural Amino Acids and Chiral Diamines. *Eur. J. Org. Chem.* **2012**, *2012*, 229-241. (f) So, S. M.; Mui, L.; Kim, H.; Chin, J. Understanding the Interplay of Weak Forces in [3,3]-Sigmatropic Rearrangement for Stereospecific Synthesis of Diamines. *Acc. Chem. Res.* **2012**, *45*, 1345-1355. (g) Lee, A.; So, S. M.; Lough, A. J.; Kim, H.; Chin, J. Mother Diamine: A Universal Building Block for Making Chiral Ligands from Daughter Diamines to Binol, Binap and Monophos Analogues. *Asian J. Org. Chem.* **2014**, *3*, 1102-

1107. (h) Kim, M.; Kim, H.; Kim, H.; Chin, J. Synthesis of Enantiopure Mixed Aryl-Alkyl Vicinal Diamines by the Diaza-Cope Rearrangement: A Synthesis of (+)-CP-99,994. *J. Org. Chem.* **2017**, *82*, 12050-12058.

(3) Maximuck, W. J.; Ganzmann, C.; Alvi, S.; Hooda, K. R.; Gladysz, J. A. Rendering classical hydrophilic enantiopure Werner salts $[M(en)_3]^{n+}$ nX^- lipophilic (M/*n* = Cr/3, Co/3, Rh/3, Ir/3, Pt/4); New chiral hydrogen bond donor catalysts and enantioselectivities as a function of metal and charge. *Dalton Trans.* **2020**, *49*, 3680-3691.

(4) Giri, N.; Davidson, C. E.; Melaugh, G.; Del Pópolo, M. G.; Jones, J. T. A.; Hasell, T.; Cooper, A. I.; Horton, P. N.; Hursthouse, M. B.; James, S. L. Alkylated organic cages: from porous crystals to neat liquids. *Chem. Sci.* **2012**, *3*, 2153-2157.

(5) Kabes, C. Q.; Maximuck, W. J.; Ghosh, S. K.; Kumar, A.; Bhuvanesh, N.; Gladysz, J. A. Chiral Tricationic Tris(1,2-diphenylethylenediamine) Cobalt(III) Hydrogen Bond Donor Catalysts with Defined Carbon/Metal Configurations; Matched/Mismatched Effects upon Enantioselectivities with Enantiomeric Chiral Counter Anions. *ACS Catal.* **2020**, *10*, 3249-3263.

(6) (a) Luu, Q. H.; Lewis, K. G.; Banerjee. A.; Bhuvanesh, N.; Gladysz, J. A. The robust, readily available cobalt(III) trication $[Co(NH_2CHPhCHPhNH_2)_3]^{3+}$ is a progenitor of broadly applicable chirality and prochirality sensing agents. *Chem. Sci.* **2018**, *9*, 5087-5099. (b) Alimohammadi, M.; Hasaninejad, A.; Luu, Q. H.; Gladysz, J. A. Λ-$[Co((S,S)\text{-dpen})_3]^{3+}$ $2I^-B(C_6F_5)_4^-$: A Second Generation Air- and Water-Stable Chiral Solvating Agent for Chiral Sensing (dpen = $NH_2CHPhCHPhNH_2$). *J. Org. Chem.* **2020**, *85*, 11250-11257.

(7) Palmer, J. W.; Basolo, F. Effect of Transition Metal Ion on Rates of Hydrogen Exchange in Metal Ammines. *J. Inorg. Nucl. Chem.* **1960**, *15*, 279-286. For the original

determinations involving the cations $[M(en)_3]^{n+}$ in this reference, the counter anions were not specified.

(8) Grinberg, A. A.; Gil'dengershel, K. I. О Кислотных Свойствах Аммиакатов И Аминатов Четырехвалентной Платины (Acidic Properties of Ammoniates and Aminates of Quadrivalent Platinum). *Izv. Akad. Nauk SSSR, Ser. Khim.* **1948**, 479-492.

(9) Goodall, D. M.; Hardy, M. J. Conjugate Bases of Tris(ethylenediamine)cobalt(III) and Nitropenta-ammine-cobalt(III) in Aqueous Hydroxide-Dimethyl Sulphoxide Mixtures. *J. Chem. Soc., Chem. Commun.* **1975**, *72*, 919-921.

(10) Giedt, D. C.; Nyman, C. J. Tris(ethylenediamine)platinum(IV) Chloride. *Inorg. Synth*. **1966**, *8*, 239-241.

(11) (a) Smirnoff, A. P. Zur Stereochemie des Platinatoms; über relativ asymmetrische Synthese bei anorganischen Komplexen. *Helv. Chim. Acta* **1920**, *3*, 177-195. (b) Dwyer, F. P.; Garvan, F. L. Stereospecific Influences in Metal Complexes Containing Optically Active Ligands. Part II. Some of the Optical Isomers of Tris-(propylenediamine)-platinum(IV) Ion. *J. Am. Chem. Soc.* **1959**, *81*, 1043-1045.

(12) Robinson, W. R. Perchlorate salts of metal complexes: Potential explosives. *J. Chem. Educ.* **1985**, *62*, 1001.

(13) Rodgers, K. R.; Murmann, R. K.; Schlemper, E. O.; Shelton, M. E. Rates of Isotopic Exchange with Solvent and Oxygen Atom Transfer Involving $[Mo_3O_4(OH_2)_9]^{4+}$. *Inorg. Chem.* **1985**, *24*, 1313-1322.

(14) Granchi, C.; Caligiuri, I.; Bertelli, E.; Poli, G.; Rizzolio, F.; Macchia, M.; Martinelli, A.; Minutolo, F.; Tuccinardi, T. Development of terphenyl-2-methyloxazol-5-(4*H*)-one derivatives as selective reversible MAGL inhibitors. *J. Enzyme Inhib. Med. Chem.* **2017**, *32*, 1240-1252.

(15) (a) Andrés, J. M.; Manzano, R.; Pedrosa, R. Novel Bifunctional Chiral Urea and Thiourea Derivatives as Organocatalysts: Enantioselective Nitro-Michael Reaction of Malonates and Diketones. *Chem. Eur. J.* **2008**, *114*, 5116-5119. (b) Almaşi, D.; Alonso, D. A.; Gómez-Bengoa, E.; Nájera, C. Chiral 2-Aminobenzimidazoles as Recoverable Organocatalysts for the Addition of 1,3-Dicarbonyl Compounds to Nitroalkenes. *J. Org. Chem.* **2009**, *74*, 6163-6168.

(16) SAINT, "Program for Data Reduction from Area Detectors", BRUKER AXS Inc., 5465 East Cheryl Parkway, Madison, WI 53711-5373 USA.

(17) SADABS, Sheldrick, G. M. "Program for Absorption Correction of Area Detector Frames", BRUKER AXS Inc., 5465 East Cheryl Parkway, Madison, WI 53711-5373 USA.

(18) Dolomanov, O. V.; Bourhis, L. J.; Gildea, R. J.; Howard, J. A. K.; Puschmann, H. *OLEX2*: a complete structure solution, refinement and analysis program. *J. Appl. Crystallogr.* **2009**, *42*, 339-341.

(19) Sheldrick, G. M. *SHELXT* – Integrated space-group and crystal-structure determination. *Acta Crystallogr.* **2015**, *A71*, 3-8.

(20) Sheldrick, G. M. A Short History of SHELX. *Acta Crystallogr.* **2008**, *A64*, 112-122.

(21) Flack, H. D. On Enantiomorph-Polarity Estimation. *Acta Crystallogr.* **1983**, *A39*, 876-881.

6. ROLE OF CHLORIDES IN REACTIVATION OF CONTAMINANT NICKEL ON FLUID CATALYTIC CRACKING (FCC) CATALYSTS†

6.1 Introduction

Fluid catalytic cracking (FCC) is an important process for the conversion of crude oil into valuable products including fuels, lubricants, and precursors for making other products. This importance is evidenced by the fact that there are more than 430 FCC units worldwide today.[1-3] First used commercially in 1942 in Baton Rouge, Louisiana (USA), the FCC process cracks high molecular weight hydrocarbon chains into lighter hydrocarbons using high temperatures (525-575 °C) and a heterogeneous catalyst.[1,4-7] Until the development of the FCC process, refineries were inefficient at making valuable products such as gasoline and liquefied petroleum gas (LPG); however, the parallel development of the FCC process and a catalyst capable of fluidization and cracking chemistry enabled refineries to upgrade less valuable fractions of crude oil into high-value diesel, gasoline, and LPG products. The FCC catalyst is primarily composed of zeolite-Y (in the form of ultra-stable zeolite Y or USY), which has a high surface area, but also features a matrix used for cracking reactions. The catalytic system can also include additional features such as nickel and/or vanadium passivation technologies and additives to tune product yields or to control emissions.

The catalyst facilitates beta scission reactions and is relatively robust – a necessity for enduring high temperatures and physical stress during operation. Additionally, FCC catalysts are often exposed to metal contaminants, which are typically introduced into the unit via the FCC feed. A common feed contaminant is nickel, which is often introduced

†Reprinted with permission from "Role of Chlorides in Reactivation of Contaminant Nickel on Fluid Catalytic Cracking (FCC) Catalysts" by Senter, C.; Clough Mastry, M.; Zhang, C. C.; Maximuck, W. J.; Gladysz, J. A.; Yilmaz, B., 2021. *Appl. Catal., A*, APCATA-D-20-01453R3, Copyright 2021 by Elsevier.

with the feed as a nickel (II) porphyrin structure.[8-9] The concentration of nickel in feed varies widely and can be as high as 100 ppm in extreme cases, although values lower than 25 ppm are more typical.[10]

A well-known dehydrogenation catalyst, nickel deposits on FCC catalyst in concentrations ranging up to 19,000 ppm. The deposited nickel induces unwanted dehydrogenation reactions, which lead to an increase in hydrogen and coke yields.[11-14] Excessive amounts of both hydrogen and coke can be problematic for refiners as they push the FCC unit closer to operating limits. For example, increased hydrogen can constrain the FCC unit's downstream compressor, and increased coke can increase the regenerator temperature towards its maximum limit. However, nickel contaminant becomes less active as it spends more time in the FCC unit. The oxidative environment in the FCC regenerator oxidizes nickel to nickel oxides. This chemical transformation immobilizes the nickel and greatly reduces its dehydrogenation tendency.[15-17] Once nickel oxide is formed, it is important to keep it in that state and inhibit its reduction to metallic nickel in the FCC environment.

There is precedence in literature that chloride ions can both mobilize and reactivate nickel oxides. Earlier work shows that NiO on activated carbon reacts with hydrochloric acid (HCl) to form $NiCl_2$, a mobile compound, which can then be further reduced by H_2 to metallic nickel, a more active dehydrogenation catalyst than NiO.[16] Another study shows the same phenomena using platinum, a metal from the same family as nickel, on zeolite that is exposed to HCl and subsequently reduced with H_2. Additionally, a further study observed a redistribution of platinum on the support following the HCl and H_2 reactions.[18-19] Another contribution showed that deactivated Ni-erionite catalyst regained its dehydrogenation activity when treated with solutions of HCl or NH_4Cl.[20] These examples demonstrate that relatively inert NiO can be reactivated for dehydrogenation

chemistry and mobilized by exposure to chloride containing compounds and set a precedence that this might be possible in the FCC environment. Indeed, industrial reports have noted a correlation between increased chloride content and an increase in unwanted hydrogen production, among other issues.

Interactions of nickel with chloride ions are relevant to the FCC environment as chloride ion sources can enter the FCC both with feed, sometimes a result of insufficient desalting operations, and with fresh catalyst as part of an alumina-based binder used in incorporated catalysts or from the use of chloride-containing precursors/chemicals in catalyst manufacturing.[14,21] The use of the alumina-based binders for incorporated catalysts is needed for particle integrity in order to control the attrition of the final product. Alumina-based binders often contain chloride as a byproduct in its manufacturing. Chloride content in fresh FCC catalyst can be as high as 1.2 wt%. Chloride sources coming from the feed vary widely. In heavily contaminated feeds, chloride can be as high as 15 ppm. Chloride sources in the feed can react with steam in the FCC to form HCl, while most of the binder-based chloride is released and converted to HCl in the high-temperature, steam partial pressure environment of the FCC regenerator.[22-24] While these chloride contaminants are well known to lead to deposits in the downstream fractionator, fouling in equipment, and having a negative impact on metallurgy, their effect on nickel contaminants in an FCC has never been formally investigated.[25]

The work described herein constitutes the first exploration of the effect of chloride ions on nickel contaminants deposited on actual FCC catalysts using simulated FCC conditions. While circulating in an FCC unit, a fraction of catalyst is continuously added and withdrawn. The continual addition and withdrawal of catalyst introduces an age-distribution of catalyst particles in periodically withdrawn samples that are tested and tracked to monitor performance. This age-distributed catalyst sample is commonly called

equilibrium catalyst (Ecat). Ecat samples taken from two different industrial FCC units were selected for this study. These samples were selected due to their differing nickel levels, marked as "high" and "low". It is important to note that the Ecat chosen for this study originate from catalysts manufactured by the "*in-situ*" manufacturing route. This route differs from conventional catalyst production process in that zeolite is grown in the microsphere after the spray drying step. The zeolite itself acts as the catalyst binder, thus *in-situ* catalysts do not use chloride-containing binders. As a result, there are no chlorides present in fresh catalyst. In addition, the refineries from which these Ecat samples originate did not report any chlorides coming from the feed. Therefore, this study represents the first time these samples are introduced to chlorides. Table 6.3 shows the total surface area (TSA), zeolite surface area (ZSA), matrix surface area (MSA), nickel, vanadium, iron, and rare earth oxides (REO, primarily lanthanum) content of the Ecat samples studied. We have not included other XRF results in Table 6.3, however it should be noted that neither sample had significant quantities of other well-known dehydrogenation metals, including copper and molybdenum. It is noted that there are slight differences in surface areas and REO content between the low and high nickel containing Ecat samples. For the purpose of this study, we note that these would not have a significant effect on the expected outcome based on the experimental design. Because the Ecat samples that fit the desired criteria (similar technology, similar manufacturing route, no additive usage, no previous chloride exposure) are limited and are based on refineries operating around the world at the moment of this experimental design, these samples represent the best compromise between using industrial Ecats and laboratory generated (deactivated) samples. Ecat samples were chosen over lab-deactivated catalyst as these samples provide the best representation of nickel age distribution in the unit, since it is known that the introduction of nickel contaminants in a laboratory can lead to a

distribution of nickel which does not mimic what is seen in an actual FCC unit.[1] To this point, extensive research is focused on the attempt to develop methods to minimize these testing artifacts.[26] Thus, performing such a study on Ecat samples provides results most relevant to industrial application.

The Ecat samples chosen for this study were exposed to chloride ions via introduction of gaseous HCl generated by reaction of aqueous HCl with sulfuric acid.[27-28] This procedure is well established in literature for generating HCl. While literature describes the introduction of HCl via liquid solutions as well, such a method was not included in this study, since FCC catalysts are not normally exposed to such liquid media during FCC operation.[20] As a result, they are not designed to withstand this type of liquid interactions; consequently, FCC structural integrity and catalytic performance can be drastically altered by exposure to liquids. The objective of exposure to HCl is to monitor any conversion of oxidized nickel on Ecat into $NiCl_2$ species. A control experiment was also run exposing Ecat to gaseous N_2. Following each introduction of chloride ions or control treatment, each catalyst sample was then exposed to H_2 to mimic the reducing environment of an FCC riser and reduce any nickel chloride species formed to metallic nickel. The effect of each treatment was then studied by evaluating the physical, chemical, structural, and catalytic changes of the catalysts using particle size measurement, surface area measurement, X-Ray Fluorescence (XRF), Scanning Electron Microscopy (SEM), Advanced Cracking Evaluation (ACE), and CO Diffuse Reflectance Infrared Fourier Transform Spectroscopy (DRIFTS) analyses. The results are presented and discussed below.

6.2 Experimental section

6.2.1 Treatment of Ecat samples (Figure 6.1)

A round-bottom flask was charged with catalyst (40 g). $HCl_{(g)}$ was produced by

dropwise addition of $HCl_{(aq)}$ (12.1 M, *ca*. 1 mL/min) into a Schlenk flask containing a stirred solution of $H_2SO_{4(aq)}$ (100 mL, 18.0 M). The generated $HCl_{(g)}$ flowed into the catalyst-containing flask via a gas dispersion tube with stirring for 1 h at room temperature and then exhausted into a KOH base trap. The catalyst was dried using a temperature furnace at 100 °C overnight.[27-28]

In a control experiment, the same procedure was repeated with a gentle stream of $N_{2(g)}$ (*ca*. 1 L/min) replacing the generated $HCl_{(g)}$. A round-bottom flask was charged with catalyst (40 g). The $N_{2(g)}$ flowed into the catalyst-containing flask via a gas dispersion tube with stirring for 1 h at room temperature and then exhausted into the atmosphere. The mixture was stirred for 1 h at room temperature. The catalyst was dried in a 100 °C furnace overnight.

The reduction process was adapted from a literature procedure.[16] A Fisher-Porter bottle was charged with treated catalyst (40 g). The system was filled with $H_{2(g)}$ and evacuated five times before being pressurized with 75 psig of $H_{2(g)}$. The system was heated to 375 °C, kept at that temperature for 30 min, and subsequently cooled (total time elapsed *ca.* 2 h).

Figure 6.1. Visual summary of zeolite treatment process.

6.2.2 Measurement of particle size of catalyst

Particle size was measured according to ASTM D4464-10 at BASF. Particle size distribution of particles in the range of 2.8 to 176 μm were measured using a Beckman Coulter LS13320 with Universal Liquid Modul and Ultrasonic unit. Material is dispersed in water, exposed to a beam of light, and the diffraction pattern of the light is used to determine the distribution of particle size.

6.2.3 Measurement of surface area of catalyst

Surface area was measured using BET method on a Micromeritics TriStar II according to ASTM methods D 3663 and D 4365 at BASF. BET uses adsorption isotherms to determine material surface area. The sample was pulverized, and outgassing was performed at 250 °C for 4 h. Surface area was measured by N_2 adsorption and desorption.

6.2.4 Elemental analysis

X-Ray Fluorescence Spectroscopy (XRF) analyses were performed using a wavelength-dispersive PANalytical PW2400 spectrometer, calibrated by linear regression to data from standards at BASF. All samples were prepared by fusion, using a lithium metaborate/lithium tetraborate flux.

6.2.5 SEM-EDX

The catalyst samples were mounted in epoxy and polished to an ultra-flat surface and carbon coated using a Denton DV-502A Vacuum Evaporation System at BASF. The BEI analysis was conducted on a Hitachi 3400S Environmental Microscope at 15-25 kV. EDX (Energy Dispersive X-Ray Spectroscopy) results were collected at 25 kV on a Bruker Quantax EDS system with Dual 30 mm^2 Silicon Drift Detectors (SDD).

6.2.6 Image processing for quantitative analyses

ImageJ was also used to calculate the circularity of all particles in each sample at BASF. A circularity index was calculated per the following equation:

$$Circularity = 4\pi * \frac{Area}{Perimeter^2}$$

A circularity of 1 equals a perfect circle while a circularity of 0 equals a straight line.

6.2.7 Fluidized catalytic cracking evaluation

Advanced Cracking Evaluation (ACE) is a laboratory-scale FCC testing unit which evaluates the activity and selectivity of FCC catalysts in a fixed-fluidized bed reactor.[29-30]As testing is carried out under fluidized conditions, it is commonly used for evaluating FCC catalysts. Ecat treated by various methods were analyzed on an ACE testing apparatus with the following conditions: Reactor temperature: 532 °C, injector height, 2.125", standard vacuum gasoil feed, variable time on stream method, 1.2 g/min feed rate, 9 g catalyst loading, 575 s catalyst strip time, liquid strip multiplier of 12, 110 °C feed temperature, 116 °C and 177 °C temperature of first and second feedline heater (respectively), and catalyst to oil ratios of 9, 7, 5, and 3 at BASF. Coke on catalyst is obtained at the end of a run on a LECO unit.

6.2.8 CO DRIFTS

A novel, BASF-developed, 3-temperature (3-T) pretreatment CO DRIFTS method was used to characterize the nickel on treated and untreated catalyst samples.[31] This method, as opposed to traditional CO DRIFTS, is needed due to the presence of other impurities, which can lead to ambiguous CO band assignments. The samples were ground into fine powders and pretreated with 2.4% H_2/Ar at 200, 400, and 600 °C sequentially for 1 hour at each temperature. The samples are cooled to 30 °C then undergo a 30 min exposure to 1% CO/Ar for adsorption and a 30 min desorption in Ar while FTIR data were collected. FTIR characterization was performed on a Thermo Fisher Nicolet iS50 FTIR spectrometer equipped with an MCT detector and a Pike Technology high-temperature

environmental chamber with a KBr window. Spectrum collection was performed under diffuse reflection mode. Bands were assigned based on CO interaction with metals of different oxidation states and the change in these band intensities with temperature was recorded, which allows the characterization of nickel reducibility upon different treatments.

6.3 Results and discussion

Ecat samples were treated with HCl or N_2, reduced by exposure to H_2, and then analyzed by several techniques. XRF, surface area, and particle size distribution of each sample were measured and compared to untreated Ecat as a means of evaluating the effect of each treatment on chemical composition and physical integrity of the catalyst. SEM images were also obtained in order to evaluate changes in catalyst particle shape and nickel distribution across different catalyst particles. An image processing method employing ImageJ was used to quantify differences seen between each SEM image. Changes in the dehydrogenation activity of nickel on Ecat following each treatment method was evaluated using ACE analysis. A standard feed was cracked over a range of catalyst to oil (C/O) ratios with each Ecat. The properties of this standard feed are given in Table 6.1.

Table 6.1. Feed properties used in ACE evaluations.

Property	Value	Distillation, °F	Value
Ni, ppm	0.3	Initial boiling point	267
V, ppm	0.2	5%	578
Na, ppm	0.3	10%	632
Fe, ppm	0.1	20%	689
Cu, ppm	0.1	30%	729
S, wt%	0.74	40%	769
CRC, wt%	0.26	50%	805
Total N, ppm	978	60%	842
Basic N, ppm	298	70%	883
UOP K	11.9	80%	926
Pour point, °F	102	90%	978
Aniline point, °F	186	95%	1017
Ref. index @ 25°C	1.5044	Final boiling point	1122
API @ 60°F	24.19		

Hydrogen and coke yields of the Ecat sample are used as a measure for dehydrogenation activity of contaminant nickel. Finally, the oxidation state of nickel, which is hypothesized to be altered by interaction with chloride ions and subsequent reduction, was evaluated by CO DRIFTS.[31] The results are described herein.

6.3.1 XRF, adsorption, and particle size distribution

Following the treatments described previously, the resulting surface area and chemical composition of the catalysts were analyzed and compared to untreated samples to evaluate how each treatment method influenced the chemical and physical properties of the catalysts. XRF results are shown in Table 6.2. Alumina, lanthanum, iron, nickel and vanadium oxides are reported. These elements (via their respective oxides) are all of interest. Alumina is present in both the matrix and zeolite phases of the catalyst. Additionally, cracking sites of the catalyst are found on the alumina which is part of the zeolite phase. Lanthanum is a rare earth element which stabilizes active cracking sites. Iron is both a contaminant and found in the structural framework of the catalyst. Vanadium is also a feed contaminant which contributes to coke and hydrogen yields. As a result, it

is important to track these elements/oxides before and after treatment methods to assess how any change in their amount might affect the reactivity or selectivity of catalyst samples. It is important to note that no other catalyst contaminant known to increase coke and H_2 were present on the catalyst in significant quantities (>50 ppm).

Table 6.2. XRF results of treated and untreated Ecat samples.

Sample	Al_2O_3, wt%	La_2O_3, wt%	Fe_2O_3, wt%	NiO, wt%	V_2O_5, wt%
High Nickel, Untreated	40.01	3.28	0.86	0.59	0.39
High Nickel, HCl	40.00	3.21	0.81	0.56	0.38
High Nickel, N_2	40.20	3.28	0.81	0.59	0.41
Low Nickel, Untreated	39.69	2.38	1.04	0.08	0.30
Low Nickel, HCl	40.02	2.40	0.99	0.08	0.29
Low Nickel, N_2	40.35	2.45	1.01	0.09	0.33

Following treatment by either HCl or N_2 and reduction with H_2, both Ecat samples contained amounts of Al_2O_3, La_2O_3, Fe_2O_3, NiO, and V_2O_5 that were within instrumental error of the untreated Ecat samples. This indicates that loss of nickel, vanadium, aluminum, iron or lanthanum does not occur during treatment (as expected) and will not influence coke and hydrogen yields in ACE analyses.

Table 6.3 shows the surface area and average particle size (APS) of the Ecat samples before and after each treatment method. These physical parameters are important to monitor, since any change in the structural integrity of the catalyst could influence coke and hydrogen yields, thus clouding any change in nickel reactivity. Neither treatment method resulted in a change in surface area or particle size that was outside of the instrumental error of the original Ecat. This indicates that HCl and N_2 treatment methods do not significantly alter the catalyst structure.

Table 6.3. Surface area and average particle size (APS) of catalyst samples.

Sample	Total Surface Area, m^2/g	Matrix Surface Area, m^2/g	Zeolite Surface Area, m^2/g	Zeolite/ Matrix Ratio	Average Particle Size, µm
High Nickel, Untreated	153	45	108	2.4	74
High Nickel, HCl	159	48	111	2.3	79
High Nickel, N_2	154	47	107	2.3	69
Low Nickel, Untreated	117	37	80	2.2	77
Low Nickel, HCl	118	38	80	2.1	77
Low Nickel, N_2	132	39	93	2.4	79

6.3.2 SEM-EDX spectroscopy

Scanning electron microscopy was performed on catalyst samples before and after treatment to understand both the change in nickel distribution and the structural integrity of the catalysts before and after exposure to chloride ions. SEM studies focused on high nickel Ecat, since the low nickel Ecat samples did not contain enough nickel for detection in SEM-EDX (Energy Dispersive X-Ray Spectroscopy).

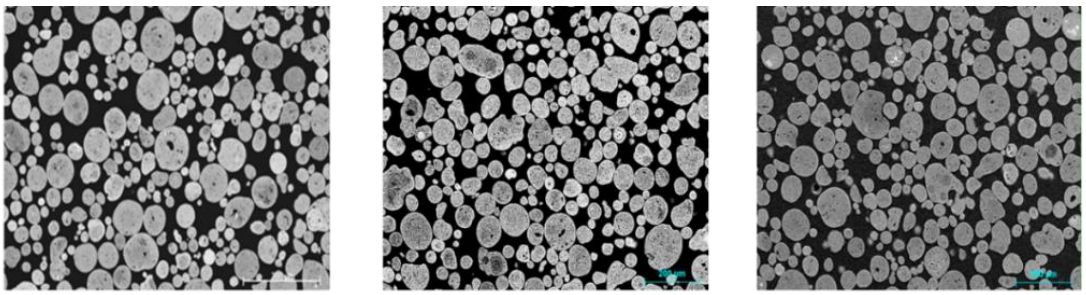

Figure 6.2. SEM backscattering images of high nickel Ecat untreated, treated by N_2, and treated by HCl.

Figure 6.2 shows the SEM back-scattering results for treated and untreated Ecat samples. No fragmentation of particles was observed, and the structural integrity of the

catalyst particles was maintained. ImageJ was used to calculate the circularity of each particle. A "circularity index" of 0 to 1 was calculated with 1 indicating a perfect circle and 0 indicating a line. The values were averaged for each treatment method and the results are shown in Table 6.4. Each catalyst sample had the same circularity index of 0.86, thus confirming that no treatment method was destructive to catalyst integrity and that these treatment methods are an effective way to introduce chloride into the catalyst without influencing the structural integrity of the catalyst particle.

Table 6.4. Circularity of catalyst particles calculated by ImageJ.

Sample	Circularity Index[1]	Number of Particles Analyzed
Untreated	0.86	221
N_2	0.86	234
HCl	0.86	214

[1]See the experimental section for the definition of circularity.

The SEM-EDX images of nickel on catalyst particles were also examined before and after treatment. Figure 6.3 shows the SEM images for nickel and aluminum overlaid for high nickel Ecat untreated and treated by N_2 and HCl.

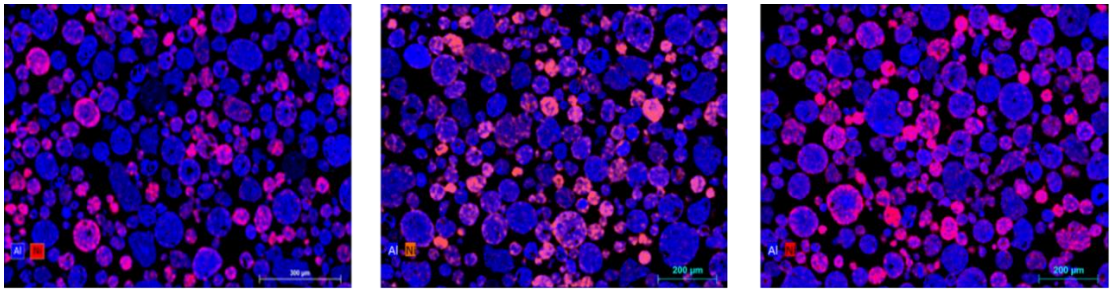

Figure 6.3. SEM images of nickel overlaid with aluminum for high nickel Ecat untreated, treated by N_2, and treated by HCl.

A redistribution of nickel is not apparent from these images; however, this is not surprising given the design of the experiment. The catalysts were not treated in a fluidized environment nor at the high temperatures experienced in an industrial FCC regenerator. As a result, while nickel chlorides can still form, the temperature and lack of fluidization would not be amenable to nickel mobility. A further study of nickel mobility in the presence of chloride ions at conditions closer to that of an FCC unit will be investigated later.

6.3.3 Catalytic testing results

Changes in the catalytic behavior of nickel contaminated Ecat following exposure to N_2 or HCl then reduced by H_2 were evaluated using ACE analyses. A standard FCC feed was cracked over a fluidized bed of Ecat at different catalyst-to-oil ratios. Since nickel is a known contaminant that produces hydrogen and coke when present on FCC catalyst, the changes in coke yield and H_2/CH_4 yield ratios during ACE evaluations were compared as a means of assessing nickel activity following different treatment methods.

Figure 6.4 shows the coke vs. conversion results from an ACE analysis of the Ecat sample containing high amounts of nickel. The results showed treatment with HCl prior to the reduction step gave roughly a 1 wt% increase in coke yield as a function of conversion. This result highlights that the introduction of chloride ions leads to increased coke yield. Since coke is a known product of dehydrogenation from nickel contamination and it is hypothesized that chloride ions facilitate activation of nickel contaminants on FCC catalyst, a higher coke yield following HCl exposure suggests the reactivation of nickel by exposure to chloride ions.

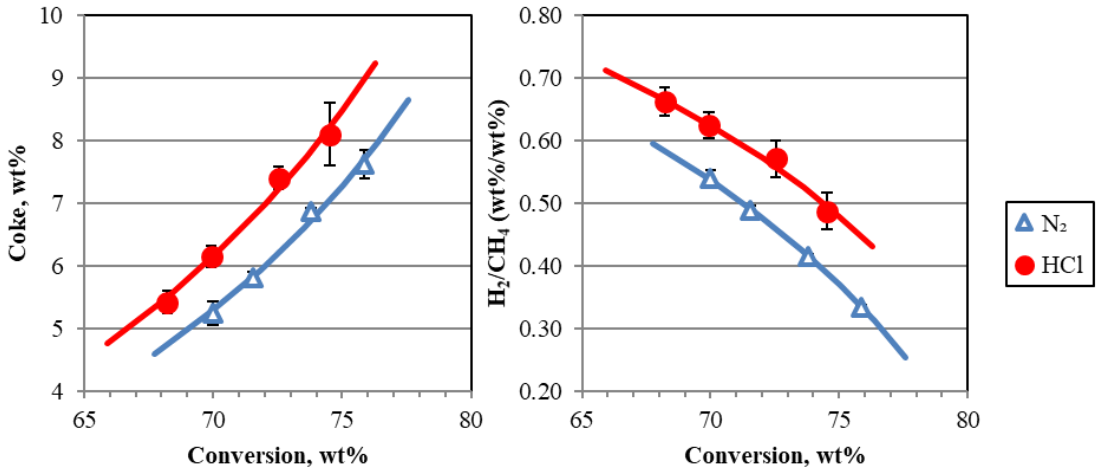

Figure 6.4. Coke and H_2/CH_4 vs. conversion of high nickel Ecat.

Figure 6.4 also shows H_2/CH_4 yield ratios as a function of conversion for the high nickel Ecat treated by N_2 and HCl. As with the coke yield, the H_2/CH_4 yield ratio was higher for Ecat exposed to HCl than Ecat exposed to N_2 (~0.08 wt%/wt%). The increase in H_2/CH_4 yield ratio with HCl treatment also suggests that there are interactions of chloride ions with nickel which increases the dehydrogenation activity of the nickel contaminants on catalyst.

The average yields at 72.5% conversion are reported in Table 6.5. There is a 0.06 wt%/wt% and 1.1 wt% increase in H_2/CH_4 ratios and coke yields, respectively, when the catalyst is treated with HCl as opposed to with N_2. These experiments confirm an average relative increase of 13% in H_2/CH_4 ratios and 18% in coke yields for samples exposed to HCl. These increases in H_2/CH_4 and coke are both significant, as the average values of 0.52 and 7.4 for H_2/CH_4 and coke yields following HCl treatment are not within the standard deviation of the H_2/CH_4 and coke values of the samples treated with N_2. Additionally, increases in 13% and 18% in H_2/CH_4 and coke would be considered significant by industry standards as well. These increases in H_2/CH_4 and coke seen in Table 6.5 agree with the trends seen in Figure 6.4, thus confirming the increased

dehydrogenation which occurs when chloride ions are introduced to the system.

The combination of increased coke and hydrogen yields following exposure to HCl indicates that nickel contaminant on the catalyst is more active, and that chloride ions play a role in reactivating nickel on the catalyst.

Table 6.5. Change in H_2/CH_4 ratios and coke yields of Ecat treated by different gaseous methods compared to untreated Ecat. High nickel reported at 72.5% conversion. Low nickel reported at 63.5% conversion.

		N_2 Treatment	HCl Treatment	% Difference (HCl vs. N_2)
High Nickel	H_2/CH_4	0.46 ± 0.006	0.52 ± 0.04	13
	Coke	6.3 ± 0.1	7.4 ± 0.2	18
Low Nickel	H_2/CH_4	0.19 ±0.005	0.25 ± 0.008	30
	Coke	3.4 ± 0.05	3.7 ± 0.2	9.8

Low nickel Ecat samples (exposed to N_2 and HCl were also analyzed via ACE. The coke yield vs. conversion are shown in Figure 6.5. There was a ~0.5 wt% increase in coke yield following exposure to HCl. However, this increase in coke is not as large as the increase seen (~1 wt%) following treatment of the high nickel Ecat sample with HCl. This is expected as there is significantly less nickel present on the Ecat, thus less nickel available for potential reactivation.

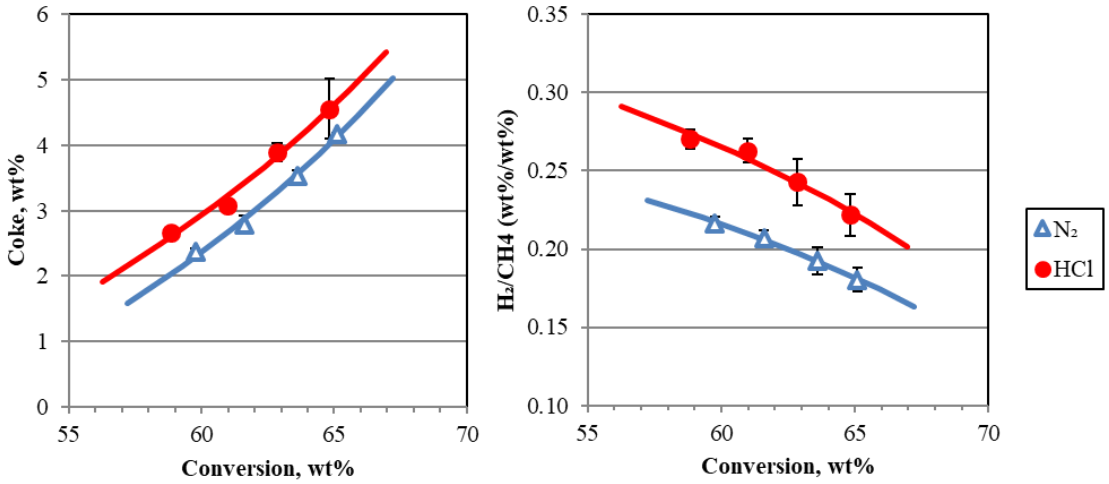

Figure 6.5. Coke and H_2/CH_4 vs. conversion yield of low nickel Ecat.

Figure 6.5 also shows the H_2/CH_4 yield ratio as a function of conversion for the Ecat samples with lower amounts of nickel. As in the high nickel case, there is an increase in H_2/CH_4 following exposure of the catalyst to HCl (+0.05 wt%/wt%). However, as was seen with coke yields, this increase in H_2/CH_4 is not as pronounced as seen in the case of catalyst containing high amounts of nickel.

Multiple ACE experiments were run with the low nickel Ecat. The coke yields and H_2/CH_4 yield ratios at constant conversion were averaged and are reported in Table 6.5. The H_2/CH_4 yield ratios at constant conversion agreed with the trend seen in Figure 6.5. There is a 0.06 wt%/wt% increase in H_2/CH_4 when HCl is introduced.

The coke yield at constant conversion agreed with the trend shown in Figure 6.5. Exposure to HCl leads to a 0.3 wt% increase in coke compared to exposure to N_2. However, it should be noted, that the increase in coke due to exposure to chlorides is almost within standard deviation of each experimental trial. This is not surprising considering the relatively low amount of nickel present on this catalyst.

6.3.4 CO-DRIFTS

CO DRIFTS experiments were performed on Ecat samples treated with N_2 or HCl then reduced by H_2. The goal of DRIFTS experiments is to determine the reducibility of the nickel contaminant. Since the Ecat samples contain 0.8-1.0% of iron, the CO adsorption on iron would show overlapped peaks in DRIFTS with the CO adsorbed on Ni. In literature, CO adsorbed on bivalent or single valent state of nickel is assigned in the range of 2100-2200 cm^{-1}, CO adsorbed on top of Ni(0) is assigned in 2000-2100 cm^{-1}, and CO adsorbed on Ni(0) can also be found at 1813-2000 cm^{-1} for single-fold or multi-fold bridged adsorption on larger particles.[32–35] CO adsorbed on iron (Fe^{2+}, Fe^{0}) is reported with similar peak positions.[36-38]

In order to differentiate the CO adsorbed on iron and the CO adsorbed on nickel, a sequential CO DRIFTS experiment at 3 temperatures is designed under the pretreatment of hydrogen reduction following the protocol reported in detail elsewhere.[31] In these CO DRIFTS experiments, samples were first treated with H_2 at 200 °C before introducing CO, which allows a partial reduction of iron or nickel to a different degree. The CO was then introduced and adsorbed on samples to reach equilibrium. After CO introduction, the CO was allowed to desorb in argon, and data were collected using FTIR. This process was then repeated at 400 and 600 °C. At each of these temperatures, the reduction degree of nickel and iron is examined by the adsorbed CO FTIR signals. As two different metal oxide materials, nickel oxide and iron oxide are expected to have different reducibilities.[39-42] The 3-temperature trend analysis of reduction allows the separation of nickel and iron when their reducibilities are different. The FTIR spectrum of the desorbed gas was processed using the IR background spectrum collected before CO was introduced, which allows the comparison of adsorbed CO bond vibration signals at the different

reduction temperatures. From this spectrum, information on the oxidation states of metals on the catalyst were determined based upon CO interaction with these sites.[43] With that, the reducibility of nickel can be isolated from the influence of iron, and the effect of N_2 or HCl treatment on the Ecat samples can be clearly examined.

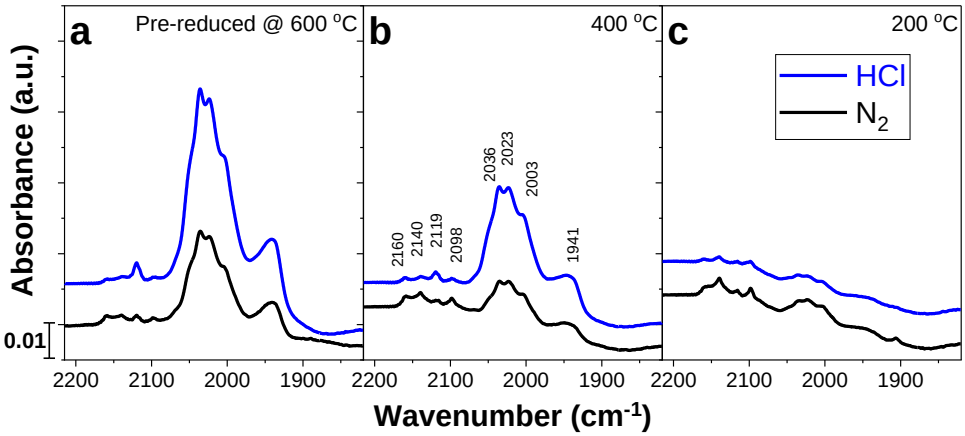

Figure 6.6. CO-DRIFTS spectra of high nickel samples treated with gaseous N_2 (lower trace) and HCl (upper trace). Samples are pre-reduced at (L to R) 600 °C, 400 °C, and 200 °C.

The CO absorbance spectra of high nickel Ecat treated by gaseous N_2 and HCl are shown in Figure 6.6. The CO absorbance spectra of low nickel Ecat samples treated with N_2 and HCl are shown in Figure 6.7.

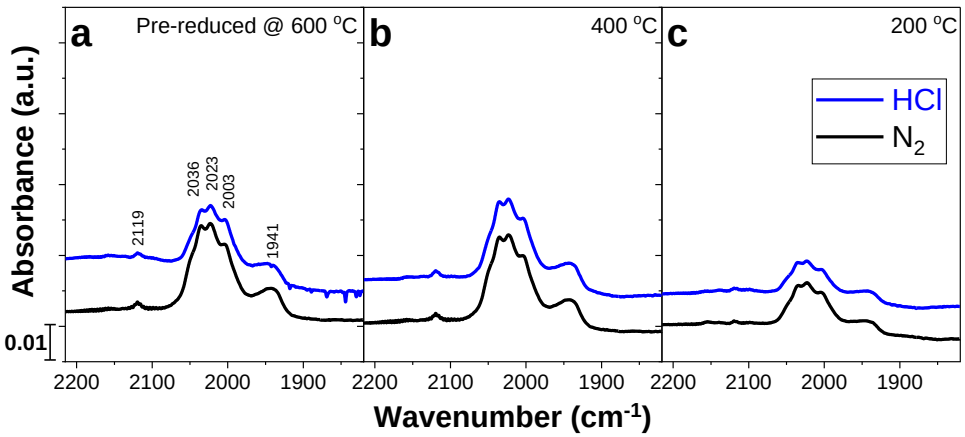

Figure 6.7. CO-DRIFTS spectra of low nickel samples treated with N_2 (lower trace) and HCl (upper trace).

The bands between 1940 cm^{-1} and 2060 cm^{-1} result from CO bound to Ni(0) and Fe(0) species. The 2090 cm^{-1} band is a result of CO bound to Ni(0). The 2120 cm^{-1} band is CO bound to Fe(II) species. The 2140 cm^{-1} and 2160 cm^{-1} bands result from Ni(II) species. Bands were deconvoluted and their areas were integrated at different reduction temperatures in order to determine differences in nickel oxidation state between treatments. The 2090 cm^{-1} and 2120 cm^{-1}, Ni(0) and Fe(II) bands, respectively, have very small areas and it was difficult to infer meaningful information from them in any sample. Thus, the analysis focused on changes in 2140 cm^{-1} and 2160 cm^{-1} band areas (Ni(II)) and the areas of the bands in the 1900-2070 cm^{-1} region (Ni(0) and Fe(0)).

Figure 6.8 shows the sum of the integrated areas of the nickel(II) derived 2140 cm^{-1} and 2160 cm^{-1} bands for the high nickel Ecat samples as a function of temperature. The CO adsorption at these two bands is much smaller than the bands in the 1900-2070 cm^{-1} region, which supports that the sample contains mostly metallic form of nickel/iron after reduction. The form of Ni(II) may include NiO or nickel aluminate in the Ecat samples, and possibly $NiCl_2$ in the HCl-treated samples. The contribution to the peaks at 2140 cm^{-1} and 2160 cm^{-1} is believed by the authors to come from NiO or nickel aluminate rather than $NiCl_2$ and are indicative of the amount of NiO/nickel aluminate compound (in short, referred to as referred to as referred to as Ni-O in discussions) present on the catalyst. This proposed peak assignments can be supported by the observation that the catalyst treated with HCl showed significantly lower band area and, therefore, less Ni-O compounds, than the sample treated with N_2. This could indicate that during treatment with HCl, chloride ions reacted with Ni-O forming $NiCl_2$, which could then be reduced to metallic nickel during the reduction step. Additionally, the N_2 treated sample showed a higher band area at 200°C and a decrease in this band area with increasing reduction temperature, while the chloride ion treated sample was essentially unchanged, indicating Ni-O remaining on Ecat

treated with N_2 is reduced at higher temperatures, while Ecat sample treated with HCl has much less Ni-O remaining. This result suggests different amount of Ni-O species remain in the Ecat samples under N_2 and HCl treatments, with a higher amount of Ni-O in the N_2-treated Ecat.

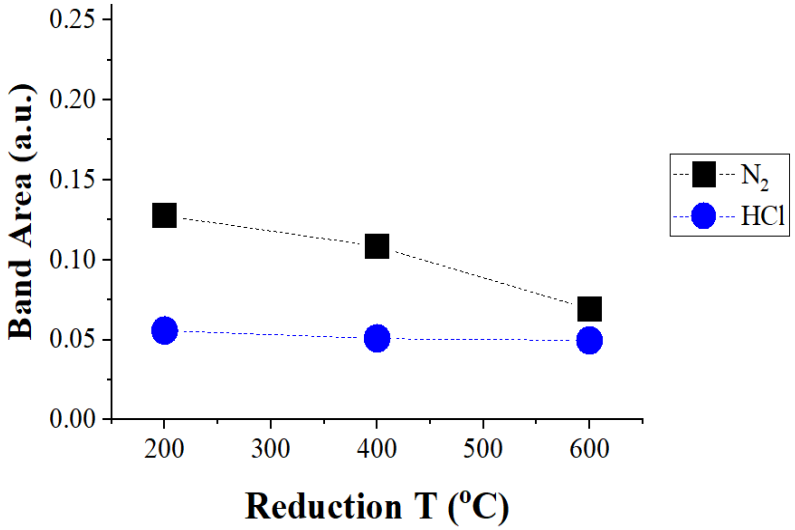

Figure 6.8. Area of the 2140 and 2160 cm^{-1} Ni(II)-IR bands of high nickel Ecat as a function of reduction temperature.

The combined band area between 1900-2070 cm^{-1} was also examined. These bands are indicative of both Ni(0) and Fe(0) species; as a result, these combined band areas are discussed for both the high nickel and low nickel catalyst samples to understand whether changes in band area are influenced by changes in Fe(0) or Ni(0) compounds, as the iron levels between the high and low nickel catalysts were similar (within 1200 ppm).

Figure 6.9 shows the combined band area of all bands in the 1900-2070 cm^{-1} region for the Ecat samples. It is expected that iron would be reduced before nickel is reduced when exposed to H_2. The formation of Ni(0) will become more obvious as the reduction temperature increases, thus the Ni(0) can be separated from Fe(0) in the CO DRIFTS.

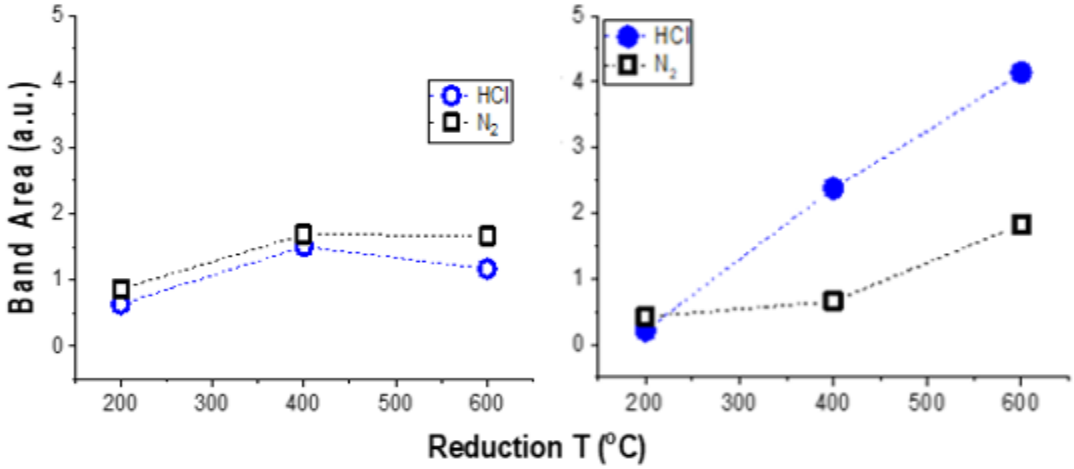

Figure 6.9. Sum of IR-band areas for low nickel (left) and high nickel (right) samples between 1900 and 2070 cm^{-1}.

For the low nickel Ecat, as the reduction temperature increases to 400 °C, the bands grow for each sample indicating more Ni(0) and Fe(0) are formed. At 600 °C, important observations can be made. For both low nickel samples, the band area does not increase, which could be an indication that all iron and nickel have been completely reduced to the zero-oxidation state at 400°C. This result has implications for the analysis of the high nickel sample. The high and low nickel catalyst samples have comparable levels of iron. Thus, a complete reduction of iron in the low nickel Ecat at 400 °C indicates that all iron will be reduced to Fe(0) in the high nickel Ecat at 400 °C as well. Consequently, any changes in band area at 600 °C for the high nickel samples can be attributed to a change in the amount of Ni(0).

The combined area of all bands in the 1900-2070 cm^{-1} region for the high nickel catalyst samples can also be seen in Figure 6.9. These band areas should reflect the amount of Fe(0) and Ni(0) present. At 200 °C, the area is similar to the low nickel samples, which is an indication that the primary species being observed here is Fe(0) since the nickel levels are very different between the two catalysts. As the temperature increases to 400 °C, the band of the HCl treated sample grows much more rapidly than the N_2 sample. At 600 °C,

both high nickel samples show an increase in band area, with the HCl treated sample showing a significantly higher increase than the N_2 treated sample. Having established that the reduction of iron to Fe(0) is completed by 400 °C, this would indicate that the increase in band area at 600 °C is due to a change in Ni(0). This difference in the change in band area would then indicate that the HCl treated sample contains more readily reducible nickel than the N_2 sample.

This large increase in Ni(0) formation vs. temperature for Ecat treated with HCl must be reconciled with the fact that its CO adsorbed on Ni-O band at 2140 and 2160 cm^{-1} does not change with a reduction temperature (Figure 6.8). One would expect a large increase in Ni(0) to correspond to a drop in Ni(II). An explanation could be that a nickel species not detected in CO DRIFTS is being reduced to Ni(0) at 600 °C in the Ecat treated with HCl. Given the HCl treatment applied, it could be that $NiCl_2$ is present on the Ecat treated by HCl and is not distinguishable in the FTIR spectra studied. As this $NiCl_2$ is exposed to H_2 at 600 °C, it is reduced to Ni(0) which is then visible in the analysis. While the exact mechanism is uncertain, the results show clearly that exposure of Ecat to HCl results in significant differences in the reducibility of nickel compared to exposure to N_2. This further supports the conclusion that differences in ACE yields are a result of a change in the reducibility of nickel, and that chloride ions are playing a major role in this transformation.

6.4 Conclusion

This work attempts for the first time to demonstrate and characterize the physiochemical and catalytic effects of chloride ions on contaminant nickel in the FCC environment. Additionally, by performing the study on catalyst from actual FCC units, the age-distribution of nickel on the catalyst studied is representative of what can be expected in actual operation. It is acknowledged that uncertainties are introduced by performing by

using actual FCC Ecat, but the method development work performed in this study has laid the groundwork to perform future studies in more carefully controlled laboratory conditions. Uncertainties which will be addressed in future work include aspects such as the use of catalyst with the same properties and non-Ni contaminants, examination of the effect of Ni passivators, and the effect of actual Cl binder.

By studying the change in physicochemical characteristics and catalytic selectivity of FCC catalysts, as well as the reducibility of the nickel on FCC catalyst, clear differences can be seen when chloride ions are introduced to catalyst contaminated with nickel Ecat which is exposed to HCl and then reduced showed increased coke and H_2 yields and resulted in less Ni-O bonds and potentially more $NiCl_2$ on the catalyst. These results bridge the gap between existing literature and the FCC environment by showing that chloride ions can interact with nickel contaminant on FCC catalyst. The interaction results in changes in the electronic environment of nickel, which makes it easier to be reduced in the FCC riser. This reduced nickel poses a significant problem to refineries since it is an active dehydrogenation catalyst which produces undesirable coke and H_2, essentially bringing the FCC unit closer to its operational constraints and inhibiting the refinery to reach the full potential of this important unit operation. The results from this study enable catalyst manufacturers and refiners to further optimize catalyst design and selection as well as operational strategies to limit H_2 and coke from nickel contaminants.

6.5 References (All titles are given in the capitalization format of the original article)

(1) Pan, S. S.; Lin, L. T. X.; Komvokis, V.; Spann, A.; Clough, M.; Yilmaz, B. Nanomaterials Fueling the World. In *Nanomaterials for Sustainable Energy*, American Chemical Society: 2015; Vol. 1213, pp 3-18.

(2) Avidan, A. A.; Edwards, M.; Owen, H. Innovative Improvements Highlight FCC's Past and Future. *Oil Gas J.* **1990**, *88*, 33-58.

(3) Vogt, E. T. C.; Weckhuysen, B. M. Fluid catalytic cracking: recent developments on the grand old lady of zeolite catalysts. *Chem. Soc. Rev.* **2015**, *44*, 7342-7370.

(4) Clough, M.; Pope, J. C.; Lin, L. T. X.; Komvokis, V.; Pan, S. S.; Yilmaz, B. Nanoporous materials forge a path forward to enable sustainable growth: Technology advancements in fluid catalytic cracking. *Microporous Mesoporous Mater.* **2017**, *254*, 45-58.

(5) NACS. Eger Murphree and the four Horsemen: FCC, Fluid Catalytic Cracking, The North American Catalysis Society, 2003.

(6) Blay, V.; Louis, B.; Miravalles, R.; Yokoi, T.; Peccatiello, K. A.; Clough, M.; Yilmaz, B. Engineering Zeolites for Catalytic Cracking to Light Olefins. *ACS Catal.* **2017**, *7*, 6542-6566.

(7) Sadeghbeigi, R. *Fluid Catalytic Cracking Handbook*, 3rd ed.; Elsevier: Amsterdam, 2012.

(8) Reynolds, J. G. Nickel in Petroleum Refining. *Pet. Sci. Technol.* **2001**, *19*, 979-1007.

(9) Busca, G.; Riani, P.; Garbarino, G.; Ziemacki, G.; Gambino, L.; Montanari, E.; Millini, R. The state of nickel in spent Fluid Catalytic Cracking catalysts. *Appl. Catal., A* **2014**, *486*, 176-186.

(10) Bai, P.; Etim, U. J.; Yan, Z.; Mintova, S.; Zhang, Z.; Zhong, Z.; Gao, X. Fluid catalytic cracking technology: current status and recent discoveries on catalyst contamination. *Catal. Rev. Sci. Eng.* **2019**, *61*, 333-405.

(11) Cerqueira, H. S.; Caeiro, G.; Costa, L.; Ramôa Ribeiro, F. Deactivation of FCC catalysts. *J. Mol. Catal. A: Chem.* **2008**, *292*, 1-13.

(12) Xu, M.; Liu, X.; Madon, R. J. Pathways for Y Zeolite Destruction: The Role of Sodium and Vanadium. *J. Catal.* **2002**, *207*, 237-246.

(13) Pinto, F. V.; Escobar, A. S.; de Oliveira, B. G.; Lam, Y. L.; Cerqueira, H. S.; Louis, B.; Tessonnier, J. P.; Su, D. S.; Pereira, M. M. The effect of alumina on FCC catalyst in the presence of nickel and vanadium. *Appl. Catal., A* **2010**, *388*, 15-21.

(14) Gambino, M.; Veselý, M.; Filez, M.; Oord, R.; Ferreira Sanchez, D.; Grolimund, D.; Nesterenko, N.; Minoux, D.; Maquet, M.; Meirer, F.; Weckhuysen, B. M. Nickel Poisoning of a Cracking Catalyst Unravelled by Single-Particle X-ray Fluorescence-Diffraction-Absorption Tomography. *Angew. Chem., Int. Ed.* **2020***, 59,* 3922-3927; Nickel Poisoning of a Cracking Catalyst Unravelled by Single-Particle X-ray Fluorescence-Diffraction-Absorption Tomography. *Angew. Chem.* **2020**, *132*, 3950-3955.

(15) Kugler, E. L.; Leta, D. P. Nickel and Vanadium on Equilibrium Cracking Catalysts by Imaging Secondary Ion Mass Spectrometry. *J. Catal.* **1988**, *109*, 387-395.

(16) Ohtsuka, Y. Influence of hydrogen chloride treatment on the dispersion of nickel particles supported on carbon. *J. Mol. Catal.* **1989**, *54*, 225-235.

(17) Cadet, V.; Raatz, F.; Lynch, J.; Marcilly, C. Nickel contamination of fluidised cracking catalysts: A model study. *Appl. Catal.* **1991**, *68*, 263-275.

(18) Foger, K.; Jaeger, H. The Effect of Chlorine Treatment on the Dispersion of Platinum Metal Particles Supported on Silica and γ-Alumina. *J. Catal.* **1985**, *92*, 64-78.

(19) Foger, K.; Jaeger, H. Redispersion of Pt-Zeolite Catalysts with Chlorine. *Appl. Catal.* **1989**, *56*, 137-147.

(20) Chen, N. Y. Reactivation of deactivated zeolite catalysts. U.S. patent 3,684,738 (filed Mar. 16, 1970); *Chem. Abstr.* **1972**, *77*, 118822.

(21) Melin, M.; Baillie, C.; McElhiney, G. Salt Deposition in FCC Gas Concentration Units. *Pet. Technol. Q.* **2009**, *Q4*, 135-139.

(22) John, R. C.; Fort, W. C. Petroleum Industry: Corrosion. In *Encyclopedia of Materials: Science and Technology*; Jürgen Buschow, K. H., Cahn, R. W., Flemings, M. C., Ilschner, B., Kramer, E. J., Mahajan, S., Veyssière, P., Eds.; Elsevier: Amsterdam, 2001; 2nd ed., pp 6840-6842.

(23) Gray, M. R.; Eaton, P. E.; Le, T. Kinetics of Hydrolysis of Chloride Salts in Model Crude Oil. *Pet. Sci. Technol.* **2008**, *26*, 1924-1933.

(24) Kaur, H.; Eaton, P.; Gray, M. R. The Kinetics and Inhibition of Chloride Hydrolysis in Canadian Bitumen. *Pet. Sci. Technol.* **2012**, *30*, 993-1003.

(25) Martin, D. O.; Allen, R. O. Preventing salt fouling in FCC main fractionators. *Pet. Technol. Q.* **2001**, *6*, 41-45.

(26) Wallenstein, D.; Farmer, D.; Knoell, J.; Fougret, C. M.; Brandt, S. Progress in the deactivation of metals contaminated FCC catalysts by a novel catalyst metallation method. *Appl. Catal., A* **2013**, *462-463*, 91-99.

(27) Maxson, R. N. Hydrogen Chloride. *Inorg. Synth.* **1939**, *1*, 147-149.

(28) Brauer, G. Handbuch der Präparativen Anorganischen Chemie. Eugen Göbel Book Printing Company: Tübingen, Germany, 1954.

(29) Kayser, J. C. Versatile Fluidized Bed Reactor. U.S. patent 6,069,012 (filed May 23, 1997); *Chem. Abstr.* **1998**, *130*, 27079.

(30) Kelkar, C. P.; Xu, M.; Madon, R. J. Laboratory Evaluation of Cracking Catalysts in a Fluid Bed: Effects of Bed Dynamics and Catalyst Deactivation. *Ind. Eng. Chem. Res.* **2003**, *42*, 426-433.

(31) A CO DRIFTS technique developed within BASF was employed. Manuscript under review.

(32) Yates, J. T., Jr.; Garland, C. W. Infrared Studies of Carbon Monoxide Chemisorbed on Nickel and on Mercury-Poisoned Nickel Surfaces. *J. Phys. Chem.* **1961**, *65*, 617-624.

(33) Kubelková, L.; Nováková, J.; Jaeger, N. I.; Schulz-Elkoff, G. Characterization of nickel species at Ni/γ-Al_2O_3 and Ni/faujasite catalysts by carbon monoxide adsorption. *Appl. Catal., A* **1993**, *95*, 87-101.

(34) Fujita, S.; Nakamura, M.; Doi, T.; Takezawa, N. Mechanisms of methanation of carbon dioxide and carbon monoxide over nickel/alumina catalysts. *Appl. Catal., A* **1993**, *104*, 87-100.

(35) Garbarino, G.; Finocchio, E.; Lagazzo, A.; Valsamakis, I.; Riani, P.; Sanchez Escribano, V.; Busca, G. Steam reforming of ethanol-phenol mixture on Ni/Al_2O_3: Effect of magnesium and boron on catalytic activity in the presence and absence of sulfur. *Appl. Catal., B* **2014**, *147*, 813-826.

(36) Zecchina, A.; Geobaldo, F.; Lamberti, C.; Bordiga, S.; Turnes Palomino, G.; Otero Areán, C. Infrared studies of the interaction of carbon monoxide and dinitrogen with ferrisilicate MFI-type zeolites. *Catal. Lett.* **1996**, *42*, 25-33.

(37) Wadayama, T.; Kubo, K.; Yamashita, T.; Tanabe, T.; Hatta, A. Infrared Reflection Absorption Study of Carbon Monoxide Adsorbed on Submonolayer Fe-Covered Cu(100), (110), and (111) Bimetallic Surfaces. *J. Phys. Chem. B* **2003**, *107*, 3768-3773.

(38) Kefirov, R.; Inanova, E.; Hadjiivanov, K.; Dzwigaj, S.; Che, M. FTIR Characterization of Fe^{3+}-OH Groups in Fe-H-BEA Zeolite: Interaction with CO and NO. *Catal. Lett.* **2008**, *125*, 209-214.

(39) Wagner, D.; Devisme, O.; Patisson, F.; Alblitzer, D. In *A Laboratory Study of the Reduction of Iron Oxides by Hydrogen*, Sohn International Symposium, San Diego, CA, August 27-31, 2006; Kongoli, F. Reddy, R. G., Eds.; *TMS*, 2008, *2*, 111-120.

(40) Pineau, A.; Kanari, N.; Gaballah, I. Kinetics of reduction of iron oxides by H_2 Part I: Low temperature reduction of hematite. *Thermochim. Acta* **2006**, *447*, 89-100.

(41) Pineau, A.; Kanari, N.; Gaballah, I. Kinetics of reduction of iron oxides by H_2 Part II: Low temperature reduction of magnetite. *Thermochim. Acta* **2007**, *456*, 75-88.

(42) Chatterjee, R.; Banerjee, S.; Banerjee, S.; Ghosh, D. Reduction of Nickel Oxide Powder and Pellet by Hydrogen. *Trans. Indian Inst. Met.* **2012**, *65*, 265-273.

(43) Bare, S. R.; Charochak, M. E.; Kelly, S. D.; Lai, B.; Wang, J.; Chen-Wiegart, Y. K. Characterization of a Fluidized Catalytic Cracking Catalyst on Ensemble and Individual Particle Level by X-ray Micro- and Nanotomography, Micro-X-ray Fluorescence, and Micro-X-ray Diffraction. *ChemCatChem* **2014**, *6*, 1427-1437.

7. SUMMARY AND CONCLUSIONS

This dissertation has described the syntheses of a variety of lipophilic Werner complexes for use as chiral hydrogen bond donors in enantioselective catalysis. Lipophilic Werner catalysts offer numerous advantages in this application. Among them, the earth-abundant cobalt(III) metal center possesses a low spin d^6 electron configuration, rendering it substitution inert and thus unable to racemize under catalytic conditions. These complexes also employ commercially available ligands that can be purchased in their enantiopure forms. The catalysts operate through second coordination sphere mechanisms through hydrogen bond donation of the NH units. As the catalytic mechanisms have not entirely been elucidated, variations to the metal, ligands, and anions present a reasonable pathway forward to identify trends that lead to the success or demise of these catalysts in organic reactions.

Section 2 dives into the effect of the central metal ion of the catalyst on the enantioselectivity and the stability. As the metal ion is not directly involved in the catalytic mechanism, the discrepancies between catalyst selectivities was not anticipated to be large. Considering that fact, the identity of the metal and its corresponding charge affect the acidity of the NH active sites. In the case of $[Pt(en)_3]^{4+}$, the base required to initiate the catalytic addition reaction may result in deprotonation of an NH group, reducing the yield and enantiomeric excess of the product. Additionally, the acidity of the lipophilic Werner complexes result in an increased hydration value in the solid state, as they have a greater propensity to function as hydrogen bond donors. Finally, thermal analyses by TGA and DSC revealed that the lipophilic catalysts decompose at temperatures just slightly above dehydration.

Section 3 details an investigation of the effects of chiral anions on enantioselectivities when paired with these catalysts. This study invited a whole new cast of characters to the table to match up with our cations than what had been previously reported. This scope of anions yielded a variety of catalyst lipophilicities, activities, and enantioselectivities. Fortunately, we were able to secure an unprecedented crystal structure of Δ-(*S*,*S*)-$[Co((S,S)\text{-dpen})_3]^{3+}$ 2(1*S*)-camph$SO_3^-BAr_f^-$. This was the first and only reported structure of a mixed salt and the first BAr_f^--containing crystal structure in the history of this project. This finding confirmed many hypotheses, including the theory that the stronger hydrogen bond accepting anions would preferentially hydrogen bond at the C_3 faces of the catalyst due to the quality and quantity of hydrogen bonds that could be forged relative to those on the C_2 face. The catalytic test reactions did not reveal any significant increase in enantioselectivity, but did provide an interesting match/mismatch effect, where the diastereomeric chiral anion pairs performed better or worse depending on the configuration of the anion.

Section 4 focuses on adapting the ligands of the catalyst. These changes present alterations in the sterics and acidities of the NH active sites, as well as the stabilities of the catalysts overall. Thanks in large part to the work carried out by Sargeson and Harrowfield, the transformations required to produce these complexes from the $[Co(en)_3]^{3+}$ precursor in a stereospecific manner were well-established. These methods featured reagents that are staples to any synthetic laboratory, which included formaldehyde, nitromethane, and ammonium hydroxide. This led to a whole new class of hexadentate complexes for us to put through the paces in our organic addition reactions. The various capping groups provided tunability in NH acidity and the number of caps affected the enantioselectivity of the product. The catalyst stability was enhanced by the

hexadentate nature of the ligand. These six "teeth" prevented the ligand loss that is possible with bidentate ligands, and leads to the formation of $[Co(en)_2(Cl)_2]^+$ Cl^- byproducts.

Section 5 covers the syntheses of functionalized (*S*,*S*)-1,2-diamine ligands and their coordination to cobalt(III) metal centers. These complexes presented some intricacies along the way and the nature of the complex varied considerably. All complexes had differing solubilities, raising difficulties in diastereomeric resolution by washing the crude product with water. Another issue presented was the variable acidity of the NH units, which led to problems in anion metathesis from acetate to chloride. Unfortunately, none of these newly installed ligands increased enantioselectivities over dpen.

Section 6 comprises an investigation of the effects of chloride on nickel contaminants in FCC catalysts. These catalysts were first exposed to gaseous HCl and then hydrogen gas at high temperature. The contaminant nickel that was present on the catalysts was redistributed and present in a reduced oxidation state, according to an abundance of analytical techniques that were employed. This nickel(0) is prone to participating in dehydrogenation reactions, leading to harmful effects in the FCC environment, including increased coke and hydrogen production.

Overall, chiral lipophilic Werner complexes have displayed promising results in enantioselectively catalyzing organic reactions. They are attractive catalysts thanks to their low cost and ease of synthesis. Still, ligand modifications and expansion of the reaction scope are avenues that are worth exploring to untap the full potential of this class of catalysts.

APPENDIX

Representative HPLC traces used for determination of ee values.

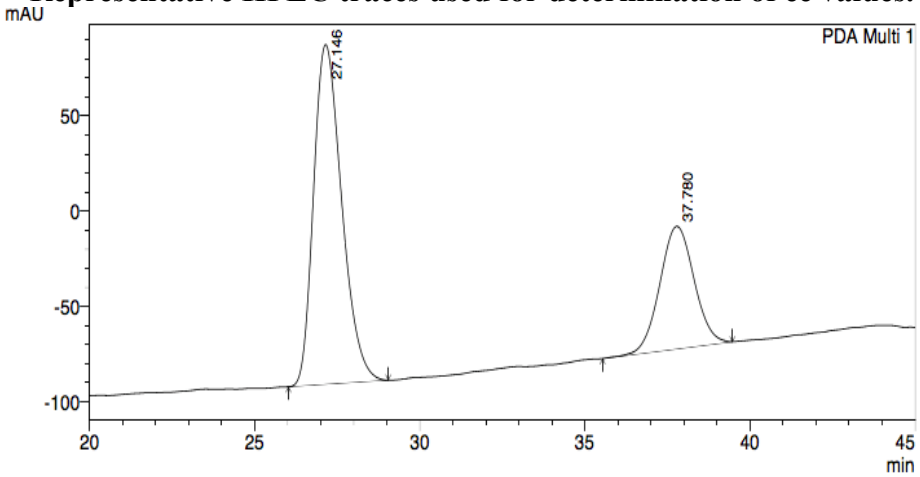

PeakTable

PDA Ch1 220nm 4nm

Peak#	Ret. Time	Area	Height	Area %	Height %
1	27.146	10569265	178400	69.453	73.470
2	37.780	4648531	64420	30.547	26.530
Total		15217796	242820	100.000	100.000

Figure A-1. HPLC trace for **1** in Figure 2.3, entry 5.

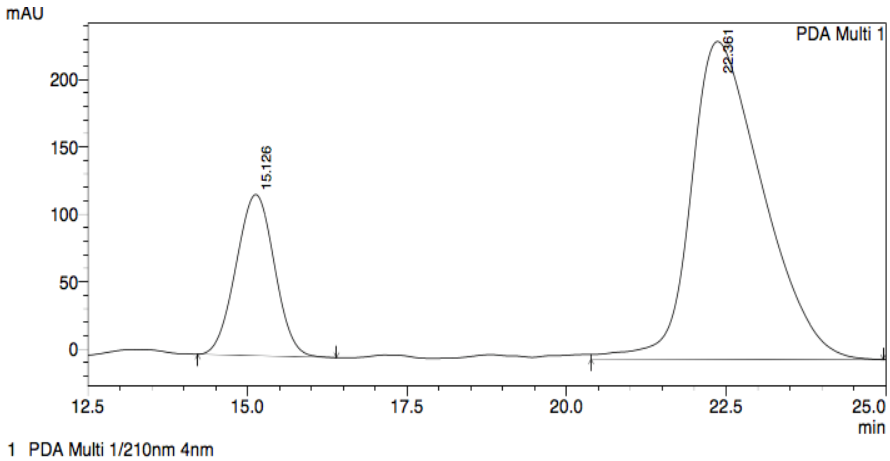

PeakTable

PDA Ch1 210nm 4nm

Peak#	Ret. Time	Area	Height	Area %	Height %
1	15.126	5007507	119434	21.386	33.636
2	22.361	18406889	235643	78.614	66.364
Total		23414395	355077	100.000	100.000

Figure A-2. HPLC trace for **2** in Figure 2.4, entry 5.

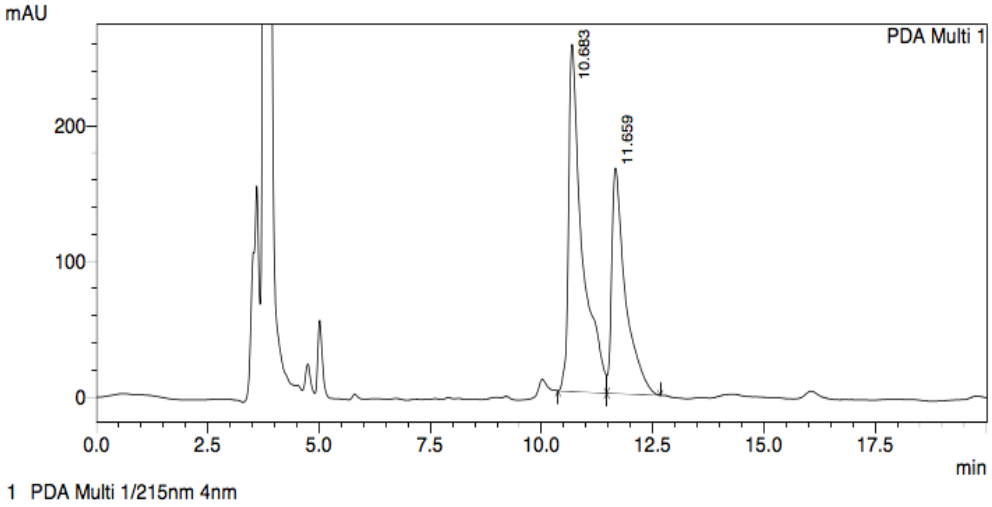

PeakTable

PDA Ch1 215nm 4nm

Peak#	Ret. Time	Area	Height	Area %	Height %
1	10.683	5453817	255985	60.376	60.643
2	11.659	3579281	166131	39.624	39.357
Total		9033098	422116	100.000	100.000

Figure A-3. HPLC trace for **3** in Figure 2.5, entry 6.

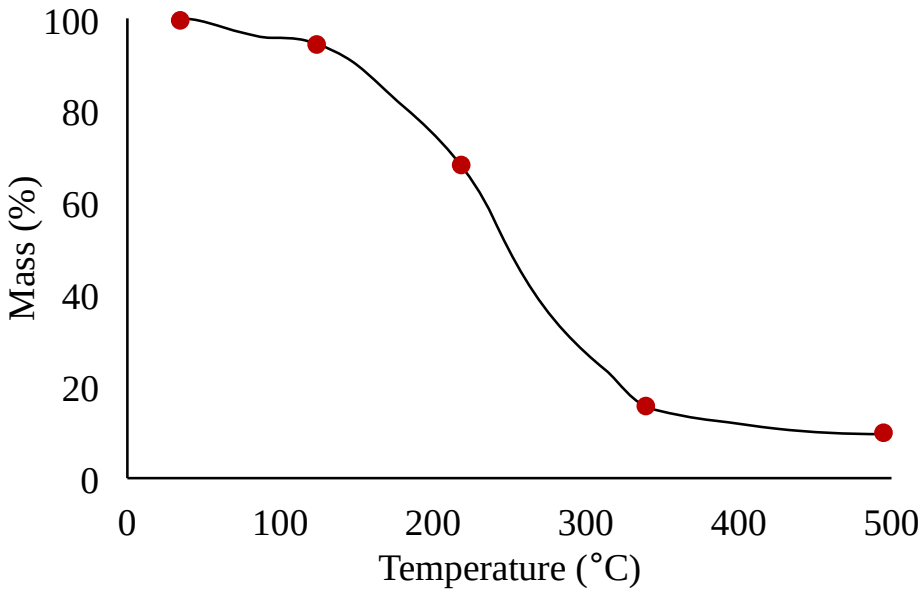

Figure A-4. TGA trace for Λ-$[Cr(en)_3]^{3+}$ $3BAr_f^-\cdot 14H_2O$.

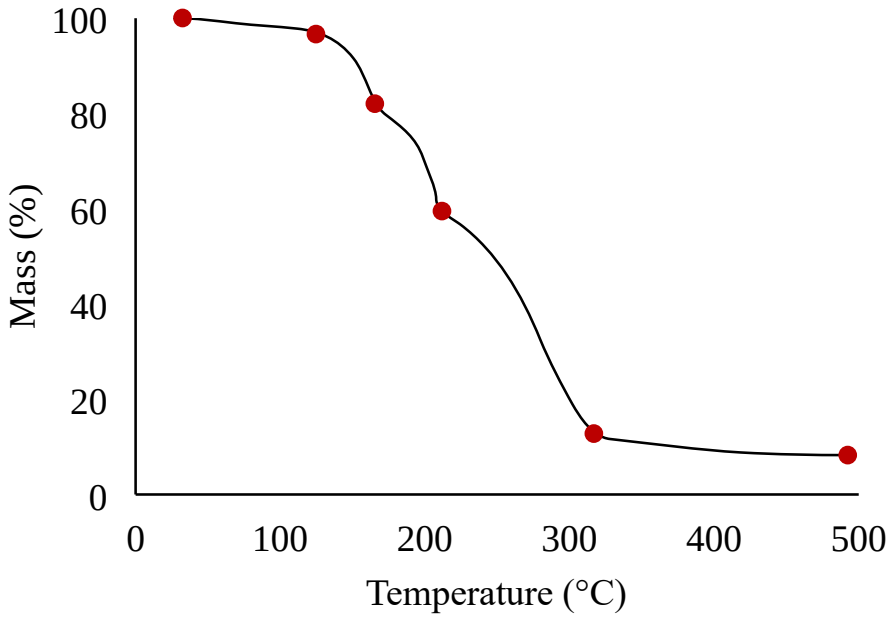

Figure A-5. TGA trace for Λ-$[Co(en)_3]^{3+}$ $3BAr_f^-\cdot 14H_2O$.

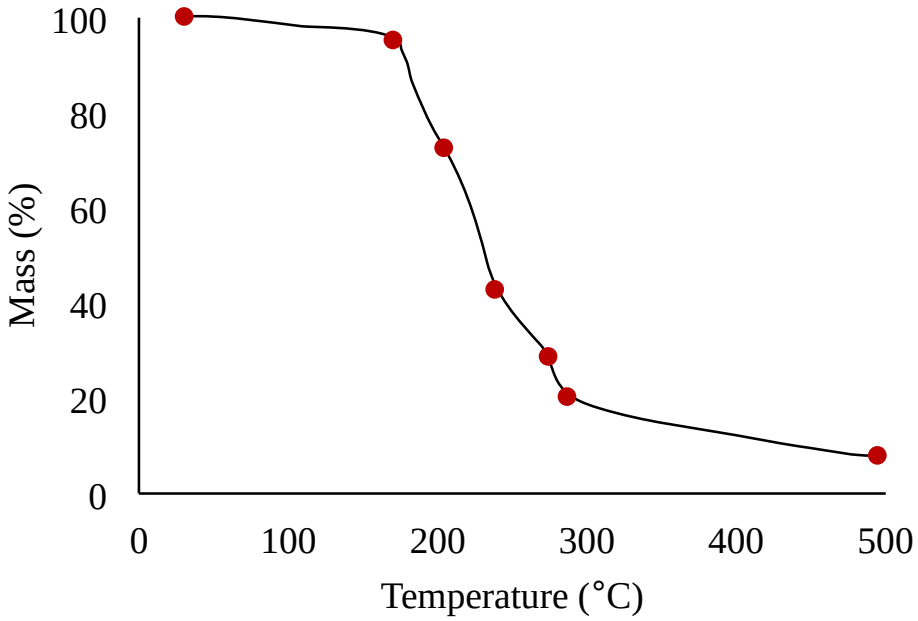

Figure A-6. TGA trace for Λ-$[Rh(en)_3]^{3+}$ $3BAr_f^-\cdot 11.5H_2O$.

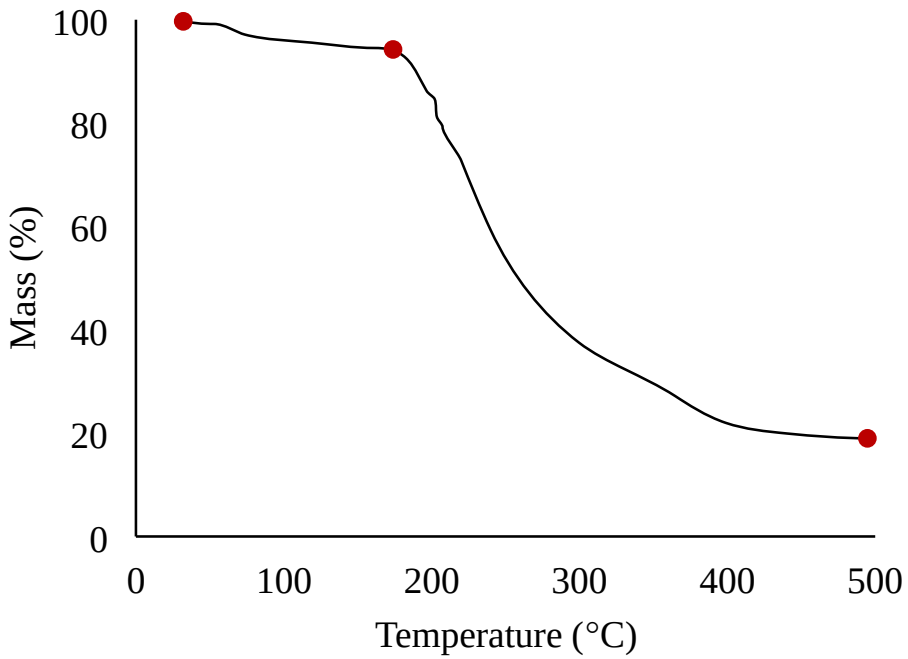

Figure A-7. TGA trace for Λ-$[Ir(en)_3]^{3+}$ $3BAr_f^-{\cdot}9H_2O$.

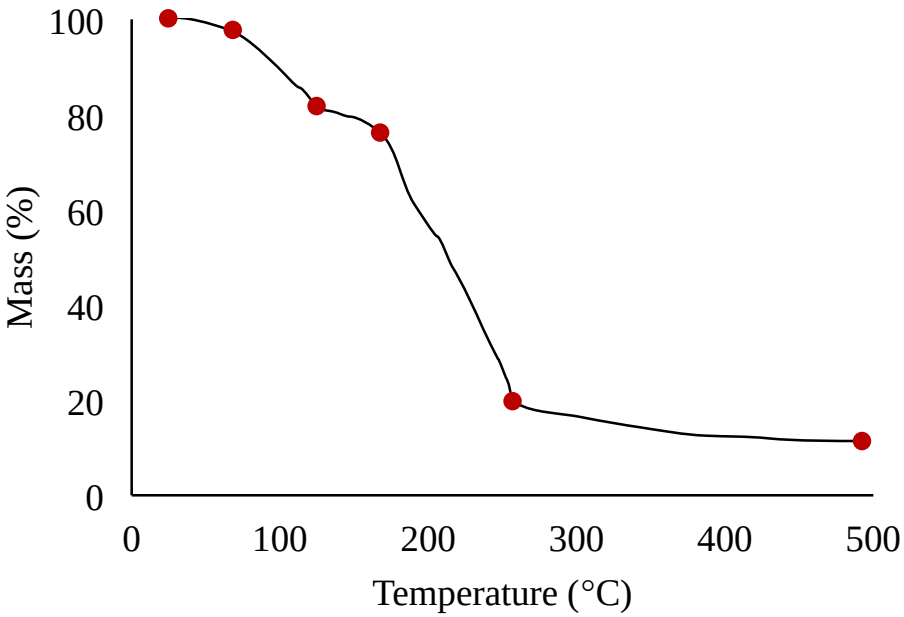

Figure A-8. TGA trace for Λ-$[Pt(en)_3]^{4+}$ $4BAr_f^-{\cdot}17H_2O$.

Table A-1. Hydration levels (z) of isolated chloride and iodide salts $[M(en)_3]^{n+}$ nX^- $\cdot zH_2O$.

M^{n+}	nX^-	z
rac-Cr(III)	$3Cl^-$	3[a]
rac-Cr(III)	$3Cl^-$	3[b]
Λ-Cr(III)	$3Cl^-$	1.6[c]
Λ-Cr(III)	$3Cl^-$	2[b]
rac-Cr(III)	$3Cl^-$	3.72[d]
rac-Cr(III)	$3I^-$	0[b]
rac-Co(III)	$3Cl^-$	4[d]
rac-Co(III)	$3Cl^-$	2.8[b]
Λ-Co(III)	$3Cl^-$	0[b]
Λ-Co(III)	$3I^-$	1[e]
rac-Co(III)	$3I^-$	1[b]
rac-Co(III)	$3I^-$	0[f]
Λ-Rh(III)	$3Cl^-$	2.3[g]
rac-Rh(III)	$3Cl^-$	3.37[d]
rac-Rh(III)	$3I^-$	0[f]
Λ-Ir(III)	$3Cl^-$	2[g]
rac-Ir(III)	$3Cl^-$	3.4[d]
rac-Ir(III)	$3I^-$	0[f]
rac-Pt(IV)	$4Cl^-$	2[h]
rac-Pt(IV)	$4Cl^-$	2.5[i]
rac-Pt(IV)	$4Cl^-$	0[j]
rac-Pt(IV)	$4I^-$	0[i]

[a]Gillard, R. D.; Mitchell, P. R. *Inorg. Synth.* **1972**, *13*, 184-186. [b]Miller, S. E.; House, D. A. *Inorg. Chim. Acta* **1989**, *157*, 29-32. [c]Galsbøl, F. *Inorg. Synth.* **1970**, *12*, 269-280. [d]Takamizawa, S.; Kohbara, M.; Akatsuka, T.; Miyake, R. *New J. Chem.* **2008**, *32*, 1782-1787. [e]Broomhead, J. A. Dwyer, F. P.; Hogarth, J. W. *Inorg. Synth.* **1960**, *6*, 183-186. [f]Moczygemba, G. A.; Lagowski, J. J. *J. Coord. Chem.* **1976**, *5*, 71-76. [g]Galsbøl, F.; Rasmussen, B. S. *Acta Chem. Scand.* **1982**, *A36*, 83-87. [h]Giedt, D. C.; Nyman, C. J. *Inorg. Synth.* **1966**, *8*, 239-241. [i]Wendlandt, W. *Texas J. Sci.* **1962**, *14*, 264-277. [j]House, J. E., Jr.; Tahir, F. M. *Thermochim. Acta* **1987**, *118*, 191-197.

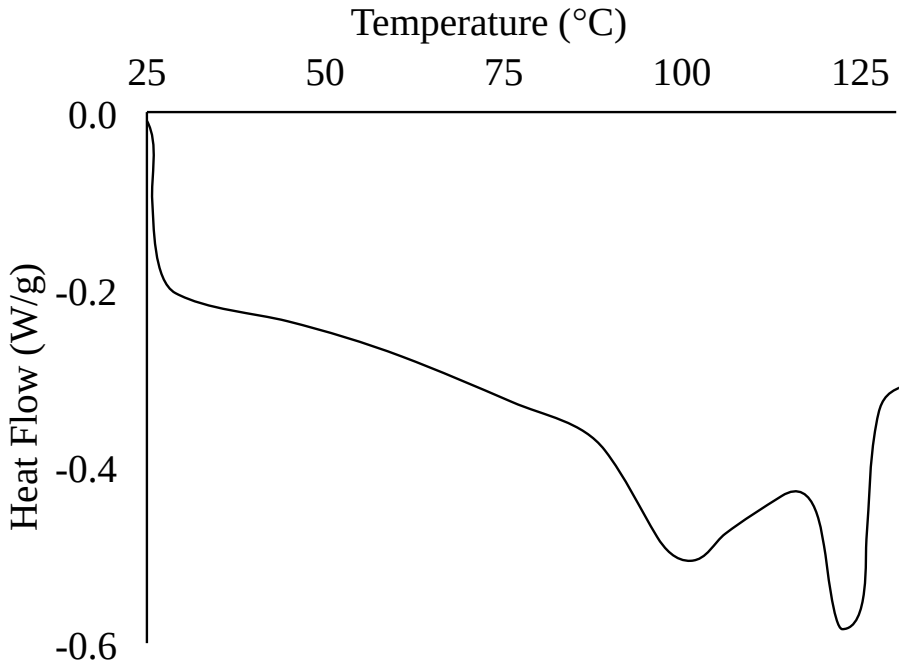

Figure A-9. DSC trace for Λ-$[Cr(en)_3]^{3+}$ $3BAr_f^-\cdot 14H_2O$.

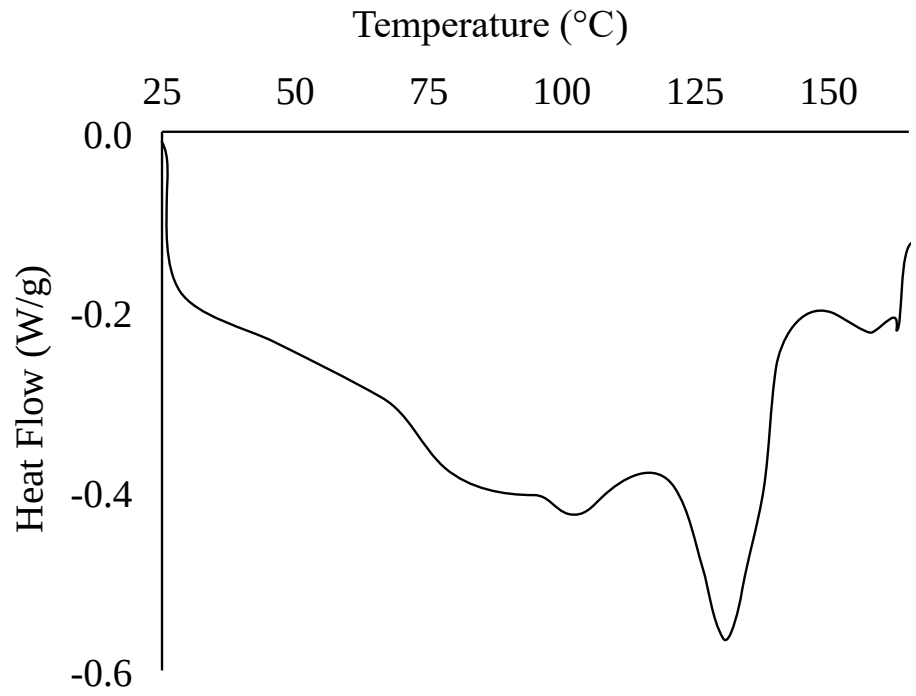

Figure A-10. DSC trace for Λ-$[Co(en)_3]^{3+}$ $3BAr_f^-\cdot 14H_2O$.

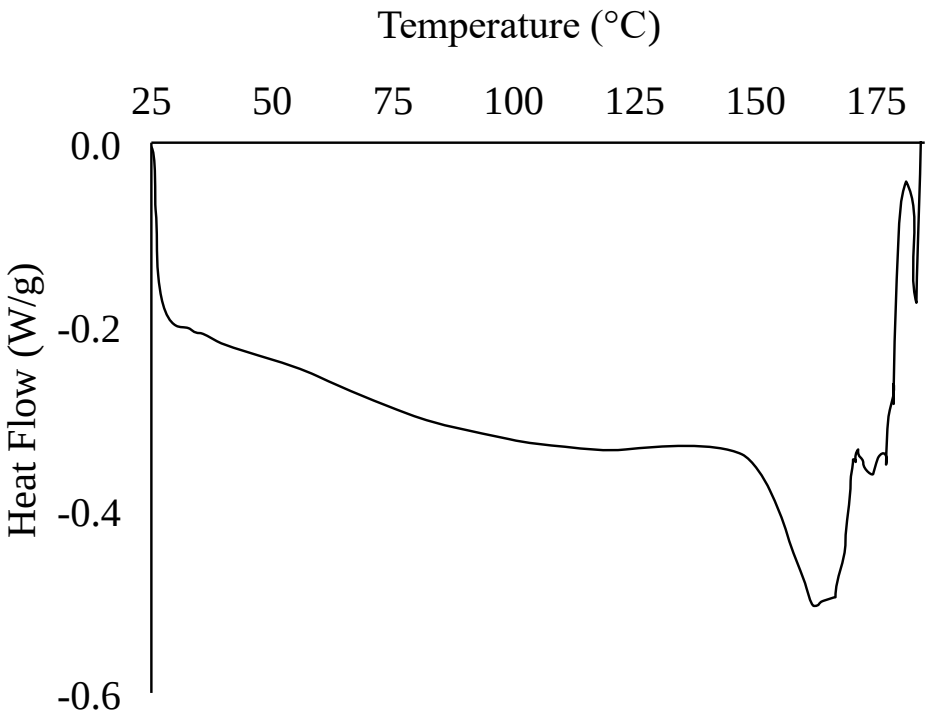

Figure A-11. DSC trace for Λ-$[Rh(en)_3]^{3+}$ $3BAr_f^-\cdot 11.5H_2O$.

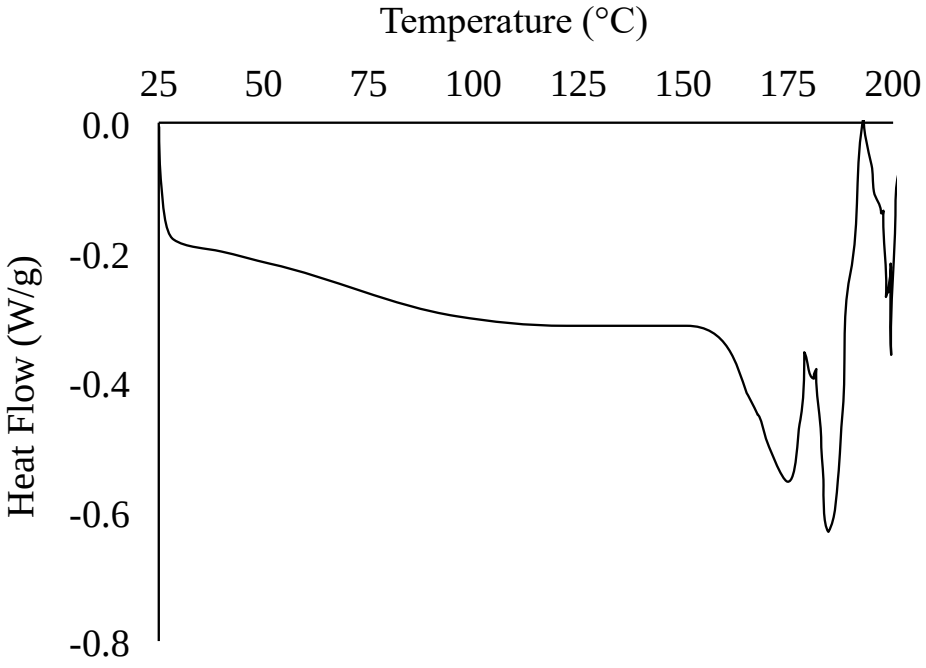

Figure A-12. DSC trace for Λ-$[Ir(en)_3]^{3+}$ $3BAr_f^-\cdot 9H_2O$.

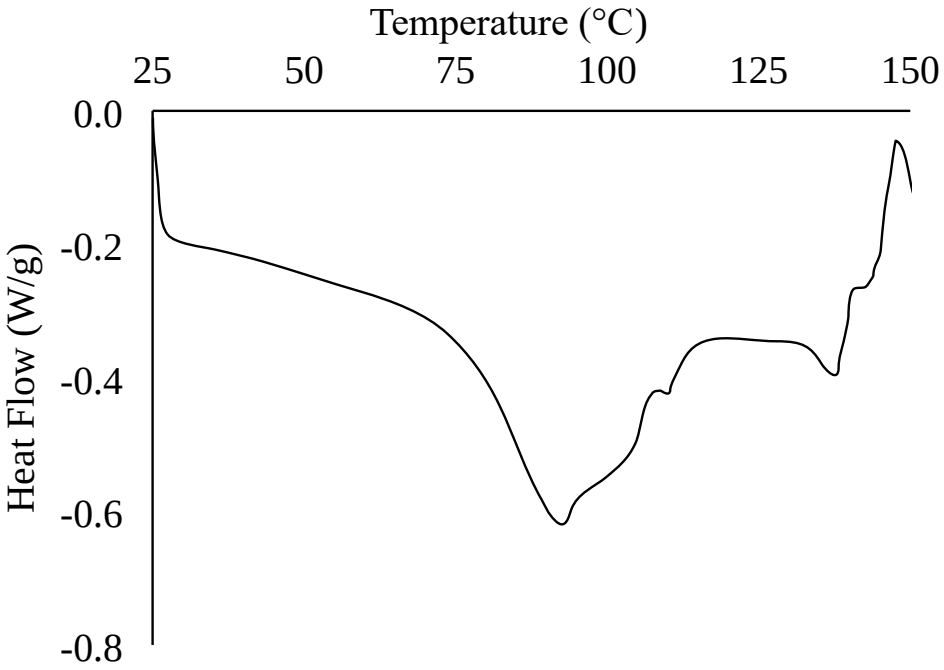

Figure A-13. DSC trace for Λ-$[Pt(en)_3]^{4+}$ $4BAr_f^-\cdot 17H_2O$.

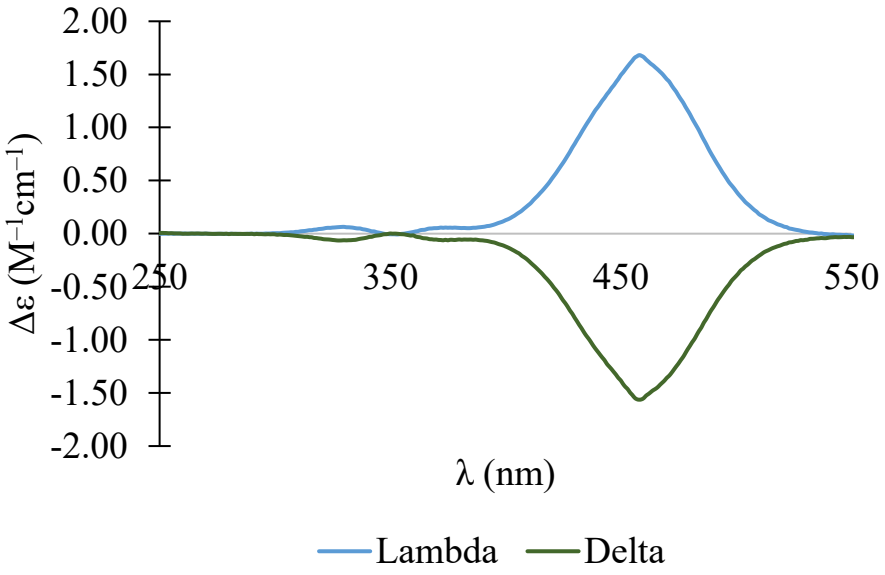

Figure A-14. CD traces for $[Cr(en)_3]^{3+}$ $3Cl^-$ in H_2O.

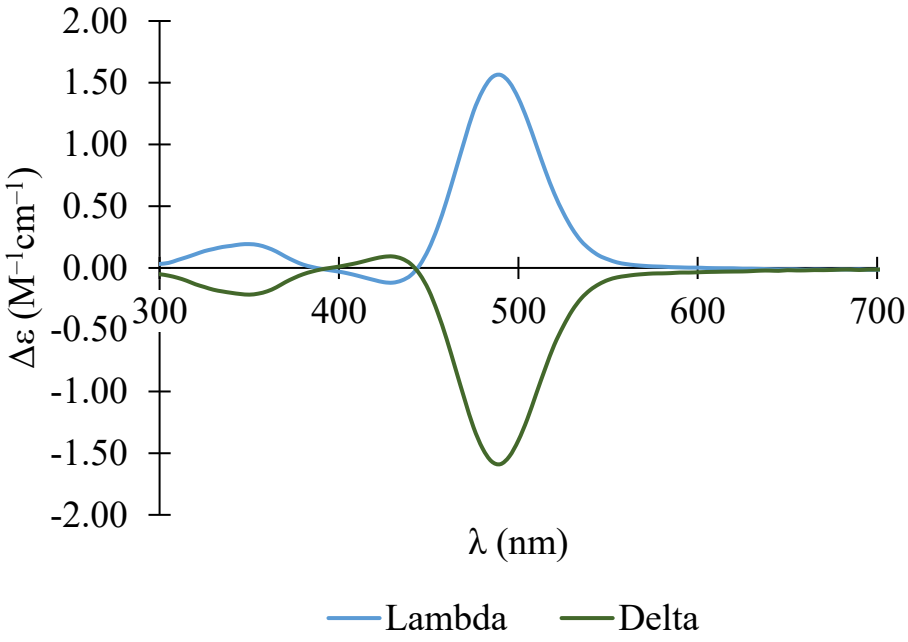

Figure A-15. CD traces for $[Co(en)_3]^{3+}$ $3I^-$ in H_2O.

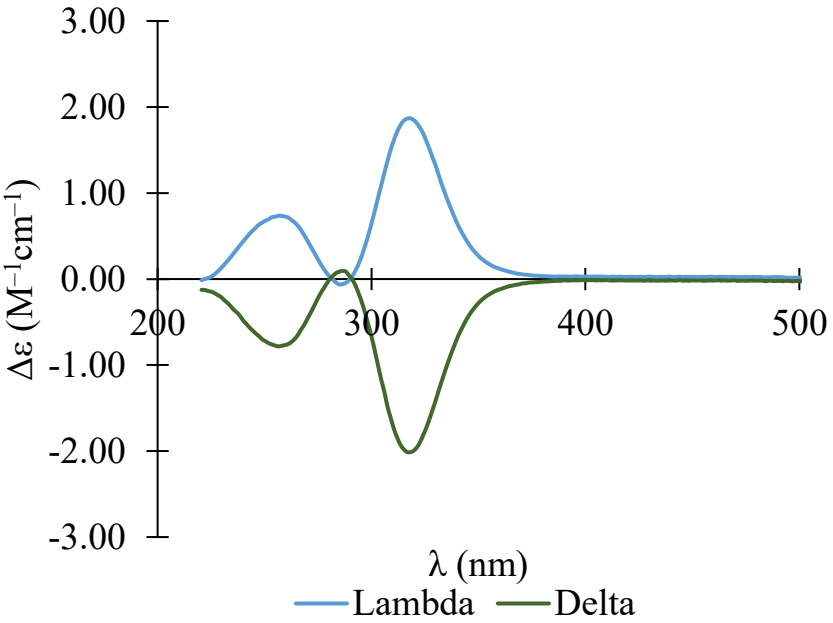

Figure A-16. CD traces for $[Rh(en)_3]^{3+}$ $3Cl^-$ in H_2O.

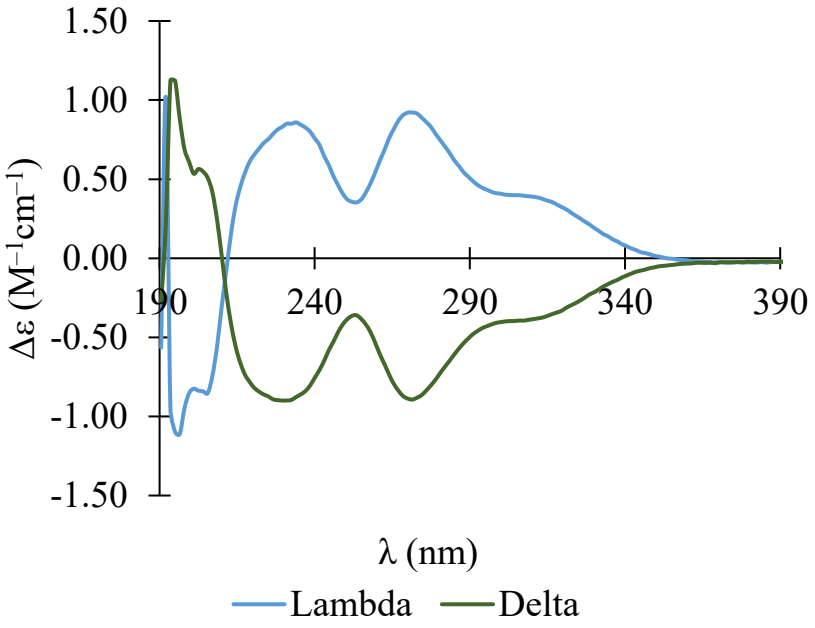

Figure A-17. CD traces for $[Ir(en)_3]^{3+}$ $3Cl^-$ in H_2O.

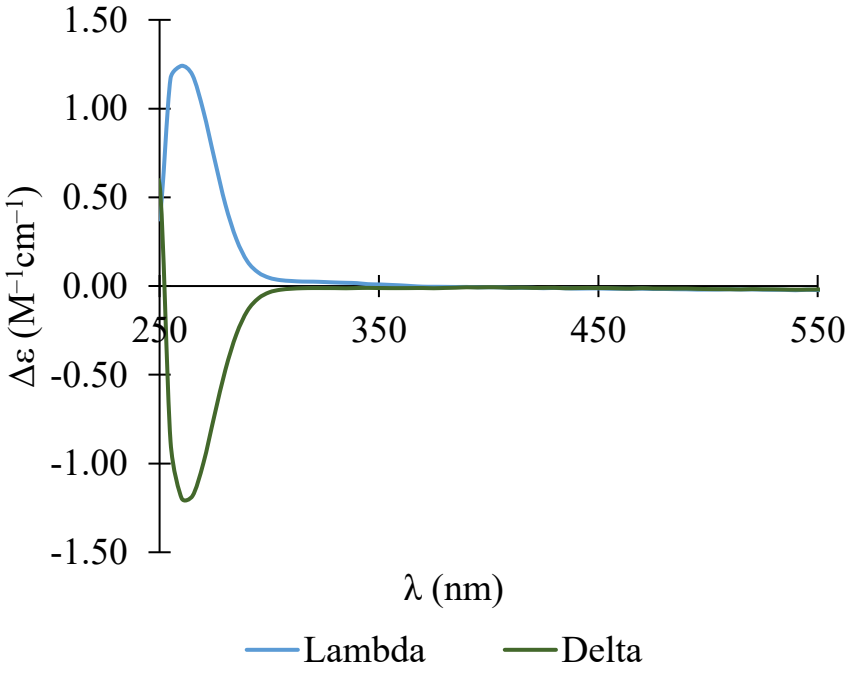

Figure A-18. CD traces for $[Pt(en)_3]^{4+}$ $4Cl^-$ in H_2O.

Dimethyl 2-(2-nitro-1-phenylethyl)malonate (**2**).

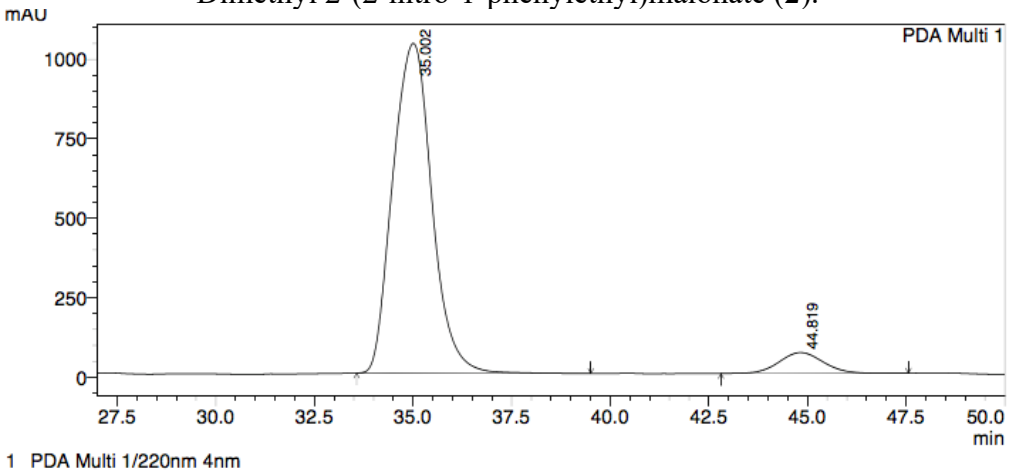

1 PDA Multi 1/220nm 4nm

PeakTable

PDA Ch1 220nm 4nm

Peak#	Ret. Time	Area	Height	Area %	Height %
1	35.002	71701778	1037932	93.391	94.071
2	44.819	5074494	65420	6.609	5.929
Total		76776271	1103352	100.000	100.000

Figure A-19. HPLC trace for Figure 3.5, entry 20 (catalyzed by Λ-(*S*,*S*)-$\mathbf{1}^{3+}$ $(Sb_2((R,R)\text{-tart}')_2)^{2-}BAr_f^-$).

N,*N*'-bis(*t*-butoxycarbonyl)-1-hydrazino-2-oxocyclopentanecarboxylic acid methyl ester (**3**).

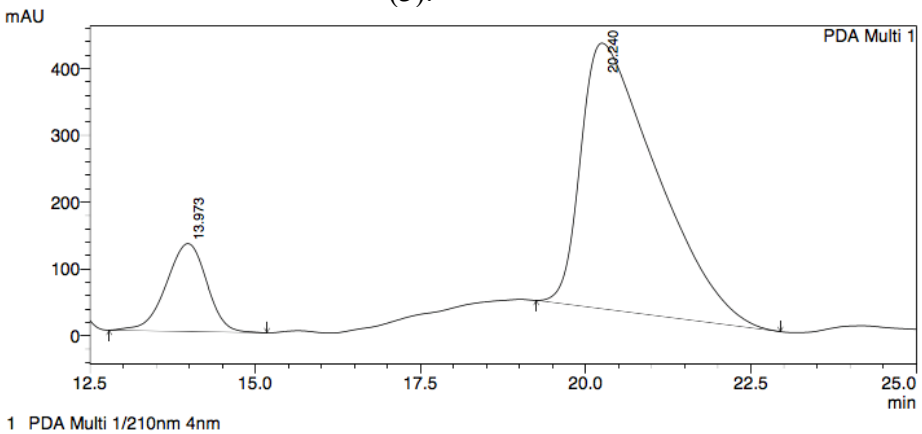

1 PDA Multi 1/210nm 4nm

PeakTable

PDA Ch1 210nm 4nm

Peak#	Ret. Time	Area	Height	Area %	Height %
1	13.973	5635111	131564	15.006	24.854
2	20.240	31916174	397776	84.994	75.146
Total		37551285	529340	100.000	100.000

Figure A-20. HPLC trace for Figure 3.6, entry 20 (catalyzed by Λ-(*S*,*S*)-$\mathbf{1}^{3+}$ $(Sb_2((R,R)\text{-tart}')_2)^{2-}BAr_f^-$).

Dimethyl 2-(2-nitro-1-phenylethyl)malonate.

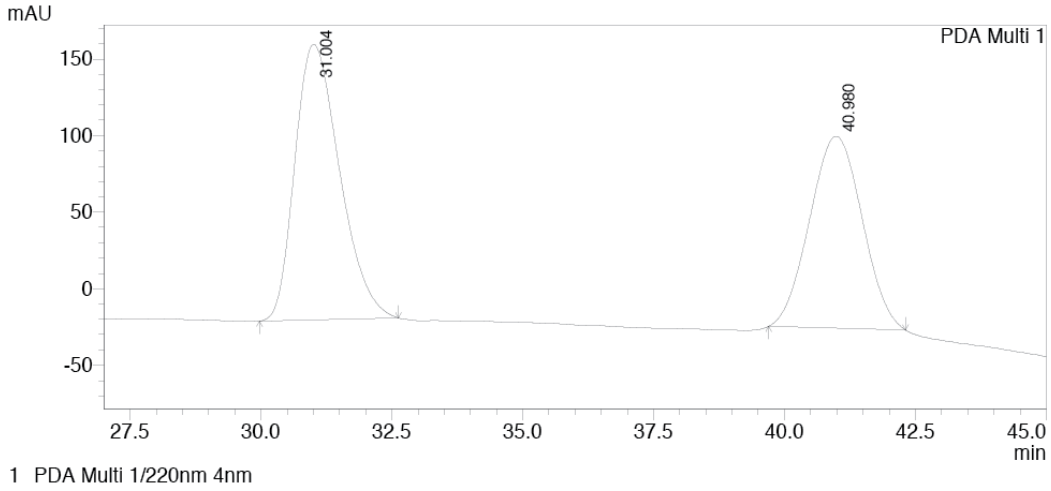

PeakTable

PDA Ch1 220nm 4nm

Peak#	Ret. Time	Area	Height	Area %	Height %
1	31.004	10700249	179875	55.054	58.931
2	40.980	8735707	125353	44.946	41.069
Total		19435956	305228	100.000	100.000

Figure A-21. HPLC trace for Figure 4.5, entry 6 (catalyzed by Λ-$[Co(sen)]^{3+}$ $3BAr_f^-$).

3-(Bis(ethoxycarbonyl)methyl)cyclopentanone.

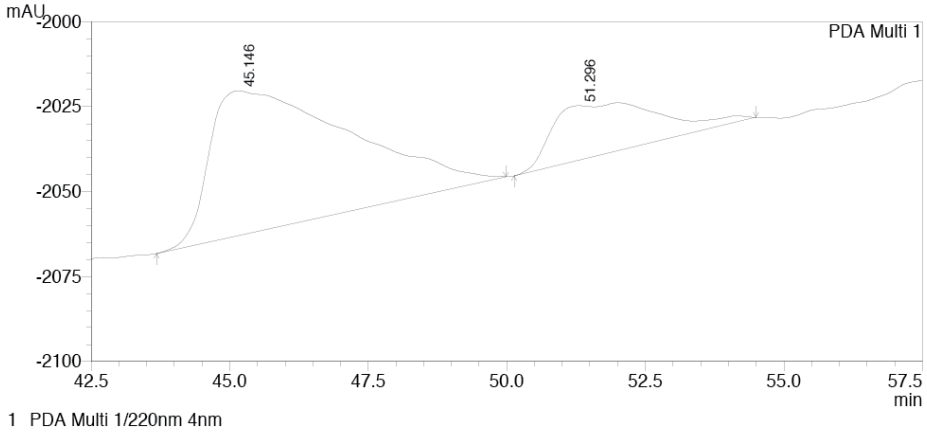

PeakTable

PDA Ch1 220nm 4nm

Peak#	Ret. Time	Area	Height	Area %	Height %
1	45.146	7372463	42685	78.319	72.680
2	51.296	2040860	16045	21.681	27.320
Total		9413323	58730	100.000	100.000

Figure A-22. HPLC trace for Figure 4.6, entry 6 (catalyzed by Λ-$[Co(sen)]^{3+}$ $3BAr_f^-$).

N,N'-Bis(t-butoxycarbonyl)-1-hydrazino-2-oxocyclopentanecarboxylic acid methyl ester.

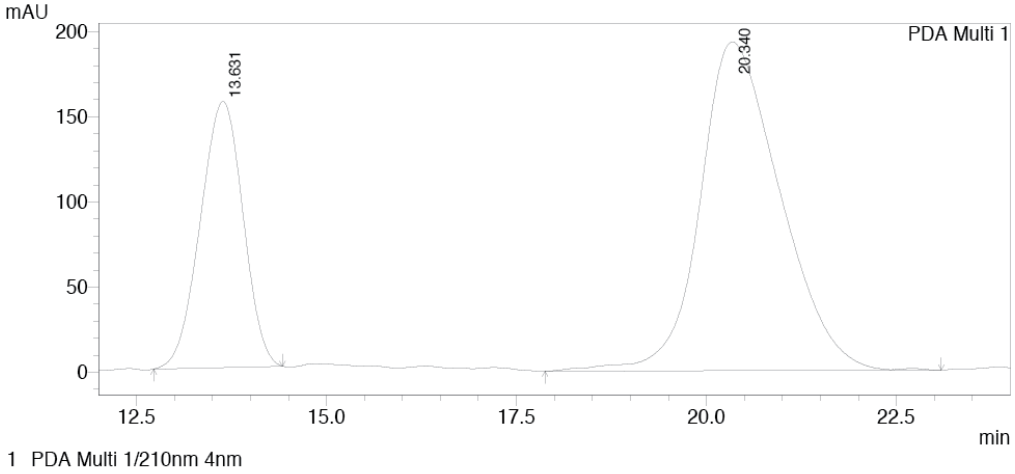

PeakTable

PDA Ch1 210nm 4nm

Peak#	Ret. Time	Area	Height	Area %	Height %
1	13.631	6121279	156316	30.129	44.731
2	20.340	14195741	193145	69.871	55.269
Total		20317020	349461	100.000	100.000

Figure A-23. HPLC trace for Figure 4.7, entry 6 (catalyzed by Λ-$[Co(sen)]^{3+}$ $3BAr_f^-$).

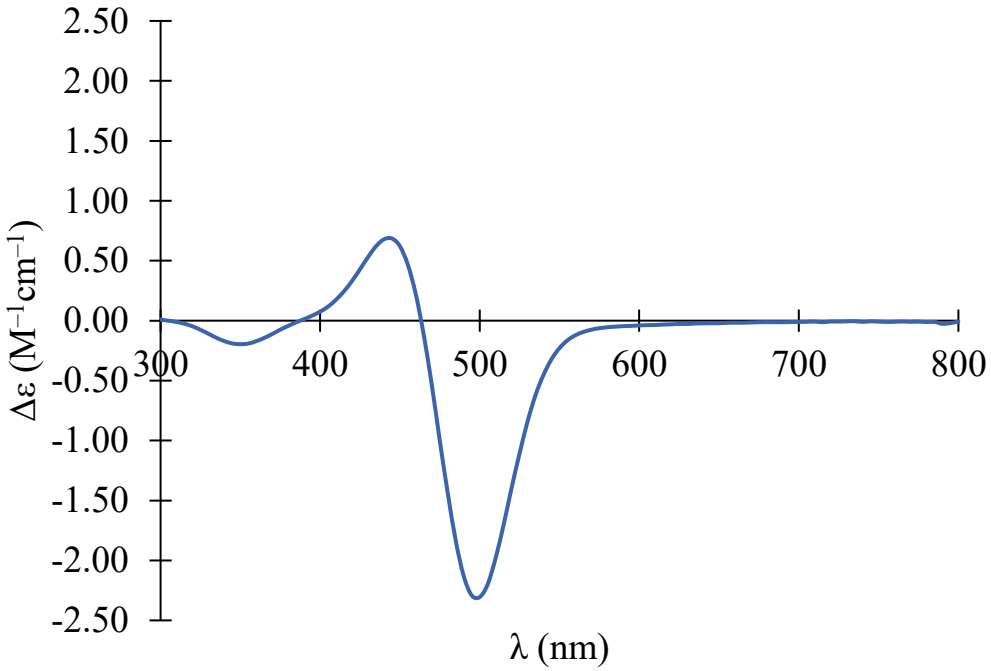

Figure A-24. CD trace for Δ-$[Co((R,R)\text{-chxn})_3]^{3+}$ $3Cl^-$ in H_2O.

Table A-2. Key interatomic distances (Å) and angles (°) in crystallographically characterized $[Pt((S,S)\text{-dpen})_2]^{2+}$ $2Cl^{-}\cdot 2CH_3OH$.

Atoms	Distances (Å)	Atoms	Angles (°)
Pt1-N1	2.034(6)	N1-Pt1-N2	83.4(3)
Pt1-N2	2.036(6)	N1-Pt1-N3	97.4(2)
Pt1-N3	2.036(6)	N1-Pt1-N4	174.4(3)
Pt1-N4	2.053(6)	N2-Pt1-N3	177.7(3)
N1-C1	1.477(10)	N2-Pt1-N4	96.2(2)
N2-C2	1.489(9)	N3-Pt1-N4	82.7(1)
N3-C15	1.470(9)	N1–H···Cl2	142.5
N4-C16	1.498(9)	N3–H···Cl2	141.8
N1···Cl2	3.280	N2–H···Cl1	147.5
N3···Cl2	3.213	N4–H···Cl1	144.9
N2···Cl1	3.296		
N4···Cl1	3.273		
N1H···Cl2	2.511		
N3H···Cl2	2.449		
N2H···Cl1	2.492		
N4H···Cl1	2.487		